R74-46

OSP 80571

MIT

STOCHASTIC MODELING OF GROUNDWATER SYSTEMS

by

Lynn W. Gelhar

Peter Y. Ko

Herman H. Kwai

John L. Wilson

RALPH M. PARSONS LABORATORY
FOR WATER RESOURCES AND HYDRODYNAMICS

Report No. 189

The work upon which this publication is based was supported in part by funds provided by the United States Department of the Interior as authorized under the Water Resources Research Act of 1964 as amended.

September 1974

DEPARTMENT
OF
CIVIL
ENGINEERING

SCHOOL OF ENGINEERING
MASSACHUSETTS INSTITUTE OF TECHNOLOGY
Cambridge, Massachusetts 02139

R74-46 DSR 80571

STOCHASTIC MODELING OF GROUNDWATER SYSTEMS

by

Lynn W. Gelhar

Peter Y. Ko

Herman H. Kwai

John L. Wilson

RALPH M. PARSONS LABORATORY

FOR WATER RESOURCES AND HYDRODYNAMICS

Department of Civil Engineering

Massachusetts Institute of Technology

Report No. 189

The work upon which this publication is based was supported in part by funds provided by the United States Department of the Interior as authorized under the Water Resources Research Act of 1964 as amended.

September 1974

ABSTRACT

This research developed important new results on the use of spectral analysis techniques to evaluate groundwater resources. The linear theory of aquifer spectral response in the frequency domain is developed, including effects of aquifer slope, vertical flow, variable transmissivity and other features. Numerical simulations of the nonlinear effects in the spectral domain are developed and show that the nonlinear effects are typically quite small, thus making the simple linear theory applicable for most field situations.

Some additional features which are explored are the effects of spatial variability of hydraulic conductivity and the influence of transient flow in the partially saturated zone above the water table. Through spectral analysis in the wave number domain, an error criterion is established for a simple observation network which is used to measure groundwater flow. The effects of storage in the partially saturated zone on the frequency spectrum of groundwater fluctuations are estimated and found to be negligible in most cases.

The theoretical results are applied to evaluate, through spectral analysis, time series of groundwater levels, precipitation and stream stage for a site in Kansas. From these data, using a procedure based on the linear spectral theory, estimates of aquifer transmissivity and storativity are developed. The procedure yields parameter estimates which are in agreement with those obtained from pumping tests.

The results of the study should be applicable under specified conditions to the estimation of aquifer parameters from natural fluctuations of groundwater level.

ACKNOWLEDGMENTS

This study was conducted at the Ralph M. Parsons Laboratory for Water Resources and Hydrodynamics at the Massachusetts Institute of Technology and was sponsored by the Office of Water Research and Technology, United States Department of the Interior under Grant No. 14-31-0001-9022 (Project C-4119), administered by the M.I.T. Office of Sponsored Programs under Project No. 80571.

The research was supervised by Dr. Lynn W. Gelhar, Associate Professor of Civil Engineering and Principal Investigator, and during the second year of the project Mr. John L. Wilson, Instructor, was responsible for coordination of the work. Dr. Ignacio Rodriguez-Iturbe provided advice on certain aspects of the spectral analysis. Messrs. Peter Ko and Herman Kwai served as research assistants on the project while doing graduate work in the Department of Civil Engineering. Portions of this report are essentially reproductions of their S.M. theses.

Mr. Jesse M. McNellis, U.S. Geological Survey in Lawrence, Kansas, provided the data which was used in the field application. Mr. Thomas Prickett, Illinois State Water Survey, Urbana, provided the computer program which was used in the numerical simulations.

TABLE OF CONTENTS

Chapter 1 INTRODUCTION

Hydrologic phenomena are generally recognized as being affected by complex natural events, the details of which cannot be anticipated precisely. Hence, the analysis of hydrologic systems is often viewed in terms of stochastic processes. However, the analysis of groundwater flow has traditionally been based on a deterministic approach to the solution of the governing partial differential equations. Natural variability, such as temporal fluctuations in groundwater recharge or water level in adjacent bodies of water and spatial variations in recharge and hydraulic conductivity, is usually dealt with only in terms of average conditions. Yet natural variability may be an important feature of groundwater flow in that it may be possible to infer aquifer properties from water table fluctuations. Also of interest are problems of aquifer management from a probabilistic point of view. In the following report, natural temporal variability in a phreatic aquifer is treated using a stationary random description rather than a deterministic approach; and the various influences of vertical flow, spatial variability, and storage of water in the unsaturated zone are investigated.

Although there has been little previous work relating to the analytical modeling of groundwater systems in a stochastic sense, there are several related studies. The interpretation of groundwater level fluctuation in order to evaluate aquifer properties has been the subject of several investigations. Jacob (1943) used a weighted average technique to relate precipitation to groundwater recharge, and thus to groundwater

level fluctuation. Tison (1965), in a review article, described a linear reservoir aquifer model with an accretion input in the form of a sine series. He found that the reservoir outflow is a function of the accretion fluctuation and is related to the aquifer area and porosity. In an adjoining discussion Tison (1965) described a linearized Dupuit equation aquifer model which was subject to a sinusoidal stream stage boundary condition. He found that the water level fluctuation (waves) created by the boundary disturbance propagates into the aquifer with decreasing amplitude, with short waves disappearing in a shorter distance. He also found that the lag time of the fluctuations increased with distance away from the stream. Pinder, et al. (1969) used a numerical model to evaluate aquifer parameters from stream stage fluctuations. In all three cases the groundwater system and inputs were treated as being deterministic rather than stochastic.

One of the simplest models that can be used to represent a phreatic aquifer is the lumped parameter linear reservoir system. Linear reservoir models of groundwater systems have been used by Kraijenhoff van de Leur (1958), Dooge (1960), van Schilfgaarde (1965) and Eriksson (1970a) to examine aquifer outflow and mean aquifer water level.

The classical Dupuit approximation provides a more realistic distributed parameter aquifer model. Deterministic solutions for this model are typically found through linearization of the equation (Cooper and Rorabaugh, 1963; Glover, 1967; Venetis, 1971; Hall and Moench, 1972), although Brooks (1961) and Singh (1969) have developed analytical solutions for specific nonlinear problems. Several numerical solutions of

the nonlinear Dupuit equation are available (Singh, 1969; Hornberger, et al., 1970).

In some situations the spatial variability of aquifer properties may have an important influence on the response of the aquifer to various inputs. Although not previously examined in the stochastic sense for groundwater, Buyevich, et al. (1969) have analyzed the related problem of flow through a porous medium with a randomly varying porosity.

Spectral analysis has been used by Eriksson (1970a,b) and Jackson, et al. (1973) for qualitative interpretations of time series of groundwater level,precipitation,and temperature.

Objectives and Scope

The general goal of the study was the development of analysis techniques which can be used to describe groundwater flow phenomena which are of a stochastic nature. More specifically, the immediate goal was to develop and apply spectral analysis techniques to the evaluation of groundwater systems, thus making use of the extensive data on water level fluctuations in aquifers. The following specific objectives were established:

(i) to develop linear analytical models for the spectral response of phreatic aquifers, including the effects of different aquifer configurations;

(ii) to evaluate the effects of nonlinearity in terms of spectral response;

(iii) to apply the theoretical spectral results to estimate aquifer parameters under field conditions;

(iv) to estimate the spectral effects of other factors such as spatial variability of hydraulic conductivity and unsaturated flow.

The theoretical analysis of the linear aquifer models was based on the representation of random functions in terms of Fourier-Stieltjes integrals. Solutions of the governing partial differential equation produced input-output spectral relationships for various aquifer configurations. The effects of aquifer slope, flow zone thickening, and vertical flow were included explicitly and the influence of the unsaturated flow zone was estimated. Some effects of the spatial variability of hydraulic conductivity were evaluated using spectral analysis in the wave number domain.

Nonlinear effects were determined from numerical simulation of the nonlinear aquifer equations in finite difference form. Spectral analysis of the nonlinear simulations was used to evaluate the nonlinear effects in the spectral domain.

Applications of the linear theory were illustrated through spectral analysis of field data on water level, precipitation and stream stage for a site in Kansas. Aquifer parameters were determined by comparing theoretical transfer functions with those determined from the field data.

Chapter 2 LINEAR THEORY OF AQUIFER SPECTRAL RESPONSE

2.1 Spectral Description in Time Series Analysis

Stationary Random Processes. A random process X(t) is said to be strictly stationary if its statistics are not affected by a shift in the time origin. In particular, the probability density function of X(t) is independent of time. That is to say that the two processes

$$X(t) \quad \text{and} \quad X(t+\tau)$$

have the same statistics for any τ. But it is very doubtful if this kind of process ever exists in nature. Since most of the methods used in time series analysis are based upon the first and second moments, i.e., means and variances, it may be more sensible to define a less restrictive type of stationary process.

A process is said to be stationary in the wide sense if its expected value is a constant and its autocorrelation depends only on τ. In terms of the probability density function, p(X),

$$m_X = E[X(t)] = \int_{-\infty}^{\infty} X\, p(X)\, dX \tag{2.1.1}$$

$$\mu_X(\tau) = E[X(t)X(t+\tau)] = \int_{-\infty}^{\infty} X(t)X(t+\tau)\, p(X)\, dX \tag{2.1.2}$$

for all t and τ.

$\mu_X(\tau)$ is the autocovariance function which is only a function of τ,

not of t. The quantity $\mu_X(0)$ is known as the variance.

Spectral Analysis. All stationary processes can be represented in the complex form as

$$X(t) = \int_{-\infty}^{\infty} e^{i\omega t}\, dZ(\omega) \qquad (2.1.3)$$

which is known as Cramer representation of a stationary process or stochastic Fourier-Stieltjes integral, with the autocovariances in the form (Granger and Hatanaka, 1964, pp. 28-29)

$$\mu(\tau) = \int_{-\infty}^{\infty} e^{i\omega\tau}\, d\,\Phi(\omega) \qquad (2.1.4)$$

where $Z(\omega)$ is the complex amplitude of the Fourier modes of frequency ω. This process is also called a process of non-correlated increments because it has the following properties:

$$\begin{aligned} E[dZ(\omega_1)\, dZ^*(\omega_2)] &= 0 \qquad \omega_1 \neq \omega_2 \\ &= d\,\Phi(\omega) = S(\omega)\, d\omega \qquad \omega_1 = \omega_2 = \omega \end{aligned} \qquad (2.1.5)$$

with

$$\Phi(\omega) = \int_{-\infty}^{\omega} S(\omega')\, d\omega' \qquad (2.1.6)$$

where the asterisk denotes the complex conjugate. $\Phi(\omega)$ is known as the power spectral distribution and $S(\omega)$ as the power spectral density or,

spectrum. Using equation 2.1.5, 2.1.4 can be written as

$$\mu(\tau) = \int_{-\infty}^{\infty} e^{i\omega\tau} \; S(\omega) \; d\omega \qquad (2.1.7)$$

Then $S(\omega)$ can be found by taking the Fourier transform of $\mu(\tau)$, the covariance function. Hence

$$S(\omega) = \frac{1}{2\pi} \int_{-\infty}^{\infty} e^{-i\omega\tau} \mu(\tau) \; d\tau \qquad (2.1.8)$$

For a real, discrete, stationary process,

$$S(\omega) = \frac{1}{2\pi} [\mu_o + 2 \sum_{j=1}^{\infty} \mu(j)\cos(j\omega)] \qquad (2.1.9)$$

Usually, for a limited amount of data, $\{X_t, t=1,2,\cdots,n\}$, $\mu(j)$ is estimated by $\hat{R}(\tau)$, where

$$\hat{R}(\tau) = \frac{1}{n-\tau} \sum_{t=1}^{n-\tau} (X_t - \bar{X})(X_{t+\tau} - \bar{X}) \qquad (2.1.10)$$

with

$$\bar{X} = \frac{1}{n} \sum_{t=1}^{n} X_t \qquad (2.1.11)$$

Therefore the estimator, $\hat{S}(\omega)$, of the power spectral density is given as

$$\hat{S}(\omega) = \frac{1}{2\pi} [\hat{R}(0) + 2 \sum_{j=1}^{n} \hat{R}(j) \cos(j\omega)] \qquad (2.1.12)$$

Since this estimate, $\hat{S}(\omega)$, is related to the periodogram, and

Hannan (1960) has shown that the periodogram does not give a consistent estimate of $S(\omega)$ and it is not at all smooth, it is customary to smooth this estimate by a set of weighting factors which is usually called a "spectral window". Among the most commonly used windows are Rectangular, Bartlett, Tukey and Parzen (see for example p. 244 of Jenkins and Watts, 1968). The narrower the base width of the lag window, the less biased is the smoothed spectrum of $\hat{S}(\omega)$; however, a narrow spectral window gives a larger variance. So it is necessary to compromise between the variance and the bias of the estimator when selecting the spectral window.

Cross-spectral Analysis. In direct analogy to the univariate case, a bivariate random process $\{X(t), Y(t)\}$ is said to be stationary, in the wide sense, if the first and second moment of this process are independent of time. Hence,

$$m_X = E[X(t)] = \int_{-\infty}^{\infty} X\, p(X)\, dX \qquad (2.1.13) \text{ cont.}$$

$$m_Y = E[Y(t)] = \int_{-\infty}^{\infty} Y\, p(Y)\, dY$$

$$\mu_X(\tau) = E[X(t)X(t+\tau)] = \int_{-\infty}^{\infty} X_k(t)X_k(t+\tau)\ p(X)\ dX$$

$$\mu_Y(\tau) = E[Y(t)Y(t+\tau)] = \int_{-\infty}^{\infty} Y_k(t)Y_k(t+\tau)\ p(Y)\ dY$$

$$\mu_{XY}(\tau) = E[X(t)Y(t+\tau)] = \int\int_{-\infty}^{\infty} X(t)Y(t+\tau)\ p(X,Y)\ dX\ dY$$

with $\mu_{XY}(\tau)$ is the cross-covariance function of the bivariate process $\{X(t),Y(t)\}$. Using the stochastic Fourier-Stieltjes integral, the series $\{X(t)\}$ and $\{Y(t)\}$ can be represented in the form of

$$X(t) = \int_{-\infty}^{\infty} e^{i\omega t}\ dZ_X(\omega) \qquad (2.1.14)$$

$$Y(t) = \int_{-\infty}^{\infty} e^{i\omega t}\ dZ_Y(\omega) \qquad (2.1.15)$$

and their covariance functions as

$$\mu_X(\tau) = \int_{-\infty}^{\infty} e^{i\omega\tau}\ S_{XX}(\omega)\ d\omega \qquad (2.1.16)$$

$$\mu_Y(\tau) = \int_{-\infty}^{\infty} e^{i\omega\tau}\ S_{YY}(\omega)\ d\omega \qquad (2.1.17)$$

$$\mu_{XY}(\tau) = \int_{-\infty}^{\infty} e^{i\omega\tau} S_{XY}(\omega)\, d\omega \qquad (2.1.18)$$

with

$$E[dZ_X(\omega_1)\, dZ_X^*(\omega_2)] = \begin{cases} 0 & \omega_1 \neq \omega_2 \\ S_{XX}(\omega)\, d\omega & \omega_1 = \omega_2 \end{cases} \qquad (2.1.19)$$

$$E[dZ_Y(\omega_1)\, dZ_Y^*(\omega_2)] = \begin{cases} 0 & \omega_1 \neq \omega_2 \\ S_{YY}(\omega)\, d\omega & \omega_1 = \omega_2 \end{cases} \qquad (2.1.20)$$

$$E[dZ_X(\omega_1)\, dZ_Y^*(\omega_2)] = \begin{cases} 0 & \omega_1 \neq \omega_2 \\ S_{XY}(\omega)\, d\omega & \omega_1 = \omega_2 \end{cases} \qquad (2.1.21)$$

Again, μ_X, S_{XX}, μ_Y and S_{YY} are the auto-covariance functions and the power spectra of the series $\{X(t)\}$ and $\{Y(t)\}$ respectively. μ_{XY} is the cross-covariance function and

$$S_{XY}(\omega) = Co(\omega) + i\, Q(\omega) \qquad (2.1.22)$$

is known as the cross-spectrum between the series $\{X(t)\}$ and $\{Y(t)\}$; $Co(\omega)$ is called the co-spectrum and $Q(\omega)$ is the quadrature spectrum. From equation 2.1.18, it can be shown that the cross-spectrum can be obtained by taking the Fourier transform of μ_{XY}. Hence,

$$S_{XY} = \frac{1}{2\pi} \int_{-\infty}^{\infty} e^{-i\omega t} \mu_{XY}(t)\, dt \qquad (2.1.23)$$

Again with a limited amount of data, $S_{XX}(\omega)$, $S_{YY}(\omega)$ and $S_{XY}(\omega)$ are estimated by $\hat{S}_{XX}(\omega)$, $\hat{S}_{YY}(\omega)$ and $\hat{S}_{XY}(\omega)$ respectively.

Coherence, Phase and Gain Factor. In direct analogy to the square of the correlation coefficient in classical statistical analysis, the coherence function $\gamma^2_{XY}(\omega)$, is a measure of the correlation between the frequency components of the two processes and is given by

$$\gamma^2_{XY}(\omega) = \frac{|S_{XY}(\omega)|^2}{S_{XX}(\omega)S_{YY}(\omega)} = \frac{Co^2(\omega) + Q^2(\omega)}{S_{XX}(\omega)\ S_{YY}(\omega)} \qquad (2.1.24)$$

The corresponding phase difference is given by

$$\theta_{XY}(\omega) = \tan^{-1}\frac{Q(\omega)}{Co(\omega)} \qquad (2.1.25)$$

and is sometimes known as the phase spectrum of the processes $\{X(t)\}$ and $\{Y(t)\}$. The phase spectrum shows the time lag, positive or negative, between the frequency components of the two processes.

The gain factor, sometimes known as the amplitude of the transfer function, is defined as

$$|G(\omega)| = \frac{|S_{XY}(\omega)|}{S_{XX}(\omega)} = \frac{\sqrt{Co^2(\omega) + Q^2(\omega)}}{S_{XX}(\omega)} \qquad (2.1.26)$$

which measures the amplitude magnification at different frequency components. For more detailed discussions on spectral analysis, readers are referred to any text on time series analysis, e.g. Jenkins and Watts (1968).

2.2 Linear Reservoir Model

One of the simplest models that can be used to represent a phreatic aquifer is the lumped-parameter linear reservoir system as shown schematically in Figure 2.1. In this model we neglect all spatial variation of water level and consider the average thickness of the saturated zone, h(t), to be solely a function of time. It is also assumed that the outflow per unit area can be represented by

$$q = a(h-H) \tag{2.2.1}$$

where a is an outflow constant and H is the elevation of the water surface in some adjacent body of water. A water balance can then be stated as

$$S \frac{dh}{dt} + a(h-H) = \varepsilon \tag{2.2.2}$$

where ε is the accretion or recharge rate and S is the average storage coefficient. Under the assumptions that S and a are constants and h, H and ε are stationary in time, taking the expected value of equation 2.2.2, we have, for the mean values,

$$a(\overline{h}-\overline{H}) = \overline{\varepsilon} \tag{2.2.3}$$

Thus it follows that the fluctuation about the mean also satisfies equation 2.2.2, namely

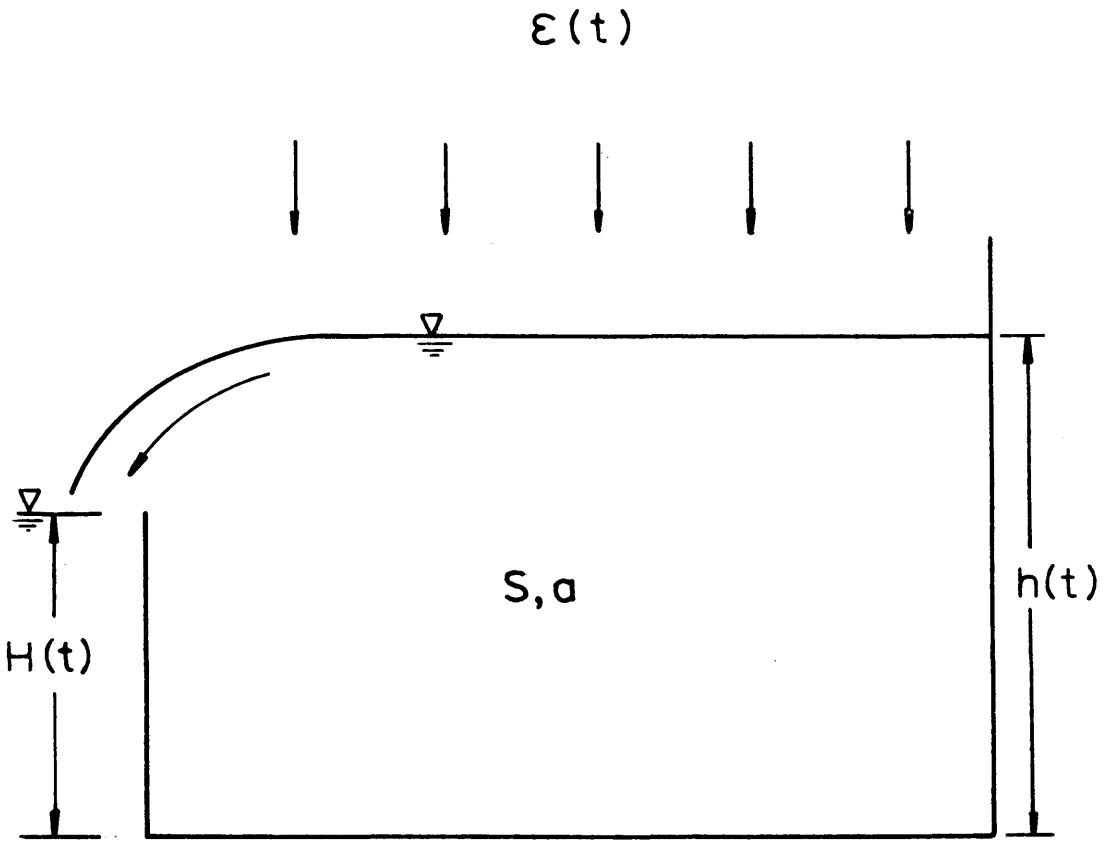

Figure 2.1 Schematic Representation of Linear Reservoir System.

$$S \frac{dh'}{dt} + a(h'-H') = \varepsilon' \qquad (2.2.4)$$

Then h', H' and ε' are stationary random processes with zero mean. Dropping the primes and using equation 2.1.3, we have

$$h(t) = \int_{-\infty}^{\infty} e^{i\omega t} \, dZ_h(\omega) \qquad (2.2.5)$$

$$H(t) = \int_{-\infty}^{\infty} e^{i\omega t} \, dZ_H(\omega) \qquad (2.2.6)$$

$$\varepsilon(t) = \int_{-\infty}^{\infty} e^{i\omega t} \, dZ_\varepsilon(\omega) \qquad (2.2.7)$$

Using equations 2.2.5, 2.2.6 and 2.2.7 in 2.2.4, the generalized Fourier amplitudes are given by

$$dZ_h(\omega) = \frac{a \, dZ_H(\omega) + dZ_\varepsilon(\omega)}{i\omega S + a} \qquad (2.2.8)$$

Using equations 2.1.19 - 21, the spectral density function becomes

$$S_{hh} = [a^2 S_{HH}(\omega) + a \, S_{H\varepsilon}(\omega) + a \, S_{\varepsilon H}(\omega) + S_{\varepsilon\varepsilon}(\omega)] / (\omega^2 S^2 + a^2) \qquad (2.2.9)$$

Similarly, the input-output cross spectra can be obtained from equation 2.2.8 to be

$$S_{\varepsilon h}(\omega) = [(a\ S_{\varepsilon H}(\omega)+S_{\varepsilon\varepsilon}(\omega))(a+i\omega S)]/(a^2+\omega^2S^2) \qquad (2.2.10)$$

$$S_{Hh}(\omega) = [(a\ S_{HH}(\omega)+S_{H\varepsilon}(\omega))(a+i\omega S)]/(a^2+\omega^2S^2) \qquad (2.2.11)$$

when only a single input is considered (e.g., H = 0 or ε = 0),say ε = 0, equation 2.2.11 reduces to

$$S_{Hh}(\omega) = \frac{a(a+i\omega S)}{(a^2+\omega^2S^2)} S_{HH} \qquad (2.2.12)$$

From equation 2.1.26, we can see that the factor

$$\left|\frac{a(a+i\omega S)}{a^2 + \omega^2S^2}\right|$$

is known as the gain factor or the transfer function from H to h. This quantity can be used in applying spectral analysis to infer values of the aquifer parameters, in this case a and S, for a groundwater system. It is of interest to compare the results of this simple lumped-parameter analysis with those for more realistically distributed systems in the following sections.

2.3 Linearized Dupuit Aquifer Analysis

Dupuit Approximation. The Dupuit approximation is probably the most powerful tool in treating unconfined flows through porous media. It requires the assumptions that the equipotential lines (in two dimensional cases) are essentially vertical and the flow essentially horizontal.

[See, e.g., Bear, 1972]. Thus, for the general case with fully penetrating stream and finite length, L, as shown in Figure 2.2, the classical Dupuit approximation leads to the following governing equation:

$$S \frac{\partial h}{\partial t} = \frac{\partial}{\partial x} [Kh \frac{\partial (h+\zeta)}{\partial x}] + \varepsilon \qquad (2.3.1)$$

where $h(x,t)$ = the thickness of the saturated zone,

x = the horizontal coordinate,

$\zeta(x)$ = the position of the impervious bottom of the aquifer,

S = the storage coefficient,

K = the hydraulic conductivity

ε = the accretion, which is assumed to be uniform over x.

Equation 2.3.1 can also be written as

$$S \frac{\partial h}{\partial t} = \frac{\partial}{\partial x} Kh \frac{\partial h}{\partial x} + \frac{\partial}{\partial x} Kh \frac{\partial \zeta}{\partial x} + \varepsilon \qquad (2.3.2)$$

Assuming $Kh = T$, the transmissivity, and $\frac{\partial \zeta}{\partial x} = \beta$, the slope of the impervious bottom, to be constant, equation 2.3.2 can be linearized to

$$S \frac{\partial h}{\partial t} = T \frac{\partial^2 h}{\partial x^2} + \beta K \frac{\partial h}{\partial x} + \varepsilon \qquad (2.3.3)$$

with boundary conditions $x = 0$, $h = H$, and $x = L$, $\frac{\partial h}{\partial x} = 0$. For a stationary random process the mean part of equation 2.3.3 is given by

$$T \frac{\partial^2 \bar{h}}{\partial x^2} + \beta K \frac{\partial \bar{h}}{\partial x} + \bar{\varepsilon} = 0 \qquad (2.3.4)$$

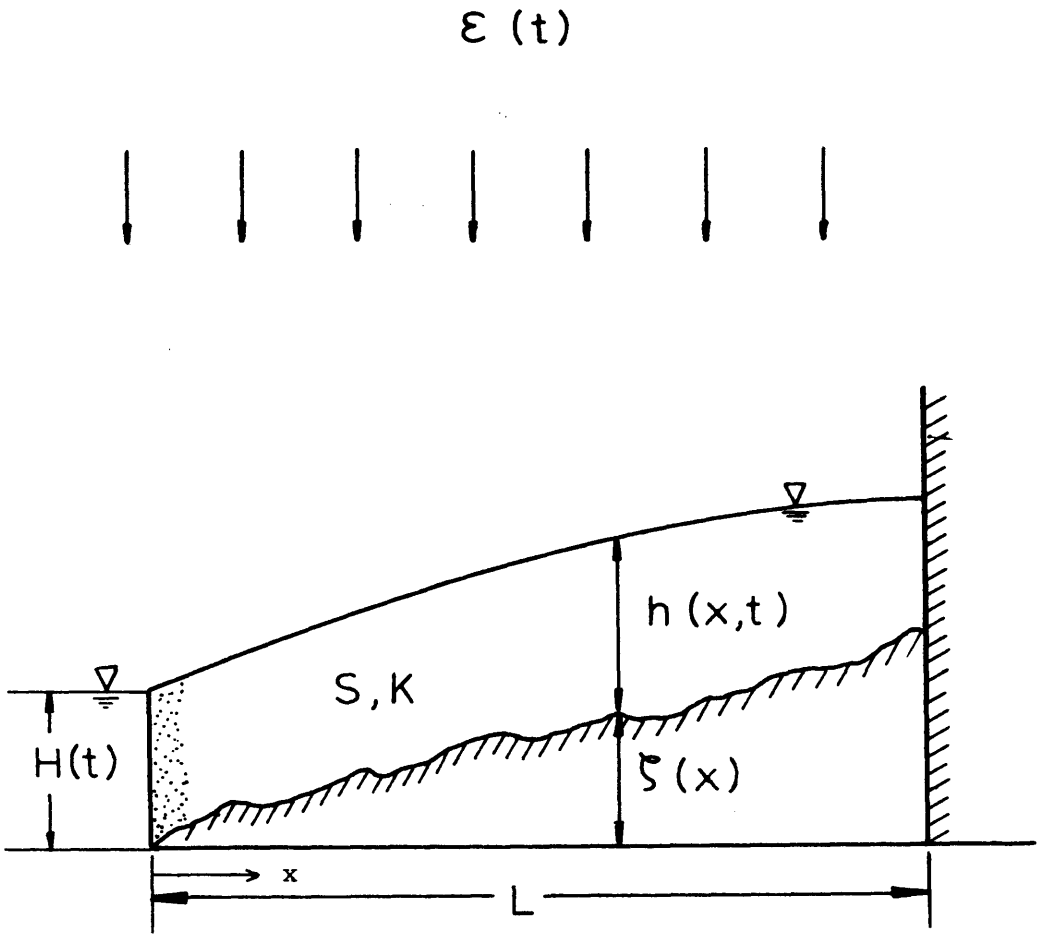

Figure 2.2 Phreatic Aquifer with Fully Penetrating Stream and Arbitrary Bottom.

By substituting

$$h = \bar{h} + h'$$

$$\varepsilon = \bar{\varepsilon} + \varepsilon'$$

$$H = \bar{H} + H'$$

where primed quantities represent the fluctuations about the mean, into equation 2.3.3 and subtracting the mean equation 2.3.4, the equation governing the fluctuations is given by

$$S \frac{\partial h'}{\partial t} = T \frac{\partial^2 h'}{\partial x^2} + \beta K \frac{\partial h'}{\partial x} + \varepsilon \qquad (2.3.5)$$

with the following boundary conditions:

$$x = 0 \qquad h' = H'$$

$$x = L \qquad \frac{\partial h'}{\partial x} = 0$$

Linearized Dupuit Analysis with constant bottom slope. Using the stochastic Fourier-Stieltjes integral, equation 2.1.3, we have

$$h' = \int_{-\infty}^{\infty} e^{i\omega t} \, dZ_h(\omega, x)$$

$$\varepsilon' = \int_{-\infty}^{\infty} e^{i\omega t} \, dZ_\varepsilon(\omega) \qquad (2.3.6)$$

$$H' = \int_{-\infty}^{\infty} e^{i\omega t} \, dZ_H(\omega)$$

Substituting equation 2.3.6 into equation 2,3.5, we have

$$T \frac{d^2}{dx^2}[dZ_h(\omega,x)] + \beta K \frac{d}{dx}[dZ_h(\omega,x)] - i\omega S\, dZ_h + dZ_\varepsilon = 0 \qquad (2.3.7)$$

with boundary conditions

$$x = 0 \qquad h' = H'(t) \qquad dZ_h(\omega,0) = dZ_H(\omega)$$

$$x = L \qquad \frac{\partial h'}{\partial x} = 0 \qquad \frac{d}{dx}[dZ_h(\omega,x)] = 0$$

The solution to equation 2.3.7 is

$$dZ_h(\omega,x) = F(\omega,x)\, dZ_H(\omega) - [1-F(\omega,x)] \frac{i dZ_\varepsilon(\omega)}{\omega S} \qquad (2.3.8)$$

where $$F(\omega,x) = \frac{\alpha_1 e^{\alpha_1 L} e^{\alpha_2 x} - \alpha_2 e^{\alpha_2 L} e^{\alpha_1 x}}{\alpha_1 e^{\alpha_1 L} - \alpha_2 e^{\alpha_2 L}}$$

and $$\alpha_1 = -\frac{\beta K}{2T} + \sqrt{\left(\frac{\beta K}{2T}\right)^2 + \frac{i\omega S}{T}}$$

$$\alpha_2 = -\frac{\beta K}{2T} - \sqrt{\left(\frac{\beta K}{2T}\right)^2 + \frac{i\omega S}{T}}$$

Thus, using equations 2.1.4, 2.1.5 and 2.1.6, we have the following relationship between the spectral density functions

$$S_{hh} = (1-F-F^*+FF^*)\frac{S_{\varepsilon\varepsilon}}{\omega^2 S^2} - \frac{i}{\omega S}[(1-F)F^* S_{\varepsilon H} - (1-F^*)F S_{H\varepsilon}] + FF^* S_{HH} \qquad (2.3.9)$$

For the particular case, $\beta = 0$, i.e., with horizontal bottom,

$$\alpha_1 = -\alpha_2 = (1+i)\left(\frac{|\omega|S}{2T}\right)^{1/2} = b$$

and

$$F = \frac{\cosh[b(x-L)]}{\cosh bL} = \frac{\cosh[bL(\frac{x}{L}-1)]}{\cosh bL}$$

Equation 2.3.9 can be shown reducible to equation 18 as given by Gelhar (1974).

It is of interest to see how the bottom slope of the aquifer will affect the spectral relationship given by equation 2.3.9 along the aquifer. It can be shown that $F(\omega,x)$ as given in equation 2.3.8, can be written as

$$F(\omega,x) = \frac{e^{-\tau L\frac{x}{L}}\left[\xi L\cosh\xi L(1-\frac{x}{L}) - \tau L\sinh\xi L(1-\frac{x}{L})\right]}{\xi L\cosh\xi L - \tau L\sinh\xi L} \qquad (2.3.10)$$

with $\Gamma = \tau L = \frac{\beta KL}{2T}$

$$\xi L = \sqrt{(\tau L)^2 + \frac{i\omega L^2}{\alpha}} \quad \text{and} \quad \alpha = \frac{T}{S}$$

Some of the curves are shown in Figures 2.3 to 2.8 for different values of Γ at different locations along the aquifer. From equation 2.3.9, it is seen that the function $f \equiv FF^* = S_{hh}/S_{HH}$ when $\varepsilon = 0$ and thus characterizes the spectral response of the aquifer to stream stage fluctuations.

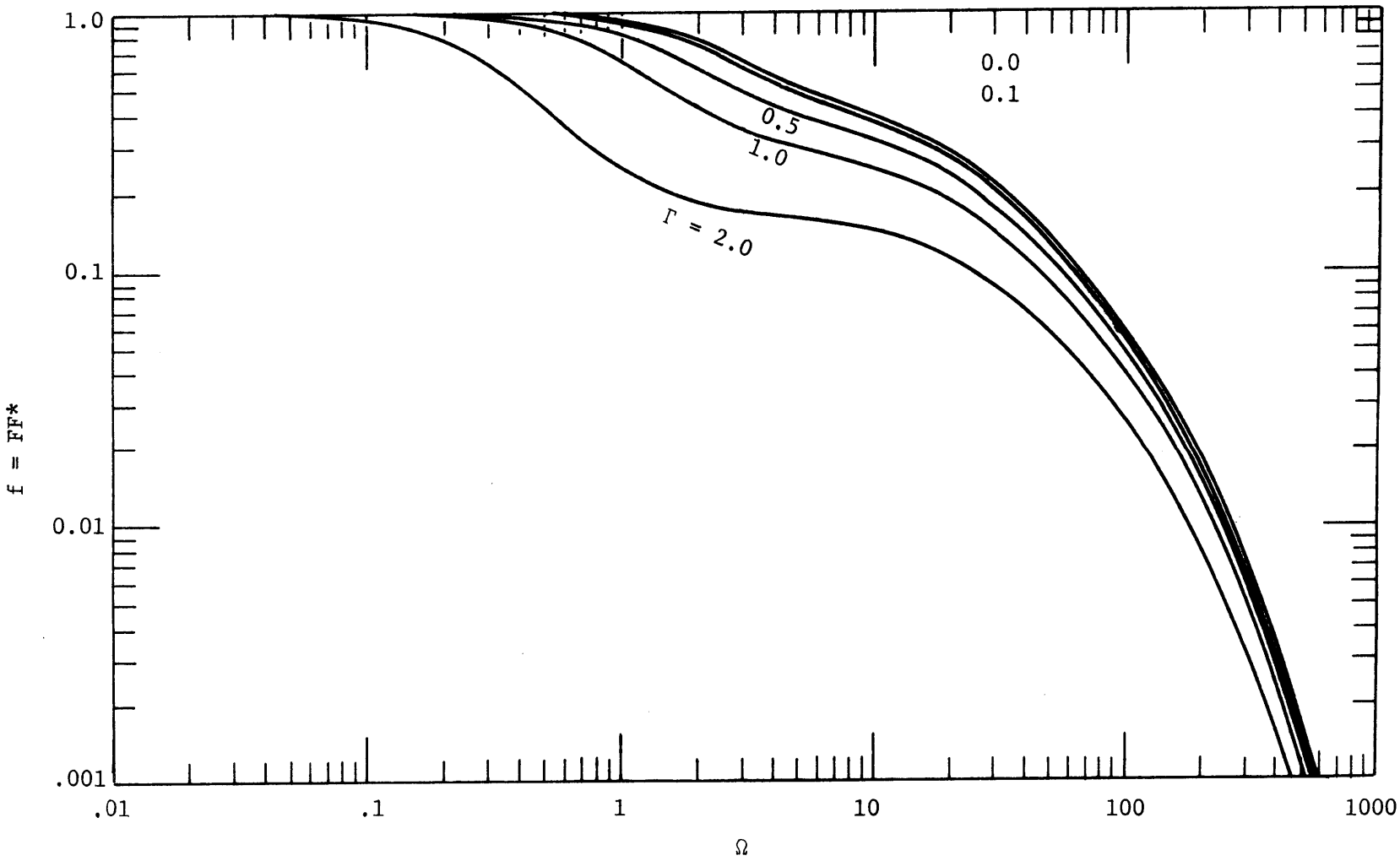

Figure 2.3 Aquifer Response to Stream Stage Fluctuations; Plot of f at x/L=0.2 with Different Values of Γ.

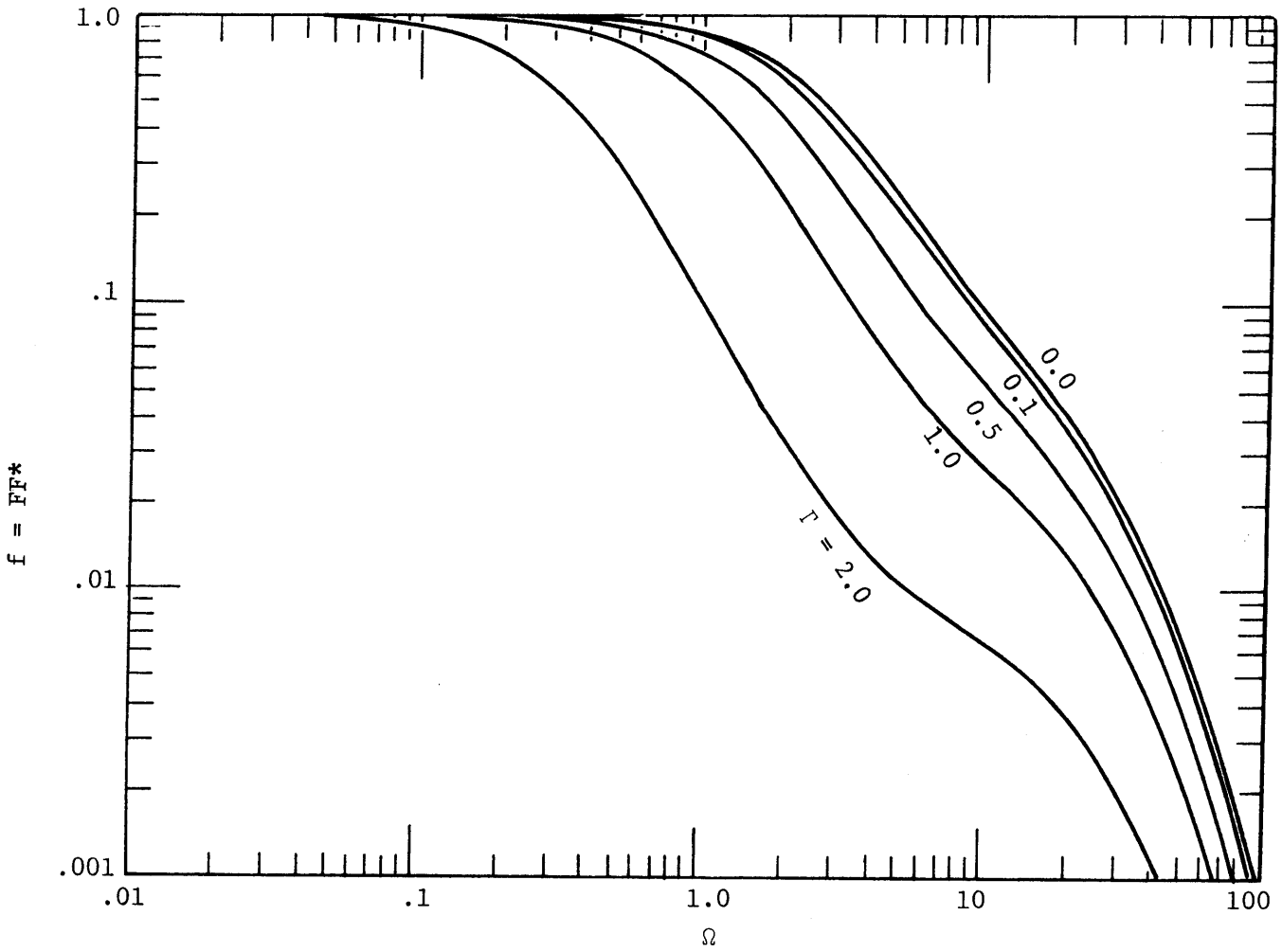

Figure 2.4 Aquifer Response to Stream Stage Fluctuations; Plot of f at x/L=.5 with Different Values of Γ.

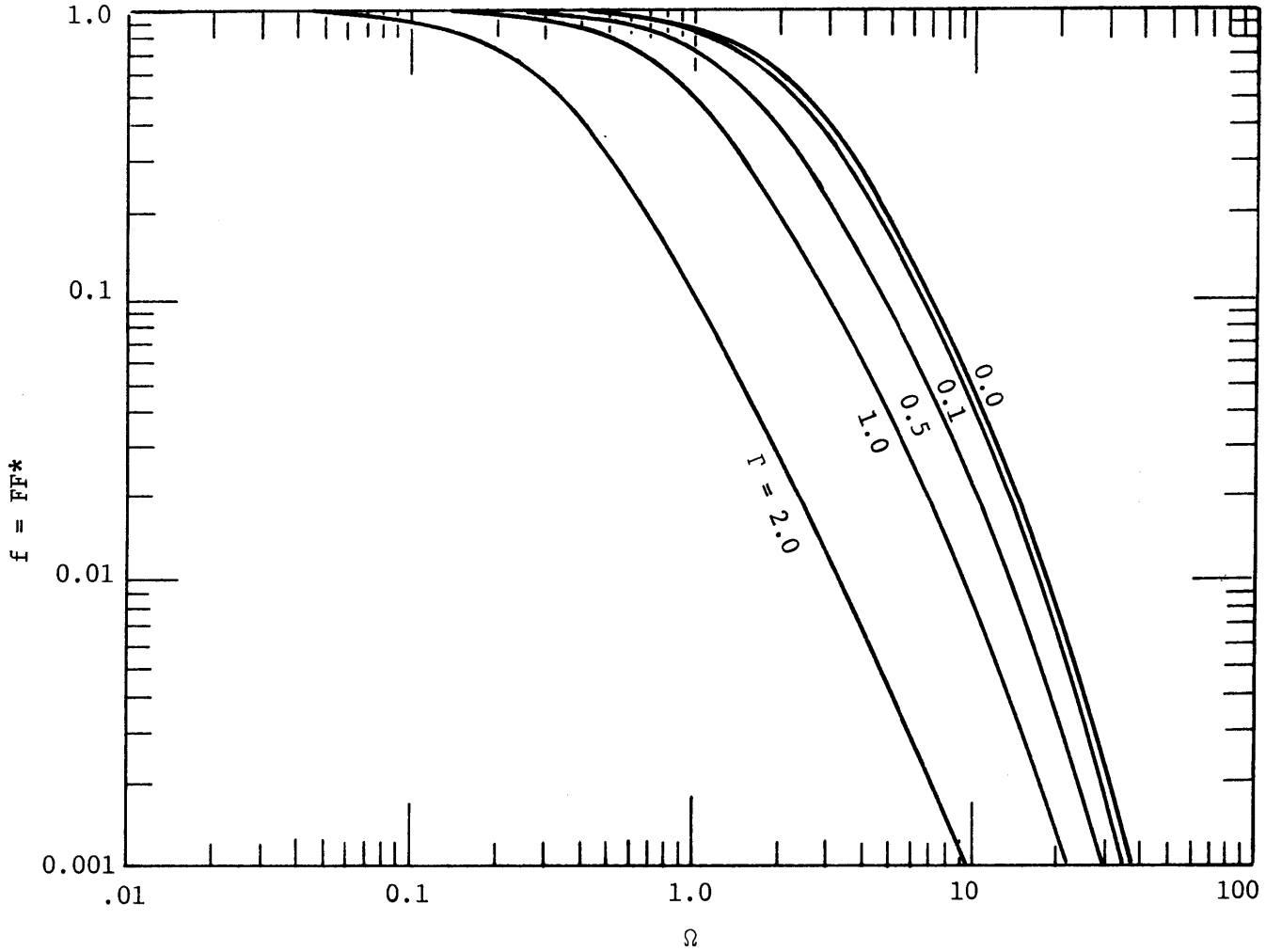

Figure 2.5 Aquifer Response to Stream Stage Fluctuations; Plot of f at x/L=.8 with Different Values of Γ.

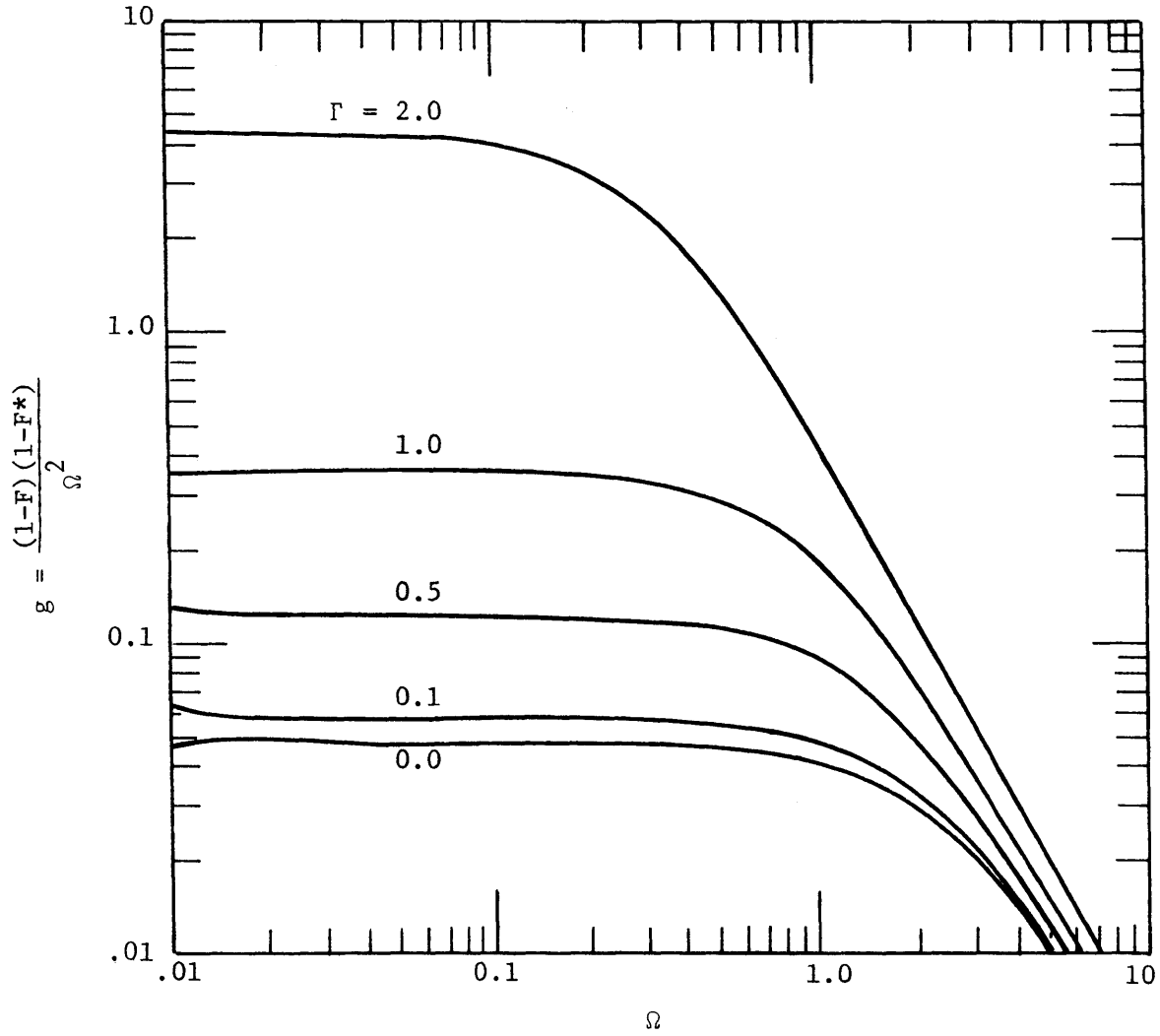

Figure 2.6 Aquifer Response to Accretion; Plot of g at x/L=.25 with Different Values of Γ.

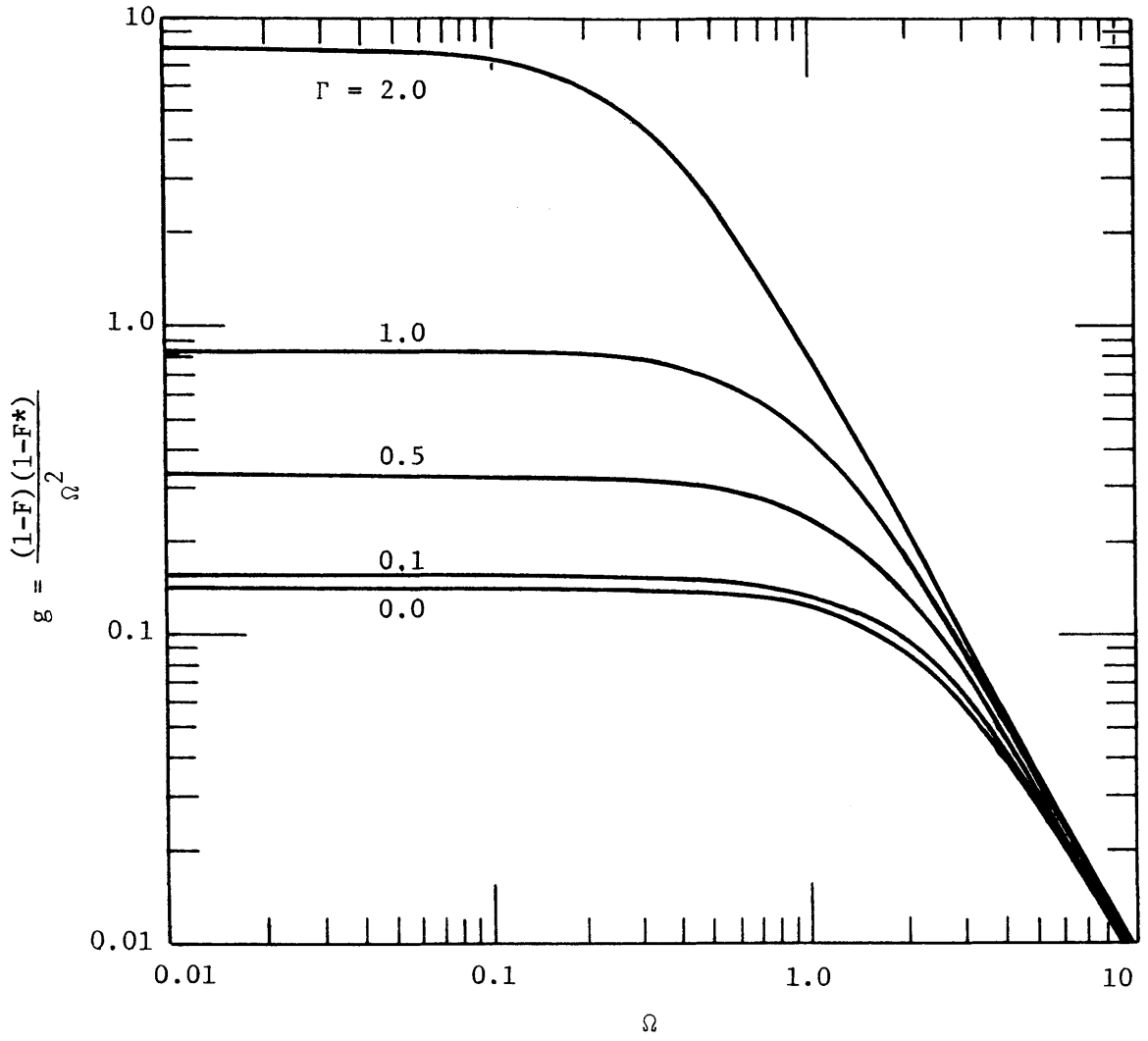

Figure 2.7 Aquifer Response to Accretion; Plot of g at x/L=.5 with Different Values of Γ.

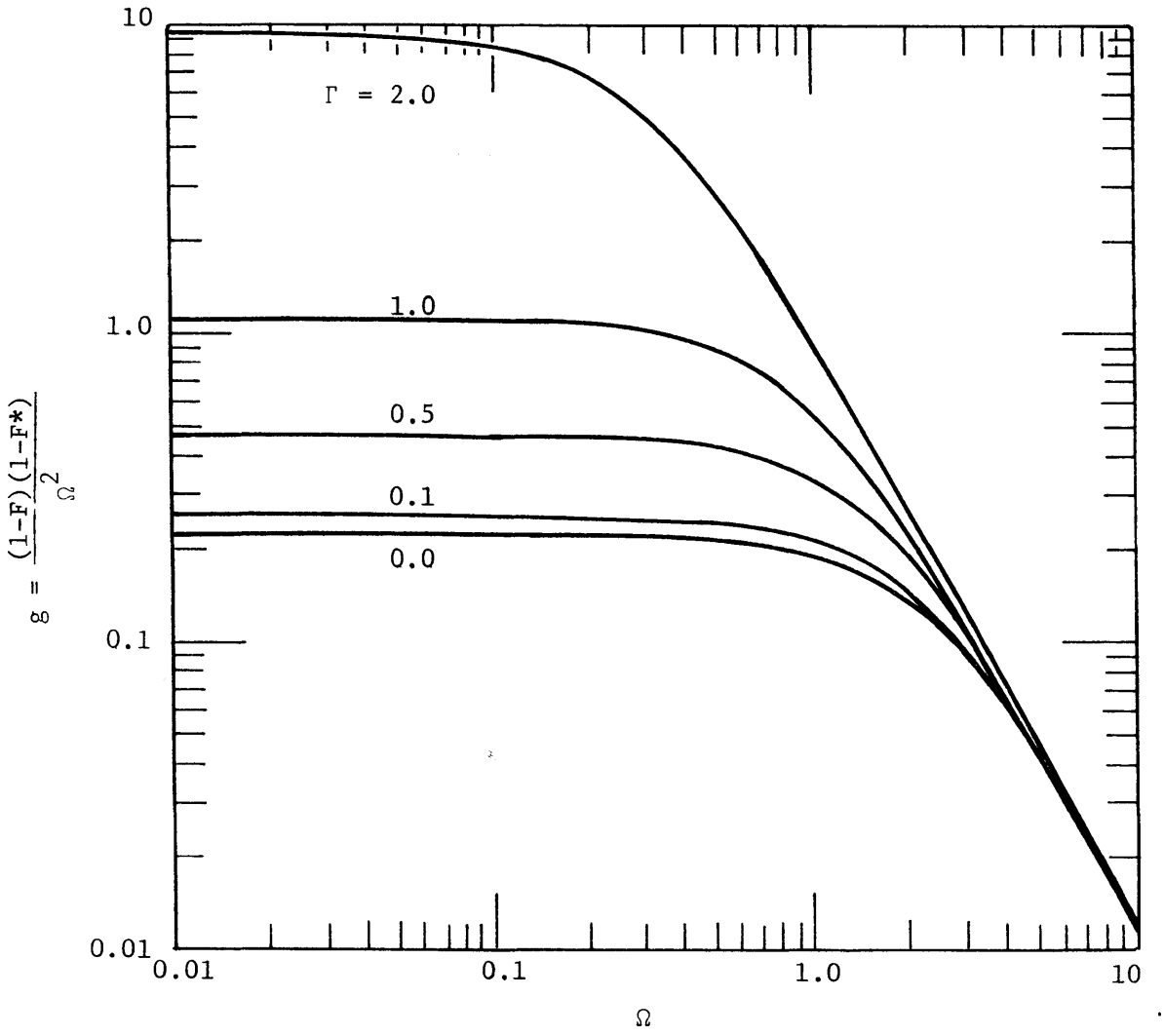

Figure 2.8 Aquifer Response to Accretion; Plot of g at x/L=.75 with Different Values of Γ.

Similarly, $g \equiv (1-F)(1-F^*)/\Omega^2 = T^2 S_{hh}/S_{\varepsilon\varepsilon} L^4)$, when $H = 0$, characterizes the dimensionless spectral response to recharge fluctuations. The parameter $\Omega = \omega L^2/\alpha$ in equation 2.3.10 is the dimensionless frequency and L^2/α can be thought of as the scale of the frequency. It is easy to see that the general effect of the sloping bottom is to damp out the high frequencies as they propagate away from the stream. As can be seen from these curves, for $\Gamma < .1$, this effect is negligible. This parameter, Γ, characterizes the bottom slope. Putting $T = Kh_o$ and $\beta L = \zeta\big|_{x=L}$, we have

$$\Gamma = \frac{\beta KL}{2T} = \frac{\zeta\big|_{x=L}}{2h_o} \qquad (2.3.11)$$

where h_o is a spatial average of the flow zone thickness. Also from the steady state equation, we have

$$T \frac{d^2}{dx^2}(h+\beta x) = - \varepsilon \qquad (2.3.12)$$

with $\quad x = 0 \quad \frac{d}{dx}(h+\beta x) = 0$

$\quad x = L \quad h = \bar{H}$

for which the solution is

$$T(h+\beta x-\bar{H}) = x(L- \frac{x}{2}) \qquad (2.3.13)$$

If the change in the saturated thickness across the aquifer,

$$\frac{h(L) - h(0)}{\bar{H}} = \frac{\Delta h}{\bar{H}} = \frac{\varepsilon L^2}{2T\bar{H}} - \frac{\beta L}{\bar{H}} \qquad (2.3.14)$$

is small (say $\left|\frac{\Delta h}{\bar{H}}\right| < \frac{1}{3}$), the linearized theory for sloping bottom should be most appropriate because then T ≃ constant. The basis for this condition is developed in the section entitled "Zone Thickening Effect".

Interaction between Linear Reservoir and Dupuit Aquifer. Considering the case as shown in Figure 2.9, with a phreatic aquifer connected to a body of water or a linear reservoir, the governing equation for the aquifer, using the Dupuit approximation, is

$$S \frac{\partial h}{\partial t} = \frac{\partial}{\partial x} Kh \frac{\partial h}{\partial x} + \varepsilon \qquad (2.3.15)$$

which can be linearized, by setting Kh = T to be constant, to

$$S \frac{\partial h}{\partial t} = T \frac{\partial^2 h}{\partial x^2} + \varepsilon \qquad (2.3.16)$$

with boundary conditions

$$x = 0 \qquad h = H$$

$$x = L \qquad \frac{\partial h}{\partial x} = 0$$

For a linear reservoir, we have

$$\ell \frac{dH}{dt} + a\, \ell(H - h_o) = T \left.\frac{\partial h}{\partial x}\right|_{x=0} \qquad (2.3.17)$$

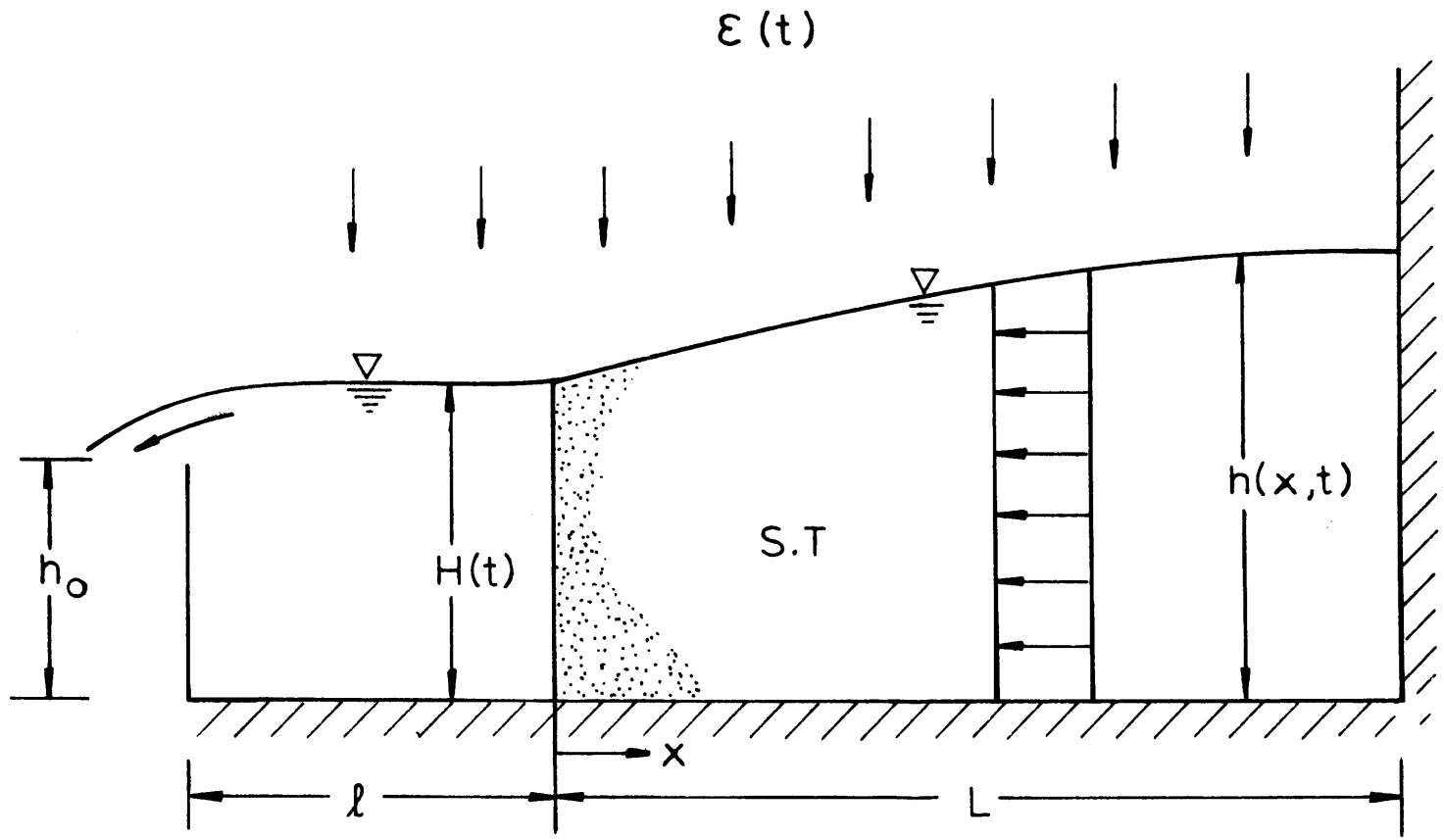

Figure 2.9 Schematic Representation of Dupuit Aquifer with Adjacent Linear Reservoir.

The term $T \left.\frac{\partial h}{\partial x}\right|_{x=0}$ is the net inflow of water to the reservoir from the phreatic aquifer. By substituting

$$h = \bar{h} + h'$$

$$H = \bar{H} + H'$$

$$\varepsilon = \bar{\varepsilon} + \varepsilon'$$

into equations 2.3.16 and 2.3.17 with the mean part removed, the equation for the fluctuations can be given as

$$\frac{dH'}{dt} + a\,H' = \frac{T}{\ell} \left.\frac{\partial h'}{\partial x}\right|_{x=0} \tag{2.3.18}$$

$$S \frac{\partial h'}{\partial t} = T \frac{\partial^2 h'}{\partial x^2} + \varepsilon' \tag{2.3.19}$$

with $x = 0 \quad h' = H'$

$x = L \quad \frac{\partial h'}{\partial x} = 0$

Substituting the stochastic Fourier-Stieltjes integral for h', ε' and H' as given in equation 2.3.6, into 2.3.18 and 2.3.19, we have

$$\frac{\ell(i\omega+a)}{T}\, dZ_H = \frac{\partial}{\partial x}\, dZ_h \Big|_{x=0} \tag{2.3.20}$$

$$i\omega dZ_h = \alpha \frac{\partial^2}{\partial x^2}\, dZ_h + \frac{dZ_\varepsilon}{S} \tag{2.3.21}$$

where $\alpha = \frac{T}{S}$

with boundary conditions

$$x = 0 \qquad dZ_h = dZ_H$$
$$x = L \qquad \frac{d}{dx} dZ_h = 0$$

Solving equations 2.3.20 and 2.3.21 simultaneously, we have, for solution, the following

$$dZ_h = (F-1)\frac{i}{\omega S} dZ_\varepsilon \tag{2.3.22}$$

with
$$F = \frac{\cosh[bL(\frac{x}{L} - 1)]}{\frac{Tb}{\ell(a+i\omega)} \sinh(bL) + \cosh(bL)}$$

and
$$b = (1+i)(\frac{\omega}{2\alpha})^{1/2}$$

Note that the term $\frac{Tb}{\ell(a+i\omega)}$ can be written as:

$$\frac{Tb}{\ell(a+i\omega)} = (bL)(\frac{SL}{\ell}) \frac{(\frac{aL^2}{\alpha}) - i(\frac{\omega L^2}{\alpha})}{(\frac{aL^2}{\alpha})^2 + (\frac{\omega L^2}{\alpha})^2} \tag{2.3.23}$$

Using equations2.1.5 and 2.1.6, we have

$$S_{hh}(\omega) = \frac{(F-1)(F^*-1)}{S^2\omega^2} S_{\varepsilon\varepsilon}(\omega) \tag{2.3.24}$$

In this coupled-system, we have two independent parameters besides the dimensionless frequency, $\Omega = \omega L^2/\alpha$, namely SL/ℓ and aL^2/α. The first one

represents the ratio of the volume in the two systems. While the second parameter can be thought of as the ratio between the response time of the two systems. However, it is not apparent how the combined effect of these two parameters may affect the spectral relationship. Some of the curves, using different combinations of these parameters, are shown in figures 2.10 - 2.14. Noting that F in equation 2.3.24 is also a function of x/L, it is also interesting to examine the ratio

$$\frac{[S_{hh}(\omega)/S_{\varepsilon\varepsilon}(\omega)]_{x/L=0}}{[S_{hh}(\omega)/S_{\varepsilon\varepsilon}(\omega)]} \qquad (2.3.25)$$

because of the fact that the resulting ratio $[S_{hh}(\omega)\big|_{x=0}/S_{hh}(\omega)]$ is a measure of the spectral response of the aquifer relative to that of a water body (a lake or reservoir). The ratio given in equation 2.3.25 is plotted against Ω, the dimensionless frequency in Figures 2.15 - 2.17.

Zone Thickening Effect. In the previous models, we have ignored the variation in transmissivity associated with the change in the thickness of the flow zone. In this section, this spatial variation has been kept in the analysis in terms of the mean flow condition. For simplicity, only the horizontal bottom has been considered. From equation 2.3.1, ignoring the bottom slope, the governing equation is

$$S \frac{\partial h}{\partial x} = \frac{\partial}{\partial x} Kh \frac{\partial h}{\partial x} + \varepsilon \qquad (2.3.26)$$

Putting $h(x) = \bar{h}(x) + h'(x)$ and $\varepsilon = \bar{\varepsilon} + \varepsilon'$, where $\bar{h}(x)$ and $\bar{\varepsilon}$ are the

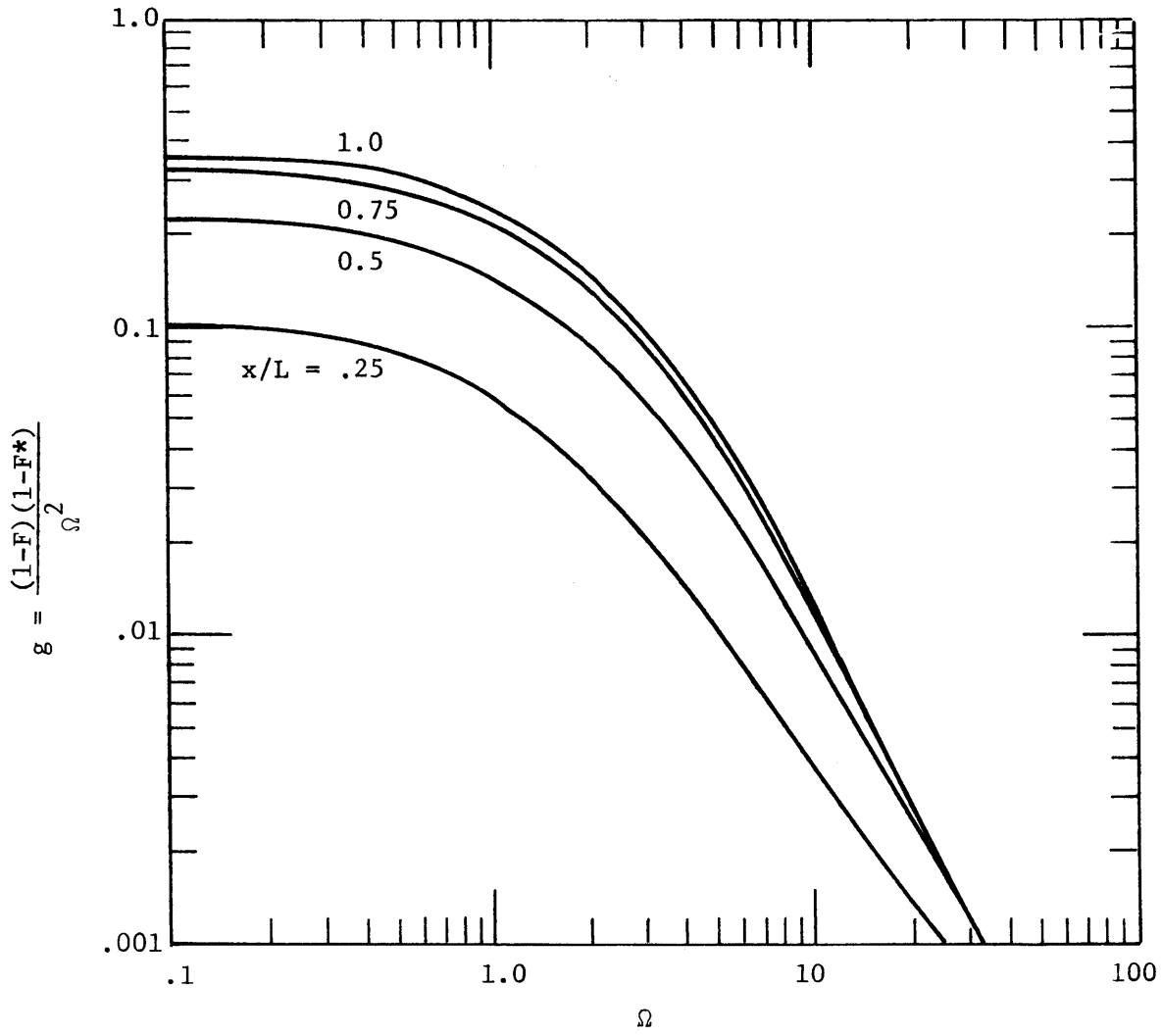

Figure 2.10 Response of the Aquifer-Reservoir System, Plot of g along the Aquifer with $aL^2/\alpha = 1.0$ and $SL/\ell = 0.1$.

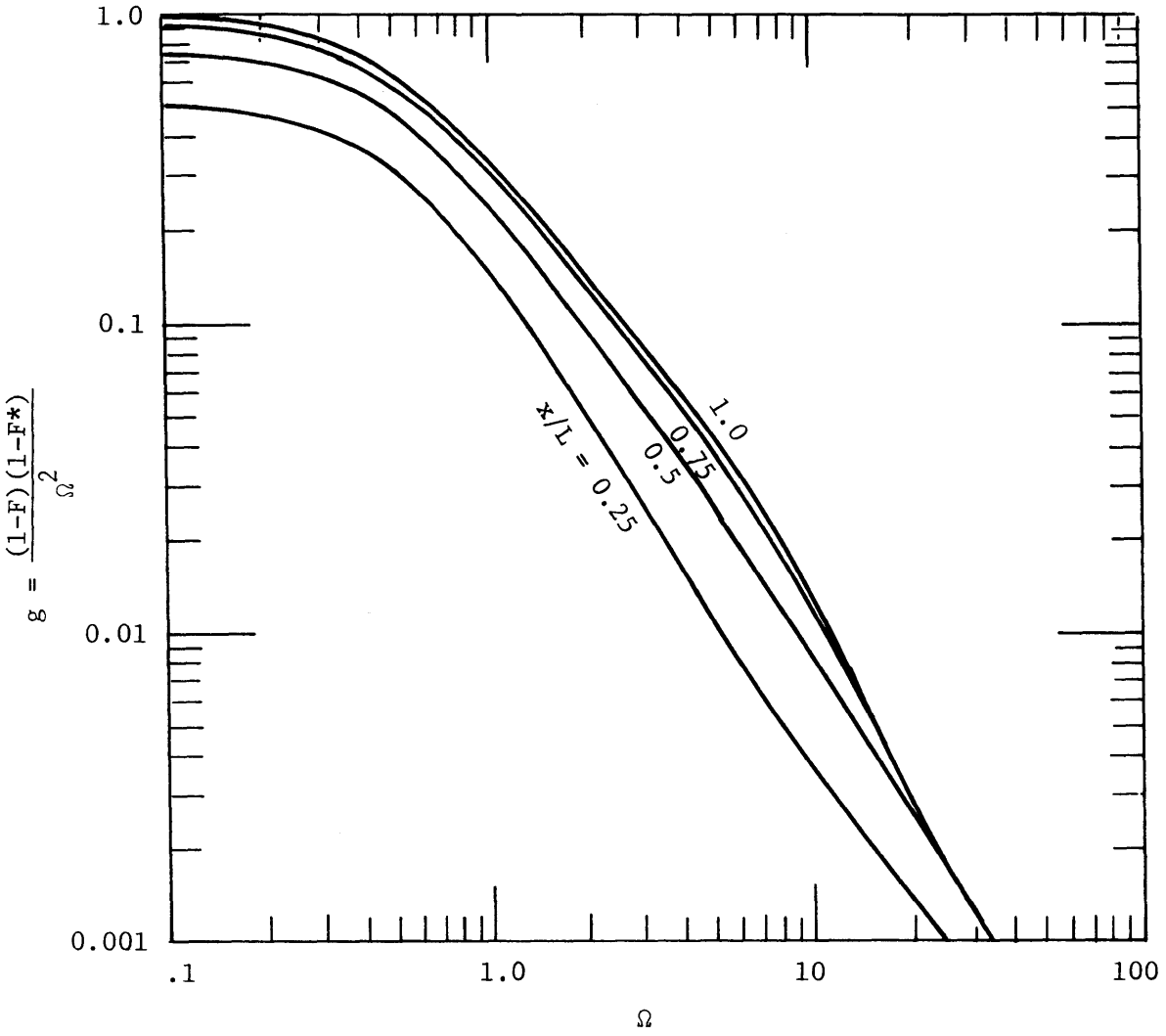

Figure 2.11 Response of the Aquifer-Reservoir System, Plot of g along the Aquifer with $aL^2/\alpha = 1.0$ and $SL/\ell = 0.5$.

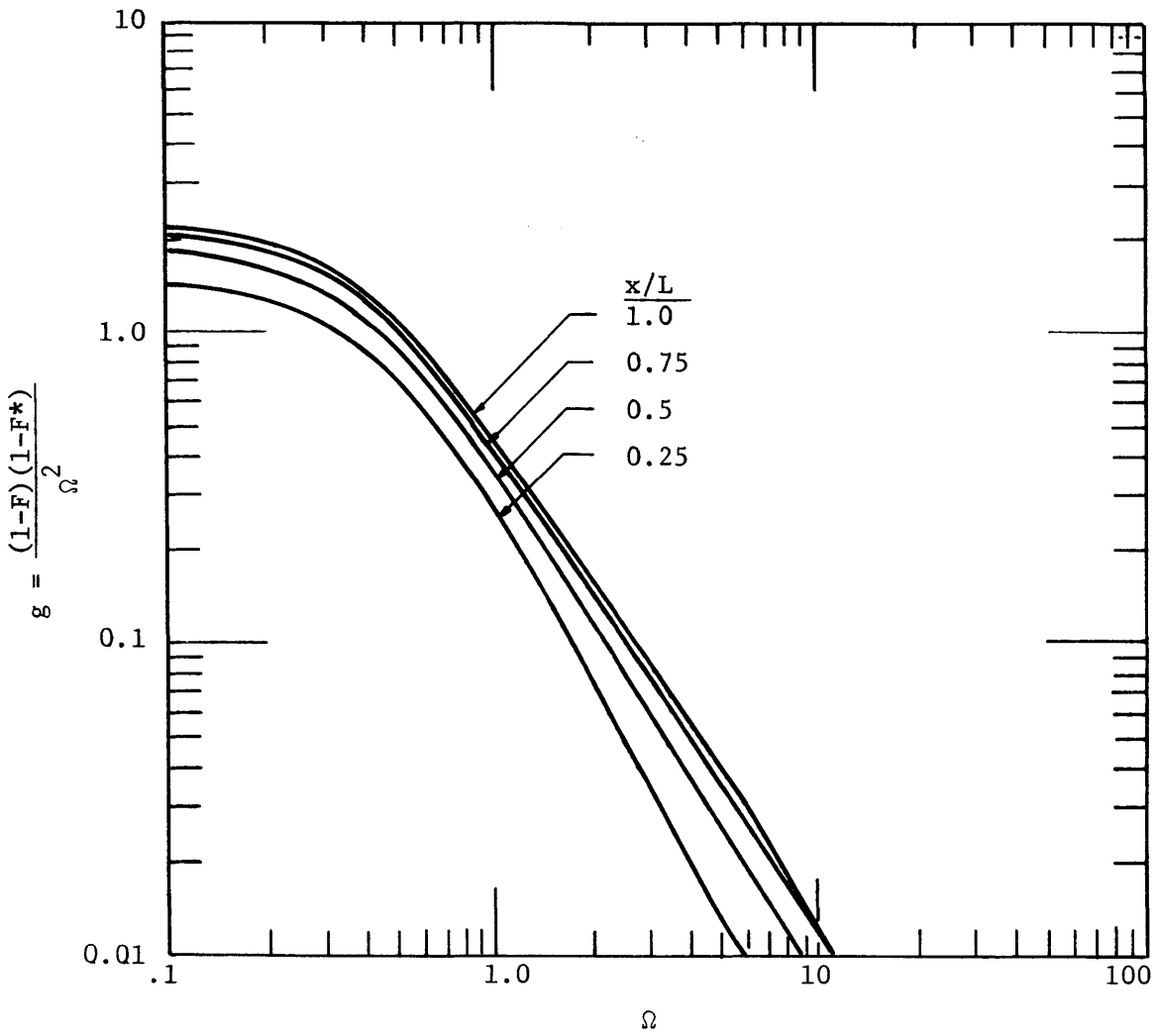

Figure 2.12 Response of the Aquifer-Reservoir System, Plot of g along the Aquifer with $aL^2/\alpha = 1.0$ and $SL/\ell = 1.0$.

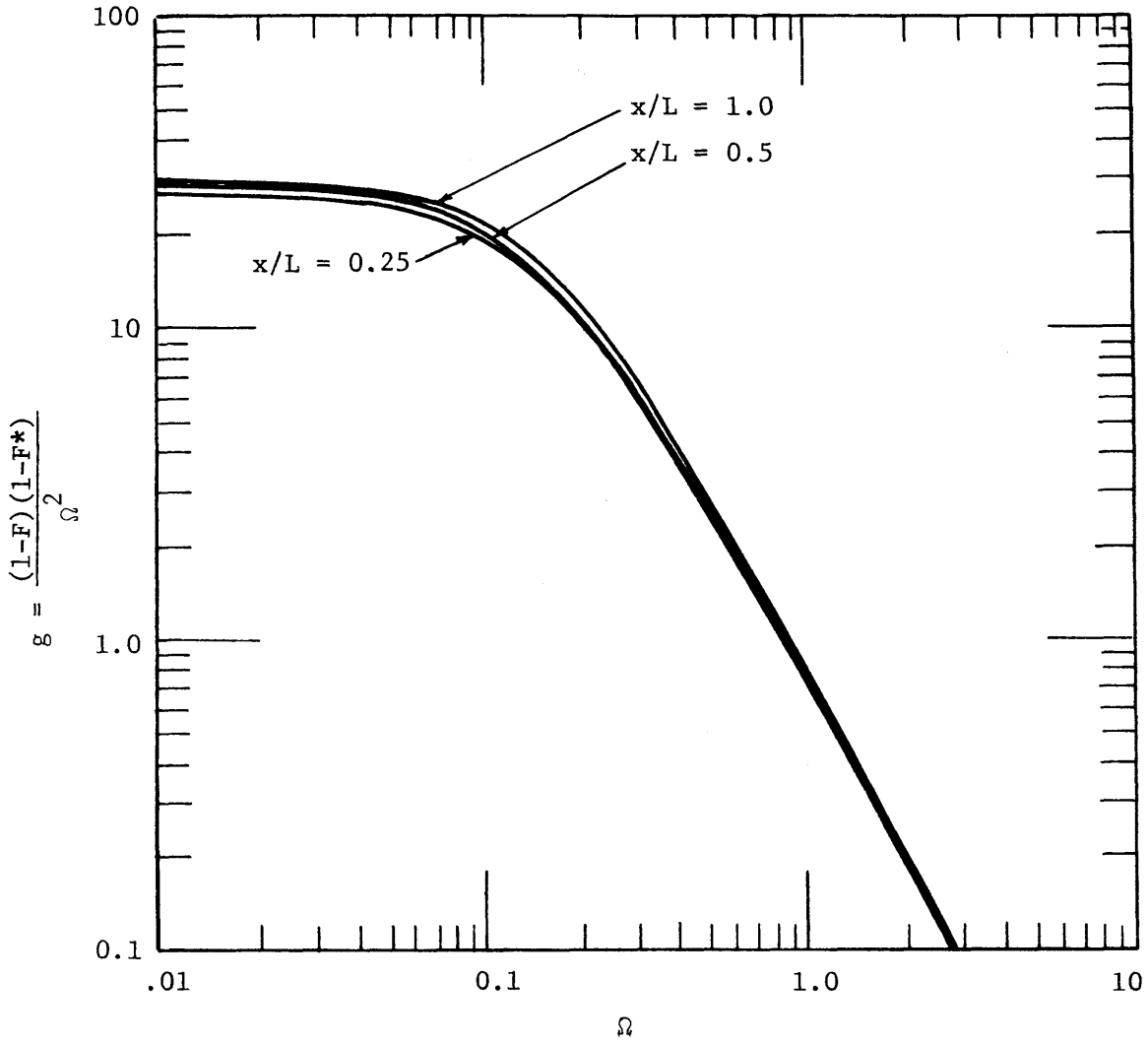

Figure 2.13 Response of the Aquifer-Reservoir System, Plot of g along the Aquifer with $aL^2/\alpha = 1.0$ and $SL/\ell = 5.0$.

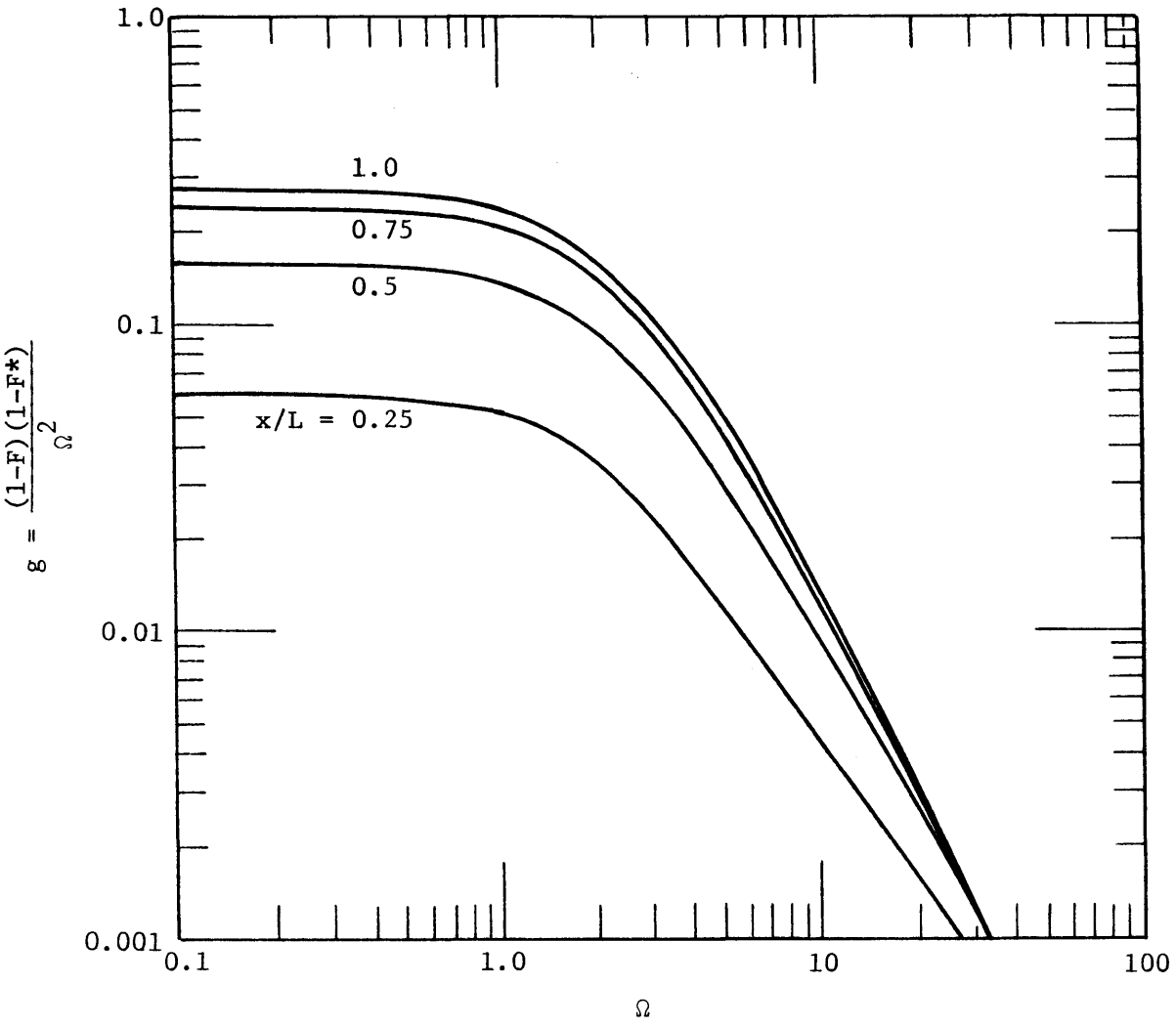

Figure 2.14 Response of the Aquifer-Reservoir System, Plot of g along the Aquifer with $aL^2/\alpha = 200$ and $SL/\ell = 5$.

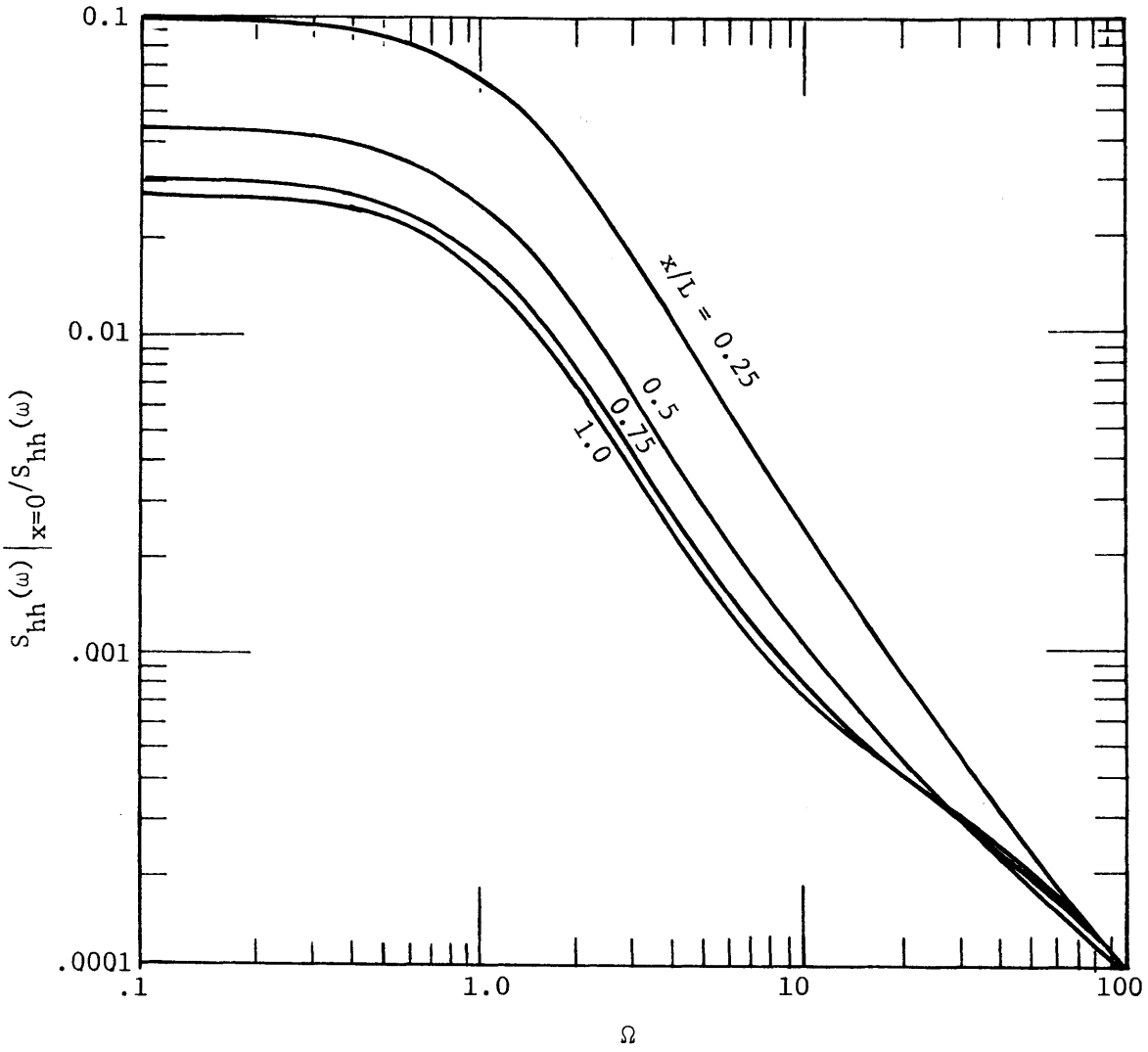

Figure 2.15 Response of the Aquifer-Reservoir System, Plot of $S_{hh}\big|_{x=0}/S_{hh}$ along the Aquifer with $aL^2/\alpha = 1.0$ and $SL/\ell = 0.1$.

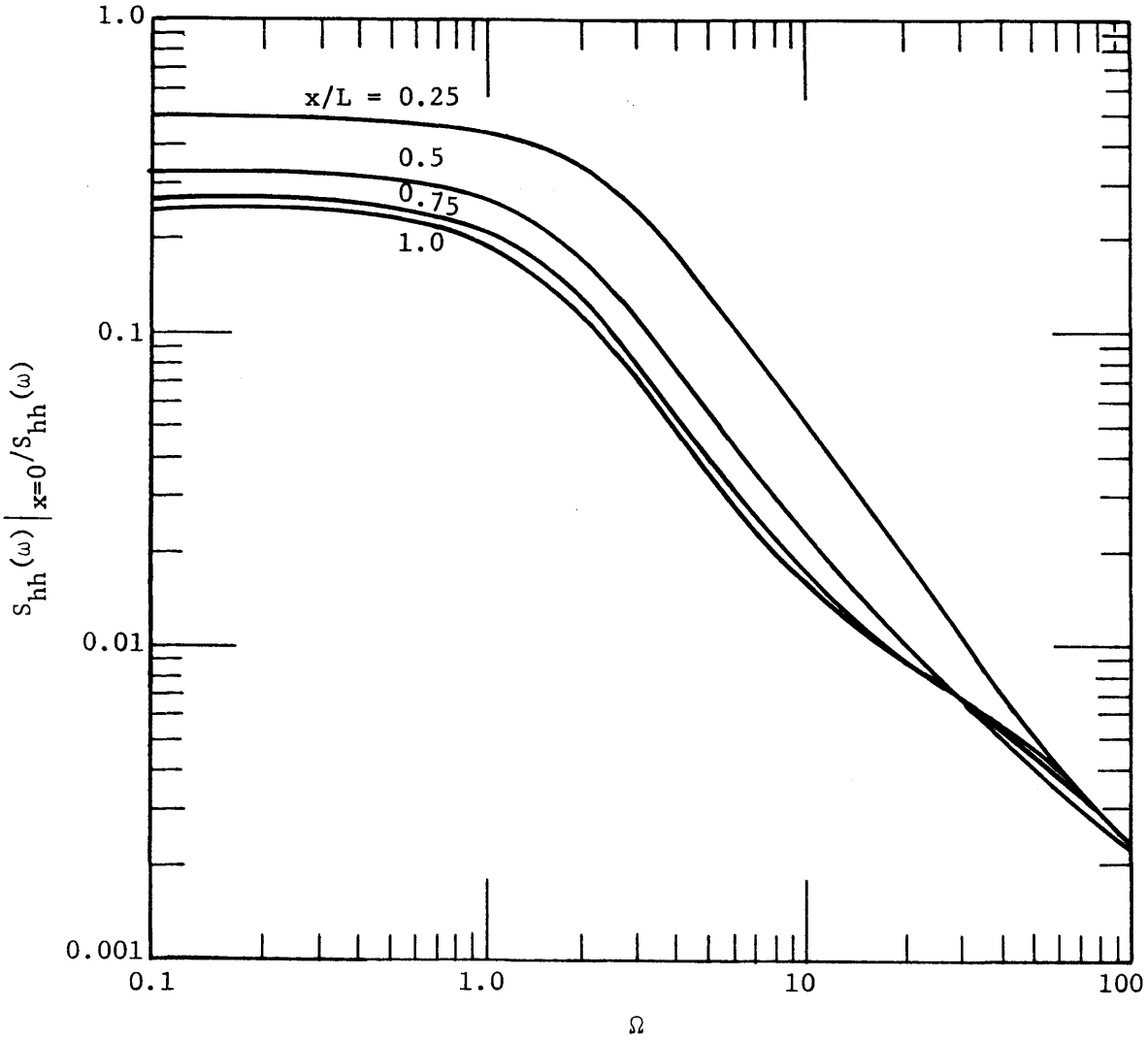

Figure 2.16 Response of the Aquifer-Reservoir System, Plot of $S_{hh}\big|_{x=0}/S_{hh}$ along the Aquifer with $aL^2/\alpha = 1.0$ and $SL/\ell = 0.5$.

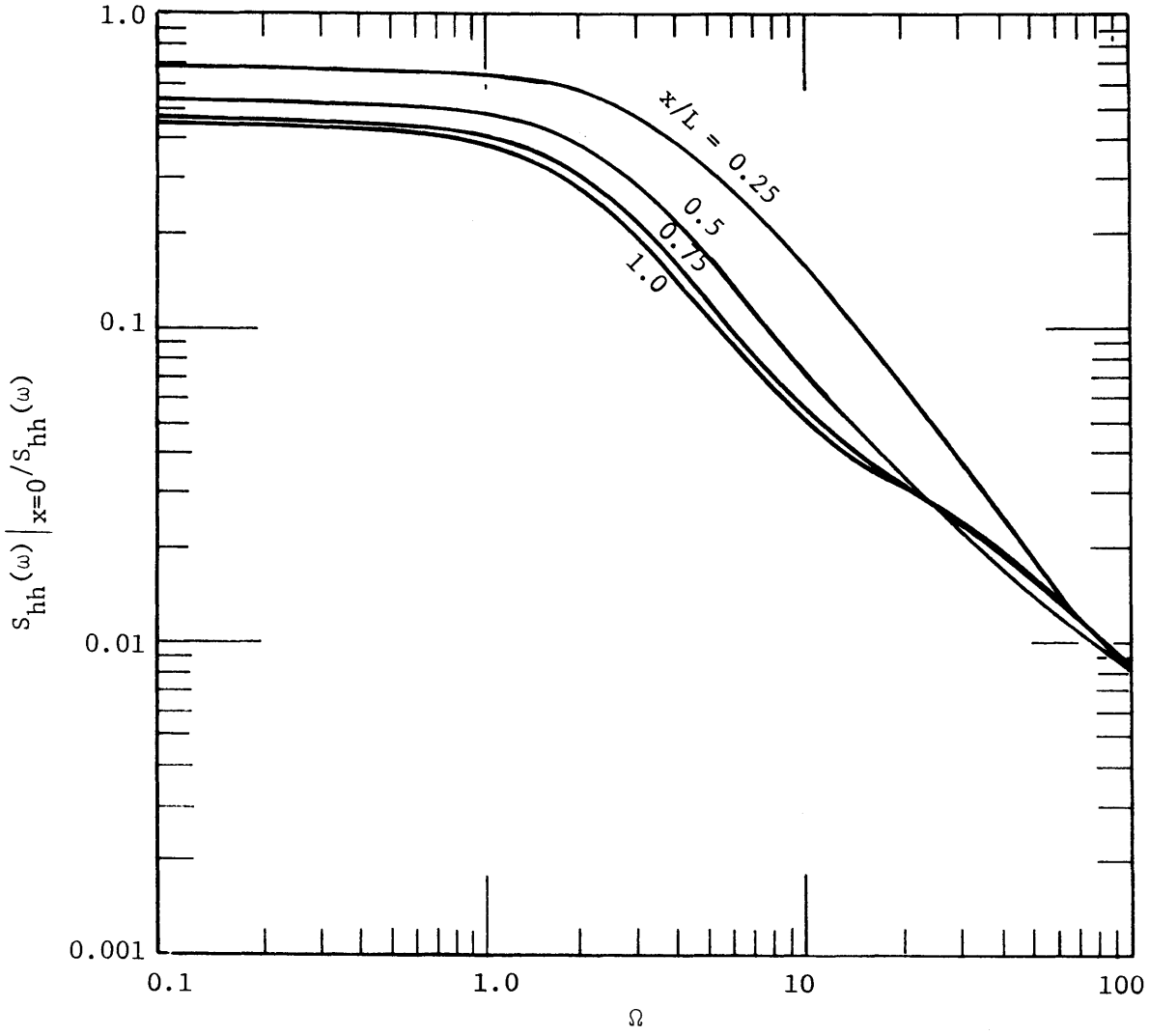

Figure 2.17 Response of the Aquifer-Reservoir System, Plot of $S_{hh}\big|_{x=0}/S_{hh}$ along the Aquifer with $aL^2/\alpha = 1.0$ and $SL/\ell = 1.0$.

expected values and $h'(x)$ and ε' are the fluctuations, equation 2.3.26 becomes

$$S[\frac{\partial \bar{h}}{\partial t} + \frac{\partial h'}{\partial t}] = \frac{\partial}{\partial x}[K\bar{h}\frac{\partial \bar{h}}{\partial x} + K\bar{h}\frac{\partial h'}{\partial x} + Kh'\frac{\partial \bar{h}}{\partial x} + Kh'\frac{\partial h'}{\partial x}] + \bar{\varepsilon} + \varepsilon' \tag{2.3.27}$$

The mean part of equation 2.3.27 can be easily extracted, neglecting terms involving products of the fluctuations

$$\frac{\partial}{\partial x} K\bar{h}\frac{\partial \bar{h}}{\partial x} = -\bar{\varepsilon} \tag{2.3.28}$$

with the following boundary conditions:

$$\begin{aligned} \bar{h} &= \bar{H} \qquad x = 0 \\ \frac{\partial \bar{h}}{\partial x} &= 0 \qquad x = L \end{aligned} \tag{2.3.29}$$

Since $\bar{h}$ is only a function of x, the partial derivatives can be replaced by total derivatives and the solution is

$$\bar{h}^2 - \bar{H}^2 = \frac{\bar{\varepsilon} x}{K}(2L-x) \tag{2.3.30}$$

For $\mu = \bar{\varepsilon}L^2/2K\bar{H}^2 < 1$, this equation can be approximated by

$$\bar{h} - \bar{H} = \mu \frac{x}{L}(2-\frac{x}{L})\bar{H} + O(\mu^2) \tag{2.3.31}$$

The remaining fluctuating part of equation 2.3.27 is

$$S \frac{\partial h'}{\partial t} = \frac{\partial}{\partial x}[K\bar{h} \frac{\partial h'}{\partial x} + Kh' \frac{\partial \bar{h}}{\partial x} + Kh' \frac{\partial h'}{\partial x}] + \varepsilon' \qquad (2.3.32)$$

Noting that the third term on the right hand side is a product of two small quantities, it has been neglected. Hence, we have for the governing equation for the fluctuations the following

$$S \frac{\partial h'}{\partial t} = \frac{\partial}{\partial x}[K\bar{h} \frac{\partial h'}{\partial x} + Kh' \frac{\partial \bar{h}}{\partial x}] + \varepsilon' \qquad (2.3.33)$$

with K as a constant. Substituting $\bar{h}$ from equation 2.3.31 into 2.3.33, we have

$$S \frac{\partial h'}{\partial t} = K\bar{H} \frac{\partial^2}{\partial x^2} \{[1+\mu \frac{x}{L}(2-\frac{x}{L}) + \cdots]h'\} + \varepsilon' \qquad (2.3.34)$$

with the following boundary conditions:

$$\begin{aligned} h' &= H' \qquad x = 0 \\ \frac{\partial h'}{\partial x} &= 0 \qquad x = L \end{aligned} \qquad (2.3.35)$$

The parameter μ characterizes the relative change of the saturated thickness as is seen from equation 2.3.31 with x = L,

$$\Delta h \equiv \bar{h}\Big|_{x=L} - \bar{H} = \mu \bar{H}$$

For small μ, we seek a perturbation solution in the form of

$$h' = h'_o + \mu\, h'_1 + \mu^2\, h'_2 + \cdots \tag{2.3.36}$$

Substituting equation 2.3.36 into 2.3.34, we have, neglecting terms of order μ^2 and higher and dropping the primes,

$$S\,\frac{\partial(h_o+\mu h_1)}{\partial t} = K\bar{H}\,\frac{\partial^2}{\partial x^2}\{h_o+\mu\,[\tfrac{x}{L}(2-\tfrac{x}{L})h_o+h_1]\} + \varepsilon \tag{2.3.37}$$

with

$$h_o + \mu\, h_1 = \bar{H} \qquad x = 0$$

$$\frac{\partial h_o}{\partial x} + \mu\,\frac{\partial h_1}{\partial x} = 0 \qquad x = L$$

Since $K\bar{H} = T$, we have, for order μ^o,

$$S\,\frac{\partial h_o}{\partial t} = T\,\frac{\partial^2 h_o}{\partial x^2} + \varepsilon \tag{2.3.38}$$

with

$$x = 0 \qquad h_o = H$$

$$x = L \qquad \frac{\partial h_o}{\partial x} = 0$$

and for order μ,

$$S\,\frac{\partial h_1}{\partial t} - T\,\frac{\partial^2 h_1}{\partial x^2} = T\,\frac{\partial^2}{\partial x^2}[h_o\,\tfrac{x}{L}(2-\tfrac{x}{L})] \tag{2.3.39}$$

with

$$x = 0 \qquad h_1 = 0$$

$$x = L \qquad \frac{\partial h_1}{\partial x} = 0$$

Upon using equations 2.1.4-5, the solution for equation 2.3.38 is

$$dZ_{h_o} = F\, dZ_H + \frac{i(F-1)}{\omega S}\, dZ_\varepsilon$$

where

$$F = \frac{\cosh bL(\frac{x}{L} - 1)}{\cosh bL} \qquad (2.3.40)$$

$$b = (1+i)(\frac{\omega}{2\alpha})^{1/2}$$

$$\alpha = \frac{T}{S}$$

Note that equation 2.3.40 is identical to that developed previously following equation 2.3.8. That is to say the nonlinearity does not affect the solution of order μ^o. Using equations 2.1.14, 2.1.15 and 2.3.40, order μ equation 2.3.39 can be written in the following form

$$\frac{\partial^2}{\partial x^2} G(x,\omega) - \frac{i\omega S}{T} G(x,\omega) = \frac{-i\omega S}{T} \frac{x}{L}(2 - \frac{x}{L})\, dZ_{h_o}$$

where $G(x,\omega) = dZ_{h_1} + dZ_{h_o} \frac{x}{L}(2 - \frac{x}{L})$ (2.3.41)

with

$$x = 0 \quad G(x) = 0$$

$$x = L \quad \frac{\partial G}{\partial x} = 0$$

Using the method of variation of parameters, solution to equation 2.3.41 can be found to be

$$G(x,\omega) = C_1 e^{bx} + C_2 e^{-bx} + G_1(x,\omega) \qquad (2.3.42)$$

where $G_1(x)$ is given by the following integral

$$G_1(x,\omega) = \int_0^{\frac{x}{L}} - bL\,\frac{s}{L}(2-\frac{s}{L})\sinh[bL(\frac{x}{L}-\frac{s}{L})]dZ_{h_o}\,d(\frac{s}{L}) \qquad (2.3.43)$$

and C_1 and C_2 are coefficients to be determined from the boundary conditions. Note the term dZ_{h_o} is given by the order μ^o solution in equation 2.3.40. Upon substitution of equation 2.3.40 for dZ_{h_o} in equation 2.3.43, G_1 can be broken up into two separate integrals as follows:

$$G_1 = \int_0^{\frac{x}{L}} - bL\,\frac{s}{L}(2-\frac{s}{L})\frac{\cosh bL(\frac{s}{L}-1)}{\cosh bL}\sinh[bL(\frac{x}{L}-\frac{s}{L})]dZ_H\,d(\frac{s}{L})$$

$$+ \int_0^{\frac{x}{L}} - bL\,\frac{s}{L}(2-\frac{s}{L})\,[\frac{\cosh bL(\frac{s}{L}-1)}{\cosh bL}-1]\sinh[bL(\frac{x}{L}-\frac{s}{L})]\frac{i}{\omega S}dZ_\varepsilon\,d(\frac{s}{L}) \qquad (2.3.44)$$

The integrations of the integrals in equation 2.3.44 and the evaluations of the coefficients C_1 and C_2 in equation 2.3.42 was developed on the computer at the Massachusetts Institute of Technology, Project MAC's Symbolic Manipulation System, using DEC PDP-10 computer and LISP programming code. The results are shown in Figure 2.18 with the symbols used in Table 2.1. It can be seen that the solution is in the form

$$G(x,\omega) = P_H(x,\omega)\;dZ_H + \frac{i}{\omega S}\,P_\varepsilon(x,\omega)\;dZ_\varepsilon \qquad (2.3.45)$$

where $P_H(x,\omega)$ and $P_\varepsilon(x,\omega)$ are coefficients for the terms dZ_H and $\frac{i}{\omega S}\,dZ_\varepsilon$ in Figure 2.18. $P_H(x,\omega)\;dZ_H$ and $P_\varepsilon(x,\omega)\;\frac{i}{\omega S}\,dZ_\varepsilon$ are shown in

Table 2.1 Directory of Symbols used in Figure 2.18.

Symbols	Equivalent Terms
B^2	$i/\omega S$
DZE	dZ_ε
DZH	dZ_H
%E	exponential
Y	bL
Z	x/L
T	s/L

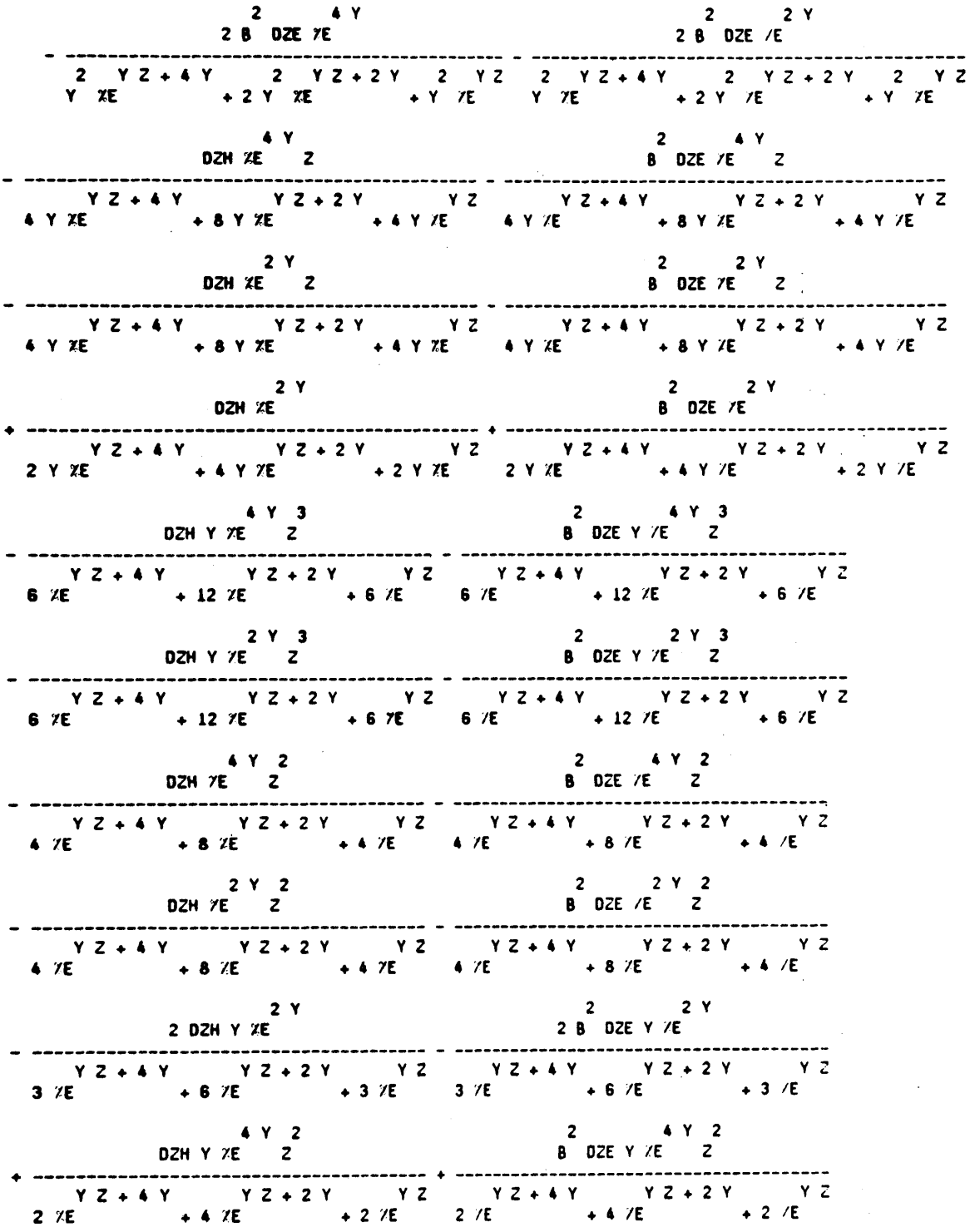

Figure 2.18 Solution to Equation 2.3.45

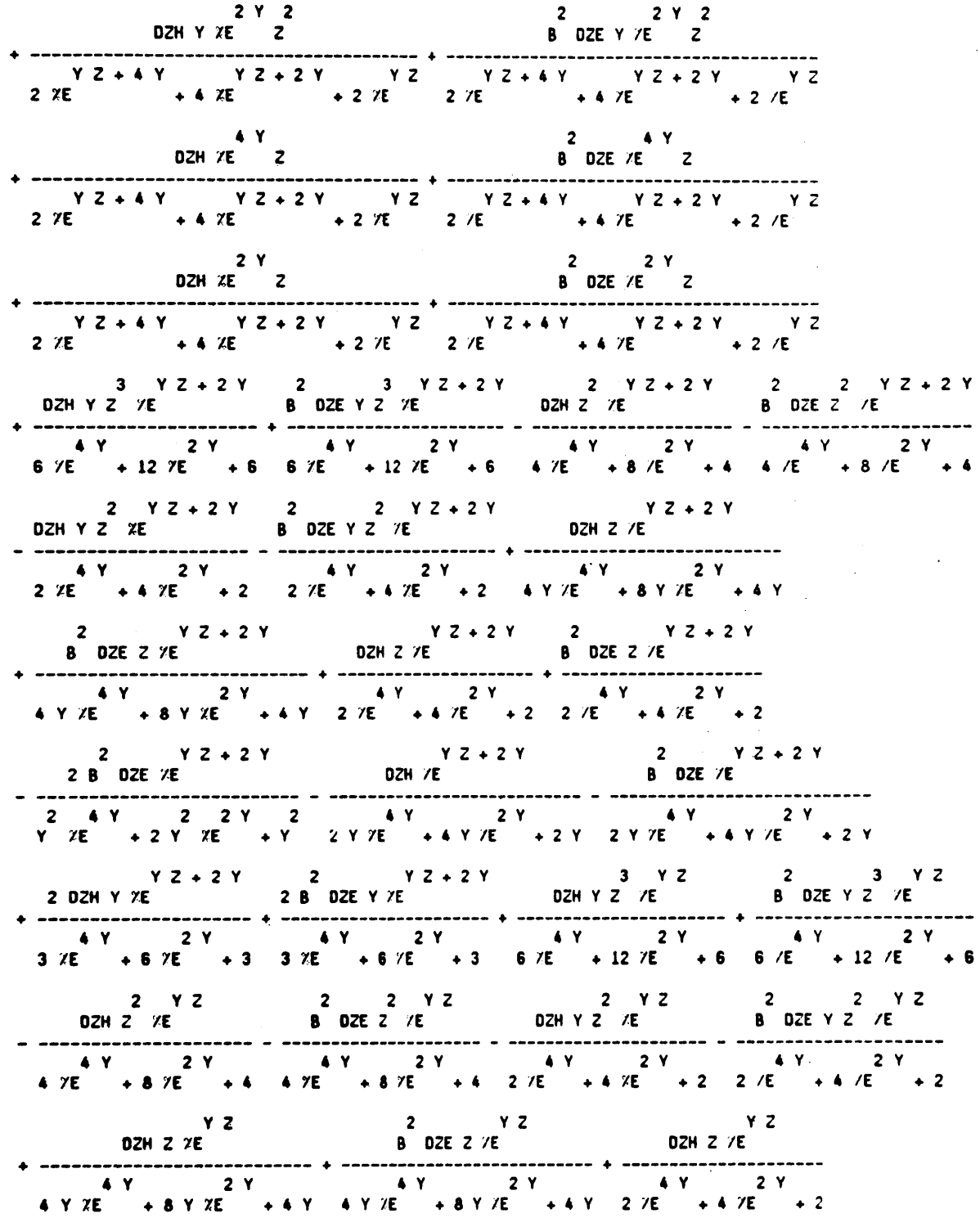

Figure 2.18 continued

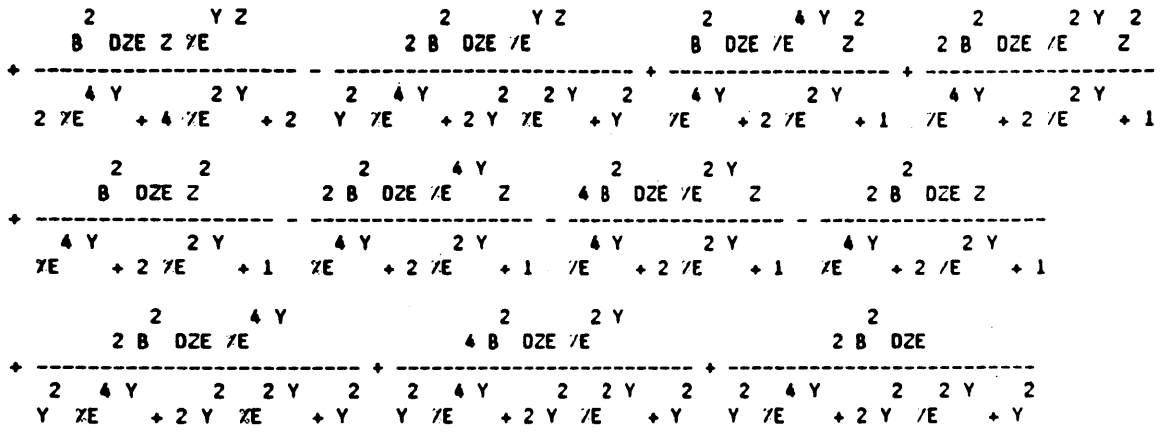

Figure 2.18 continued

Figures 2.19 and 2.20 with the substitutions of

$$T = e^{bL(\frac{x}{L})} + 4e^{bL} + 2e^{bL(\frac{x}{L})} + 2e^{bL} + e^{bL(\frac{x}{L})} \tag{2.3.46}$$

$$TT18 = e^{4bL} + 2e^{2bL} + 1 \tag{2.3.47}$$

Now $G(x,\omega)$ in equation 2.3.42 has been found. From equation 2.3.36, we have

$$dZ_h = dZ_{h_o} + \mu\, dZ_{h_1} + O(\mu^2) \tag{2.3.48}$$

Using equation 2.3.41 in the above equation, we have

$$dZ_h = dZ_{h_o} + \mu\, [G - \tfrac{x}{L}(2 - \tfrac{x}{L})\, dZ_{h_o}] \tag{2.3.49}$$

Hence, we have, upon using equations 2.1.19 - 21, and retaining only $O(\mu)$ terms, the spectral relation

$$S_{hh} = f\, S_{HH} + \Omega^2 g \frac{S_{\varepsilon\varepsilon}}{\omega^2 S^2} - \frac{i}{\omega S}\{[1-2\mu\tfrac{x}{L}(2-\tfrac{x}{L})]F(F^*-1)+2\mu\, Re[P_H(F^*-1)]\}\, S_{H\varepsilon}$$

$$+ \frac{i}{\omega S}\{[1-2\,\tfrac{x}{L}(2-\tfrac{x}{L})]F^*(F-1)+2\mu\, Re[P_\varepsilon F^*]\}\, S_{\varepsilon H} \tag{2.3.50}$$

where $f = \{[1-2\mu\tfrac{x}{L}(2-\tfrac{x}{L})]FF^*+2\mu\, Re[P_H F^*]\}$

and $\Omega^2 g = \{[1-2\mu\tfrac{x}{L}(2-\tfrac{x}{L})](F-1)(F^*-1) + 2\mu\, Re[P_\varepsilon(F^*-1)]\}$

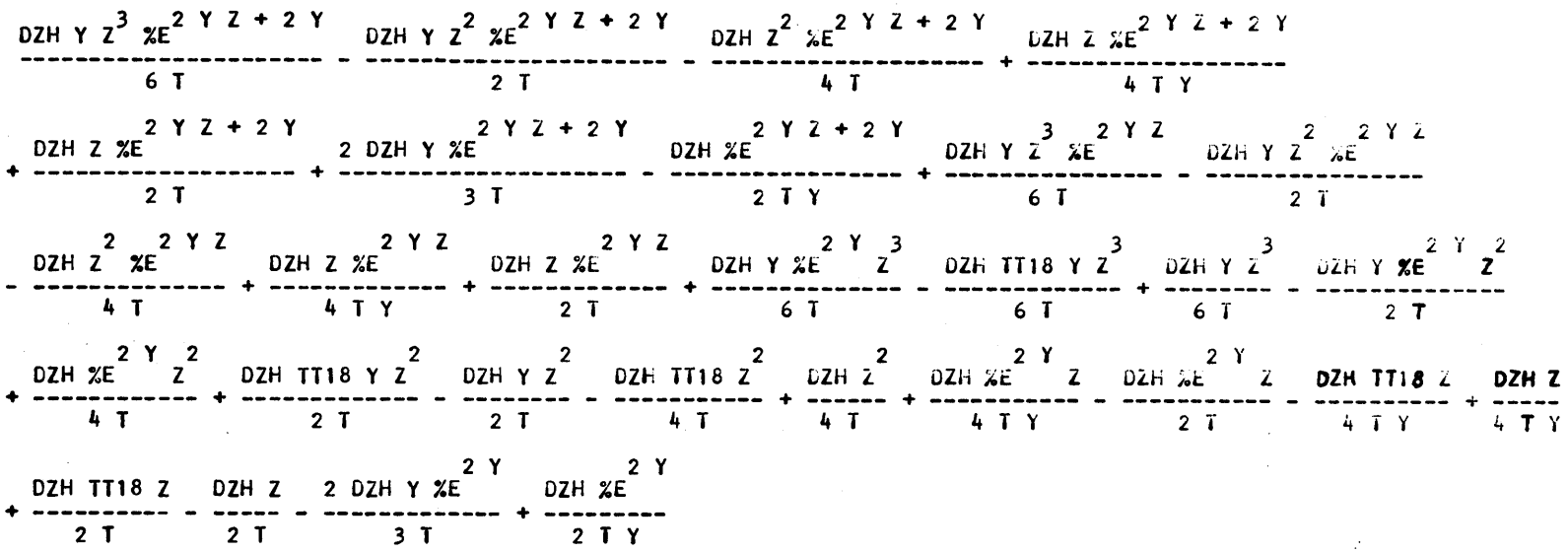

Figure 2.19 $P_H(x,\omega)dZ_H$ in Equation 2.3.45.

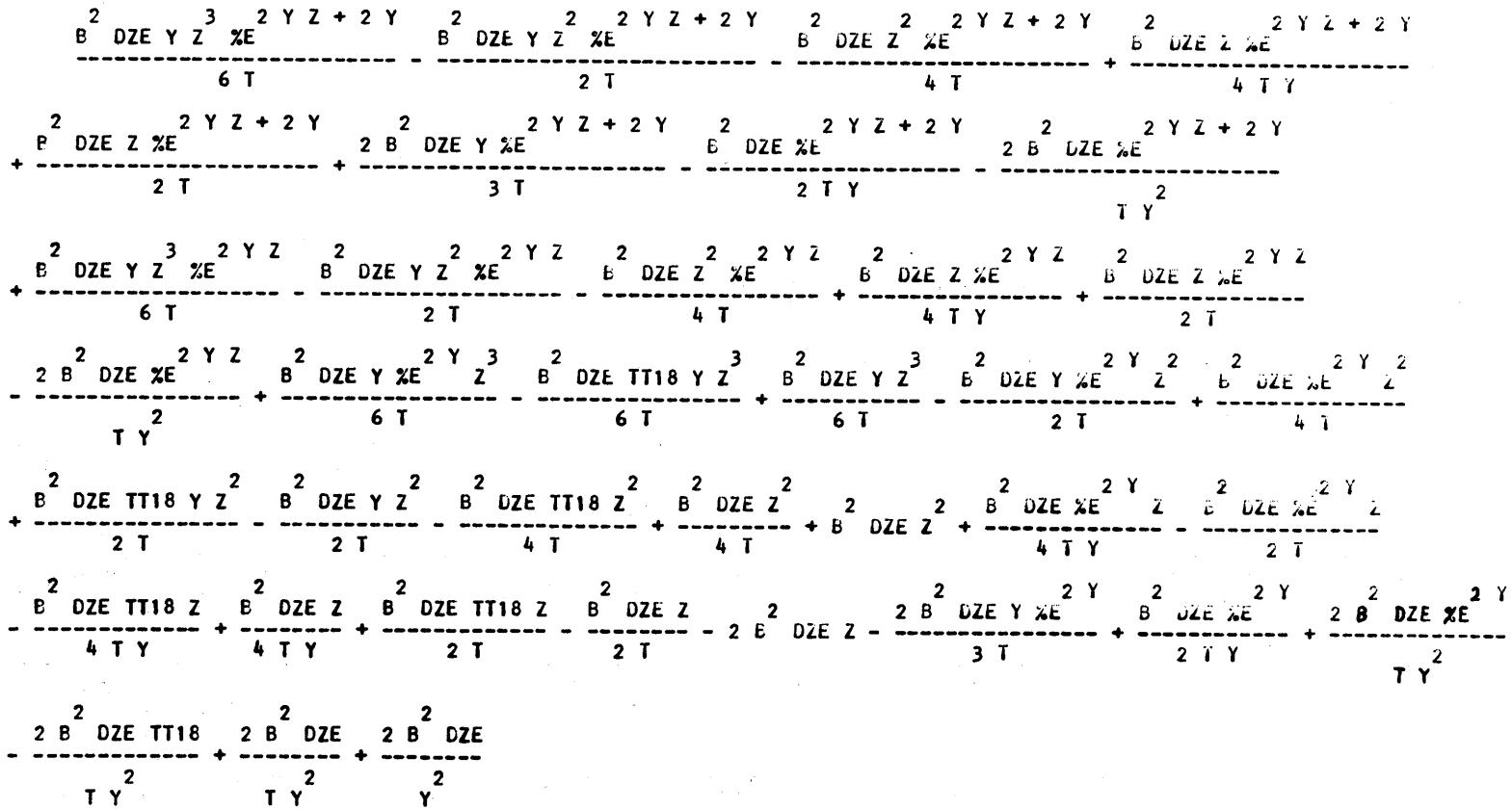

Figure 2.20 $\frac{i}{\omega S} P_{\varepsilon}(x,\omega) dZ_{\varepsilon}$ in Equation 2.3.45.

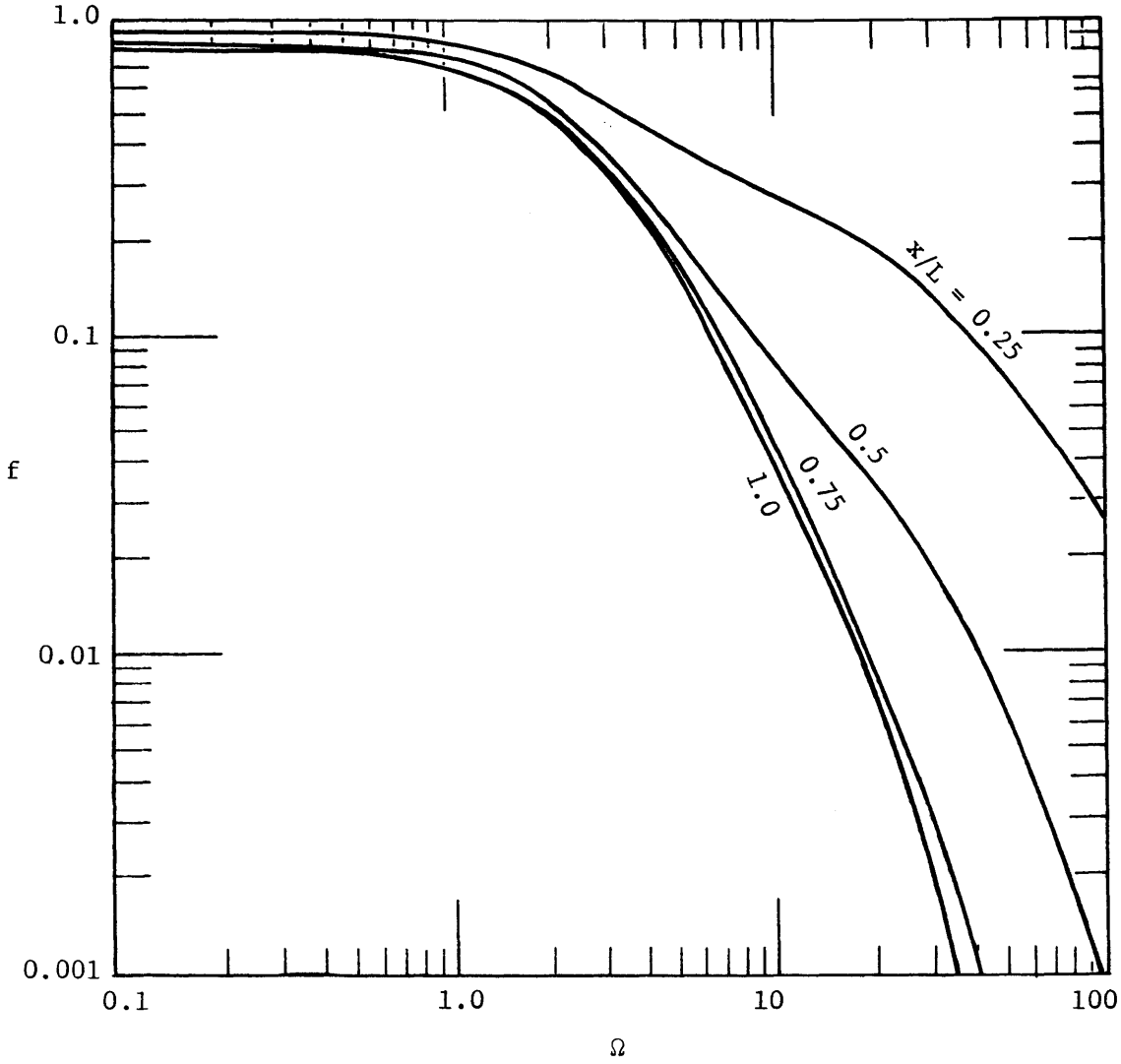

Figure 2.21 Plot of f in Equation 2.3.50 with μ = 0.1.

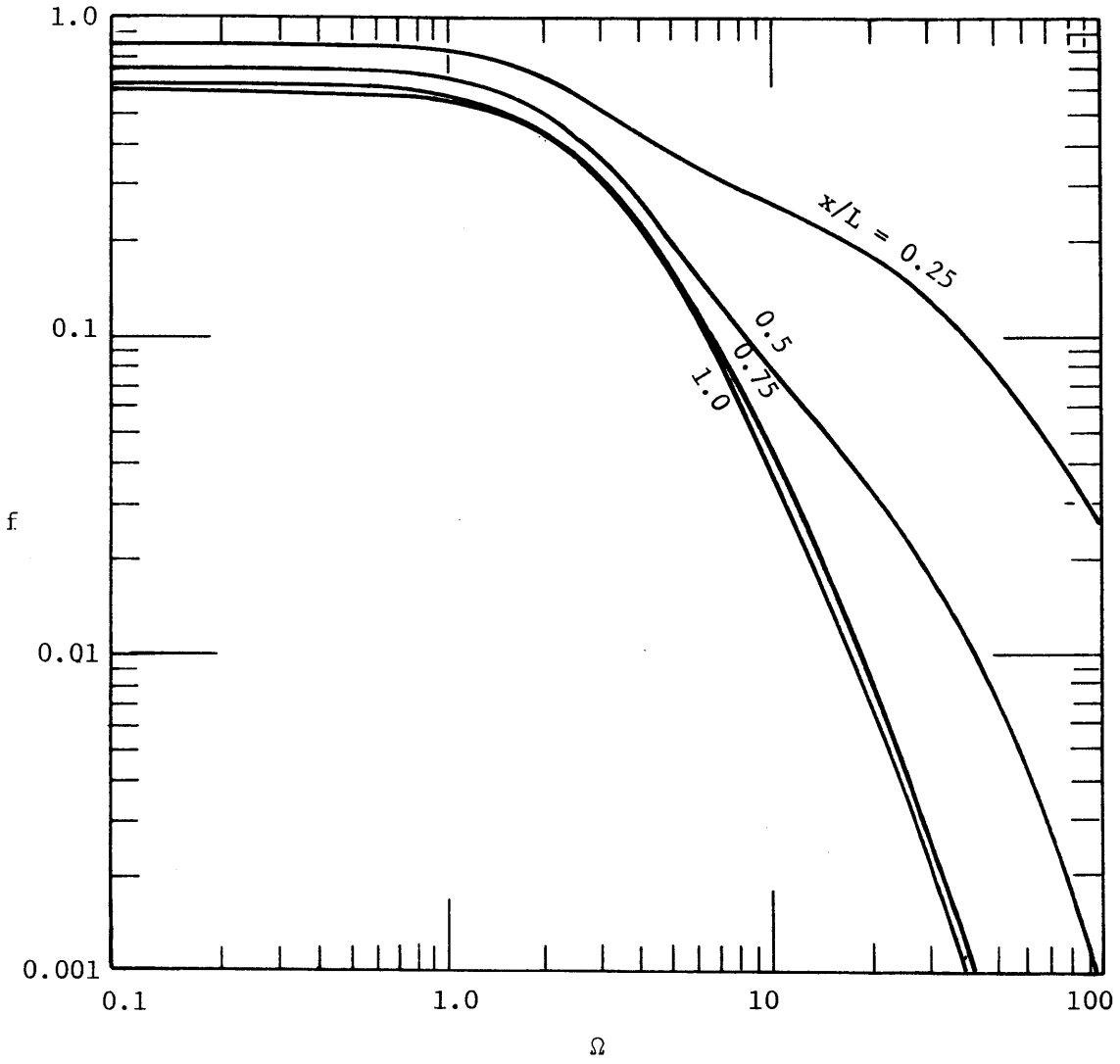

Figure 2.22 Plot of f in Equation 2.3.50 with $\mu = 0.2$.

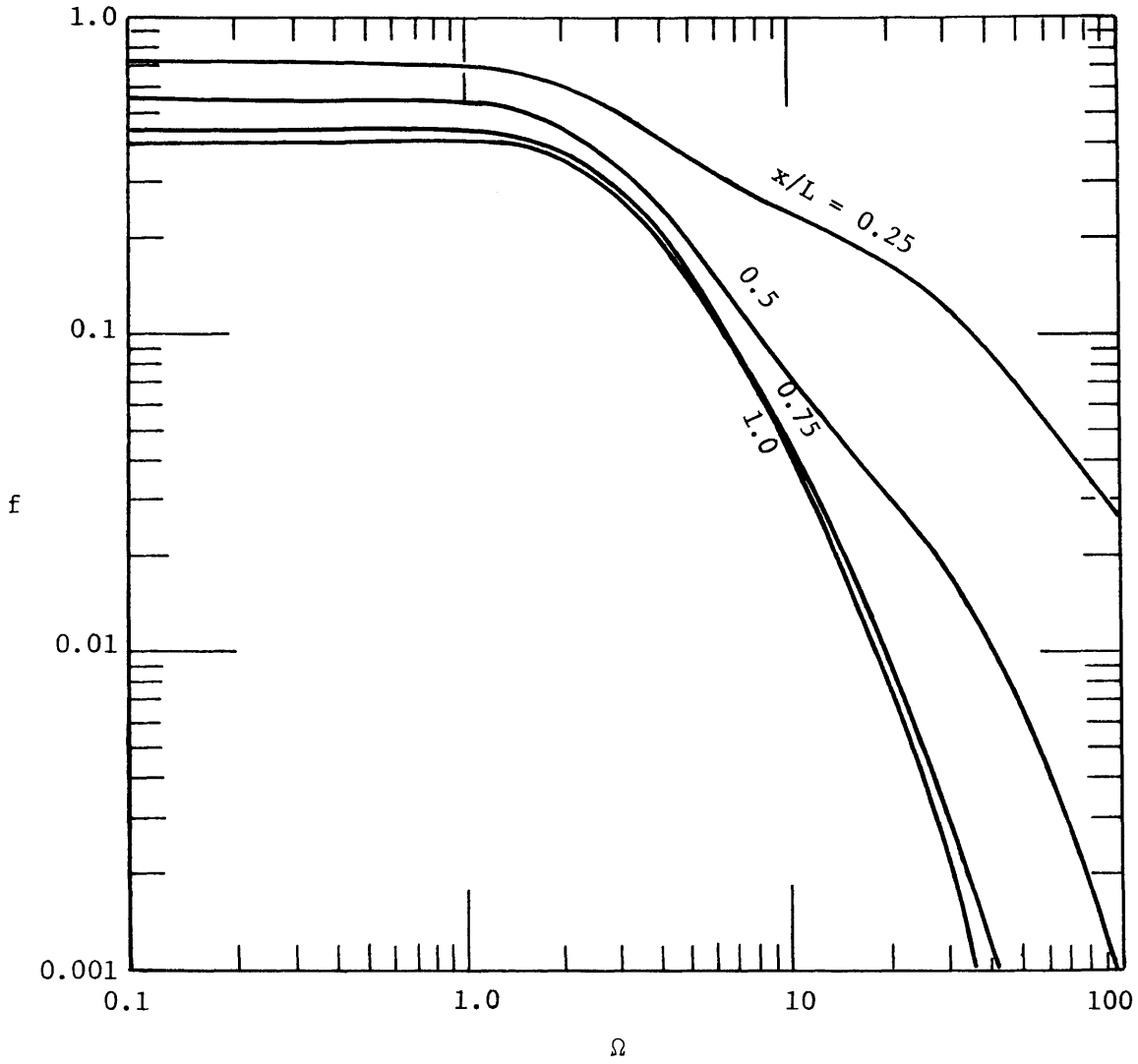

Figure 2.23 Plot of f in Equation 2.3.50 with μ = 0.3.

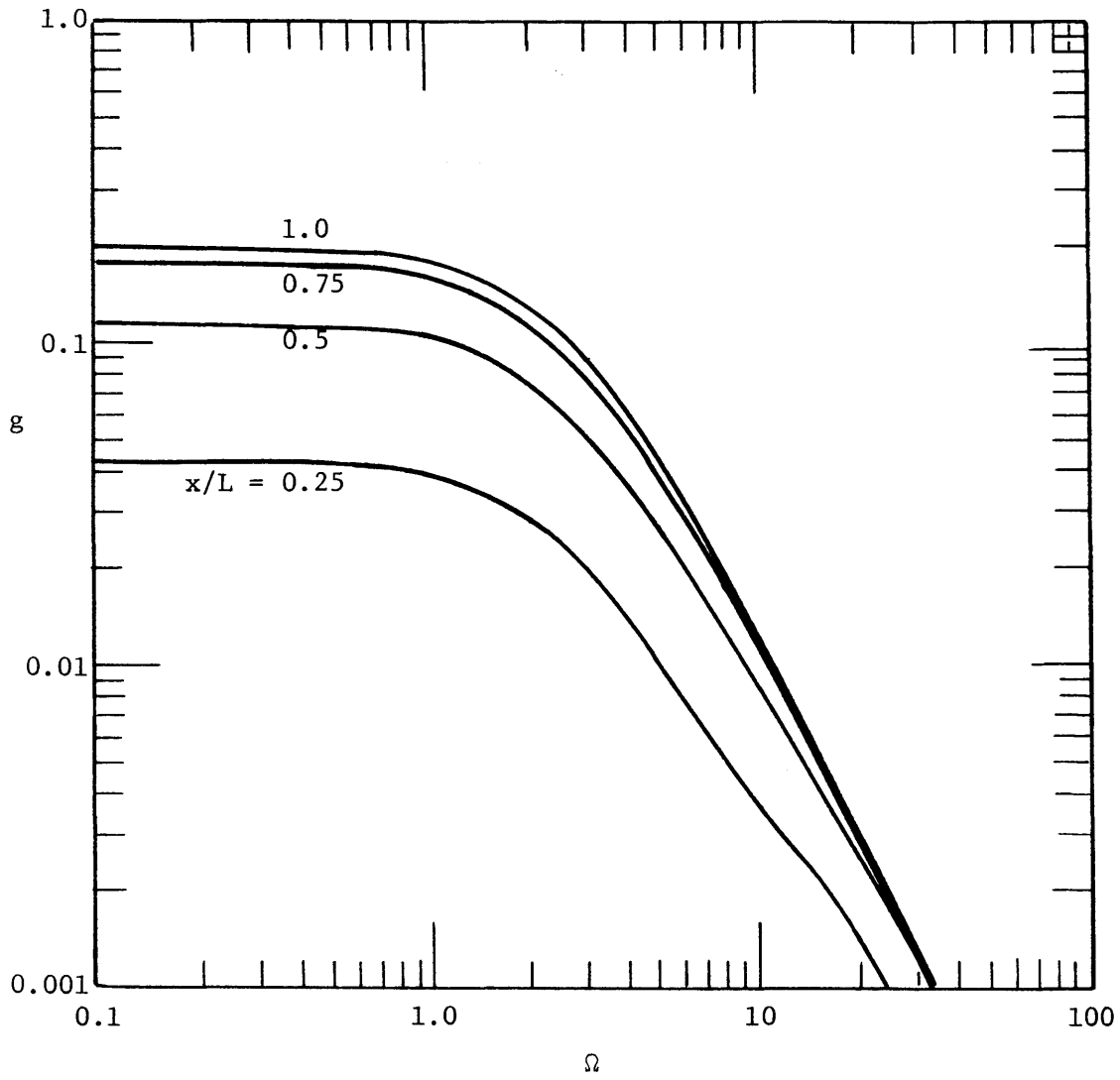

Figure 2.24 Plot of g in Equation 2.3.50 with $\mu = 0.1$.

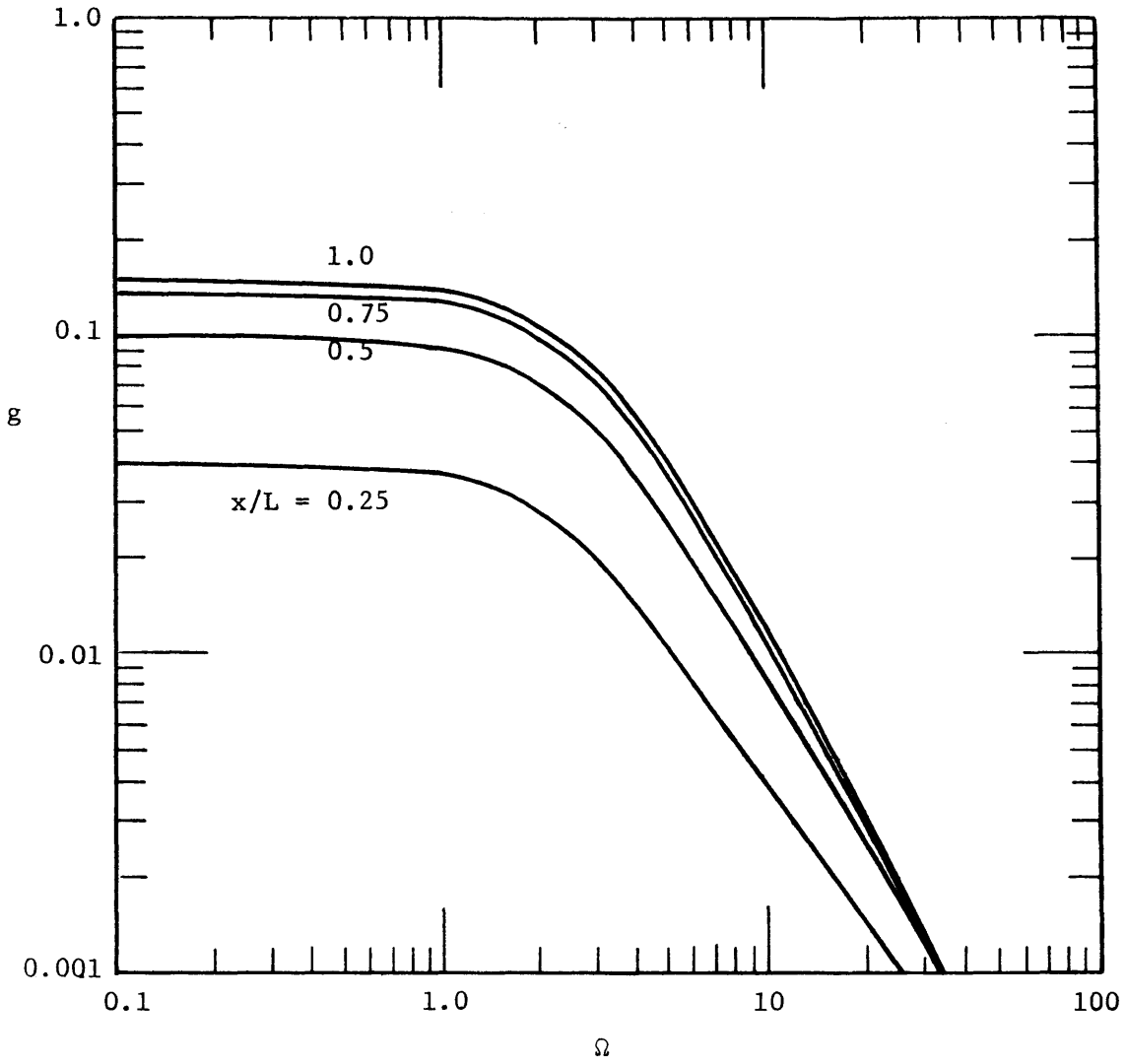

Figure 2.25 Plot of g in Equation 2.3.50 with $\mu = 0.2$.

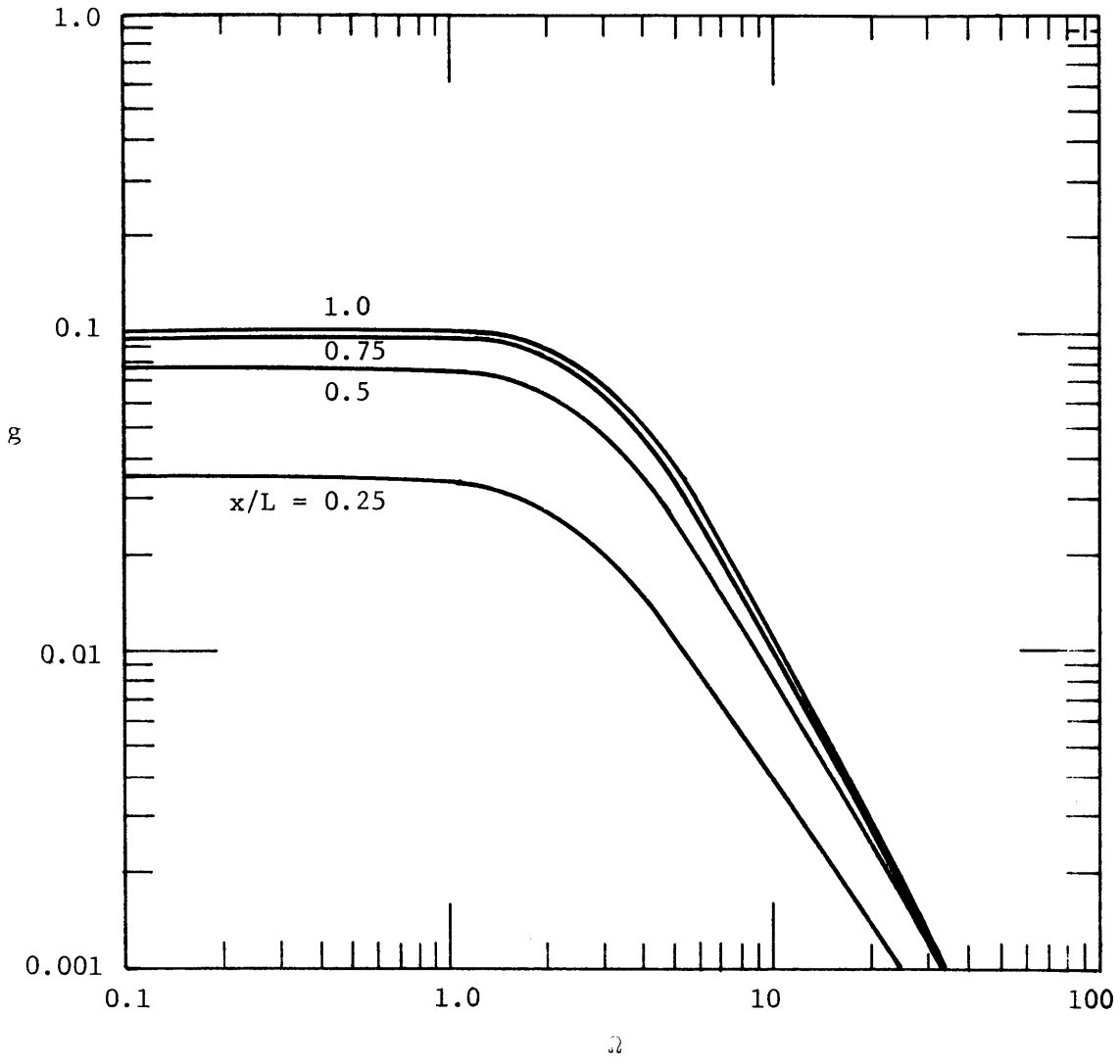

Figure 2.26 Plot of g in Equation 2.3.50 with $\mu = 0.3$.

the functions f and g are shown in Figures 2.21 - 26 with different values of μ. It can be seen that the value of μ does not have much effect in the higher frequency domain while the change may be noticeable at low frequencies (compare with Figures 2.5 - 2.8 with $\Gamma = 0$).

2.4 The Laplace Aquifer

The above analyses of the Dupuit aquifer can be expected to provide a reasonable representation of relatively shallow aquifers at location away from the stream. However, for relatively deep anisotropic aquifers with partially penetrating streams, the assumption of predominantly horizontal flow becomes inadequate. An analysis of the dynamic effects of vertical flow will be developed in this section.

The flow in a vertical section of a two dimensional homogeneous anisotropic phreatic aquifer, as depicted in Figure 2.27 is described by

$$K_x \frac{\partial^2 \phi}{\partial x^2} + K_z \frac{\partial^2 \phi}{\partial z^2} = 0 \qquad (2.4.1)$$

where $\phi(x,z,t)$ is the piezometric head, and K_x and K_z are the principal components of the hydraulic conductivity tensor whose principal axes coincide with x and z. The linearized phreatic surface boundary condition is

$$n \frac{\partial \phi}{\partial t} + K_z \frac{\partial \phi}{\partial z} = \varepsilon \ , \qquad z = \eta(x,t) \simeq 0 \qquad (2.4.2)$$

where n is the effective porosity. It is consistent with this linearization to apply the condition at $z = 0$ as done by Dagan (1964) and Hunt

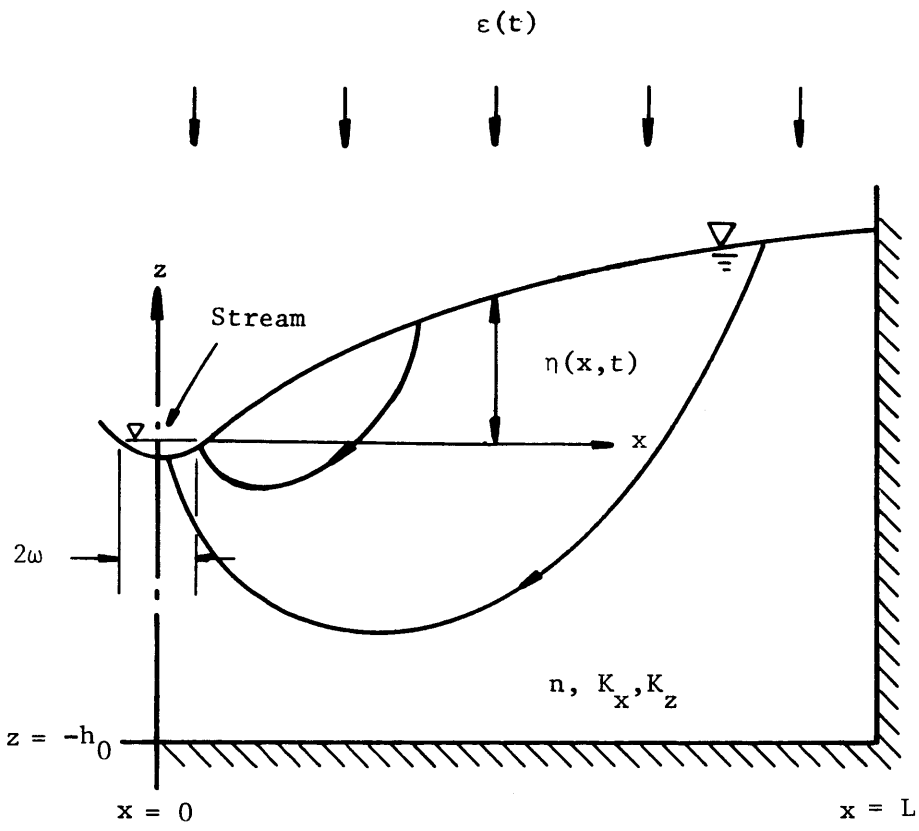

Figure 2.27 The Laplace Aquifer

(1971) in related deterministic problems. The shape of the phreatic surface $\eta(x,t)$ is related to the piezometric head through the constant pressure condition $\phi(x,\eta,t) = \eta(x,t)$ and under this linearization it is consistent to apply this condition at $z = 0$, i.e.,

$$\phi(x,0,t) = \eta(x,t) \tag{2.4.3}$$

The conditions of no flux through impervious boundaries are

$$z = -h_o \qquad \frac{\partial \phi}{\partial z} = 0 \tag{2.4.4}$$

$$x = L \qquad \frac{\partial \phi}{\partial x} = 0 \tag{2.4.5}$$

In addition, at the stream of width $2w$ we require that

$$\phi = \eta = 0 \quad \text{at} \quad z = 0, \quad x = w \tag{2.4.6}$$

which implies that any seepage face at the stream is negligible.

The mean flow condition is found by taking an ensemble average of equations (2.4.1 - 2.4.6). Explicit solutions [Dagan, 1964, Eq. 14] have been given for the steady mean flow in the case $h_o \to \infty$. However, for a stationary random process the fluctuations of ϕ, η and ε are also governed by the linear system (2.4.1 - 2.4.6) and the mean flow is not explicitly involved.

With ϕ, η, ε now denoting fluctuations with zero mean, the representations

$$\phi = \int_{-\infty}^{\infty} e^{i\omega t}\, dZ_{\phi}(\omega,x,z) \tag{2.4.7}$$

$$\eta = \int_{-\infty}^{\infty} e^{i\omega t}\, dZ_{\eta}(\omega,x) = \int_{-\infty}^{\infty} e^{i\omega t}\, dZ_{\phi}(\omega,x,0) \tag{2.4.8}$$

are introduced along with

$$\varepsilon(t) = \int_{-\infty}^{\infty} e^{i\omega t}\, dZ_{\varepsilon}(\omega) - \delta(x) \int_{-\infty}^{\infty} e^{i\omega t}\, dZ_{q}(\omega) \tag{2.4.9}$$

where $\delta(x)$ is the Dirac delta function. The last term in equation 2.4.9 represents outflow to the stream which is approximated in the form of a point sink. Note that this representation of the stream does not introduce the shape of the stream cross section explicitly. The shape of the stream is given implicitly by the condition $\phi = 0$. Because equipotentials near a sink are circular, the stream boundary will be practically circular in the transformed (y,z) system or elliptical in (x,z) when $w << L$.

With equations (2.4.7), (2.4.8), and (2.4.9), and the notation $\Phi \equiv dZ_\eta(\omega)$, $c \equiv dZ_\varepsilon(\omega)$, $q \equiv dZ_q(\omega)$, $y = (K_z/K_x)^{1/2}\, x$, $\ell = (K_z/K_x)^{1/2} L$, $N \equiv dZ_\eta(\omega)$ and system (2.4.1 - 2.4.6) becomes

$$\frac{\partial^2\Phi}{\partial y^2} + \frac{\partial^2\Phi}{\partial z^2} = 0 \tag{2.4.10}$$

$$i\omega n\Phi + K_z \frac{\partial\Phi}{\partial z} = c - \delta(y)q\,, \quad z = 0 \tag{2.4.11}$$

$$\Phi = N, \quad z = 0 \tag{2.4.12}$$

$$\frac{\partial\Phi}{\partial z} = 0, \quad z = -h_o \tag{2.4.13}$$

$$\frac{\partial\Phi}{\partial y} = 0, \quad y = \ell \tag{2.4.14}$$

$$\Phi = 0, \quad z = 0, \quad y = w' = w(K_z/K_x)^{1/2} \tag{2.4.15}$$

With symmetry about $y = x = 0$, the solution of the system equations (2.4.10 - 2.4.15) will be of the form

$$\Phi = \frac{a_o}{2} + \sum_{m=1}^{\infty} a_m \cos \lambda_m y \cosh \lambda_m (z+h_o) \tag{2.4.16}$$

which satisfies (2.4.10), (2.4.13) and (2.4.14) with $\lambda_m = m\pi/\ell$. Using the Fourier series representation of the delta function

$$\delta(y) \sim \frac{b_o}{2} + \sum_{m=1}^{\infty} b_m \cos \lambda_m y \ , \quad b_m = 1/\ell \tag{2.4.17}$$

equation (2.4.11) requires that

$$a_o = (2c - q/\ell) \ / \ (i\omega n) \tag{2.4.18}$$

$$a_m = - \ (q/\ell)(i\omega n \cosh \lambda_m h_o + K_z \lambda_m \sinh \lambda_m h_o)^{-1}, \ m > 0 \tag{2.4.19}$$

and from equation (2.4.15)

$$0 = \frac{a_o}{2} + \sum_{m=1}^{\infty} a_m \cos \lambda_m w' \cosh \lambda_m h_o \tag{2.4.20}$$

which, with equation (2.4.18), yields

$$a_o = \frac{4b\ell\sigma/K_z}{1 + i\ 2\xi\sigma}$$

$$\sigma = \sum_{m=1}^{\infty} \cos \lambda_m w' (m\pi \tanh \lambda_m h_o + i\xi)^{-1} \quad , \quad \xi = n\ell\omega/K_z \tag{2.4.21}$$

The complete solution for Φ then becomes, from equations (2.4.18), (2.4.19) and (2.4.21),

$$dZ_\phi \equiv \Phi \frac{2\ell b}{(1 + i2\xi\sigma)K_z} \left[\sigma - \sum_{m=1}^{\infty} \frac{\cosh \lambda_m(z+h_o)\cos \lambda_m y}{m\pi \sinh \lambda_m h_o + i\xi \cosh \lambda_m h_o}\right] \quad (2.4.22)$$

The generalized Fourier amplitudes of η are found from equation (2.4.22) with $z = 0$, $c = dZ_\varepsilon$ and equation (2.4.12) as

$$dZ_\eta(\omega,y) = dZ_\varepsilon(\omega) \frac{2\ell / K_z}{1 + i2\xi\sigma} \sum_{m=1}^{\infty} \frac{\cos \lambda_m w' - \cos \lambda_m y}{m\pi \tanh \lambda_m h_o + i\xi}$$

Thus following equation (2.1.19), the spectral density functions are related by

$$\frac{S_{\eta\eta}}{S_{\varepsilon\varepsilon}} \frac{K_x K_z}{4L^2} = G(\Omega, x/L, h_o/\ell, w/L)$$

$$= r^{-1} \sum_{m=1}^{\infty} A_m \sum_{m=1}^{\infty} A_m^* = r^{-1} \left[\left(\sum_{m=1}^{\infty} u_m\right)^2 + \left(\sum_{m=1}^{\infty} v_m\right)^2\right]$$

$$r = 1 - 4\xi\sigma_i + 4\xi^2(\sigma_r^2+\sigma_i^2) \ , \ \sigma = \sigma_r + i\sigma_i \ , \ \xi = \Omega h_o/\ell \ , \ \Omega = nL \ / K_x h_o$$

$$A_m = u_m + iv_m = \frac{\cos \lambda_m w' - \cos \lambda_m y}{m\pi \tanh \lambda_m h_o + i\xi} \quad (2.4.23)$$

The variable Ω is the equivalent of the dimensionless frequency variable used for the Dupuit aquifer when $n = S$ and $K_x h_o = T$. The sums in equa-

tion (2.4.23) were evaluated by digital computer; the series are convergent but several hundred terms may be required to obtain accuracy of a few per cent, especially when w/L is very small. Some typical results of the numerical evaluation are shown in Figures 2.28 and 2.29. Figure 2.28 shows, in a logarithmic form which is similar to that used in the Dupuit aquifer presentation, the effects of relative horizontal position in the aquifer; the trends are similar to those for the Dupuit aquifer. Note the G is related to the Dupuit aquifer response function, g by $G = (K_z/K_x)(L/h_o)^2\, g/4$. In Figure 2.29 the dependent variable $\psi = 4\Omega(h_o/\ell)^2 G$ is used because this is equivalent to the dependent variable $\Omega g(\Omega)$ for the Dupuit aquifer when $T = K_x h_o$ and $S = n$. This form of presentation provides a direct graphical indication of the importance of different frequencies in the transfer relationship $S_{hh}/S_{\varepsilon\varepsilon}$. Because ψ is proportional to $\omega S_{hh}/S_{\varepsilon\varepsilon}$ and

$$\overline{h^2} = \int_{-\infty}^{\infty} S_{hh}\, d\omega = 2 \int_{-\infty}^{\infty} \omega S_{hh}\, d\, \ell n\, \omega$$

the incremental area under the curves in Figure 4 directly represents the contribution of a given frequency to the total mean square fluctuation when the input accretion is represented by white noise ($S_{\varepsilon\varepsilon}$ = constant). Figure 2.29 illustrates the effects of the additional parameters for the Laplace aquifer (w/L, h_o/ℓ) in comparison with the Dupuit result. The response curves for the Laplace aquifer are seen to have shapes quite similar to the Dupuit aquifer but the amplitudes can differ significantly depending on the parameters. The trends indicated in Figure 2.29 are intuitively reasonable; an increase in the stream width (w/L) reduces

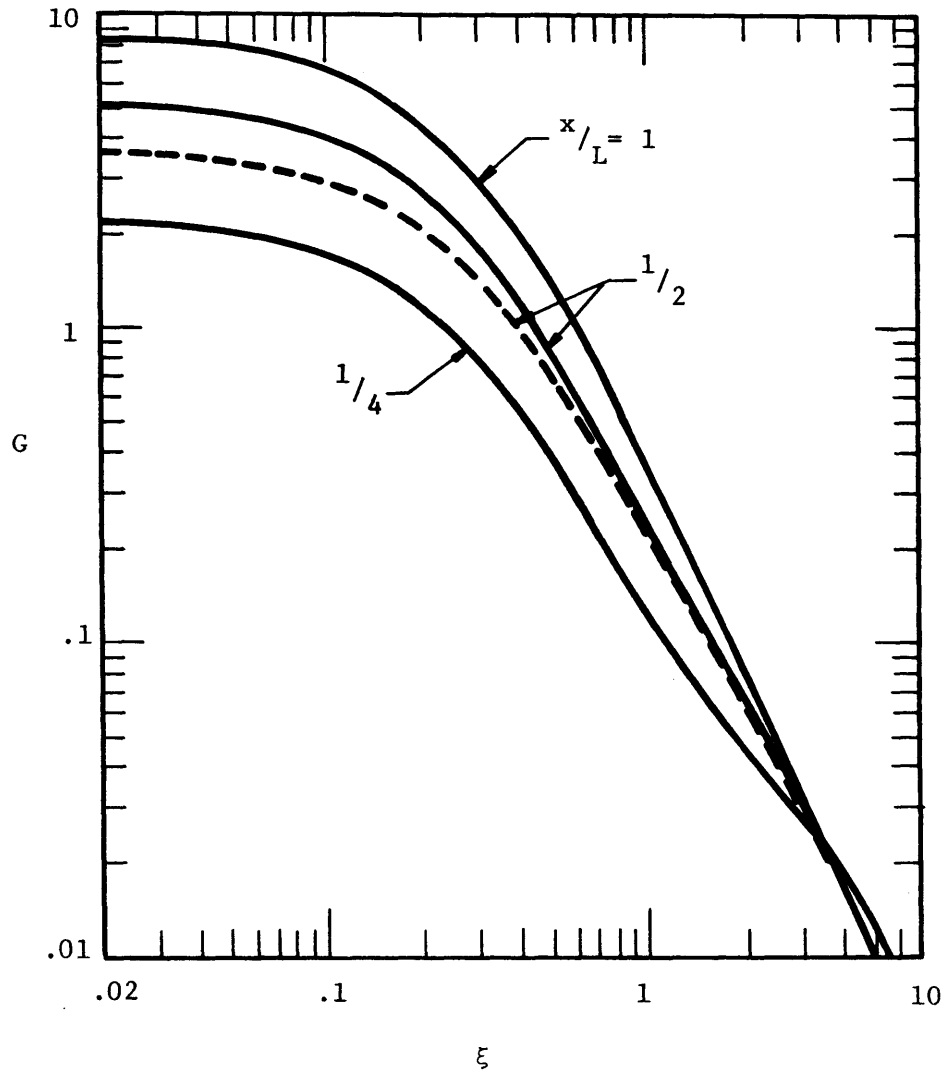

Figure 2.28 Spectral Response of the Laplace Aquifer; Solid Lines Represent the Laplace Aquifer with $h_o/\ell = 0.1$ $w/L = 0.01$ and the Dashed Lines the Dupuit Aquifer.

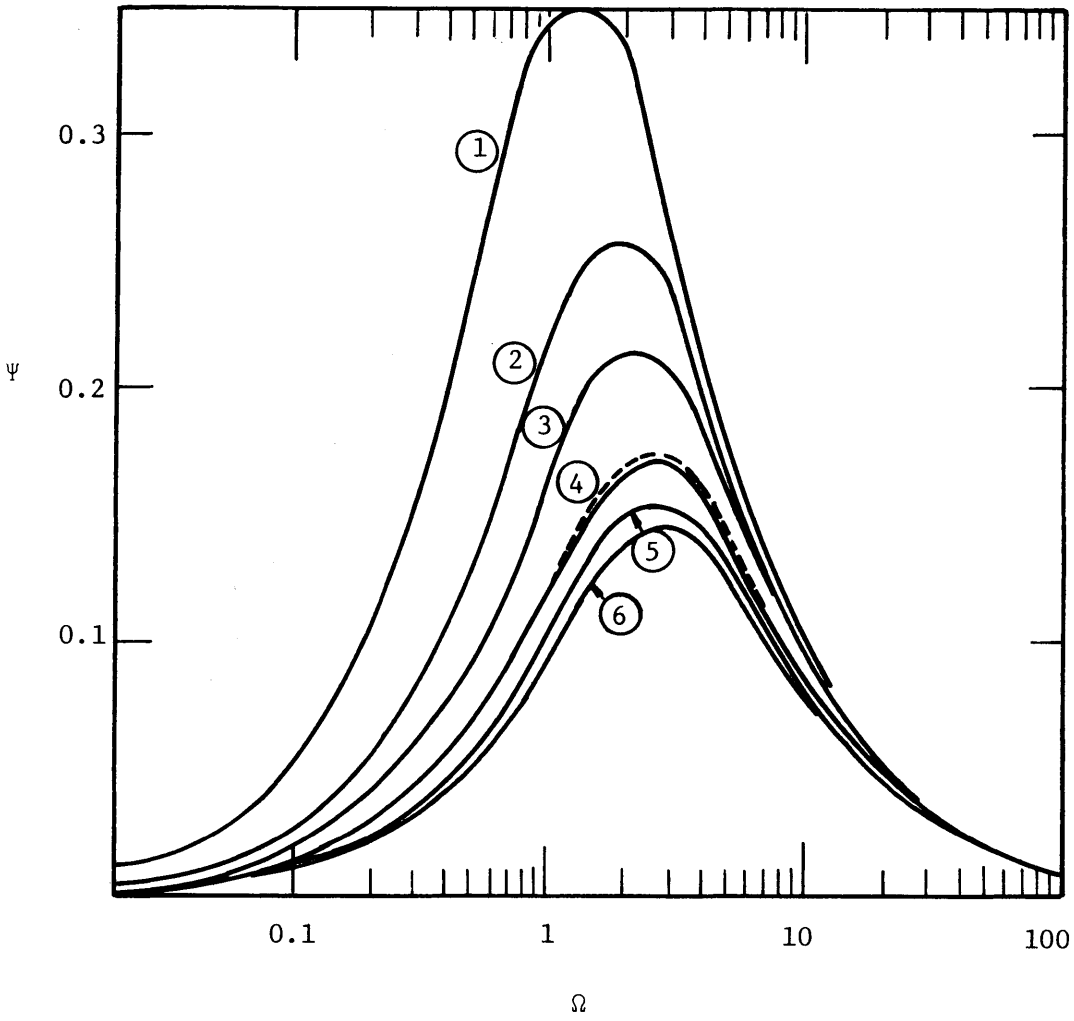

Figure 2.29 Laplace Aquifer Spectral Response at x/L = 1/2, where $\psi = 4\Omega(h_o/\ell)^2 G$ and $\Omega = \omega L^2 n/(K_x h_o)$; Curve 1, $h_o/\ell = 0.5$, w/L = 0.05; Curve 2, $h_o/\ell = 0.1$, w/L = 0.003; Curve 3, $h_o/L = 0.1$, w/L = 0.01; Curve 4, $h_o/\ell = 0.02$ and 0.0002, w/L = 0.01; Curve 5, $h_o/\ell = 0.1$, w/L = 0.05; and Curve 6, $h_o/\ell = 0.02$ and 0.002, w/L = 0.05. The Dashed Line Represents the Dupuit Aquifer (x/L = 1/2).

the amplitude of the fluctuations and an increase in the relative thickness of the aquifer (h_o/ℓ) increases the amplitude.

The rather significant differences between the Laplace and Dupuit aquifers for some values of the parameters may have some bearing on the applicability of the Dupuit approximation. However, no precise conclusions can be drawn because the boundary conditions for the Laplace aquifer problem, with a partially penetrating stream of finite width, and the Dupuit aquifer, with a fully penetrating stream, are not exactly equivalent. Based on previous work on deterministic problems, we would expect the Laplace and Dupuit aquifers to become equivalent when $h_o/\ell \ll 1$. From numerical solutions of nonlinear Dupuit and Laplace problems, Verma and Brutsaert (1971) found agreement when the length of the aquifer was four times its initial saturated thickness even with complete drawdown at the stream.

A careful analysis of the solution for the Laplace aquifer equation (2.4.23) in the limit $h_o/\ell \to 0$ shows that there is a finite limit for the function ψ depending on the parameter w/L. The results in Figure 2.29 reflect this feature for the cases w/L = 0.01 and 0.05. The function ψ becomes independent of h_o/ℓ when $h_o/\ell < 0.02$. It is seen that the Dupuit aquifer is equivalent to the Laplace aquifer with s/L = 0.01 when h_o/ℓ is very small.

In general, the results for the Laplace aquifer show that nonhydrostatic effects can be quite important in a natural system when the anisotropy K_x/K_z is large and the relative stream width w/L is very small.

2.5 Spatial Variability of Hydraulic Conductivity

In addition to the temporal fluctuations analyzed in the previous sections, there will be changes in the characteristics such as hydraulic conductivity or accretion from point to point within the aquifer. The analysis of spatial variability is considerably more complicated than the temporal phenomena because the variability appears in the coefficients in the equations and because the spatial statistics may not be homogeneous when influenced by boundary conditions. However, some insight can be developed by analyzing the effects of small spatial perturbations in an aquifer system for which spatially homogeneity is assured. Spectral techniques may then be applied in the wave number domain to evaluate some statistical features of the flow. The results of the analysis are applied to evaluate the errors in a flow-observation system in relation to the spatial variability of hydraulic conductivity.

We analyze the flow in a sloping aquifer governed by equation 2.3.1 and linearize by introducing the following quantities in terms of a mean and a small perturbation

$$h = \bar{h} + h'$$

$$y = h + \zeta = \bar{y} + y'$$

$$\zeta = \bar{\zeta} + \zeta'$$

$$\varepsilon = \bar{\varepsilon} + \varepsilon'$$

$$K = \bar{K} + K'$$

Neglecting all products of primed quantities, equation 2.3.1 reduces to

$$S \frac{\partial h'}{\partial t} = \frac{\partial}{\partial x} \left[\bar{K}\bar{h} \frac{\partial \bar{y}}{\partial x} + \bar{K}\bar{h} \frac{\partial \bar{y}'}{\partial x} + \bar{K} \frac{\partial \bar{y}}{\partial x} h' + \bar{h} \frac{\partial \bar{y}}{\partial x} K' \right] + \bar{\varepsilon} + \varepsilon' \qquad (2.5.1)$$

and since the mean of the primed quantities is zero, the mean flow is given by

$$\frac{\partial}{\partial x}\left(\bar{K}\bar{h}\frac{\partial \bar{y}}{\partial x}\right) + \bar{\varepsilon} = 0$$

The mean flow will be taken as one of constant depth $\bar{h} = h_o$ down an incline of constant slope $\beta(\zeta=\beta x)$, in which case $\bar{\varepsilon} = 0$ is implied. The flow configuration is depicted in Figure 2.30.

We consider the case of statistically homogeneous steady input perturbations which are represented by Fourier-Stieltjes integrals in wave number k, as follows:

$$\zeta' = \int_{-\infty}^{\infty} e^{ikx}\, dZ_\zeta(k),\quad K' = \int_{-\infty}^{\infty} e^{ikx}\, dZ_K(k),\quad \varepsilon' = \int_{-\infty}^{\infty} e^{ikx}\, dZ_\varepsilon(k) \qquad (2.5.2)$$

Similarly, the water level perturbation is represented by

$$y' = \int_{-\infty}^{\infty} e^{ikx}\, dZ_y(k) \qquad (2.5.3)$$

and upon substitution of these expressions, with $h' = y' - \zeta'$, into equation 2.5.1, we obtain the following relationship between the generalized Fourier amplitudes

$$dZ_y = \frac{ik\beta(h_o dZ_K - \bar{K} dZ_\zeta) + dZ_\varepsilon}{\bar{K}h_o k^2 - ik\bar{K}\beta} \qquad (2.5.4)$$

This result can be used to construct the wave number spectrum $\Phi_{yy}(k)$ of the water level fluctuations in terms of the spectra and cross spectra of the input perturbations. Because cross-spectral input information is lacking,

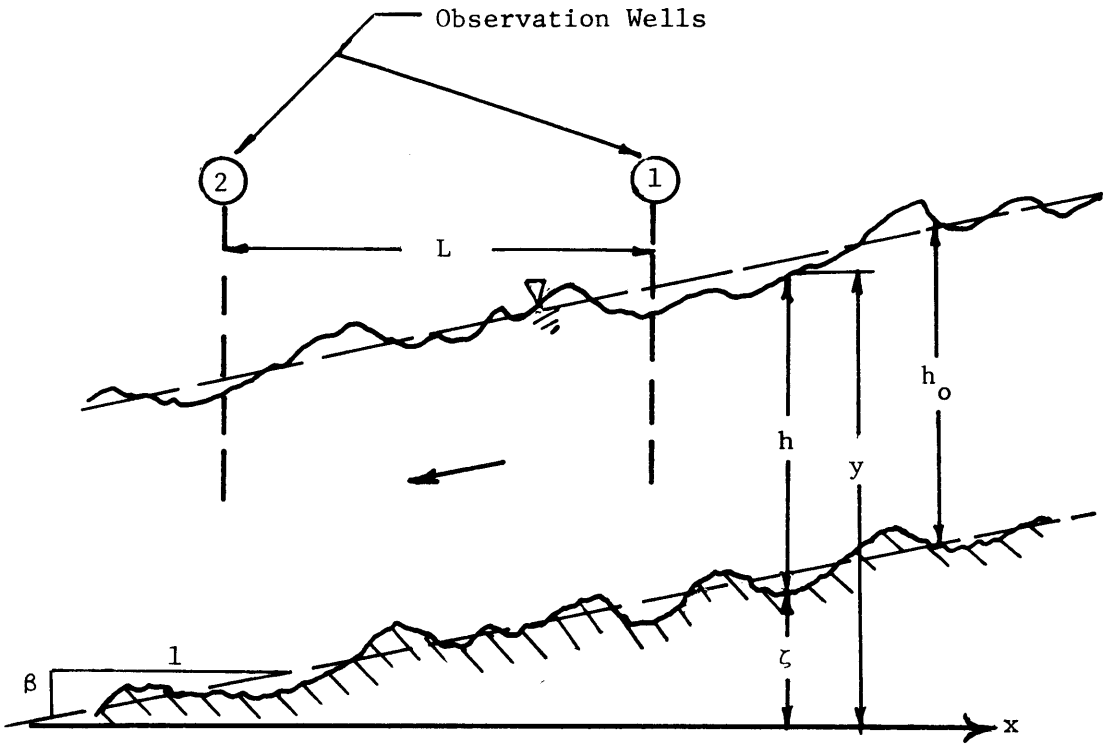

Figure 2.30 Sloping Aquifer with Spatial Variability

the behavior of the system will be evaluated in terms of a single input representing fluctuations of hydraulic conductivity. In this case equation 2.5.4 reduces to

$$dZ_y = \frac{ikh_o\beta}{Tk^2-ik\bar{K}\beta} dZ_K, \quad T = \bar{K}h_o \tag{2.5.5}$$

and following the equivalent of equation 2.1.5 in wave number space,

$$\Phi_{yy}(k) = \frac{(h_o\beta)^2}{T^2k^2+(\bar{K}\beta)^2} \Phi_{KK}(k) \tag{2.5.6}$$

where $\Phi_{KK}(k)$ is the wave number spectrum of the hydraulic conductivity fluctuations. In order to obtain explicit results Φ_{KK} must be given; for this analysis we will assume a simple exponential form for the autocovariance

$$R_{KK}(\xi) = E[K'(x+\xi)K'(x)] = \int_{-\infty}^{\infty} e^{ik\xi} \Phi_{KK}(k)\, dk = \overline{K'^2}\, e^{-|\xi|/\lambda} \tag{2.5.7}$$

where $\overline{K'^2}$ is the variance of K' and λ is the integral scale defined by

$$\lambda = \int_0^{\infty} (R_{KK}(\xi)/\overline{K'^2})\, d\xi$$

The integral scale indicates the average distance over which the conductivity is correlated. The spectrum Φ_{KK} is found from the inverse Fourier transform

$$\Phi_{KK}(k) = \frac{1}{2\pi} \int_{-\infty}^{\infty} e^{-ik\xi} R_{KK}(\xi) d\xi = \lambda\overline{K'^2}/(1+(k\lambda)^2)\pi \tag{2.5.8}$$

and the variance $\overline{y'^2}$ from

$$\overline{y'^2} = R_{yy}(0) = \int_{-\infty}^{\infty} \Phi_{yy}(k)dk$$

The integration using equations 2.5.6 and 2.5.8 yields

$$\overline{y'^2}/h_o^2 = (\overline{K'^2}/\bar{K}^2)\left[r/(1+r)\right] \qquad (2.5.9)$$

where $r = \beta\lambda/h_o$ is the ratio of a length scale for the conductivity fluctuations (λ) to a length scale of the aquifer (h_o/β). Since the slope of the phreatic surface is typically small ($\beta = 10^{-2}$ to 10^{-4}), this result indicates that the water level fluctuation relative to the aquifer depth will generally be much smaller than the relative conductivity fluctuation unless the integral scale is much larger than the aquifer depth.

Also of interest is autocovariance of y which is found by taking the Fourier transform of equation 2.5.6

$$R_{yy}(\xi) = \overline{y'^2}(e^{-\beta\xi/h_o} - re^{-\xi/\lambda})/(1-r) \qquad (2.5.10)$$

and the cross covariance of K and y

$$R_{Ky}(\xi) = E\left[K'(x+\xi)y'(x)\right] = \int_{-\infty}^{\infty} e^{ik\xi}\Phi_{Ky}(k)dk \qquad (2.5.11)$$

where Φ_{Ky} is the cross spectrum which is found, using equation 2.5.6 in the spatial equivalent of equation 2.1.21, as

$$\Phi_{Ky}(k) = \Phi_{KK}(k)(-ikh_o\beta)/(Tk^2+ik\bar{K}\beta)$$

This expression for Φ_{Ky}, with Φ_{KK} from equation 2.5.8, is used in equation

2.5.11 to find

$$R_{Ky}(\xi) = \overline{K'y'} \begin{cases} e^{-\xi/\lambda} , & \xi \geq 0 \\ \left[2e^{\beta\xi/h_o} - (1+r)e^{\zeta/\lambda}\right]/(1-r), & \xi \leq 0 \end{cases} \tag{2.5.12a}$$

$$\overline{K'y'} \equiv R_{Ky}(0) = -(\overline{K'^2}/\bar{K}^2)Tr/(1+r),$$

It can easily be shown that

$$R_{yK}(\xi) = E\left[y'(x+\xi)K'(x)\right] = R_{Ky}(-\xi) \tag{2.5.12b}$$

The various spectral and covariance functions for this system are shown in Figure 2.3.1 for r = 1/2.

The results of this analysis can be applied to evaluate the error structure of a simple two piezometer network which is to be used to estimate the amount of flow through an aquifer. Observation wells are used to measure the water levels y_1 and y_2 at two points a distance L apart as shown in Figure 2.3.0. In addition, two essentially point observations of hydraulic conductivity (K_1, K_2) are available (say, from well pumping tests or cores) at the two wells. An estimate of the flow per unit width of aquifer, $\hat{Q}$, is obtained from the Darcy equation in the form

$$\hat{Q} = \frac{K_1+K_2}{2} \; \frac{h_1+h_2}{2} \; \frac{y_1 - y_2}{L} \tag{2.5.13}$$

and by introducing mean plus perturbation quantities in equation 2.5.13

$$\hat{Q} = \bar{K}h_o\beta + \beta h_o(K_1'+K_2')/2 + \bar{K}\beta(h_1'+h_2')/2 + \bar{K}h_o(y_1'-y_2')/L \tag{2.5.14}$$

where $(\bar{y}_1-\bar{y}_2)/L = \beta$, $\bar{h}_1 = \bar{h}_2 = h_o$, $\bar{K}_1 = \bar{K}_2 = \bar{K}$. The term $\bar{K}h_o\beta$ is the

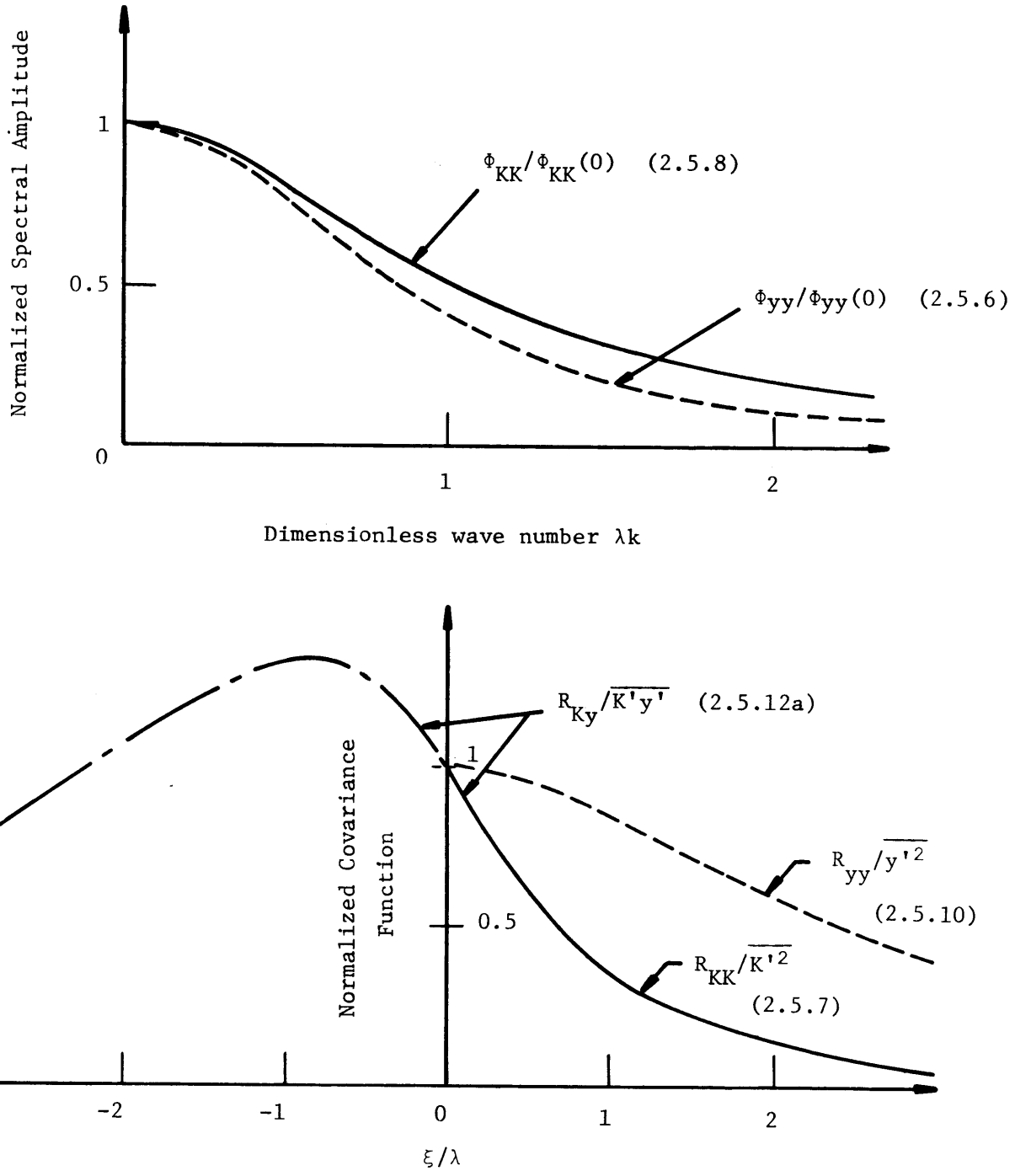

Figure 2.31 Normalized Spectral and Covariance Functions for r = 1/2

actual flow Q through the aquifer and the difference $Q' = \hat{Q}-Q$, when squared and averaged, yields

$$\overline{Q'^2}/Q^2 = (\overline{K'^2}+\overline{K_1'K_2'})/(2\bar{K}^2) \qquad [\text{I conductivity variation}]$$

$$+ 2(\overline{y'^2}-\overline{y_1'y_2'})/(L\beta)^2 \qquad [\text{II surface slope variation}]$$

$$+ (\overline{y'^2}+\overline{y_1'y_2'})/2h_o^2 \qquad [\text{III depth variation}]$$

$$+ (\overline{K_2'y_1'} - \overline{K_1'y_2'})/(\beta\bar{K}L) \qquad [\text{IV surface slope-conductivity correlation}]$$

$$+ (2\overline{K'y'} + \overline{K_1'y_2'} + \overline{K_2'y_1'})/(2\bar{K}h_o) \qquad [\text{V depth-conductivity correlation}]$$

(2.5.15)

where statistical homogeneity has been used, i.e.,

$$\overline{K_1'^2} = \overline{K_2'^2},\ \overline{y_1'^2} = \overline{y_2'^2},\ \overline{y_1'y_2'} = \overline{y_2'y_1'}$$

The origin of each of the terms in equation 2.5.15 is indicated on the right. Using the previous results for the covariances of the terms in equation 2.5.14 can be expressed in terms of $\overline{K'^2}/\overline{K^2}$. Noting the following identities

$$\overline{K_1'K_2'} \equiv R_{KK}(L) \qquad [\text{equation 2.5.7}]$$

$$\overline{y_2'} \equiv R_{yy}(0) \qquad [\text{equation 2.5.9}]$$

$$\overline{y_1'y_2'} \equiv R_{yy}(L) \qquad [\text{equation 2.5.10}]$$

$$\overline{K_2'y_1'} \equiv E[y'(x+L)K'(x)] = R_{yK}(L) = R_{Ky}(-L) \qquad [\text{equations 2.5.12 a \& b}]$$

$$\overline{K_1'y_2'} \equiv E[K'(x+L)y'(x)] = R_{Ky}(L) \qquad [\text{equation 2.5.12a}]$$

$$\overline{K'y'} \equiv R_{Ky}(0) \qquad [\text{equation 2.5.12a}]$$

and using the indicated equations, the expression for the relative mean square error becomes

$$
\begin{aligned}
Q'^2/Q^2 = (K'^2/K^2)\{ & (1+e^{-L/\lambda})/2 && [I]\\
& + (2h_o/\beta L)(\lambda/L)\left[1-e^{-rL/\lambda}-r(1-e^{-L/\lambda})\right]/(1-r^2) && [II]\\
& + r\left[1+e^{-rL/\lambda}-r(1+e^{-L/\lambda})\right]/2(1-r^2) && [III]\\
& - (2\lambda/L)(e^{-rL/\lambda}-e^{-L/\lambda})/(1-r^2) && [IV]\\
& - r((1-r)+e^{-rL/\lambda}-re^{-L/\lambda})/(1-r^2)\} && [V]
\end{aligned}
$$

(2.5.16)

where the origin of each of the terms is identified as in equation 2.5.16.

The application of these results is illustrated by considering several different values of piezometer spacing in an aquifer with a specified integral scale of the hydraulic conductivity variations (λ = 100ft). The parameters for the example and the numerical results are given in Table 2.2. Several important features are apparent from these numerical results. The variance of the estimated flow rate is substantially smaller than the variance of the hydraulic conductivity. This is because the phreatic surface slope-conductivity correlation (IV) nearly compensates for the variance of conductivity (I) and phreatic surface slope (II). In addition, counter to ones likely intuition for this case, the error is seen to be smallest for the smallest well spacing. This is because the compensatory effect of the slope-conductivity correlation is greatest for the smallest spacing. This analysis does not, of course, consider the limitations of

Well Spacing	L - ft	10	100	1000
Contributions to the Relative Variance Ratio $\overline{(Q'^2/Q^2)}/\overline{(K'^2/K^2)}$	I	0.95	0.68	0.50
	II	0.95	0.72	0.16
	III	0.02	0.02	0.02
	IV	- 1.86	- 1.23	- 0.16
	V	- 0.04	- 0.04	- 0.04
Total $\overline{(Q'^2/Q^2)}/\overline{(K'^2/K^2)}$		0.02	0.16	0.48

Parameters: h_o = 50ft, $\beta = 10^{-2}$, λ = 100ft, $r = 2 \times 10^{-2}$

TABLE 2.2 Errors in Flow Estimates for Several Observation Well Spacings

the device used to measure the water levels; such considerations would determine the minimum spacing that is appropriate for a specific application. If a normal distribution is assumed for Q' and $\overline{K'^2}/\overline{K^2}$ is known, the probability that Q is within a specified range can be estimated from results of the type in Table 2.2.

Although the simple analysis developed in this section can be used to evaluate elementary flow observation networks, it is probably more important in terms of the insight it provides on the general problem of spatial variability in subsurface flows. It illustrates the importance of spatial correlation structure. Some other problems that should be investigated in future studies of this general area are systems with simultaneous temporal and spatial variability, multi-dimensional spatial

variability, and the effects of large amplitude fluctuations of hydraulic conductivity.

2.6 The Unsaturated Zone

The natural temporal variability of groundwater recharge or accretion is a function of precipitation subject to several complicated moderating influences. The modification occurs at the ground surface and in the unsaturated zone above the water table. In a simple view of the rainfall-runoff-infiltration process a certain portion of the precipitation (P) runs off as overland flow, while the remainder infiltrates into the soil and/or is subject to evaporation and transpiration. Some of the water which enters the soil moisture phase of the unsaturated zone eventually percolates down to the water table. The rate at which it enters the saturated zone is described by the term accretion (ε). In considering the unsaturated zone we are concerned with this process of infiltration, evapotranspiration, percolation and, additionally, soil moisture storage. Because unsaturated soils have a certain portion of air-filled pores they can store additional water. Similarly, water can drain from formerly saturated pores to deplete storage and supply additional water for evapotranspiration or accretion.

The resulting system can be schematized as in figure 2.32. In this system the net infiltration is $I = P - E - R_0$ where E is evapotranspiration and R_0 is the runoff. The net infiltration enters the soil moisture zone where it is stored and eventually percolates through to the groundwater as accretion, ε. The amount of stored moisture is

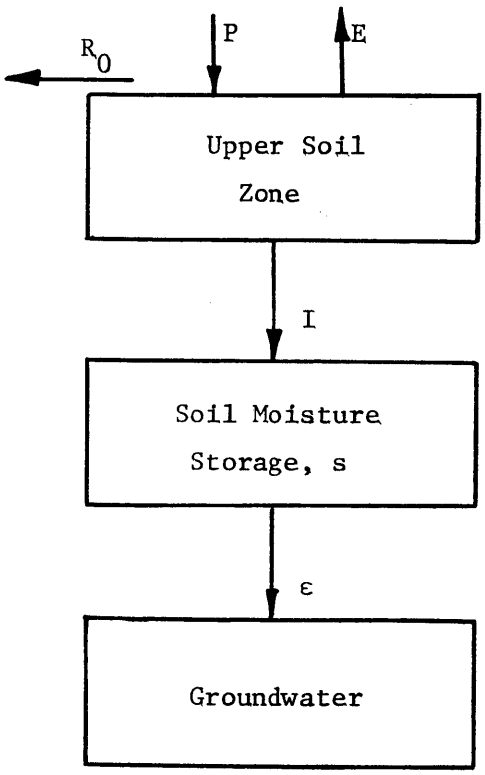

Figure 2.32 Schematic of the Unsaturated Zone

denoted by s. From a mass balance of water the change in storage is given by

$$\frac{ds}{dt} = I - \varepsilon \qquad (2.6.1)$$

where the accretion outflow to the groundwater will be a function of stored moisture. Consider the accretion outflow to be represented by

$$\varepsilon = a'(s-s_0) \qquad (2.6.2)$$

where a' is an outflow constant and s_0 is the minimum moisture storage. Then the soil moisture storage is represented as a lumped parameter linear reservoir system, in which the vertical and horizontal spatial

variability of stored moisture has been neglected.

The total stored moisture is given by

$$s = \int_0^b \theta dz \qquad (2.6.3)$$

where θ is the moisture content, z is a vertical coordinate (positive downward) and b is the depth from the surface to the water table. The minimum moisture storage is given by

$$s_0 = \int_0^b \theta_r dz$$

where θ_r is, say, field capacity.

The representation of the soil moisture zone as a lumped parameter linear reservoir can be established by comparing this simple system to a more complicated spatially distributed system. For example, a common problem encountered in irrigation is the vertical drainage of a soil column to a stationary water table. If the soil column is initially saturated ($s = nb = s_n$) and is then allowed to drain, the total volume of outflow as a function of time results from the solution of the partial differential equation for Darcy type flow in an unsaturated porous medium (Bear, 1972)

$$\frac{\partial \theta}{\partial t} = \frac{\partial}{\partial z}\left[-K(\theta)\left(\frac{\partial z}{\partial \theta} + \frac{\partial \eta}{\partial \theta}\right)\frac{\partial \theta}{\partial z}\right] \qquad (2.6.4)$$

where $\eta = -p/\gamma$, $\phi = -(z+\eta)$, with initial and boundary conditions

$$\theta = n \qquad \theta \leq z \leq b \qquad t = 0$$

$$\theta = n \qquad z = b \qquad t > 0$$

$$\frac{\partial \theta}{\partial z} = \text{constant} \qquad z = 0 \qquad t > 0$$

The last boundary condition is a linearized approximation of a no flux condition, $\partial\phi/\partial z = 0$, $z = 0$. Retaining only the first term of the series solution to this problem and integrating over z, the total volume of outflow from the column as a function of time is (Swartzendruber, 1969)

$$\frac{\Psi(t)}{\Psi_\infty} \simeq 1 - \left(\frac{32}{\pi^3}\right) e^{-\left(\frac{\pi}{2b}\right)^2 Nt} \qquad (2.6.5)$$

where $\Psi(t) = s_n - s(t)$, $\Psi_\infty = \Psi(t \to \infty)$, $N = -K(\theta)(\partial z/\partial\theta + \partial\eta/\partial\theta) = -K(\theta)\cdot\partial z/\partial\theta + D(\theta)$, and $D(\theta)$ is the soil moisture diffusivity. The solution assumes N to be a constant. This exponential relationship for outflow has a reasonable experimental basis (Youngs, 1960 and Gardner, 1962) and is also characteristic of the outflow from a linear reservoir.

For the particular soil moisture model of this section, under the equivalent conditions of drainage

$$s = s_n \qquad t = 0$$
$$I = 0 \qquad t > 0$$

the solution of equations 2.6.1 and 2.6.2 is

$$(s - s_0) = (s_n - s_0)\, e^{-at} \qquad (2.6.6)$$

The total volume of outflow for the linear reservoir model is $\Psi = s_n - s(t)$ or $\Psi = (s_n - s_0)(1-e^{-at})$. As $t \to \infty$, $\Psi \to \Psi_\infty = s_n - s_0$. Thus,

$$\frac{\Psi}{\Psi_\infty} = (1 - e^{-at}) \qquad (2.6.7)$$

and the linear reservoir (2.6.7) and distributed soil moisture models (2.6.5) have equivalent outputs since $32/\pi^3$ is near unity, where the outflow constant is given by

$$a' = \frac{\pi^2 N}{4b^2} \tag{2.6.8}$$

Thus a linear reservoir can be used to approximate the storage and release of moisture in the unsaturated zone.

The amount of net infiltration is given by $I = P - E - R_0$, and if I, P and E are considered as random stationary processes (the R_0 variability will be neglected) the fluctuation of infiltration about the mean is given by $I' = P' - E'$, with the spectral relationship

$$S_{II}(\omega) = S_{PP}(\omega) - S_{PE}(\omega) - S_{EP}(\omega) + S_{EE}(\omega) \tag{2.6.9}$$

An analysis identical to the linear reservoir (see Section 2.2) yields from equation 2.6.1 and 2.6.2,

$$S_{\varepsilon\varepsilon} = a'^2 S_{II}/(\omega^2+a'^2) \tag{2.6.10}$$

if the accretion and soil moisture storage are considered to be stationary random processes.

For precipitation input only ($S_{II} = S_{PP}$) the effect of the unsaturated zone can be studied by examining the square of the amplitude of the normalized transfer function of precipitation to aquifer response. In this case (equation 2.2.9 with H = constant)

$$S_{hh} = S_{\varepsilon\varepsilon}/(\omega^2 S^2+a^2) \tag{2.6.11}$$

where S is storativity and a is the linear reservoir constant for the aquifer. The transfer function is (equations 2.6.10 - 2.6.11)

$$\frac{S_{hh}}{S_{PP}} = \frac{a'^2}{(\omega^2 S^2+a^2)(\omega^2+a'^2)}$$

or, in normalized terms

$$g = T^2 S_{hh}/L^2 S_{PP} = \frac{A^2}{(\Omega^2+\beta^2)(\Omega^2+A^2)} \qquad (2.6.12)$$

where $a = \beta T/L^2$, $\Omega = SL^2\omega/T$, $A = (L^2N/b^2T)\beta' S$ and $a' = \beta' N/b^2$. For the linear reservoir aquifer $\beta = 3$ (see Section 2.7) while for the unsaturated zone $\beta' = \pi^2/4$ (equation 2.6.8). Reasonable values of the other parameters are in the range: $L/b \cong 100$, $N/T \cong .003$, and $S = .25$, or, say, $A^2 = 65$.

Relative to its value at $\Omega = 0$ the transfer function is

$$g(\Omega)/g(0)\big|_I = A^2\beta^2/((\Omega^2+\beta^2)(\Omega^2+A^2)) \qquad (2.6.13)$$

This is compared to the transfer function for the case which ignores storage in the unsaturated zone (equation 2.6.11 where $S_{PP} = S_{\varepsilon\varepsilon}$)

$$g(\Omega)/g(0)\big|_{II} = \beta^2/(\Omega^2+\beta^2) \qquad (2.6.14)$$

in Figure 2.33. There is no significant difference of the response for the two cases in the lower frequency range. It is only as the dimensionless frequency (Ω) approaches a value of 10 that the response of the

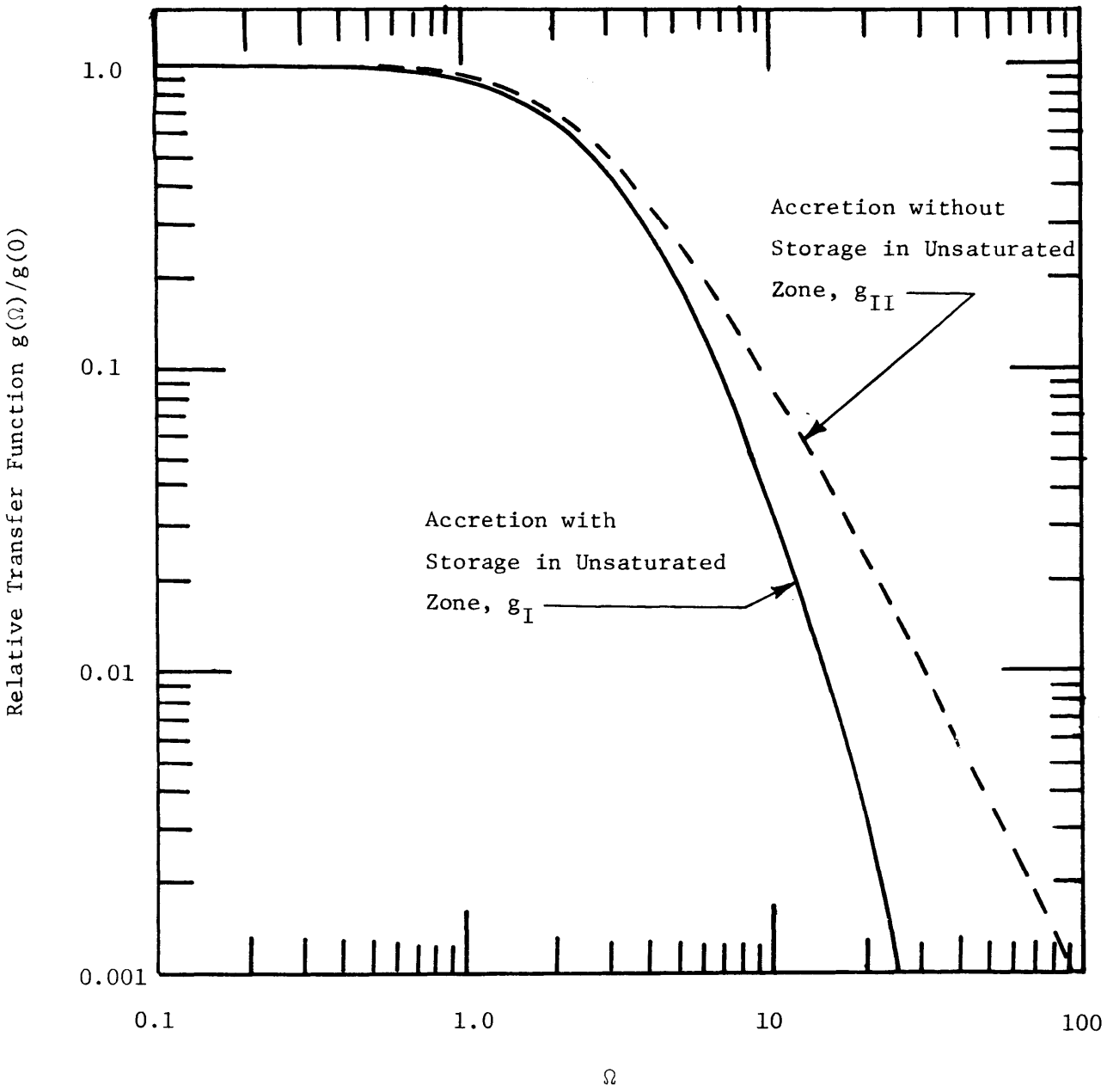

Figure 2.33 Comparison of the Groundwater Linear Reservoir in Response to Accretion with and without Storage in the Unsaturated Zone.

simple system ignoring the soil moisture storage (g_{II}), deviates. At $\Omega = 10$ this deviation is only 5% of the response function g(0). Some of the high frequency fluctuation of the precipitation is filtered out by the soil moisture storage, which supplies water to the groundwater table more uniformly than precipitation supplies water to the soil. This mechanism has been observed deterministically in the field and laboratory (Freeze and Banner, 1970). Because, however, the deviations are associated only with low energy, high frequency fluctuations, the distortion of the input due to the presence of the unsaturated zone, can be considered quite small for the range of frequencies of interest when monthly data are used, as in Chapter 4. If smaller sampling interval is used the distrotion would become more significant.

Although the effect of soil moisture storage can be neglected, it is important to consider what the effect of evapotranspiration may be on the accretion input. Evapotranspiration removes water from the surface and upper soil layers that would otherwise infiltrate or produce runoff. Thus, in the simplest form the net accretion can be expressed as a fraction of precipitation

$$\varepsilon = \gamma P$$

where the proportionality coefficient is a constant. This is the form of accretion input from precipitation records that is used in Chapters 3 and 4. More realistic estimates may be based on a deterministic variation of $\overline{\gamma}$ with seasonal fluctuations, or perhaps, the spectral relationship of the net infiltration to E as well as P. Future research can be directed toward this last suggestion. Since temperature records

are widely available, assume that the net evapotranspiration can be estimated from temperature data alone. For example, the Thornthwaite method utilizes a power law relationship for estimating E as a function of temperature (Thornthwaite, 1948). In the present case assume that

$$E = a + bT$$

where T is temperature, a stationary random process, and a and b are constants. Then

$$S_{EE} = b^2 S_{TT}$$

and the spectrum for the net infiltration can be found from

$$S_{II} = S_{PP} - bS_{PT} - bS_{TP} + b^2 S_{TT}$$

In field applications the spectra on the right-hand side can be estimated from an analysis of evapotranspiration data (b), temperature (S_{TT}), and precipitation (S_{PP}) records (plus S_{PT}, S_{TP}). The net infiltration (S_{II}) can then be used as an input to the soil moisture-groundwater system. This procedure should be investigated in future research.

2.7 Discussion

Earlier in this chapter, we developed several different models to approximate the spectral response for a phreatic aquifer in the frequency domain. They are (i) the linear reservoir model, in which no spatial variation has been considered; (ii) the linearized Dupuit approximation, in which we have assumed $K h_o = T$, a constant; (iii) the coupled-system

of the linear reservoir and the Dupuit aquifer, in which we have looked at the interaction between the said systems; (iv) "Zone Thickening Effect", in which we have retained some nonlinear effect by employing a perturbation type solution and (v) the Laplace aquifer which includes the effects of vertical flow. The linearized Dupuit approximation is probably the most widely applicable model because it is simple but retains a certain degree of physical reality.

One would expect that the linear reservoir model is comparable to the spatial average of the linearized Dupuit aquifer with horizontal bottom. Taking the spatial average of equation 2.3.6, we have

$$< h'(x,t) > = \int_{-\infty}^{\infty} e^{i\omega t} \frac{1}{L} \int_{0}^{L} dZ_h(x,\omega)\, dx \qquad (2.7.1)$$

Then it can be shown that the spectral response of the spatial average of the aquifer is given by

$$S_{<h><h>} = [\frac{\tanh bL}{bL}][\frac{\tanh bL}{bL}]^* S_{HH} + \frac{i}{\omega S}[\frac{\tanh bL}{bL} - 1][\frac{\tanh bL}{bL}]^* S_{\varepsilon H}$$

$$- \frac{i}{\omega S}[\frac{\tanh bL}{bL} - 1]^*[\frac{\tanh bL}{bL}] S_{H\varepsilon}$$

$$+ \frac{1}{\omega^2 S^2}[\frac{\tanh bL}{bL} - 1][\frac{\tanh bL}{bL} - 1]^* S_{\varepsilon\varepsilon} \qquad (2.7.2)$$

Compared to equation 2.2.9 of the linear reservoir model, we can expect some kind of equivalence between the two forms of the response function, i.e., $\frac{a^2}{\omega^2 S^2 + a^2}$ and $[\frac{\tanh bL}{bL}][\frac{\tanh bL}{bL}]^*$ for the input series H, and

$\frac{1}{\omega^2 S^2 + a^2}$ and $[\frac{\tanh bL}{bL} -1][\frac{\tanh bL}{bL} -1]^*$ for the input series ε. Taking a in the form of $a = \beta_o T/L$ where β_o is a numerical constant,

$$\frac{a^2}{\omega^2 S^2 + a^2} = \frac{1}{[1+(\Omega/\beta_o)^2]} \qquad (2.7.3)$$

and

$$\frac{1}{\omega^2 S^2 + a^2} = \frac{1}{\omega^2 S^2}[\frac{1}{1+(\beta_o/\Omega)^2}] \qquad (2.7.4)$$

By employing the least square method, $\beta_o = 2.722$ with the sum of squares = 0.00955 for the series H, and $\beta_o = 3.021$ with the sum of squares = 4.712×10^{-4} for the series ε. These two comparisons are shown in Figures 2.34 and 2.35 . These values of β_o can be compared with those by Gelhar (1974) for a steady state ($\beta_o = 3$) and for a falling sinusoidal water table ($\beta_o = \pi^2/4 = 2.467$).

The above analysis shows that the linear reservoir model can provide crude overall estimates for the spectral response of a phreatic aquifer. The linearized Dupuit approximation is a more realistic model for obvious reasons. However, in applying the linearized Dupuit approximation, care has to be taken about the bottom geometry and the degree of nonlinearity. In particular for the bottom slope, if β satisfied equation 2.3.14, we have T = constant which is required to use the linearized theory. However, judging by the figures 2.3 - 2.8, if the value of Γ is larger than 0.1, the effect of the sloping bottom begins to show.

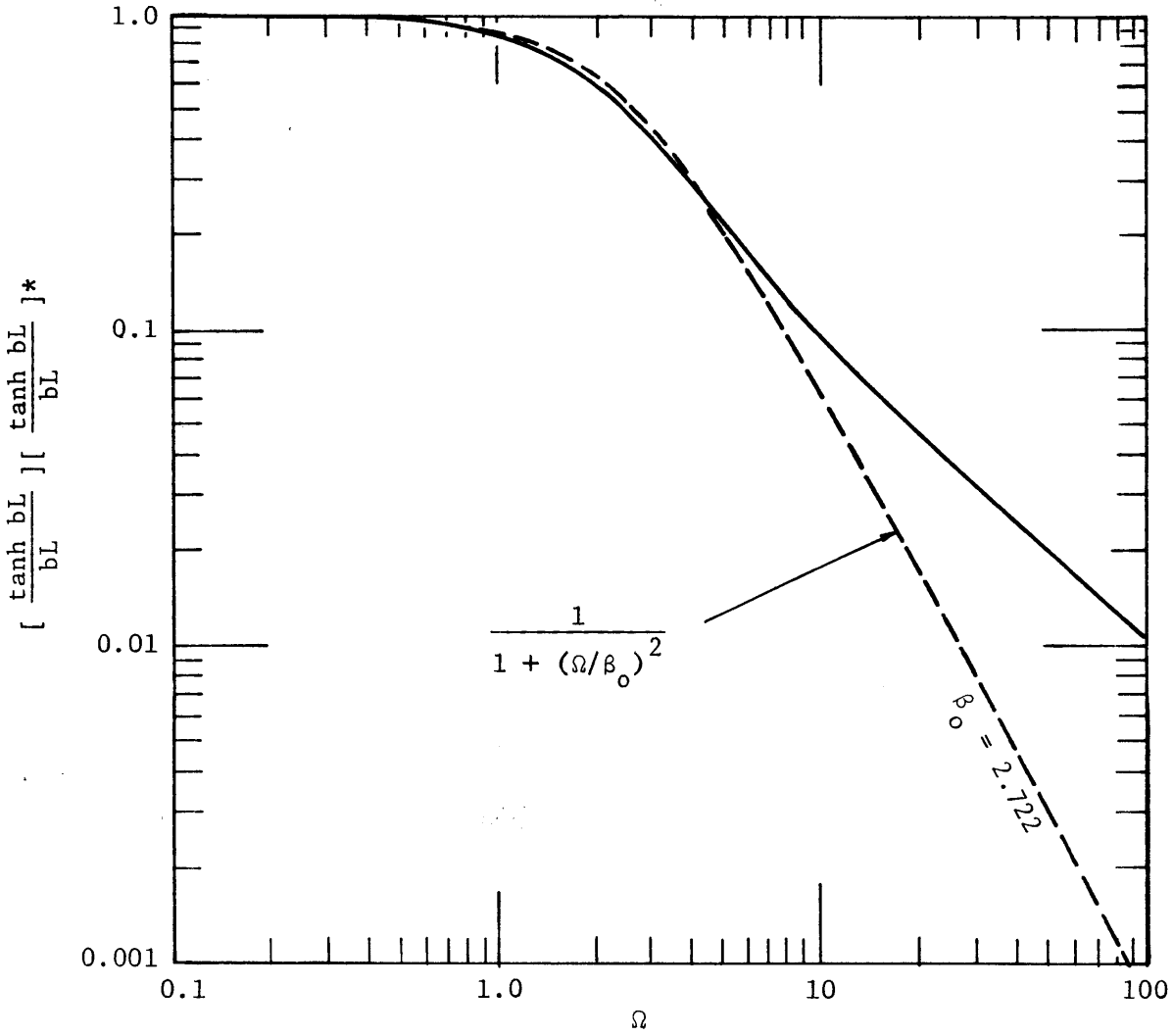

Figure 2.34 Comparison of the Linear Reservoir and the Spatial Average of the Linearized Dupuit Aquifer for the Input Series H.

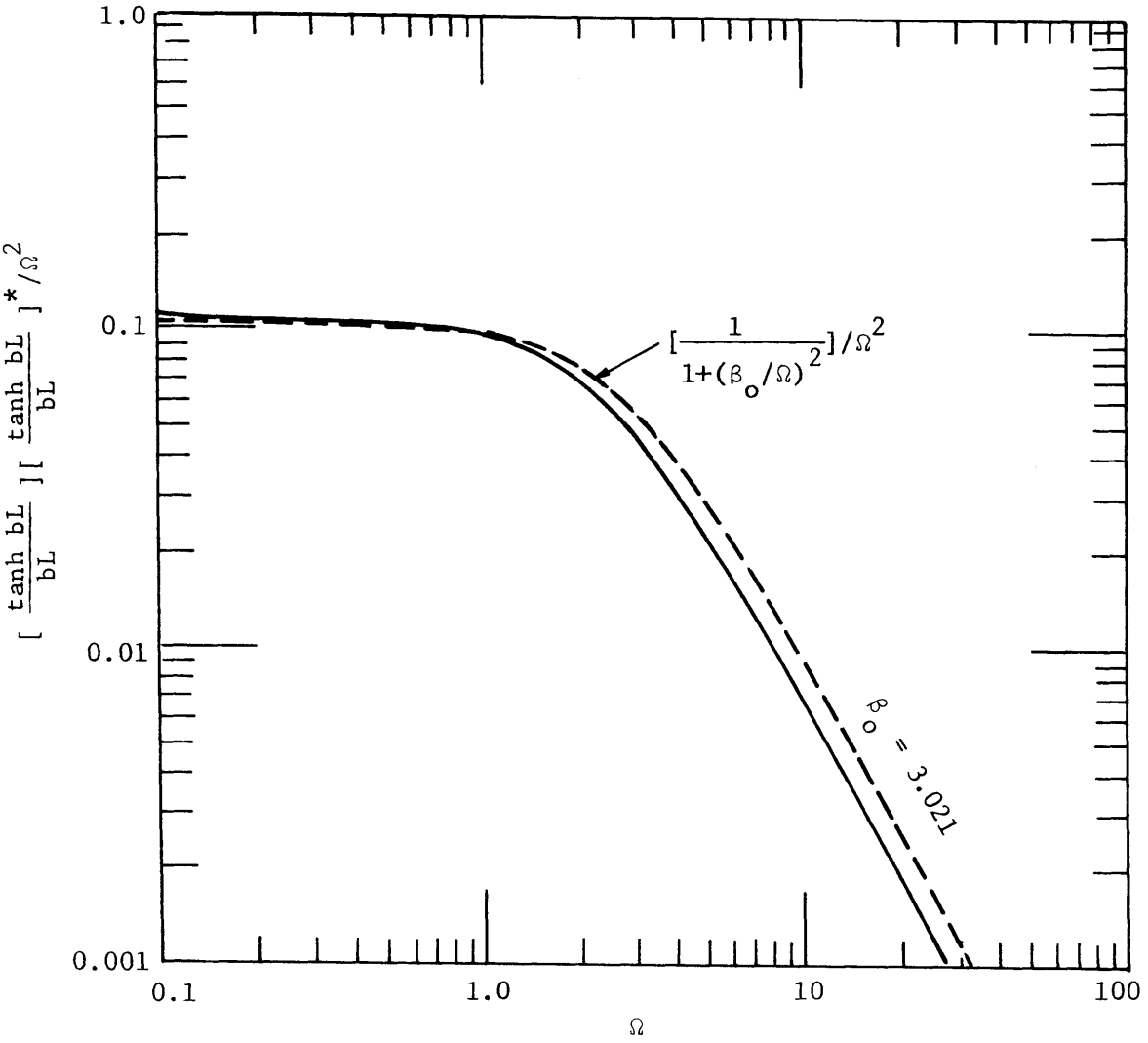

Figure 2.35 Comparison of the Linear Reservoir and the Spatial Average of the Linearized Dupuit Aquifer for the Input Series ε.

For the "Zone Thickening Effect", the value of $\mu = \varepsilon L^2/2K\bar{H}^2$ measures the degree of nonlinearity of the system due to accretion, and is also a function of the aquifer parameters. However, for the value of μ up to 0.1, the nonlinear effect is not too important in the low frequencies and is not felt in the high frequencies. The comparisons between these effects are shown in figures 2.36 and 2.37 for $x/L = 0.5$. They are the forms for the horizontal bottom to be used in the data analysis later in Chapter 4.

If a surface water reservoir, e.g., a lake or a reservoir, is present, the coupled-system of the linear reservoir and the Dupuit aquifer can then be used. Under the assumption that accretion is uniform in space, the spectral response of a phreatic aquifer is completely determined by the accretion. Also by knowing the response of the surface water reservoir, we can estimate the aquifer response by means of equation 2.3.25. However, we have to estimate two parameters, namely aL^2/α and SL/ℓ, the ratio of the response time and the ratio of water mass of the two systems respectively. The combination of these two parameters characterizes the spectral response along the aquifer. For example, in figure 2.13, the combination of $aL^2/\alpha = 1$ and $SL/\ell = 5$ resulted in a spectral response almost uniform along the aquifer.

The analysis of the Laplace aquifer indicates that vertical flow effects can produce significant differences between the spectral response of the Dupuit and Laplace aquifers. As shown in figure 2.29, even for very shallow aquifers ($h_o/\ell < 0.02$), there can be differences depending on the relative stream width w/L. When $w/L = 0.01$ and h_o/ℓ

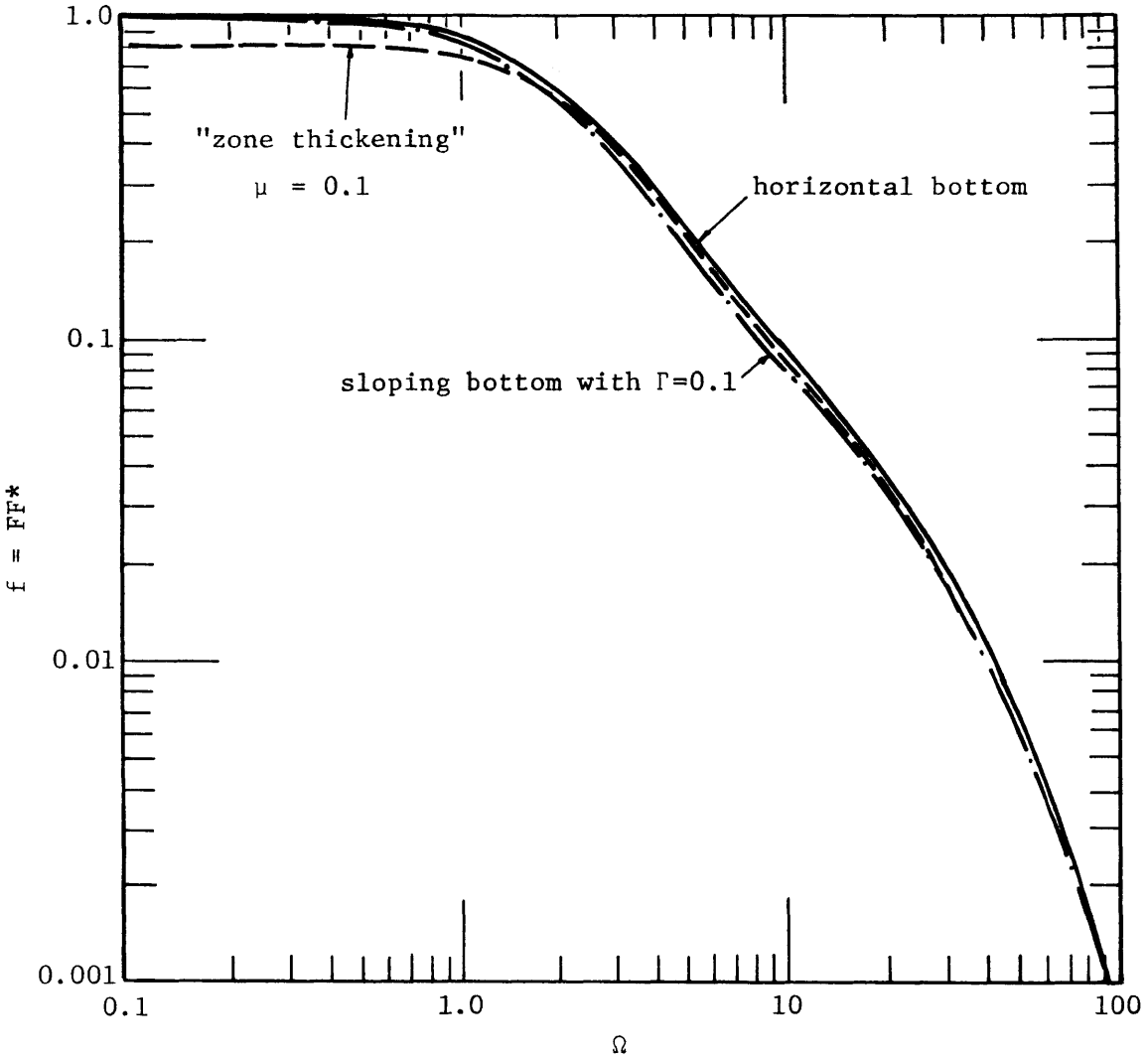

Figure 2.36 Comparison Between the Horizontal Bottom, the Sloping Bottom and the "zone thickening" Effects for the Input Series H, the Stream Stage, at x/L = 0.5.

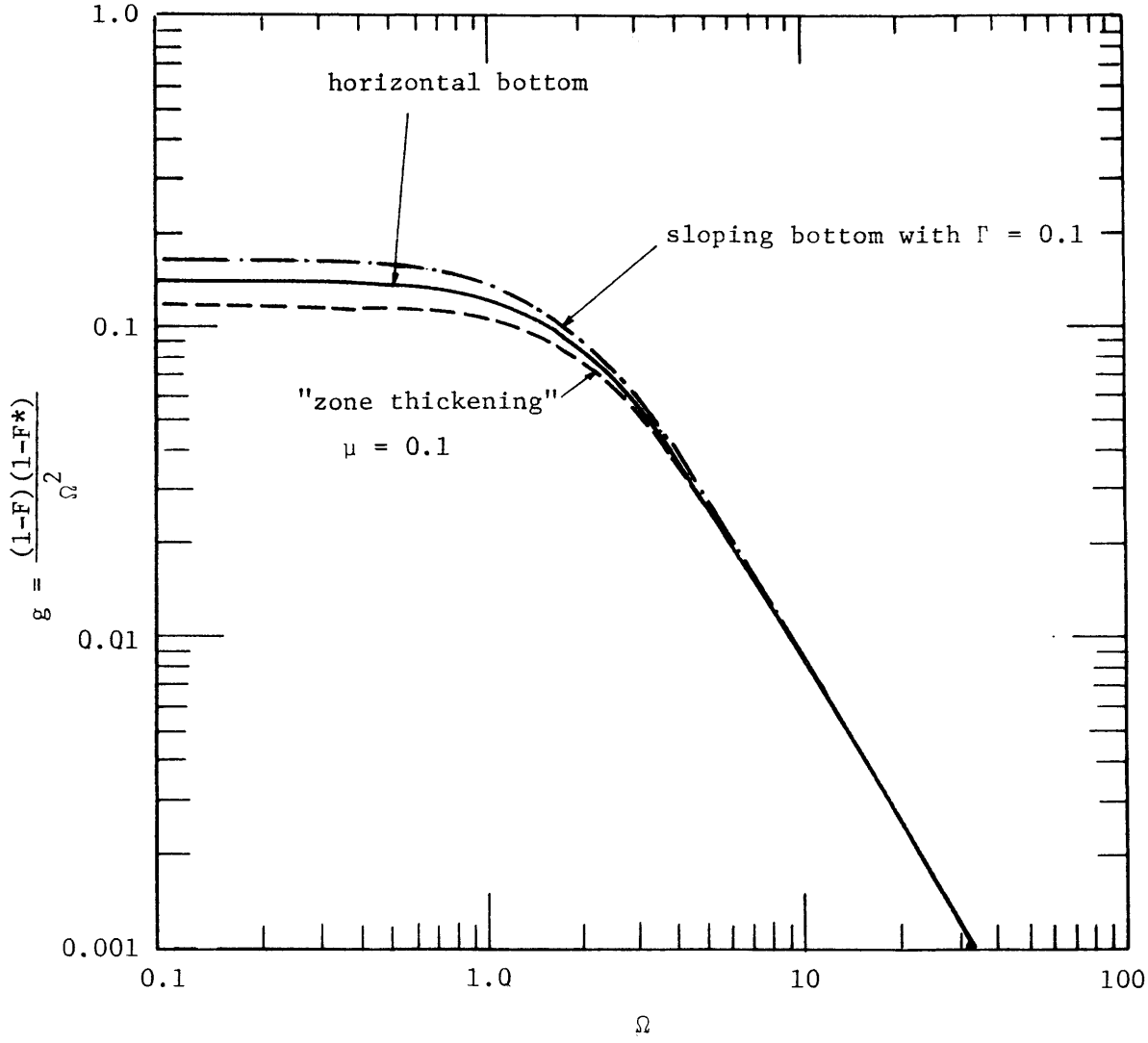

Figure 2. 37 Comparison Between the Horizontal Bottom, the Sloping Bottom and the "zone thickening" Effects For the Input Series ε, the Accretion, at x/L=0.5.

small, the Dupuit and Laplace aquifers are practically equivalent but for other values there are differences. The Laplace aquifer result will be more appropriate for many field conditions but its applicability is limited by our ability to estimate the necessary parameters. The relative stream width can probably be estimated quite well but h_o/ℓ, being dependent on the anisotropy ratio K_x/K_z is not routinely available. It may be possible to determine K_x/K_z from cross spectral analysis of piezometric levels from two wells of different depth within the same aquifer; however, feasibility of such a procedure remains to be demonstrated and in many cases extensive records for wells at different depths will not be available.

The analysis of spatial variability in Section 2.5 provides some important initial insight on this complex problem. It was demonstrated that the variance of the water level fluctuation due to hydraulic conductivity variation is typically much smaller than the variance of hydraulic conductivity. For the analysis of the two well flow observation networks it was shown that the errors in the flow estimate will be substantially smaller than that indicated by the relative variance of the hydraulic conductivity, and that the errors are smallest for closely spaced observation wells (Table 2.2). The error is also much smaller than that which would be obtained assuming that the variables are statistically independent in space. In that case the only terms that will remain in equation 2.5.14 are

$$\overline{Q'^2}/\bar{Q}^2 = \overline{K'^2}/2\bar{K}^2 + 2\overline{y'^2}/(L\beta)^2 + \overline{y'^2}/2h_o^2$$

This result implies an error which is at least one half of the relative variance of the hydraulic conductivity. The contribution to the error by the variance of the water level $\overline{y'^2}$ is seen to increase sharply as the well spacing L is decreased; this is the opposite of the behavior found when realistic spatial correlation structure is included. Thus, it is important to deal with the spatial correlation structure in future work on spatial variability of subsurface flows.

The analysis of the unsaturated zone indicates that the effects of moisture storage are minor for low frequencies, and can be neglected for the range of frequencies of interest when monthly data is used, as in Chapter 4. A simple proportionality ($\varepsilon = \gamma P$) relating accretion to precipitation is introduced which can be used to determine the net recharge to the groundwater aquifer. However, more precise means of evaluating evapotranspiration in order to find the net accretion should be investigated in future work.

CHAPTER 3 NONLINEAR SIMULATION OF AQUIFER SPECTRAL RESPONSE

3.1 Physical and Theoretical Basis of Phreatic Aquifers

The Physical Basis

The understanding of the physical groundwater system is not only helpful in the formulation of mathematical models but is also useful in the scaling and evaluation of this study. The latter refers to the physical configuration and dimensions of the system that are important in the determination of the parameters which appear significant in the nonlinear effects.

The type of groundwater system to be studied is the phreatic aquifer shown schematically in Figure 2.2, which can be regarded as a transformation system with two inputs and one output. The transformation system is the spatially distributed structure of the saturated porous medium of which two major physical properties, transmissivity and storage coefficient, are of interest to this study. The two inputs are the accretion rate and stream stage. The percolation of water from the ground surface to the water table is the process of accretion which may be regarded as another transformation system. Stream stage fluctuation is the rise and fall of water level at the boundary between the aquifer and the stream. These inputs are complicated hydrologic processes and they are spatially and time dependent. In addition, their occurrences in time and space are random. The output of the system is the piezometric head in the aquifer (i.e., the water level in a well). It is characterized as random, spatially and time dependent because both the inputs and the transformation system have such characteristics. The physical boundaries are the water table, the stream

stage fluctuation and the impervious boundary at the bottom. For a finite length of the aquifer, there is the boundary at which no flow of water is allowed.

Intuitively, it can be seen that the larger the inputs, the larger is the output as the system is enclosed in the described boundaries. Hence one effective measure of the system is the amplitude of response which forms the major analysis in this study. The other physical characteristic is the delay response time of the output with respect to the inputs. This is the time for which a disturbance of the phreatic surface travels from one location to the other and hence it could be a measure of transmissivity of the aquifer system. This will be studied briefly.

Mathematical Models

Mathematical models are abstractions of complex physical phenomena. A model should be sufficiently complete in its description so as to produce useful results, yet simple enough to be manageable. The most commonly used mathematical equation to describe unsteady, unconfined groundwater flow is the Dupuit-Forchheimer equation. Its basic assumptions are that the flow is essentially horizontal and that the equipotential surfaces are vertical (see Bear, 1972). The assumptions are implied by the fact that the slope of the phreatic surface is small in real situations. The validity of these assumptions were discussed by Murray & Monkmeyer (1973) who found that for steady flow, the free surface slope must not be greater than 1:10 if results are expected to be 99% accurate. For the unsteady case, it was found that the equation describes a rising water table condition more exactly than it does a falling one.

The general form of the equation is given by

$$S \frac{\partial h}{\partial t} = \nabla \cdot [T \nabla (h + \zeta)] + \varepsilon$$

where S = storage coefficient

h = thickness of the saturated zone above the impervious base whose elevation is given by ζ

T = aquifer transmissivity

ε = accretion rate.

This part of the study is restricted to one dimensional horizontal aquifers, thus reducing the governing equation 2.3.2

$$S \frac{\partial h}{\partial t} (x,t) = \frac{\partial}{\partial x} [T(x,t) \frac{\partial h}{\partial x} (x,t)] + \varepsilon(x,t) \qquad (3.1.1)$$

For unconfined aquifers the transmissivity is defined as the product of the hydraulic conductivity, K, and the thickness of the saturated flow zone, h(x,t), or T = Kh. Hence we have

$$S \frac{\partial h}{\partial t} (x,t) = \frac{\partial}{\partial x} [Kh(x,t) \frac{\partial h}{\partial x}] + \varepsilon(x,t) \qquad (3.1.2)$$

This partial differential equation is nonlinear and has been solved for various boundary conditions in approximate linearized form by analytical techniques (see Glover, 1964; Haushild, 1960; Kriz, 1967; Polubarinova-Kochina, 1962; and Singh, 1969) and in nonlinear form by numerical methods (see Hornberger et al., 1970; Karadi et al., 1968; Kriz et al., 1966; and Yeh, 1970) for one and two dimensional, and axisymmetric geometries. The boundary conditions for this mathematical model are vertical accretion onto the phreatic surface which is implied in the equation, stream-aquifer interaction and a groundwater divide-no flow condition. Mathematically, the last two of these conditions are

represented as

$$\text{(a)}\quad h(o,t) = H(t)$$

$$\text{(b)}\quad \left.\frac{\partial h}{\partial x}\right|_{x=L} = 0 \qquad (3.1.3)$$

where x = horizontal space coordinate

L = length of aquifer

and, H(t) is the stream stage. The physical system is represented symbolically in Figure 2.2.

The primary characteristic of this analysis is that the inputs, accretion and stream stage, are random. Hence the output at the various locations along the aquifer is also random. A secondary characteristic is that the effective porosity or storage coefficient (S) and the hydraulic conductivity (K) usually are spatially distributed. This characteristic leads to a complex stochastic transformation system. For simplicity, assumptions are generally made that S and T are constants and that ε is only temporally distributed. This simplification leads to the well known linearized Dupuit model which is

$$S\,\frac{\partial h}{\partial t}(x,t) = T\,\frac{\partial^2 h}{\partial x^2}(x,t) + \varepsilon(t) \qquad (3.1.4)$$

This equation can be solved analytically and it constitutes the basis of the analytical study. Other forms of the equation, which is nonlinear, are to be compared with this simple model. They are :

(a) nonlinear Dupuit model with T = Kh(x,t)

(b) nonlinear Dupuit model with spatially distributed input, $\varepsilon=\varepsilon(x,t)$

The method used to solve the nonlinear equation is a numerical simulation using an implicit finite difference method discussed later.

But first, for a better understanding of the behavior of the physical system, it is useful to develop analytical solutions to the Dupuit model.

Linear Theory

The objectives of this section are two-fold: first, to understand the system in its simplest case; and second, to compare the simple analytical models to the finite difference model developed later. The accuracy of the nonlinear numerical simulation is based on such comparisons.

The linearized Dupuit model represented in equation 3.1.4 is subject to the boundary conditions in equation 3.1.3. In order to solve this equation by numerical simulation it is advantageous to transform the equation in dimensionless form:

$$\begin{aligned} \eta &= \frac{h}{m} \\ \eta_0 &= \frac{H}{m} \\ \xi &= \frac{x}{L} \\ \tau &= \frac{T}{SL^2}\, t \\ \rho &= \frac{L^2}{Tm}\, \varepsilon(t) \end{aligned} \tag{3.1.5}$$

where m is a typical thickness of the saturated zone. Usually this is the mean of the fluctuation at stream, or $m = \bar{H}(t)$. Hence the dimensionless equation becomes

$$\frac{\partial \eta}{\partial \tau} = \frac{\partial^2 \eta}{\partial \xi^2} + \rho(\tau) \tag{3.1.6}$$

subject to the boundary conditions

$$\eta(0,\tau) = \eta_0(\tau)$$

$$\left.\frac{\partial \eta}{\partial \xi}\right|_{\xi=1} = 0 \qquad (3.1.7)$$

In order to solve this equation explicitly the inputs into the system, η_0 and ρ, must be specified. Since these inputs are random in temporal distribution, they may be best represented by a harmonic function with a single frequency and amplitude. A variety of functions, which are almost periodic in nature, can be constructed by the superposition of harmonic functions with a large range of frequency and amplitude. The almost periodic function is close to a random function if the frequency intervals, which are used to specify the almost periodic function, approach zero.

The sinusoidal function is characterized by its amplitude and frequency. The inputs are represented in complex form as

$$\rho(\tau) = \alpha_0 + \alpha e^{i\Omega_\alpha \tau} \qquad (3.1.8)$$

$$\eta_0(\tau) = \beta_0 + \beta e^{i\Omega_\beta \tau} \qquad (3.1.9)$$

where α_0 and β_0 are the mean of accretion rate and stream fluctuation respectively; α and β are the respective amplitudes of fluctuation, and Ω_α and Ω_β are the respective dimensionless frequency. The dimensionless frequency Ω is related to the real frequency ω as

$$\Omega\Delta\tau = \omega\Delta t \qquad (3.1.10)$$

Hence from equation (3.1.5)

$$\Omega = \frac{SL^2}{T}\omega \qquad (3.1.11)$$

By the principle of superposition, the solution to this equation is simply the sum of the three cases, namely the steady case, accretion case and the stream interaction case.

(a) Steady case - accretion rate is constant

$$\rho = \alpha_0 \ , \ \beta = 0 \ , \ \beta_0 = 1$$

$$\eta_1(\xi,\tau) = 1 + \alpha_0\xi(1 - \frac{1}{2}\xi) \tag{3.1.12}$$

(b) Accretion case - accretion rate varies sinusoidally, i.e.,

$$\rho(\tau) = \alpha e^{i\Omega_\alpha \tau} \qquad \text{with}$$

$$\alpha_0 = 0 \quad \text{and} \quad \eta_0 = 0$$

$$\eta_2(\xi,\tau) = \frac{i\alpha}{\Omega_\alpha}\left[\frac{\cosh[\sqrt{i\Omega_\alpha}\ (1 - \xi)]}{\cosh\sqrt{i\Omega_\alpha}} - 1\right] e^{i\Omega_\alpha \tau} \tag{3.1.13}$$

(c) Stream interaction case - stream stage varies sinusoidally, i.e.,

$$\eta_0(\tau) = \beta e^{i\Omega_\beta \tau}$$

$$\eta_3(\xi,\tau) = \beta\,\frac{\cosh[\sqrt{i\Omega_\beta}\ (1 - \xi)]}{\cosh\sqrt{i\Omega_\beta}}\ e^{i\Omega_\beta \tau} \tag{3.1.14}$$

Therefore the superposition of the three solutions gives

$$\eta(\xi,\tau) = \eta_1 + \eta_2 + \eta_3 \tag{3.1.15}$$

It can be seen that the output is sinusoidal with the same frequency as that of the inputs. The only difference is the change in amplitude and a phase shift. This is the basic response behavior of the linear system. If the input $X(\tau)$ is given by

$$X(\tau) = Ae^{i\Omega\tau} \tag{3.1.16}$$

where A = amplitude of fluctuation and the output $Y(\tau)$ is in the form

$$Y(\tau) = AG(\Omega)e^{i\Omega\tau} \tag{3.1.17}$$

where $G(\Omega)$ = gain factor or transfer function, the ratio of $Y(\tau)$ to $X(\tau)$ is

$$\frac{Y(\tau)}{X(\tau)} = |G| e^{i\theta} \tag{3.1.18}$$

which is the frequency response function. The amplitude response or amplitude of transfer function is

$$|G(\Omega)| = \left|\frac{Y(\tau)}{X(\tau)}\right| \tag{3.1.19}$$

and its phase response is

$$\theta = \arg \left|\frac{Y(\tau)}{X(\tau)}\right| \tag{3.1.20}$$

Using these formulae, we find the response for both the accretion and stream interaction cases as follows:

Let $\cosh \gamma\xi' \cos \gamma\xi' = B$

$\cosh \gamma \cos \gamma = C$

$\sinh \gamma\xi' \sin \gamma\xi' = D$

$\sinh \gamma \sin \gamma = E$

where $\gamma = \sqrt{\Omega_\alpha/2}$ (Accretion case)

$= \sqrt{\Omega_\beta/2}$ (Stream Interaction case) and $\xi' = 1 - \xi$

Accretion case:

$$|G_1(\Omega_\alpha)| = \frac{\alpha}{\Omega_\alpha}\left[\frac{(B-C)^2 + (D-E)^2}{C^2 + E^2}\right]^{1/2} \tag{3.1.21}$$

$$\theta_1 = \theta_{\rho\eta}(\Omega_\alpha) = \tan^{-1}\left[\frac{E(B-C) - C(D-E)}{E(D-E) + C(B-C)}\right] \tag{3.1.22}$$

Stream interaction case:

$$G_2(\Omega_\beta) = \left[\frac{B^2 + D^2}{C^2 + E^2}\right] 1/2 \tag{3.1.23}$$

$$\theta_2 = \theta_{\eta_0\eta}(\Omega_\beta) = \tan^{-1}\left[\frac{BE - DC}{BC + DE}\right] \tag{3.1.24}$$

$|G_1|$, $|G_1|^2$, $|G_2|$, $|G_2|^2$ and $\theta_{\eta_0\eta}$ are plotted for the frequency range from $\Omega = 0.1$ to $\Omega = 100$ in Figures 3.1 (a), (b) and 3.2 (a), (b) and 3.3 respectively. The transfer function and the phase response function thus obtained is exactly equivalent to those obtained in the linear spectral theory. (See Chapter 2). The equivalence is due to the similar form of the input, $X(\tau)$. In the sinusoidal theory the input is represented by a single amplitude, whereas in the spectral theory, it is represented by the superposition of a number of amplitudes in the frequency domain as the Fourier-Stieltjes integral

$$X(\tau) = \int_{-\infty}^{\infty} e^{i\Omega\tau}\, dZ_X(\Omega) \tag{3.1.25}$$

where dZ_X = complex amplitude of input. The output $Y(\tau)$ is similarly represented as

$$Y(\tau) = \int_{-\infty}^{\infty} e^{i\Omega\tau}\, dZ_Y(\Omega) \tag{3.1.26}$$

The substitution of these equations into the linear Dupuit equation would hence lead to the same results as from the sinusoidal theory. The frequency response function is given by dZ_Y/dZ_X in the spectral theory and Y/X in the sinsusoidal theory. The former theory has the advantage that it deals with a more general random stationary function, while the latter is of advantage in solving the problem with less difficulty.

The dimensionless frequency, Ω must be related to the physical significance of the system. From equation 3.1.11

$$\Omega = \frac{SL^2}{T}\omega$$

where Ω is radians/dimensionless time

ω is radians/time unit.

Hence the frequency of input depends on the physical parameters and dimension of the system. For a typical aquifer with L = 1 mile, S = 0.3, $T = 10^4$ gal/day/ft^2 and real time interval as one month we obtain approximately

$$\omega \simeq \frac{1}{5}\Omega \text{ radians/month}$$

$$= \frac{1}{10\pi}\Omega \text{ cycle/month.}$$

For $\Omega = 100$

$$\omega \simeq \frac{10}{\pi} \text{ cycles/month} \simeq 3 \text{ cycles/month}$$

which is a very high value for the inputs, accretion and stream stage. At such a high frequency, there is no doubt that noise other than the characteristic response frequency (e.g., annual cycle of precipitation) is brought in.

For $\Omega = 0.1$

$$\omega \simeq \frac{1}{100\pi} \text{ cycle/month} \simeq 0.003 \text{ cycle/month.}$$

The frequency is very small compared to characteristic frequency of the system response. Hence the range from Ω=0.1 to Ω=100 represents a fairly large range of aquifer response behavior.

The relatively insensitive response at low frequency, from Ω=0.1 to Ω=1, as shown in Figures 3.1 (a),(b) and 3.2 (a),(b) has an obvious physical significance. At such low frequencies (0.003 cycle/month) there is virtually no damping effects on the response. One significant difference between the response amplitude for these cases is that the stream response is damped out faster than the accretion response, particularly when the well is farther away from the stream. Also the accretion response is much the same for all locations at higher frequency (Ω >50). The amplitude of the response is an important concept in this study, particularly with respect to the determination of the physical parameters (S and T) of the system.

The other important mathematical property which has an associated physical meaning is the phase lag of the response with respect to the input. This is particularly true for the stream interaction case. The phase lag represents the delay of a signal from the response location to the stream. The delay response time (τ_D) is related to the phase lag θ_{XY} in a linear system as

$$\tau_D = \frac{\theta_{XY}}{\Omega} \qquad (3.1.27)$$

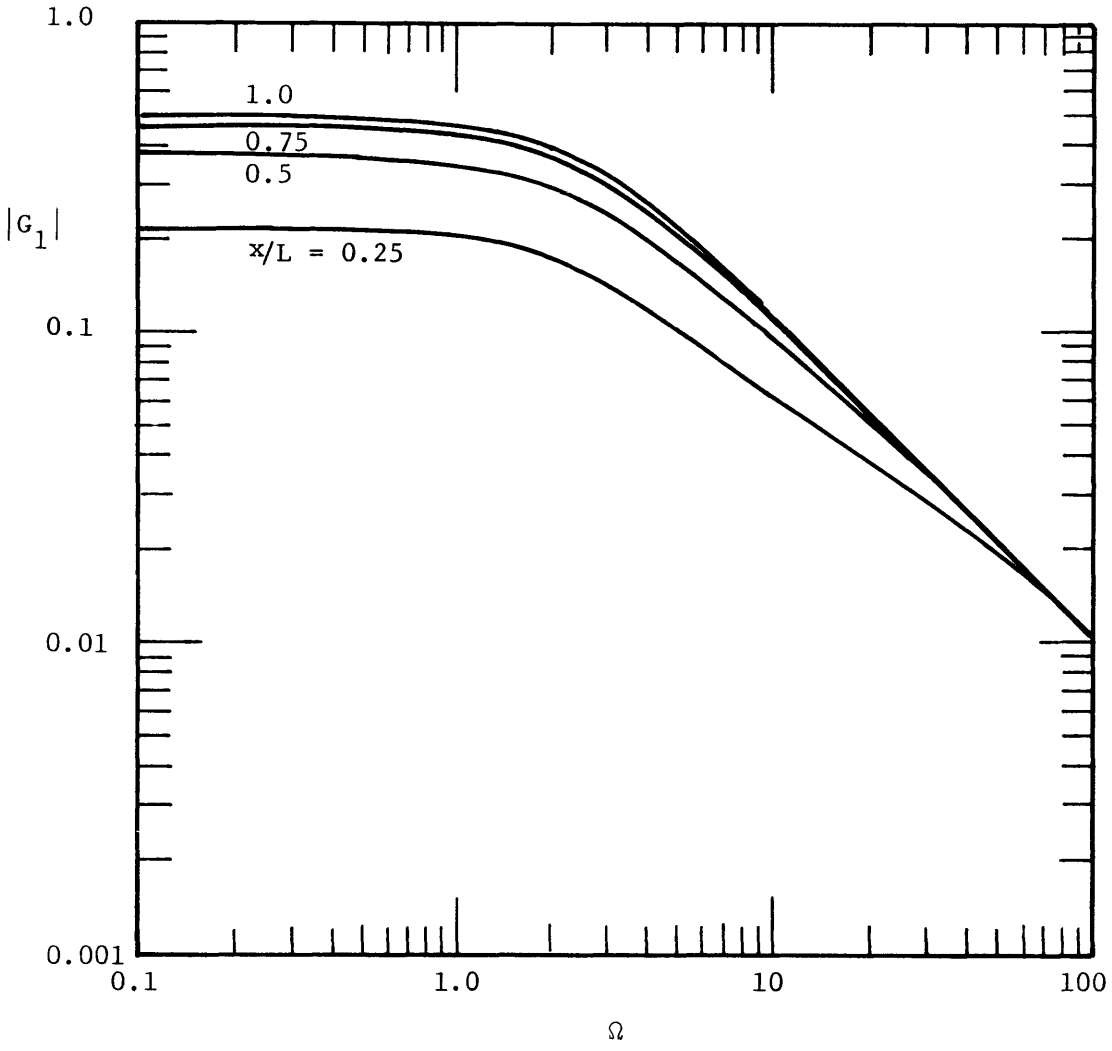

Figure 3.1 (a) Amplitude of the Transfer Function of the Aquifer System with Accretion Input

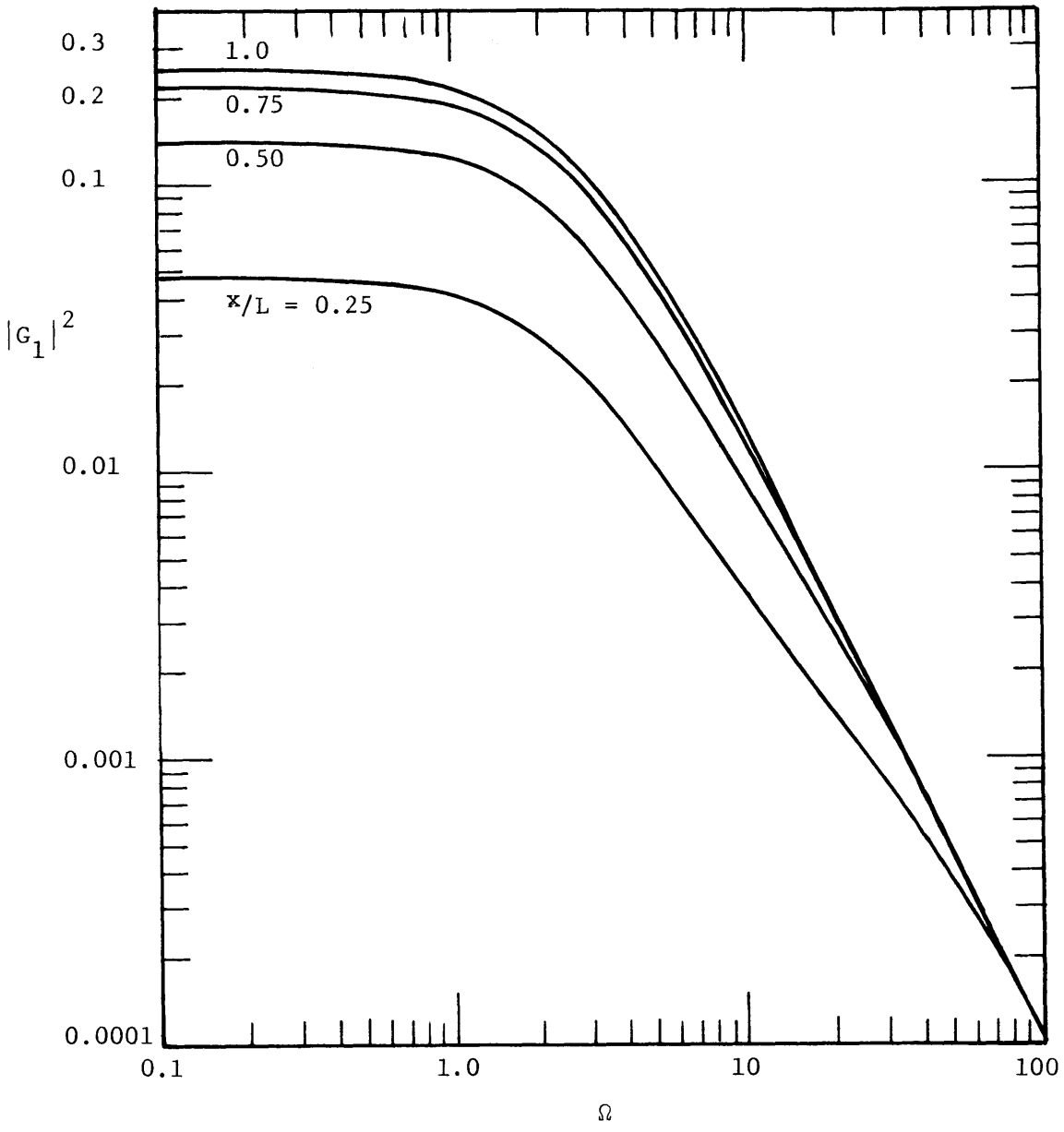

Figure 3.1(b) Square of the Amplitude of Transfer Function of the Aquifer System with Accretion Input

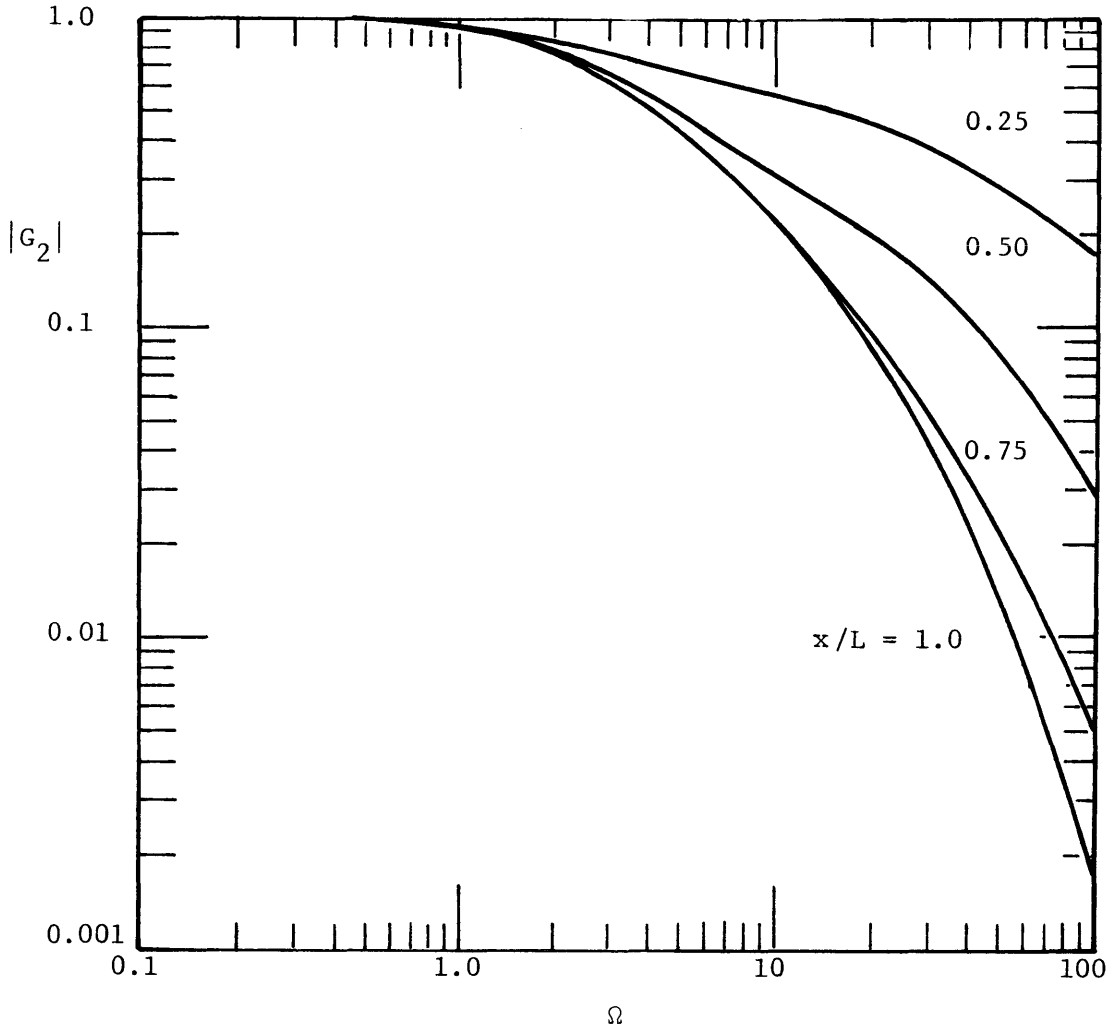

Figure 3.2(a) Amplitude of Transfer Function of the Aquifer System with Stream Stage Input (Also the Amplitude of the ratio in equation 2.5.7 for $\beta=1$)

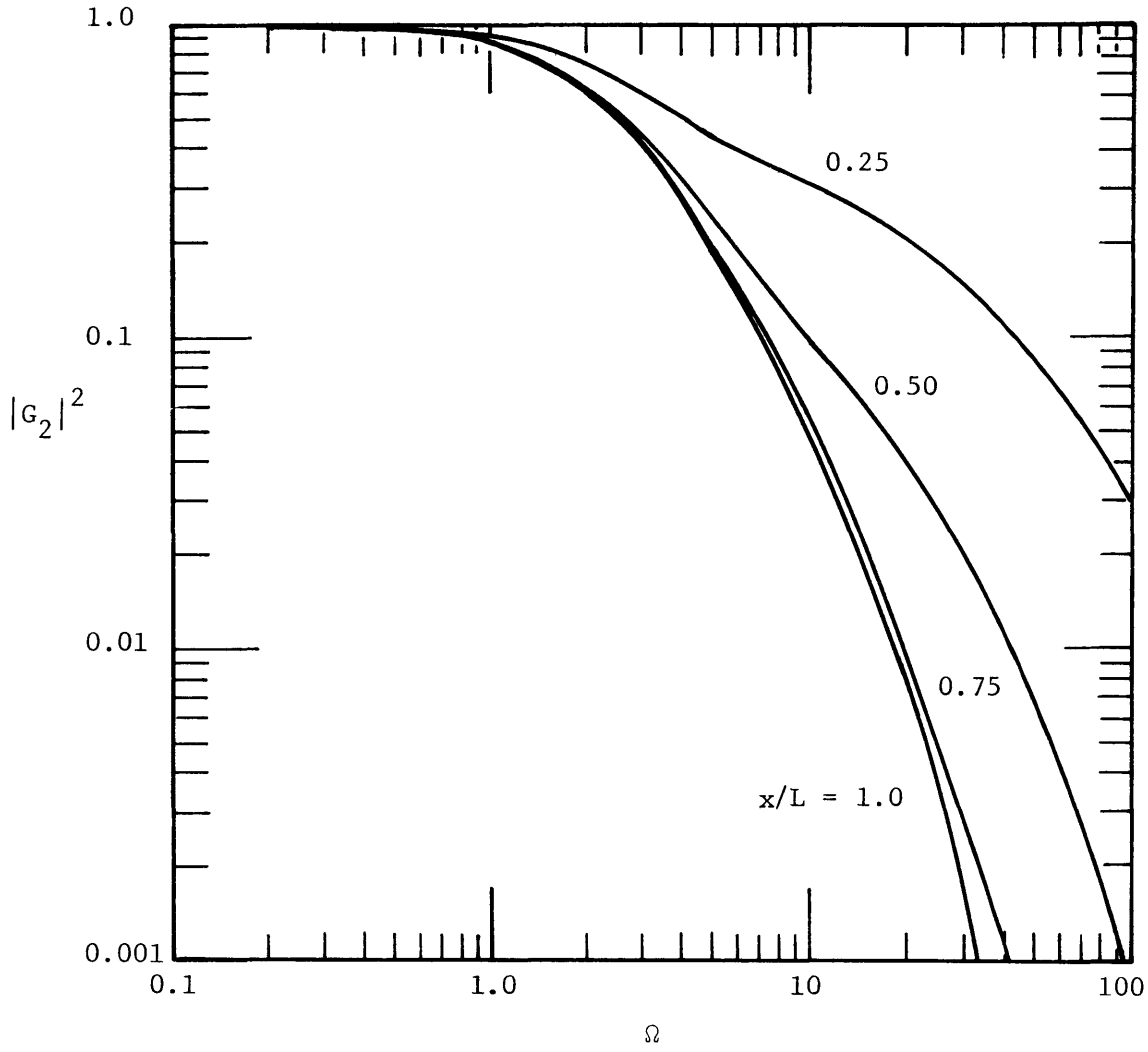

Figure 3.2(b) Square of the Amplitude of the Transfer Function of the Aquifer System with Stream Stage Input

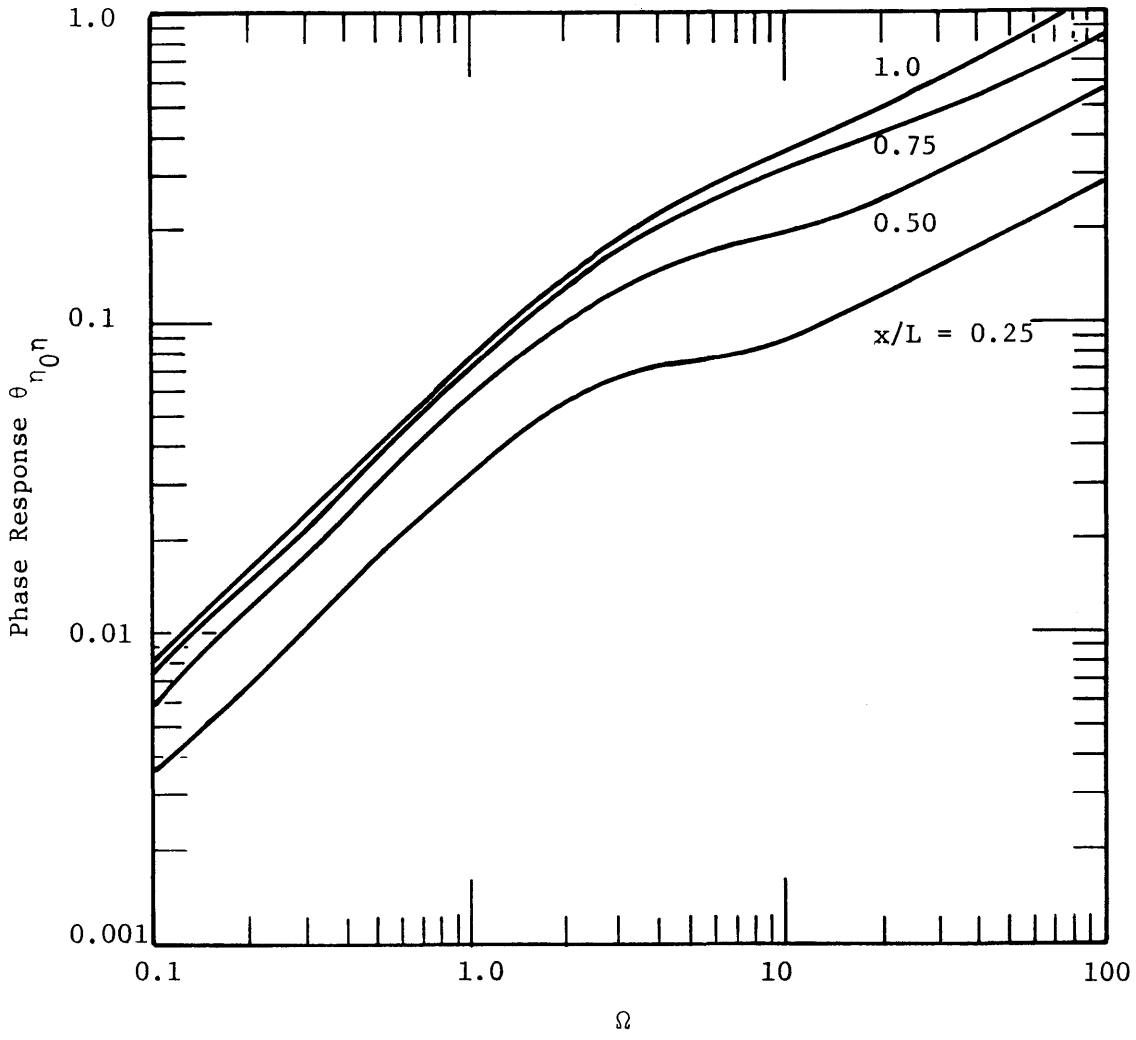

Figure 3.3 Phase Response of the Aquifer System with Stream Stage Input

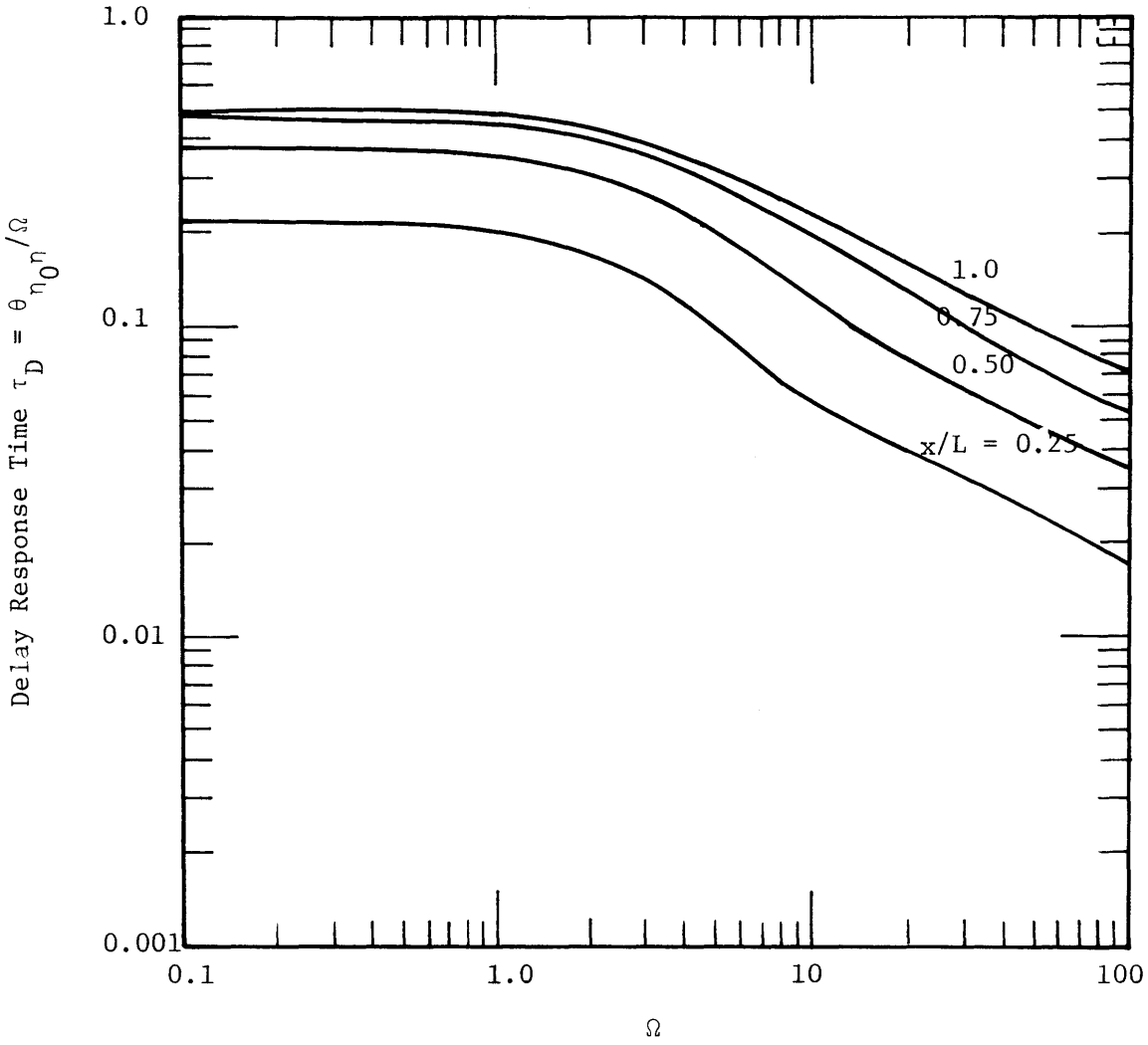

Figure 3.4 Delay Response Time of the Aquifer System with Stream Stage Input

where X is the input

Y is the output

Ω is the dimensionless frequency of the input.

For the stream interaction case, θ_{XY} and τ_D are shown in Figures 3.3 and 3.4 respectively. It can be seen that is takes less time for a wave to reach a nearer location. Also it takes less time for the signal to travel to a nearer location. It can be noted that the response time is relatively insensitive to frequency changes, particularly when Ω ranges from 0.1 to 1. Intuitively, this means that waves at such low frequency are damped out so slowly that they respond almost simultaneously as that at the stream. For the accretion case, there is hardly any phase lag for all locations. From the basic assumption of the Dupuit model, water flow is essentially horizontal, the vertical recharge onto the system would have insignificant effects. Hence this is not to be studied in detail.

Summing up, the study of the behavior of this linear groundwater system is based on its amplitude and phase responses, with particular emphasis on the former. The evaluation of nonlinear effects is also based on these physical properties.

Nonlinear Theory for Steady Accretion and Stream Stage

In general it is not possible to solve the nonlinear Dupuit equation analytically. Steady flow situations are an exception however, and one such case is examined here. The equation and boundary conditions are

$$\frac{\partial \eta}{\partial \tau} = \frac{\partial}{\partial \xi}\left(\eta \frac{\partial \eta}{\partial \xi}\right) + \alpha_0 \tag{3.1.28}$$

$$\eta(0,\tau) = 1 \tag{3.1.29}$$

$$\left.\frac{\partial \eta}{\partial \xi}\right|_{\xi=1} = 0 \tag{3.1.30}$$

where α_0 is a constant, and the solution is

$$\eta(\xi) = (1 + 2\alpha_0\xi - \alpha_0\xi^2)^{1/2} \tag{3.1.31}$$

whereas the linear solution to this problem is given by

$$\eta(\xi) = 1 + \alpha_0\xi + \frac{\alpha_0\xi^2}{2} \tag{3.1.32}$$

Expanding the nonlinear solution in a Taylor series we obtain

$$\eta(\xi) \simeq \left(1 + \alpha_0\xi - \frac{\alpha_0\xi^2}{2}\right) - \frac{1}{8}(2\alpha_0\xi - \alpha_0\xi^2)^2 + \frac{3}{48}(2\alpha_0\xi - \alpha_0\xi)^2 \tag{3.1.33}$$

We can examine the nonlinear effects and see that when α_0 is small, the linear solution is close to the nonlinear one. It can also be seen that for a fixed ξ, the difference between the two solutions increases somewhat quadratically as the mean of accretion α_0 increases. For a fixed α_0, the difference increases as ξ increases. The solutions to both linear and nonlinear cases are plotted in Figure 3.5 for α_0=1. It is seen that the maximum difference is about 8%. This deviation increases as the horizontal spatial coordinate, x/L increases. In conclusion, α_0 is the basic nonlinear parameter in the steady state nonlinear system.

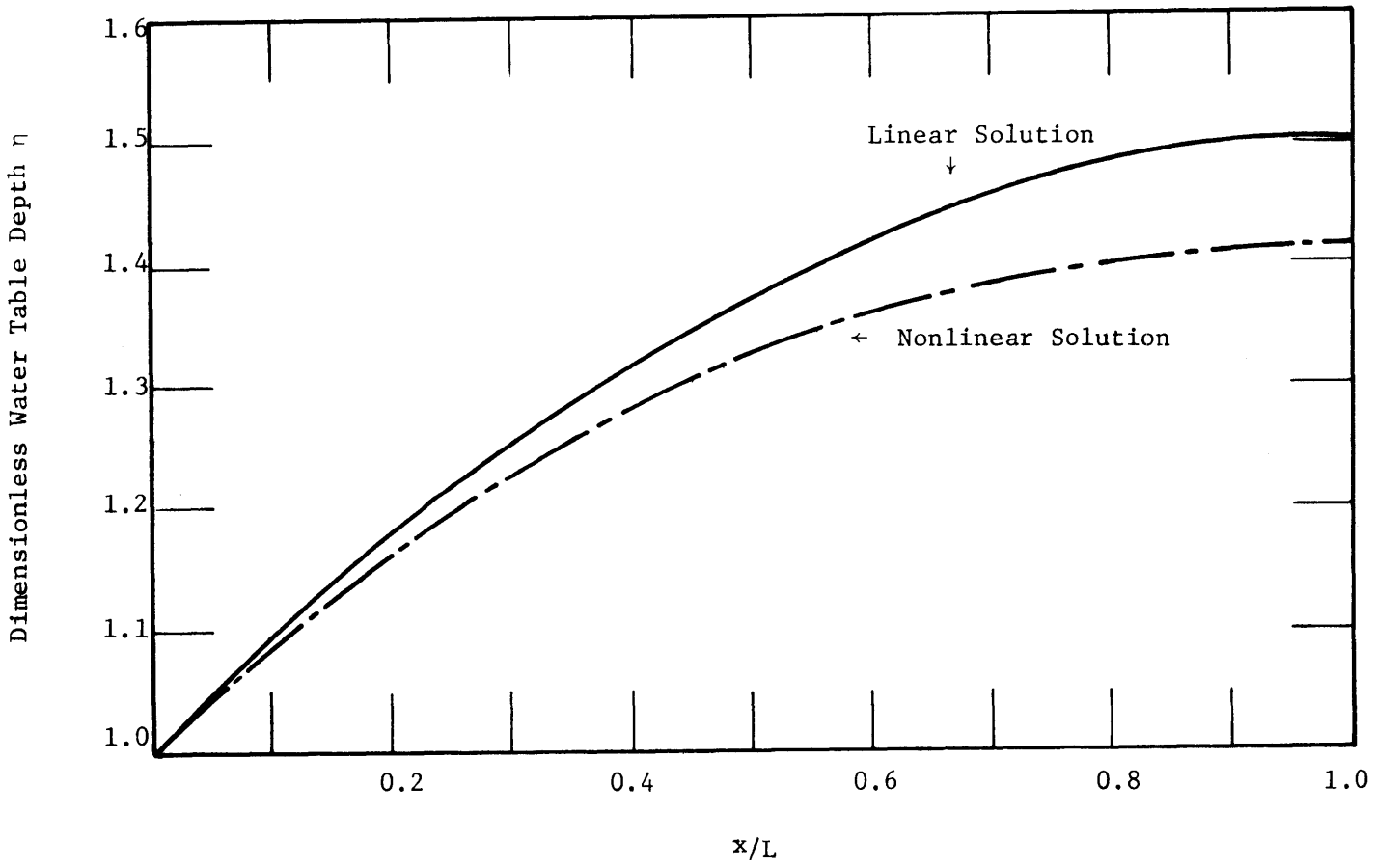

Figure 3.5 Analytical Solution of the Linear Case and the Nonlinear Steady State Cases

A Simple Evaluation of Nonlinearity

Since analytical solutions to the nonlinear equation do not in general exist, it is difficult to evaluate the nonlinear effects directly. However, a crude estimate may be based on the linear solution of the equation by investigating how the nonlinear effects are sensitive to changes of the input parameters α_0, β_0, α, β. The mean of accretion, α_0 has already been identified in the previous section and β_0 is fixed to be one for all cases. The evaluation of α, β and Ω is based on the transient state solutions of both accretion and stream interaction cases.

In the stream interaction case with no accretion, the equation is

$$\frac{\partial \eta}{\partial \tau} = \frac{\partial}{\partial \xi} \left(\eta \frac{\partial \eta}{\partial \xi}\right) \tag{3.1.34}$$

which can be expanded to

$$\frac{\partial \eta}{\partial \tau} = \left(\frac{\partial \eta}{\partial \xi}\right)^2 + \eta \frac{\partial^2 \eta}{\partial \xi^2} \tag{3.1.35}$$

Let $$\eta = 1 + f \tag{3.1.36}$$

and substitute into equation (2.5.2) to obtain

$$\frac{\partial f}{\partial \tau} = \frac{\partial^2 f}{\partial \xi^2} + \left(\frac{\partial f}{\partial \xi}\right)^2 + f \frac{\partial^2 f}{\partial \xi^2} \tag{3.1.37}$$

The first term on the right hand side is the well known linear Dupuit equation, i.e.

$$\frac{\partial f}{\partial \tau} = \frac{\partial^2 f}{\partial \xi^2}$$

or, (3.1.38)

$$\frac{\partial^2 f}{\partial \xi^2} \Big/ \frac{\partial f}{\partial \tau} = 1$$

The two nonlinear terms are investigated using linear solutions of f. This evaluation is based on the assumption that the true nonlinear solution has a sinusoidal shape similar to the linear solution, and that there is sufficiently small phase lag between the two solutions. The validity of this assumption will be tested in the nonlinear simulation with sinusoidal inputs.

From the linear solution equation 3.1.13 the ratio of the first nonlinear term to $\partial f/\partial \tau$ is

$$\frac{(\frac{\partial f}{\partial \xi})^2}{(\frac{\partial f}{\partial \tau})} = \beta \frac{\sinh^2[\sqrt{i\Omega_\beta}\ (1-\xi)]e^{i\Omega_\beta \tau}}{\cosh\ [\sqrt{i\Omega_\beta}\ (1-\xi)]\ \cosh\sqrt{i\Omega_\beta}} \tag{3.1.39}$$

and for the second term is

$$\frac{(f\ \frac{\partial^2 f}{\partial \xi^2})}{(\frac{\partial f}{\partial \tau})} = \beta \frac{\cosh[(1-\xi)\ \sqrt{i\Omega_\beta}]e^{i\Omega_\beta \tau}}{\cosh\sqrt{i\Omega_\beta}} \tag{3.1.40}$$

Clearly, it can be seen both nonlinear terms are proportional to the amplitude of fluctuation, β. With respect to frequency dependence, the amplitudes of both terms are computed and are shown in Figure 3.6 and Figure 3.2(a) respectively for $\beta=1$. As it can be seen, the amplitudes of both nonlinear terms decrease at high frequency particularly when $\Omega > 50$. For a well farther away from the stream, the nonlinear terms decrease more significantly. Also it may be noticed that the amplitude of the first nonlinear term, $|(\partial f/\partial \xi)^2/(\partial f/\partial \tau)|$, as shown in Figure 3.6, increases at low frequency $\Omega=0.1$ to a maximum at about $\Omega=8$. From these results, it may be concluded that for small amplitude, β and higher

frequency, the linear approximation is a good one.

In the accretion case, the equation is

$$\frac{\partial f}{\partial \tau} = \frac{\partial^2 f}{\partial \xi^2} + \rho + \left(\frac{\partial f}{\partial \xi}\right)^2 + f \frac{\partial^2 f}{\partial \xi^2} \tag{3.1.41}$$

From the solution, equation 2.3.10, the two nonlinear terms become

$$\frac{\left(\frac{\partial f}{\partial \xi}\right)^2}{\left(\frac{\partial f}{\partial \tau}\right)} = \frac{i\alpha}{\Omega_\alpha} \left[\frac{\sinh^2 \sqrt{i\Omega_\alpha}\,(1-\xi)}{\cosh \sqrt{i\Omega_\alpha}\,(1-\xi) - \cosh \sqrt{i\Omega_\alpha}}\right] \frac{e^{i\Omega\tau}}{\cosh \sqrt{i\Omega_\alpha}} \tag{3.1.42}$$

$$\frac{\left(f \frac{\partial^2 f}{\partial \xi^2}\right)}{\left(\frac{\partial f}{\partial \tau}\right)} = \frac{i\alpha}{\Omega_\alpha} \left[\frac{\cosh(1-\xi)\sqrt{i\Omega_\alpha}}{\cosh \sqrt{i\Omega_\alpha}}\right] e^{i\Omega_\alpha \tau} \tag{3.1.43}$$

the amplitudes of which are shown in Figure 3.7 and Figure 3.8 respectively. Similar to the stream interaction case, the two nonlinear terms are directly proportional to the amplitude, α. However, they are fairly sensitive to the change in frequency. At lower frequency (Ω=0.1 to Ω=1), the nonlinear terms remain relatively large, while at higher frequency they decrease significantly.

In conclusion, the effects of nonlinearity are significant in the lower range of frequency for the accretion case. By contrast, the effects are negligibly small for the stream interaction case. Furthermore, the nonlinear effects are directly proportional to the amplitudes of accretion and stream stage fluctuation.

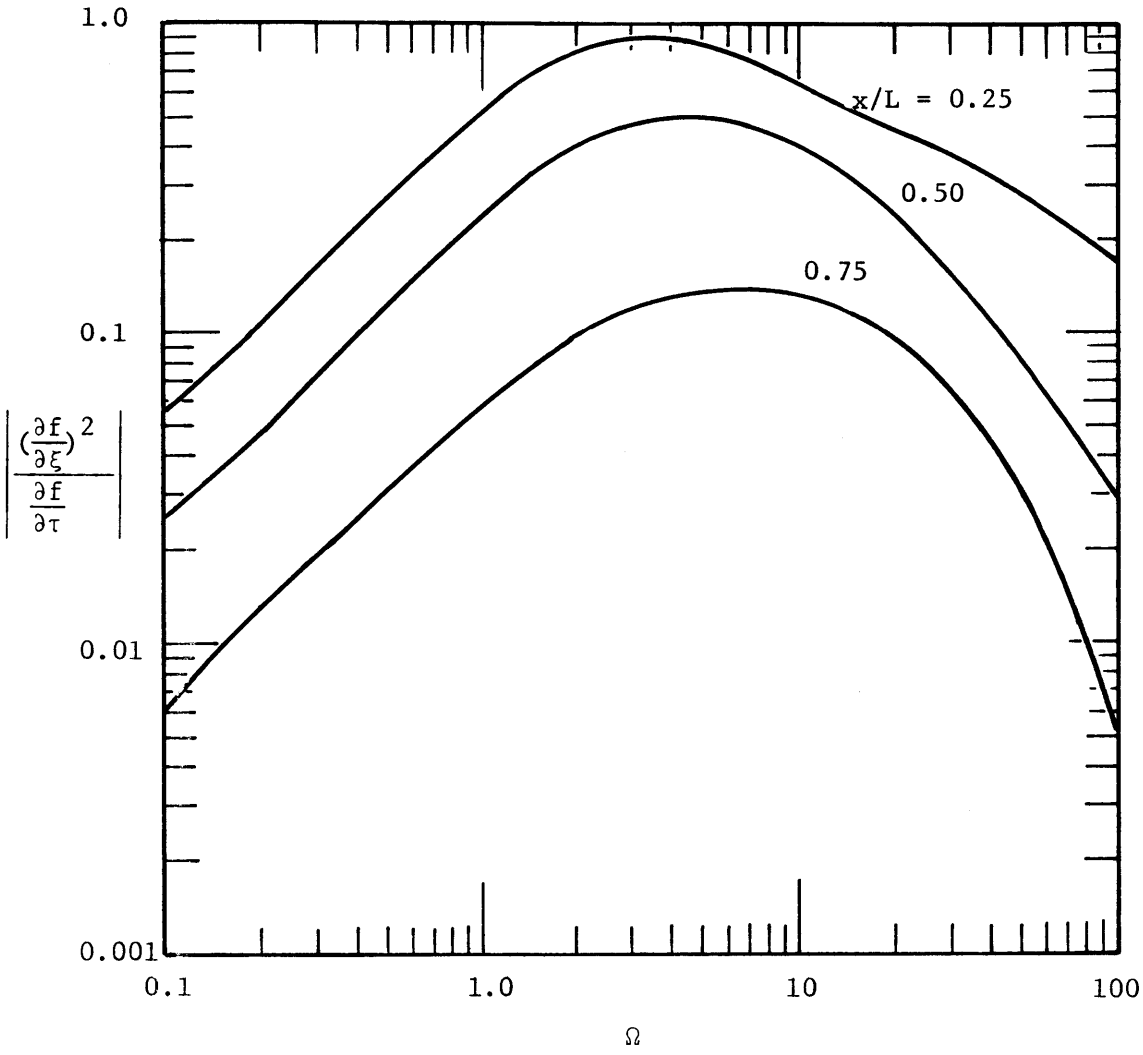

Figure 3.6 Amplitude Ratio of the First Nonlinear Term for the Stream Interaction Case with $\beta=1$

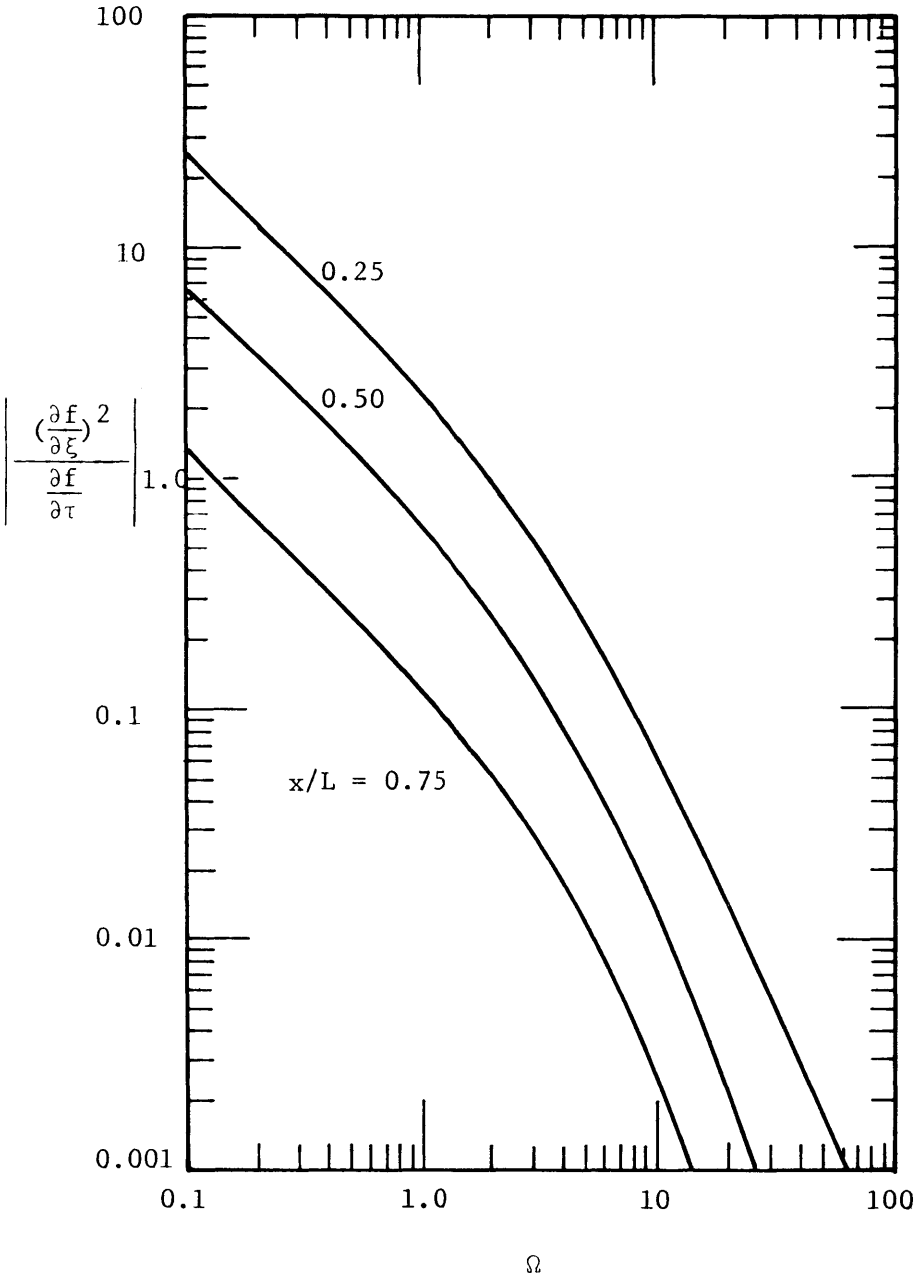

Figure 3.7 Amplitude Ratio of the First Nonlinear Term for the Accretion Case with α=1

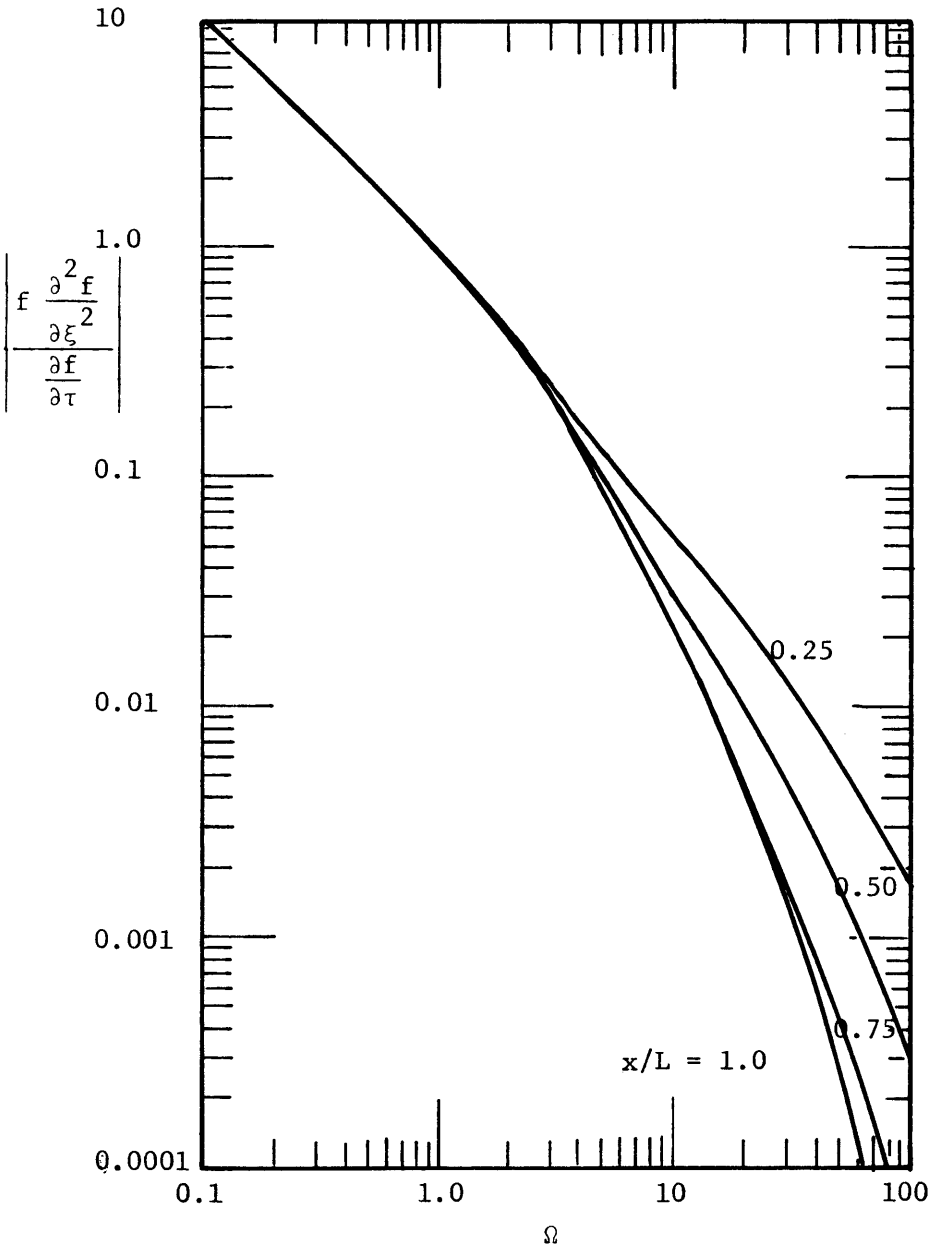

Figure 3.8 Amplitude Ratio of the Second Nonlinear Term for the Accretion Case with α=1

Linear Theory with a Spatially Distributed Input

The irregular and random distribution of vegetation on the ground surface, topography and porous medium properties in the unsaturated zone above the water table shown schematically in Figure 2.2, constitute another complicated transformation system. Hence the accretion reaching the water table can hardly be regarded as spatially uniform in realistic situations.

The simple linear model discussed earlier is implemented with a spatially distributed parameter in the input accretion as:

$$\rho(\xi,\tau) = \alpha' e^{i(\Omega\tau - k\xi)} \tag{3.1.44}$$

where α' = amplitude of spatial fluctuation

k = dimensionless wave number in radians

Ω = dimensionless frequency

This equation represents a moving harmonic wave in the horizontal direction from $\xi=0$ to $\xi=1$ with frequency Ω and harmonic number k. The solution to the linear equation 3.1.6 with boundary conditions 3.1.7 with $\eta_0 = 0$, is found to be

$$\eta(\xi,\tau) = -\frac{\alpha'}{k^2 + i\Omega}\left[\frac{\cosh\sqrt{i\Omega}(1-\xi)}{\cosh\sqrt{i\Omega}} e^{ik\xi} - 1 - \frac{ik}{\sqrt{i\Omega}}\frac{\sinh\sqrt{i\Omega}\xi}{\cosh\sqrt{i\Omega}} e^{-ik(1-\xi)}\right] e^{i(\Omega\tau - k\xi)} \tag{3.1.45}$$

As one can see, for k=0 the solution reduces to the case without spatially variability (equation 3.1.13). However, the present solution

has some limitations for the purpose of this study. These include:

(a) The input harmonic wave is moving in one direction only.

(b) There is no specification of the wave number, k.

(c) There is no comparison of the amplitude of spatial variability of temporal fluctuation to that of spatially uniform temporal fluctuation.

To overcome these difficulties, the input wave is changed to a standing wave:

$$\rho = \frac{1}{2}\left(\alpha' e^{i\Omega\tau - k\xi} + \alpha' e^{i\Omega\tau + k\xi}\right)$$

$$= \alpha' e^{i\Omega\tau}\cos k\xi \qquad (3.1.46)$$

Hence the solution can be obtained from equation 2.6.2 by superposition as

$$\eta(\xi,\tau) = -\frac{\alpha'}{k^2 + i\Omega}\left(F - \cos k\xi - \frac{k \sinh\sqrt{i\Omega}\xi}{\sqrt{i\Omega}\cosh\sqrt{i\Omega}} \sin k\right)e^{i\Omega\xi}$$

where $$F = \frac{\cosh\sqrt{i\Omega}\,(1-\xi)}{\cosh\sqrt{i\Omega}} \qquad (3.1.47)$$

In order that the mean of accretion remains constant in all cases, the wave number, k, must satisfy the condition $k = 2\pi N$ where N is an integer. Hence equation 2.6.4 becomes

$$\eta(\xi,\tau) = -\frac{\alpha'}{k^2 + i\Omega}\left(F - \cos k\xi\right)e^{i\Omega\tau} \qquad (3.1.48)$$

Now we may consider the accretion input as being made up of the following components:

$$\rho = \underset{\text{Steady}}{\alpha_0} + \underset{\substack{\text{Spatially Uniform} \\ \text{Temporal Fluctuation}}}{\alpha e^{i\Omega\tau}} + \underset{\substack{\text{Spatially Variable} \\ \text{Temporal Fluctuation}}}{\alpha' e^{i\Omega\tau}\cos k\xi}$$

where α_0 = mean of accretion

α = amplitude of the temporal fluctuation

α' = amplitude of the spatial fluctuation

The unsteady part of the output is therefore given by:

$$\eta(\xi,\tau) = \alpha\left[\frac{i}{\Omega}(F-1) - \frac{\alpha'}{\alpha}\left(\frac{1}{k^2 + i\Omega}\right)(F - \cos k\xi)\right]e^{i\Omega\tau} \tag{3.1.49}$$

The transfer function of this system is evaluated by comparing the output to the spatially uniform input. This is given by:

$$G = \frac{\eta}{\alpha e^{i\Omega\tau}} \tag{3.1.50}$$

The square of the amplitude of the transfer function is given by:

$$|G|^2 = GG^* = \frac{(F-1)(F^*-1)}{\Omega^2} - \frac{\alpha'}{\alpha}\left\{\frac{i(F-1)(F^* - \cos k\xi)}{\Omega(k^2 - i\Omega)} + \frac{i(F^* - 1)(F - \cos k\xi)}{\Omega(k^2 + i\Omega)}\right\} + \left(\frac{\alpha'}{\alpha}\right)^2 \frac{(F - \cos k\xi)(F^* - \cos k\xi)}{k^4 + \Omega^2} \tag{3.1.51}$$

where G* and F* are complex conjugates of G and F respectively.

Two major parameters must be identified in this system. They are the wave number, k, and the ratio of the amplitudes of the spatially variable component of accretion to the spatially uniform component, α'/α. The wave number measures the intensity of the spatial variability of accretion, i.e., the higher k is, the greater is the variability. However, the total amount of accretion over the aquifer at any time is identical to the total accretion for the spatially uniform input. On the other hand, α'/α measures the amount of the change of accretion over space. It can be regarded as some measure of deviation from the spatially uniform temporal fluctuation. The wave number is similar in concept to frequency. The maximum wave number, k_c, for a system can be determined based on the sampling theorem for the frequency domain as

$$k_c = 2\pi\left(\frac{1}{2\Delta\xi}\right) = \frac{\pi}{\Delta\xi} \qquad (3.1.52)$$

where $\Delta\xi$ is the smallest spatial interval for which there is significant variability of accretion.

In the numerical model described later or in realistic situations, $\Delta\xi$ can be determined or estimated. Hence the maximum wave number can be related to the physical properties of the system. The smallest possible maximum wave number is 2π.

For equation 3.1.51 one can see that the first term on the right hand side is the solution for the case without spatial variability, and the other terms are multiplied by the ratio α'/α. For example, Figure 3.9 shows a spatial variability case with $k = 2\pi$ different values of α'/α at x/L=0.5. It indicates that the amplitude of the transfer

function decreases at all frequencies as α'/α increases.

The wave number has little significant contribution to the difference. For low wave numbers (2π or 4π) there is a slight difference between the cases with and without spatial variability. But for higher wave numbers, there is virtually no difference. An example with $\alpha'/\alpha = 0.707$ and $k = 10\pi$ is shown in Figure 3.10 for which the plotted curves are essentially identical to the case with no spatial variability as in Figure 3.1(b). The higher wave number indicates higher spatial variability of the system.

The nonlinear Dupuit equation with spatially variable accretion can be evaluated by the approach given previously. From equation 3.1.49 the nonlinear terms $(\frac{\partial f}{\partial \xi})^2$ and $f\frac{\partial f}{\partial \xi}$ depend on α'/α in addition to α. This means that the ratio α'/α is another nonlinear parameter. It is expected that the effects of nonlinearity will increase as this parameter increases.

In conclusion, the transfer function in the case with spatially variable accretion is little different from the case without the spatial variability. The basic parameter that increases the deviation is the ratio, α'/α. The wave number, k, is also relatively unimportant for this comparison. In addition, the effects of nonlinearity for such a system should be negligibly small for small α'/α and high k. The simple linear system without spatial variability of accretion can hence be used to represent a large variety of cases.

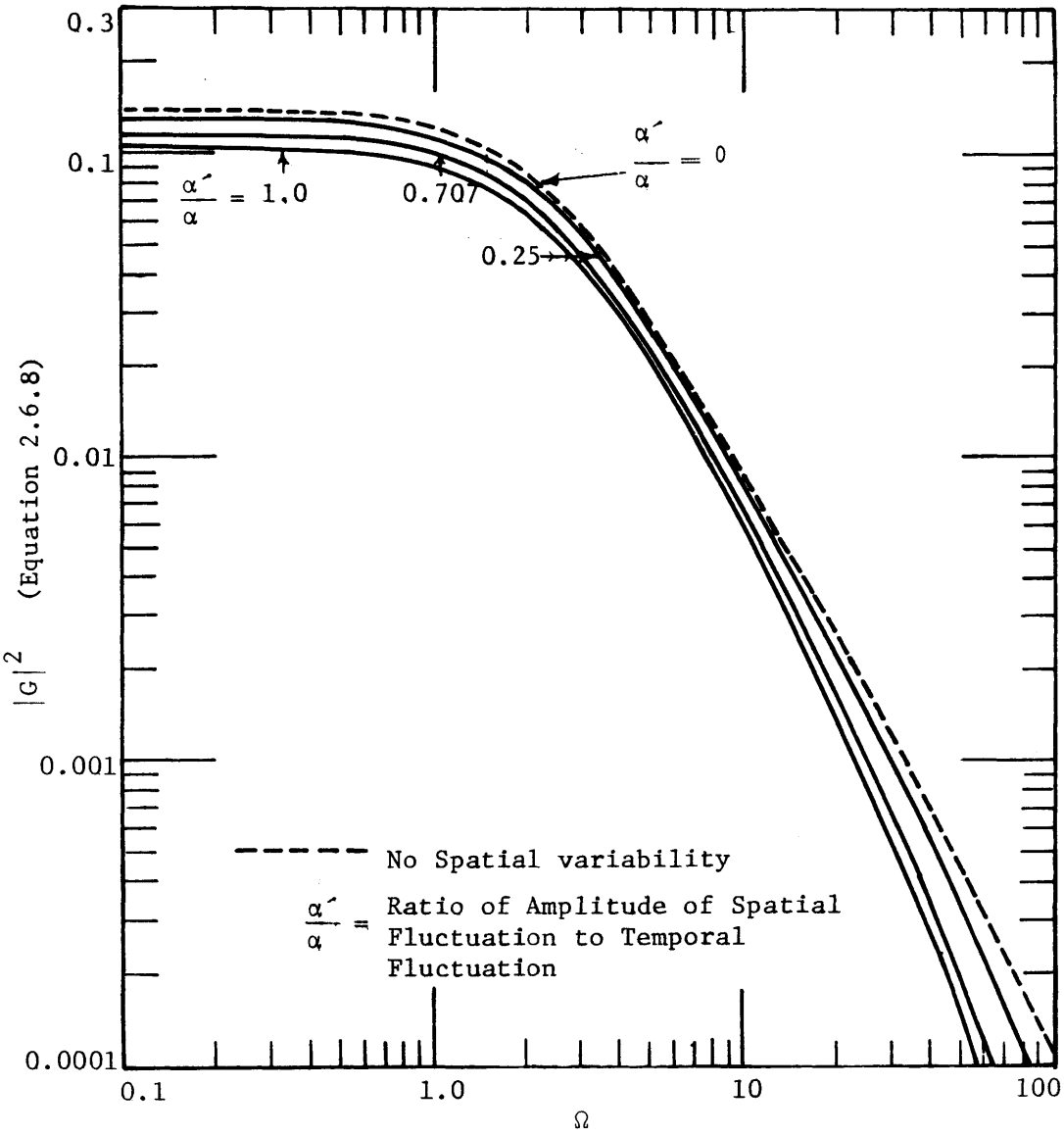

Figure 3.9 Square of the Amplitude of the Transfer Function for the Accretion Input System with Spatial Variability at x/L = 0.50

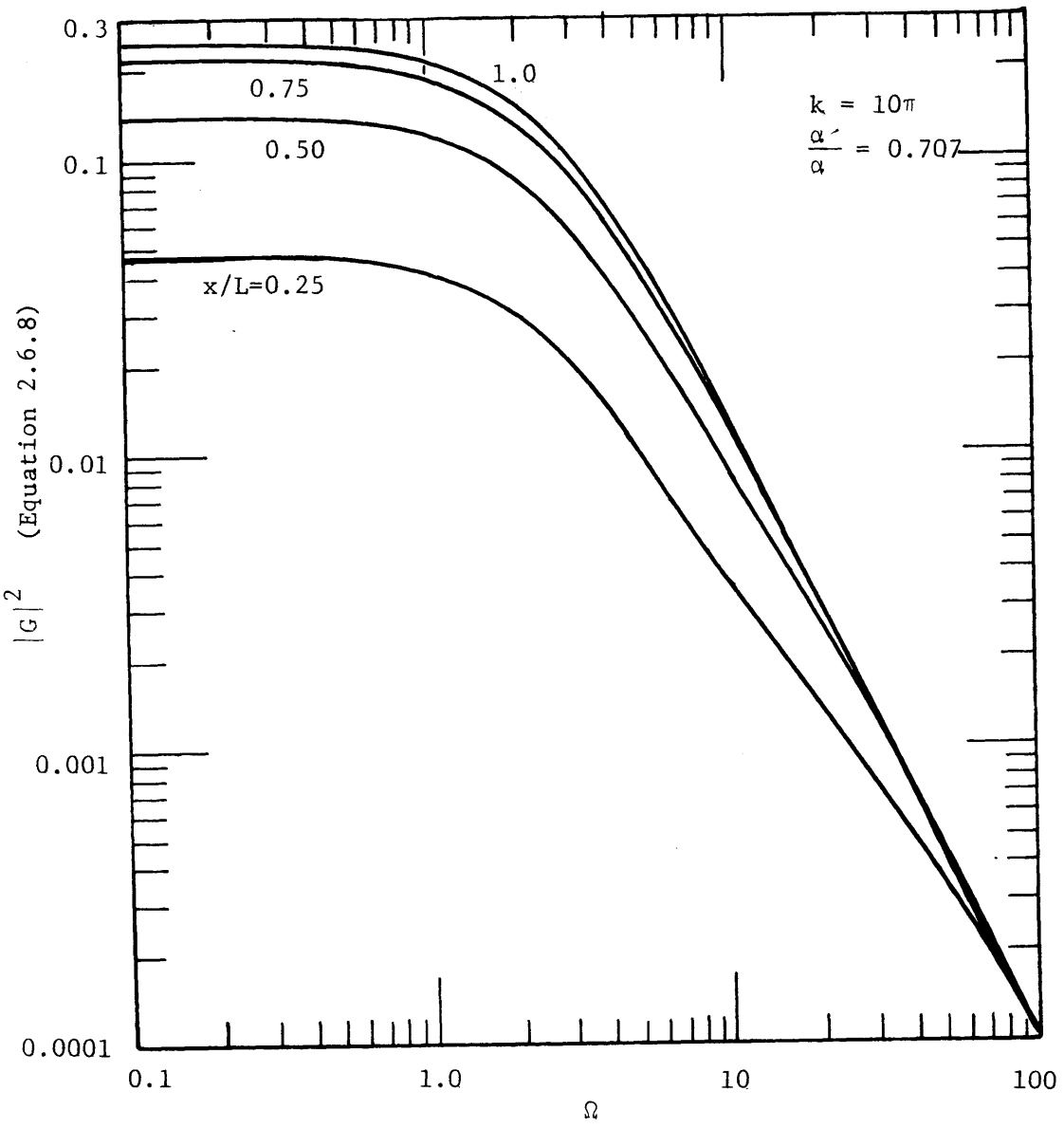

Figure 3.10 Square of the Amplitude of the Transfer Function for the Accretion Input System with Spatial Variability, $k = 10\pi$, $\frac{\alpha'}{\alpha} = 0.707$

3.2 The Numerical Model: Deterministic Simulation and Model Evaluation

Introduction

The objective of this section is to discuss the numerical model which is used to study the nonlinearity of the Dupuit equation. The advantage of such a model is that it can be easily implemented in the stochastic simulation described in the next section and that we can explore some of the complexities that can not be achieved in the linear analytical study. On the other hand, it is expensive to solve the problem numerically and a careful analysis is required in relation to the accuracy and efficiency of the model. In this study a number of cases in deterministic linear and nonlinear simulation are examined; the former serves as verification and accuracy test of the program, while the latter provides some background for nonlinear evaluation in the stochastic simulation.

The Finite Difference Approximation

Numerical approximations to solutions of the Dupuit equation may be obtained by the stepwise solution of an associated difference equation. In this study, an alternating-direction implicit scheme proposed by Peaceman and Rachford in 1955 is utilized in a revision of the basic computer program written by Prickett and Lonnquist (1971).

The presentation of the Dupuit equation is in two dimensional form according to Prickett and Lonnquist.

$$S \frac{\partial h}{\partial t} = \frac{\partial}{\partial x} \left(T \frac{\partial h}{\partial x}\right) + \frac{\partial}{\partial y} \left(T \frac{\partial h}{\partial y}\right) + \varepsilon(x,y,t) \qquad (3.2.1)$$

The finite difference approximation to this equation can be obtained in

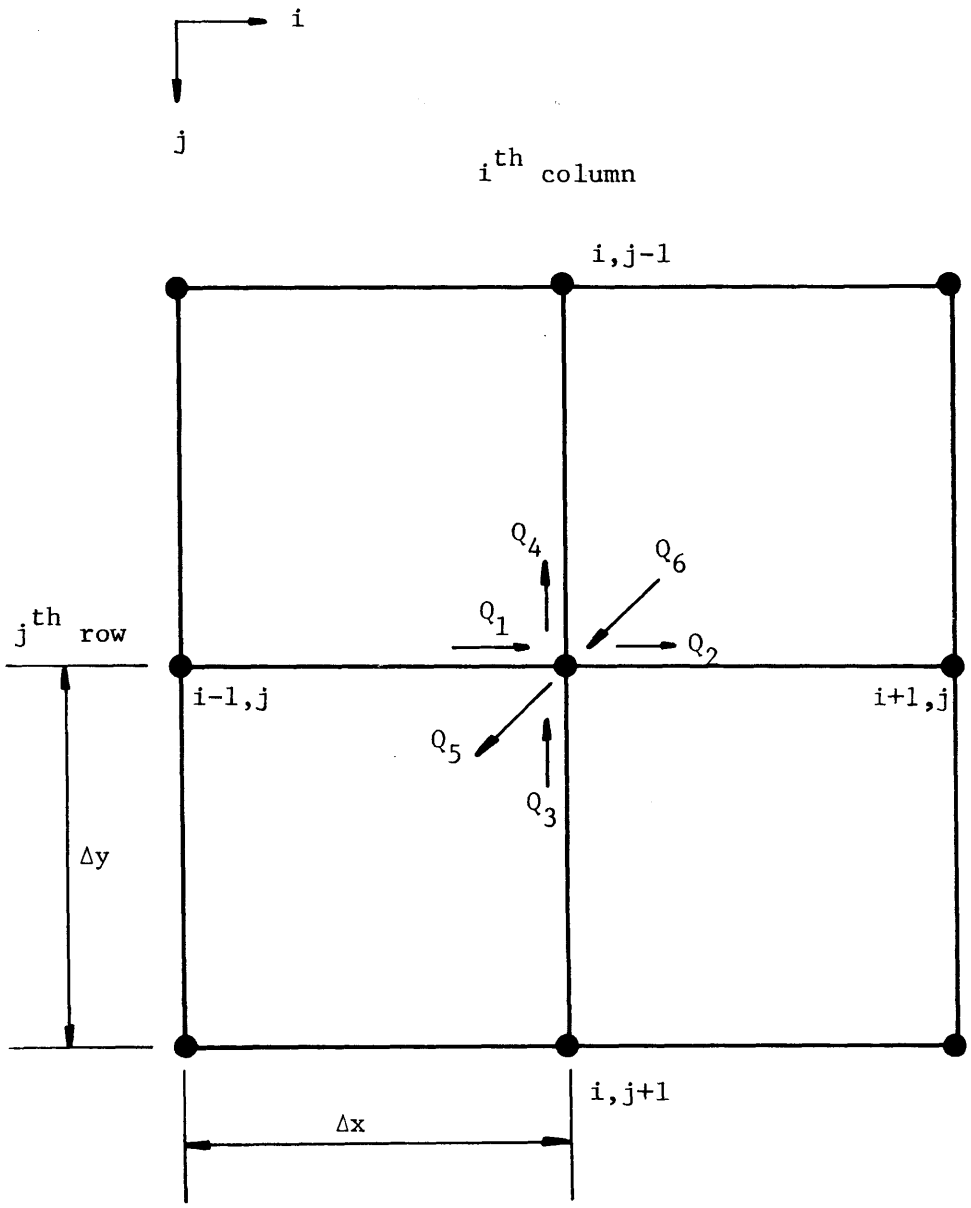

Figure 3.11 Finite Difference Grid

two ways, i.e. from the physical viewpoint that the principle of conservation of mass and Darcy's law are observed, or from the mathematical viewpoint using finite difference approximations for the derivatives for equation 3.2.1. The physical viewpoint is to be described in this study. This approach makes use of the finite difference grid illustrated in Figure 3.11. The aquifer is subdivided into volumes with area $\Delta x \Delta y$. The differential ∂x and ∂y are approximated by Δx and Δy respectively. The intersection of the grids form nodes which are the discrete point locations on the aquifer. Flow rates Q_1, Q_2, Q_3, Q_4, Q_5 and Q_6 are assigned as shown in Figure 3.11. Q_1, Q_2, Q_3 and Q_4 represent node to node water transfer rates. Using Darcy's law

$$
\begin{aligned}
Q_1 &= T_{i-1,j,2}(h_{i-1,j} - h_{i,j}) \frac{\Delta y}{\Delta x} \\
Q_2 &= T_{i,j,2}(h_{i,j} - h_{i+1,j}) \frac{\Delta y}{\Delta x} \\
Q_3 &= T_{i,j,2}(h_{i,j+1} - h_{i,j}) \frac{\Delta x}{\Delta y} \\
Q_4 &= T_{i,j-1,1}(h_{i,j} - h_{i,j-1}) \frac{\Delta x}{\Delta y}
\end{aligned}
\qquad (3.2.2)
$$

where $T_{i,j,1}$ = transmissivity between nodes i,j and i,j+1

$T_{i,j,2}$ = transmissivity between nodes i,j and i+1,j

$h_{i,j}$ = calculated heads at the end of a time increment measured from an arbitrary reference level

Q_5 is the flow rate associated with the amount of water taken into or released from storage per unit time increment Δt.

$$
Q_5 = \frac{S \, \Delta x \Delta y (h_{i,j} - h\phi_{i,j})}{\Delta t} \qquad (3.2.3)
$$

where S = storage coefficient

$h\phi_{i,j}$ = calculated head, at node (i,j) at the end of the previous time increment.

The flow rate Q_6 is the accretion at node (i,j),

$$Q_6 = \varepsilon_{i,j} \Delta x \Delta y \qquad \text{where } \varepsilon_{i,j} = \text{rate of accretion} \tag{3.2.4}$$

Using continuity equations for all flow rates we obtain

$$Q_1 + Q_3 + Q_6 = Q_2 + Q_4 + Q_5 \tag{3.2.5}$$

Substituting equations (3.2.2), (3.2.3) and (3.2.4) into this and rearranging the terms we obtain the finite difference form of the differential equation

$$\frac{T_{i-1,j,2}(h_{i-1,j} - h_{i,j})}{\Delta x^2} + \frac{T_{i,j,2}(h_{i+1,j} - h_{i,j})}{\Delta x^2}$$

$$+ \frac{T_{i,j,1}(h_{i,j+1} - h_{i,j})}{\Delta y^2} + \frac{T_{i,j-1,1}(h_{i,j-1} - h_{i,j})}{\Delta y^2}$$

$$+ \varepsilon_{i,j} = \frac{S(h_{i,j} - h\phi_{i,j})}{\Delta t} \tag{3.2.6}$$

The solution of this difference equation is by iterative alternating direct implicit method which involves reducing a large set of simultaneous equations down to a number of small sets for a given time increment. For a more detailed description, see Peaceman and Rachford (1955) for its theoretical development and Prickett and Lonnquist (1971) for its modification. The advantages of using this method are the rapid convergence of the solution and its unconditional stability regardless of the size of the time increment.

The basic aquifer simulation program by Prickett and Lonnquist (1971) is adopted throughout this study with some modifications. These include the following items:

(a) One dimensional case - The equation we study is a one dimensional form instead of two as that in the numerical model. The change is made by retaining the minimum number of nodes along one direction (y-axis). In this program the minimum number of y nodes is two.

(b) Number of nodes along the aquifer (x-axis) - The number of nodes chosen depends on the tradeoff between the accuracy of the model and the cost involved. In a similar problem, Remson (1971) adopted 21 nodes in the finite difference model. In fact, it has been tested in this program that a choice of 31 nodes does not increase accuracy significantly (0.1%), whereas the computer cost increases significantly (over 20%). Hence, the choice of 21 nodes is considered to be appropriate. Given 21 nodes, we have 20 divisions, i.e. $\Delta x = 1/20$. For simplicity, the other increment, Δy is made equal to this horizontal increment.

(c) Boundary conditions - From the physical picture of the system, we see that there are four physical boundaries, i.e. the boundary between the stream and aquifer, the water table above, the impervious boundary at the bottom and the vertical impervious boundary at the end of the aquifer. In the difference equation model, the fluctuation of stream H(t) is represented as

$$h(i,j) = H(t) \quad \text{for } i=1,\ j=1 \text{ and } 2 \text{ respectively}$$

In addition it must be assured that the water level at this boundary node does not change due to the flow in the aquifer. This condition can

be handled in the computer program by assigning relatively large values of storage factors along the boundary. The storage factor is defined to be the product of storage coefficient and the unit area of the aquifer. This storage factor is given a value of 10^8 throughout the numerical study. The water table boundary condition is implied by the accretion condition which can be easily represented in terms of temporal and spatial dependent values. The no flow condition at the end of the aquifer horizontal axis is represented in the model as

$$h_{n-1,j} = h_{n+1,j} \qquad \text{for } j=1 \text{ and } 2 \text{ respectively.}$$

(d) Water table conditions - This is the condition for the non-linear Dupuit model where the transmissivities depend on the aquifer thickness, i.e. T = Kh. For a linearized Dupuit model, this could be done by setting all transmissivities to be constant. There are two major methods to approximate the head, h. They are the geometric mean and the arithmetic mean methods. The second method is chosen for the simple reason that we do not know exactly the shape of the water table which behaves differently under the random boundary conditions. The arithmetic mean method assigns the transmissivity between two nodes as the arithmetic average head between the two nodes, i.e.

$$T_{i,j,2} = PERM_{i,j,2} \left(\frac{h_{i,j} + h_{i+1,j}}{2}\right)$$

$$T_{i,j,1} = PERM_{i,j,1} \left(\frac{h_{i,j} + h_{i,j+1}}{2}\right)$$

where $PERM_{i,j,2}$ = hydraulic conductivity of aquifer between (i,j) and (i+1,j)

$PERM_{i,j,1}$ = hydraulic conductivity of aquifer between (i,j) and (i,j+1).

Model Evaluation

The accuracy of the numerical model is one of the important issues in this study. Direct mathematical error analysis is not available due to the complexicity of the boundary conditions and the system. Direct verification of the results is based on the linearized numerical model with deterministic sinusoidal inputs, the analytical solutions of which were already found.

Numerical models of differential equations are subject to two major types of errors; truncation error and numerical (round-off) error. Truncation error depends on the size of grid interval (Δx and Δy) to be chosen. In this numerical scheme, the derivation of the difference equation is based on the central-difference approximation with transmissivities assigned to the successive nodes as weights, i.e.

$$\frac{\partial}{\partial x}\left(T \frac{\partial h}{\partial x}\right) \simeq \frac{T_{i-1,j,2}\, h_{i-1,j} - T_{i-1,j,2} h_{i,j} - T_{i,j,2} h_{i,j} + T_{i,j,2} h_{i+1,j}}{(\Delta x)^2} \tag{3.2.7}$$

$$\frac{\partial}{\partial y}\left(T \frac{\partial h}{\partial y}\right) \simeq \frac{T_{i,j-1,1} h_{i,j-1} - T_{i,j-1,1} h_{i,j} - T_{i,j,1} h_{i-1,j} + T_{i,j,1} h_{i,j+1}}{(\Delta y)^2} \tag{3.2.8}$$

Hence, the truncation error for such a scheme is in the order of $(\Delta x)^2 + (\Delta y)^2$. For a choice of 21 nodes in the model, this error is in the order of 0.005.

The round-off error is due to the difference between solving the difference equation exactly and the numerical model by computer. The condition for stability is the case when this error approaches zero over

the whole region of solution. This numerical model, as it has been pointed out by Peaceman and Rachford (1955), has the advantage of being unconditionally stable regardless of the size of the time increment.

The total error of the model is made up of the truncation error and the round-off error. The truncation error is due to the form selected for the finite difference equation, and is often the larger part of the total error. However, for a particular model like this with inputs as exogenous variables feeding into the system, we need a more direct evaluation of the total error as a function of the parameters of the inputs. These parameters are the amplitude, mean and frequency. Using some typical values of these parameters, it is possible to estimate the error of the linear simulation study. Before discussing these results, it is important to understand the efficiency of this numerical model. This is a problem of choosing the proper time step, Δt, which would lead to rapid solution. In general, the smaller the Δt, the smaller the number of iterations (see Prickett and Lonnquist, 1971) for the numerical solution to reach a predetermined error criterion (E). This error criterion controls the sum of the changes in head during iterations over the entire model and assures that computed heads have converged to answers within a specified tolerance. This depends on the time step of the model.

The frequency of a sinusoidal input function is directly related to this time step. For a given time step, the higher the frequency, the less information is obtained due to the discrete time step of the numerical model. To retreive this information it is necessary to reduce the time step by a proportional amount. The efficiency of the model re-

quires that the time step is chosen in such a way that the cost of running the computer model is kept to a minimum. For a number of initial runs of the model, it was estimated that Δt is chosen approximately as

$$\Delta t \simeq \frac{0.1}{\Omega} \quad \text{for } \Omega > 1 \tag{3.2.9}$$

For $\Omega<1$, Δt is chosen to be 0.1 in all cases. Henceforth, the error criterion E can be estimated for a given Δt used in the model. From Figures 3.1(a) and 3.2(a) the magnitude of the amplitude response $\Omega \leq 1$ is approximately one. From equation 3.2.9, Δt is found approximately to be 0.1. In order that the error criterion, E, be 1% in order of magnitude, the formula for relating E and Δt is estimated as

$$E \simeq \frac{1}{10} \Delta t \tag{3.2.10}$$

or

$$\simeq \frac{1}{100\Omega}$$

As Ω increases, this error criterion decreases but correspondingly, the amplitude of the response function also decreases at an equal or smaller rate. Hence, in the range of Ω from 0.1 to 100, we have error criterion of 1%.

In the simulation study, it usually takes some time for the solution to reach quasi-steady state. It was found that it takes four or five cycles for a sinusoidal input to reach this state. A typical example is shown in Figure 3.12 which shows simulation results of the stream interaction case with input frequency equal to 20 and amplitude 1 at location x/L = 0.5. The linear simulation with inputs at some typical frequencies and amplitudes and means are compared to the analytical

Figure 3.12 Linear Simulation versus Linear Theory with Stream Stage Input $\eta_0 = 1 + \beta \sin \Omega_\beta \tau$, β=0.5, Ω_β=20

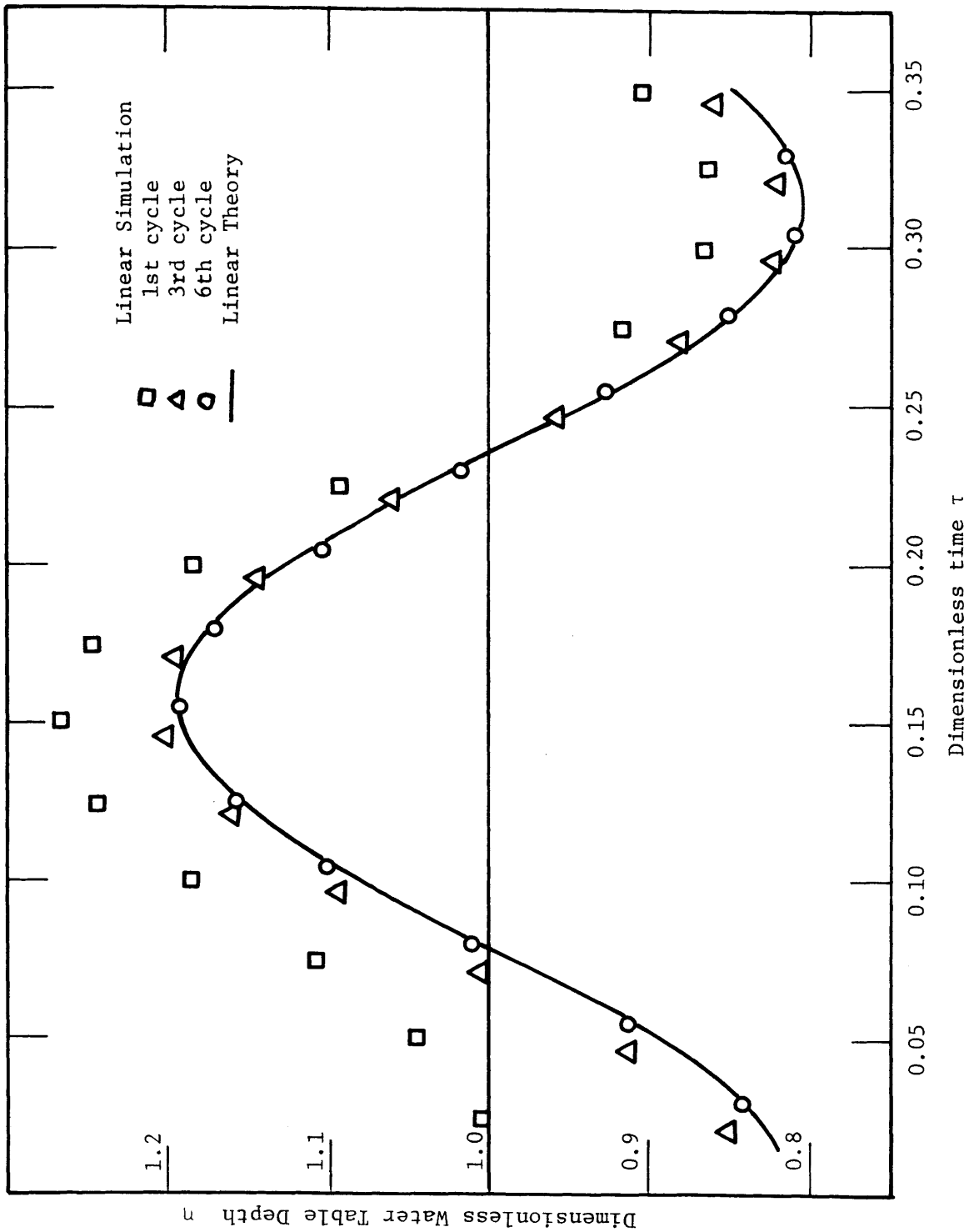

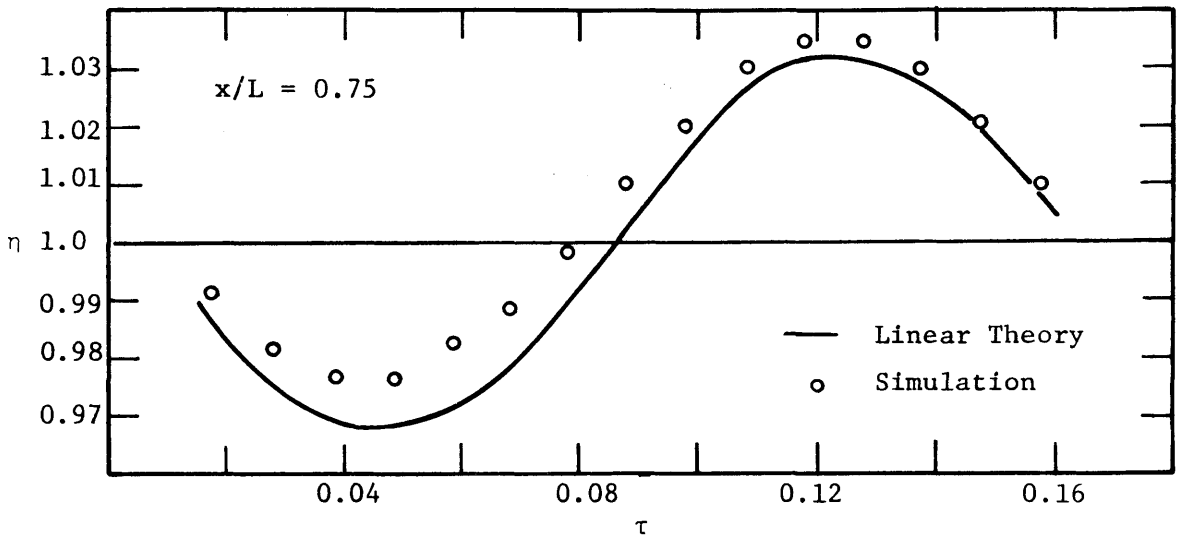

Figure 3.13(a) Linear Simulation versus Linear Theory with Stream Stage Input, $\eta_0 = 1 + \beta \sin \Omega_\beta \tau$, β=0.5, Ω_β=40

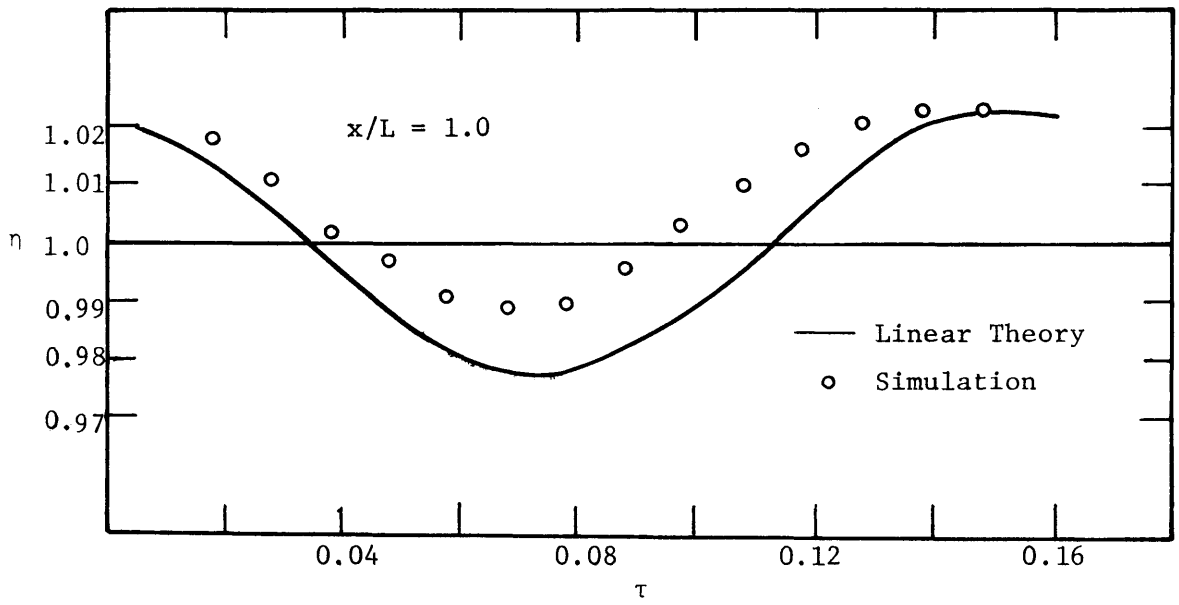

Figure 3.13(b) Linear Simulation versus Linear Theory with Stream Stage Input, $\eta_0 = 1 + \beta \sin \Omega_\beta \tau$, β=0.5, Ω_β=40

solutions. Other linear simulations show that results do not depend on the amplitudes and frequency. One simulated result is shown in Figure 3.13(a) and (b) respectively. The results show that the error increases slightly as a function of the distance away from the stream. Errors are less than 1% in all of the simulation results. On the other hand, the mean of accretion has slightly increased the error as shown in Figure 3.14. However, the results show that all errors are less than 2% which is sufficient for the purpose of this study. In conclusion, the only parameter that would slightly increase the error of the numerical model is the spatial horizontal distance from the stream. For a range of α_0 from 0 to 3 there is sufficiently small error which may be neglected for the purpose of this study. A listing of the computer program is given in Appendix A.

Nonlinear Simulation with Deterministic Inputs

The objective of this section is to discuss nonlinear simulation results and their deviations from the linear theory. The nonlinear numerical model is exactly the same as the linear model discussed previously, except that the transmissivity at each node of the grid is assigned varying values with the condition that both models are in dimensionless form (which means the dimensionless head has order of magnitude of about one). It is reasonable to assume that the numerical error of the nonlinear model is similar to that of the linear model. Since this error is sufficiently small, we may further assume that the difference between the restults of the nonlinear simulation results and those of the linear theory is primarily due to the nonlinear effects or deviations

rather than to numerical error. For the steady state case with constant accretion, there exists analytical solutions for both linear and nonlinear cases (see 2.1 and 3.15) shows the relatively small numerical error for the nonlinear simulation and this has a trend similar to the numerical error of the linear simulation (compare to Figure 3.14). These results further confirm our assumptions. On the other hand, Figure 3.16 shows significant nonlinear effects for the steady state case with constant accretion. It is noticed that such deviations increase significantly when α_0, the mean of accretion is greater than 1. This is one of the major nonlinear parameters in the system.

The nonlinear simulation for the transient state solutions (both for accretion and stream interaction cases) is tested using simple sinusoidal inputs with typical amplitudes and frequencies. The purpose of these tests is twofold; to understand the general behavior of the nonlinear system and to verify the simple theory developed in section 3.1 regarding the evaluation of the nonlinear terms. The following table (Table 3.1) and figures (Figures 3.17 - 3.25) show various cases being tested for the two deterministic inputs:

Accretion case:

$$\rho(\tau) = \alpha_0 + \alpha \sin \Omega_\alpha \tau \tag{3.2.11}$$

Stream interaction case:

$$\eta_0(\tau) = \beta_0 + \beta \sin \Omega_\beta \tau \tag{3.2.12}$$

All these are represented in dimensionless forms. In the stream interaction case, the mean β_0 is set to 1; hence the maximum value for β is equal to 1 in all cases.

Figure Number	Stream or Accretion case	α_0	α	β	Ω_α or Ω_β
3.17	Stream	0	0	0.5	0.5
3.18	Stream	0	0	0.5	10,20,50
3.19	Stream	0	0	0.2	10,20,50
3.20	Accretion	1	1	0	0.5
3.21	Accretion	2	1	0	0.5
3.22	Accretion	0	1	0	10,50
3.23	Accretion	1	1	0	10,20,50
3.24	Accretion	1	2	0	10,20,50
3.25	Accretion	2	1	0	10,50

Table 3.1 List of Nonlinear Simulations with Deterministic Sinusoidal Inputs at x/L = 0.5

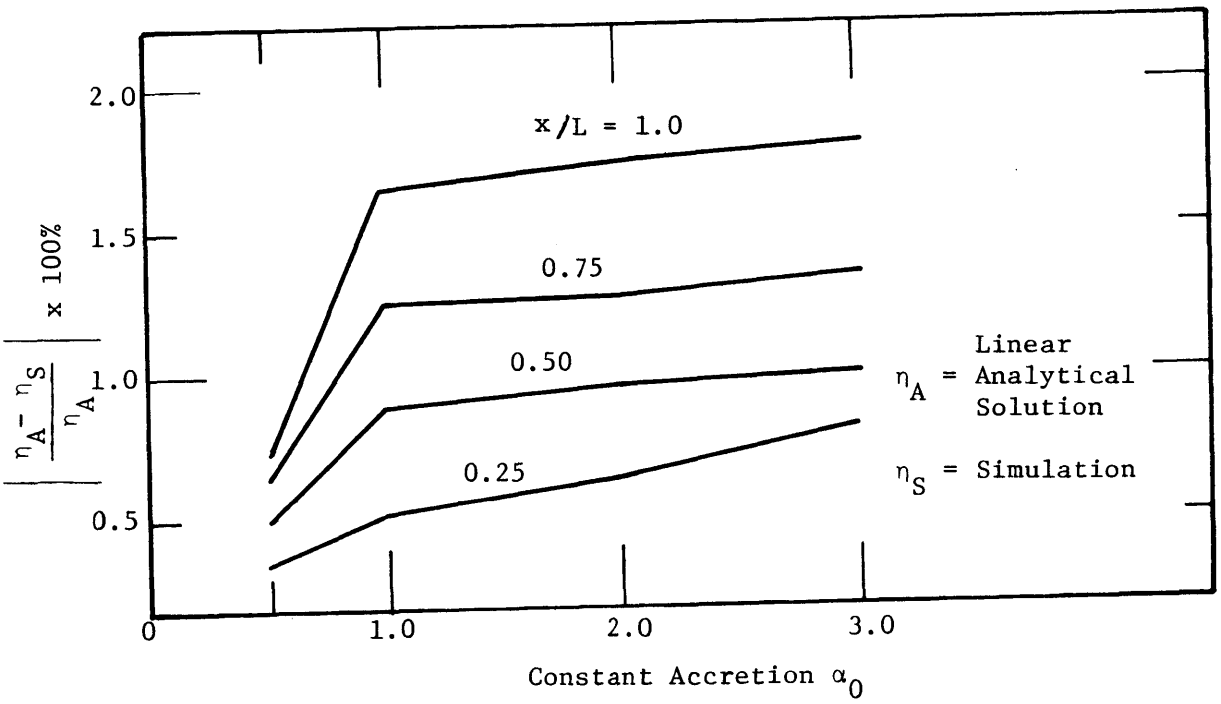

Figure 3.14 Numerical Error of Linear Simulation for Steady State Constant Accretion Case

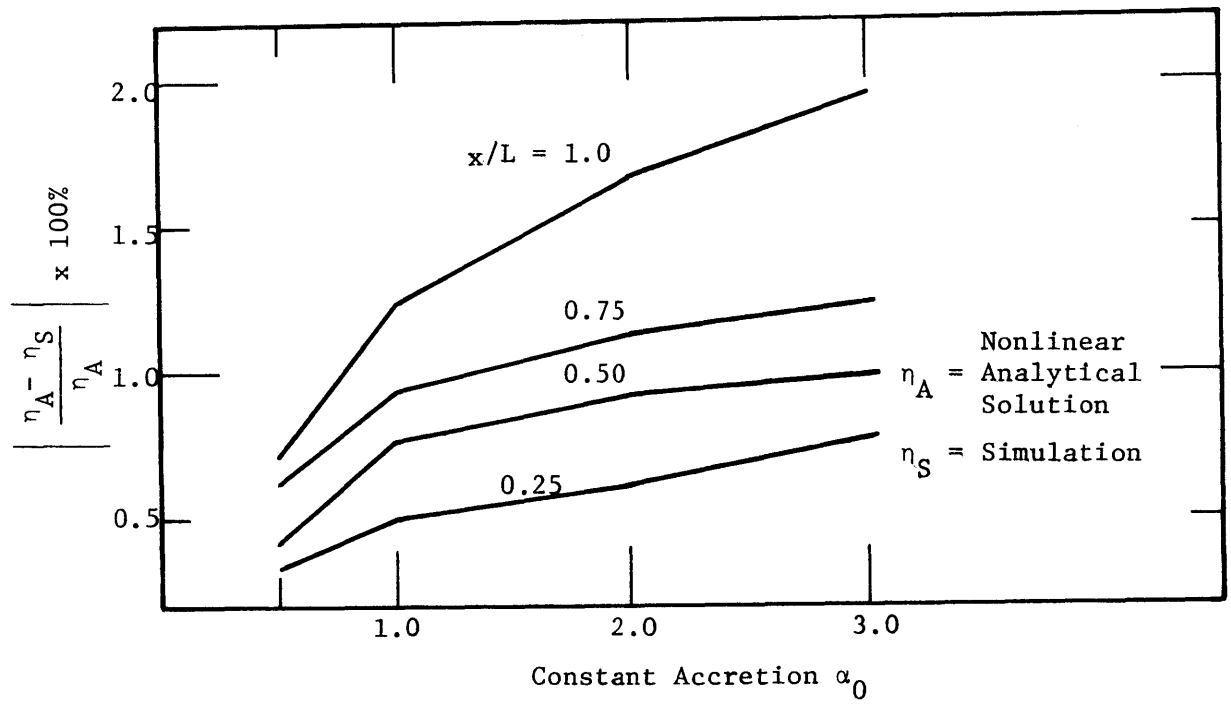

Figure 3.15 Numerical Error of Nonlinear Simulation for Steady State Constant Accretion Case

Figure 3.16 Comparison of Nonlinear Simulation versus Linear Theory for Steady State Constant Accretion Case

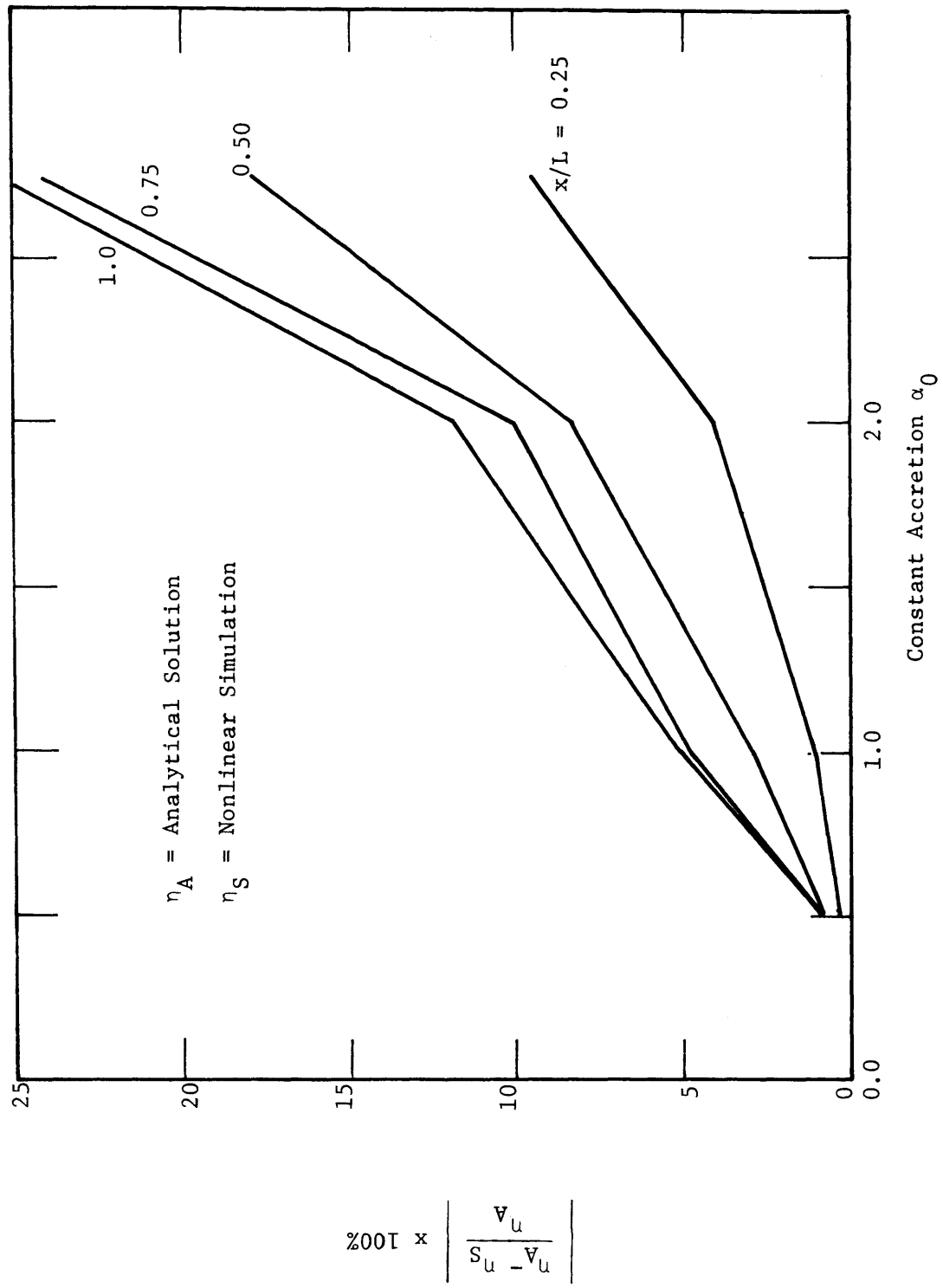

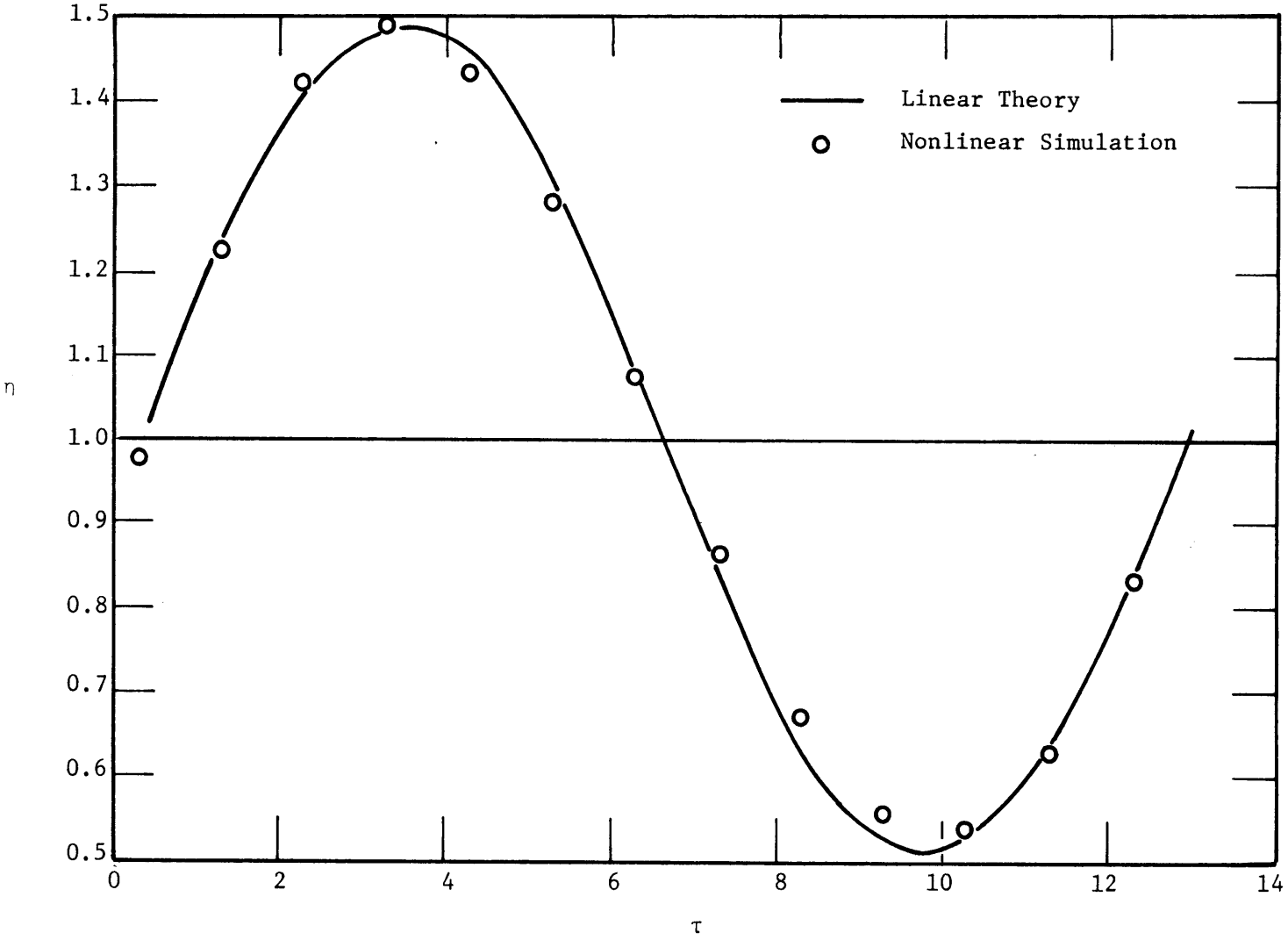

Figure 3.17 Nonlinear Simulation versus Linear Theory at x/L = 0.50 with Stream Stage Input, $\eta_o = 1 + \beta \sin \Omega_\beta \tau$, β=0.5, Ω_β=0.50

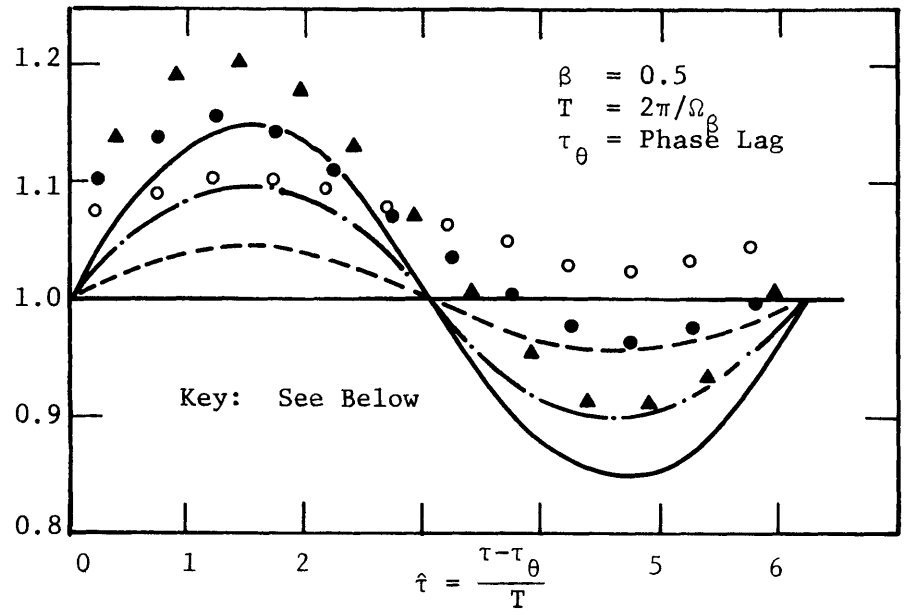

Figure 3.18 Nonlinear Simulation at x/L = 0.50 with Stream Stage Input, $\eta_0 = 1 + \beta \sin \Omega_\beta \tau$

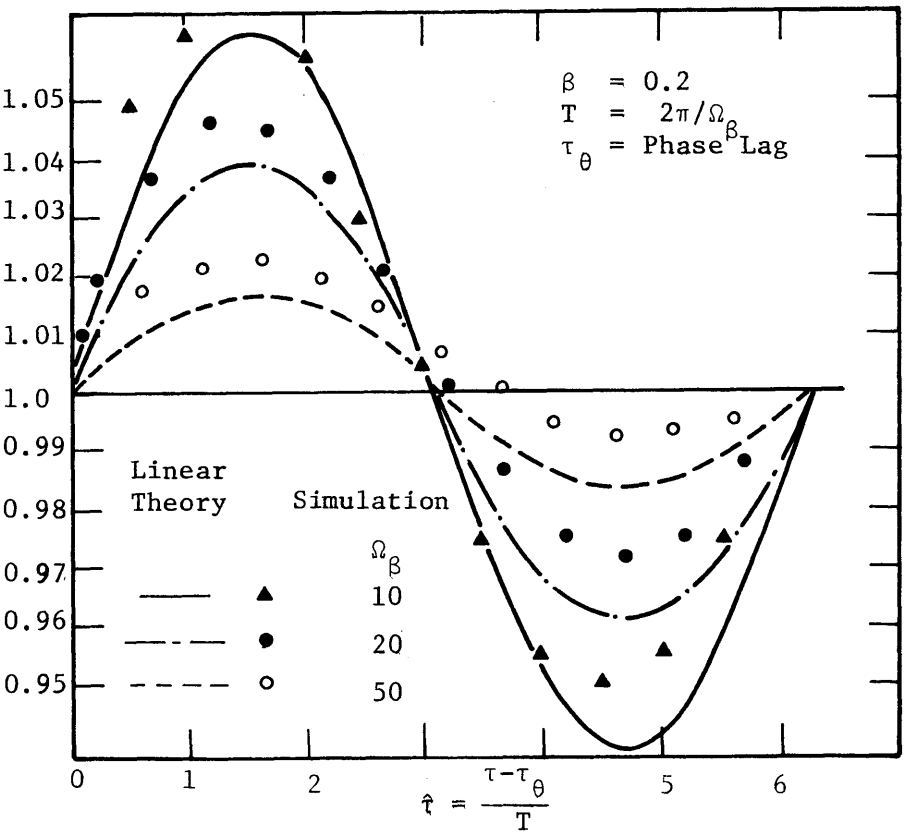

Figure 3.19 Nonlinear Simulation at x/L = 0.50 with Stream Stage Input, $\eta_0 = 1 + \beta \sin \Omega_\beta \tau$

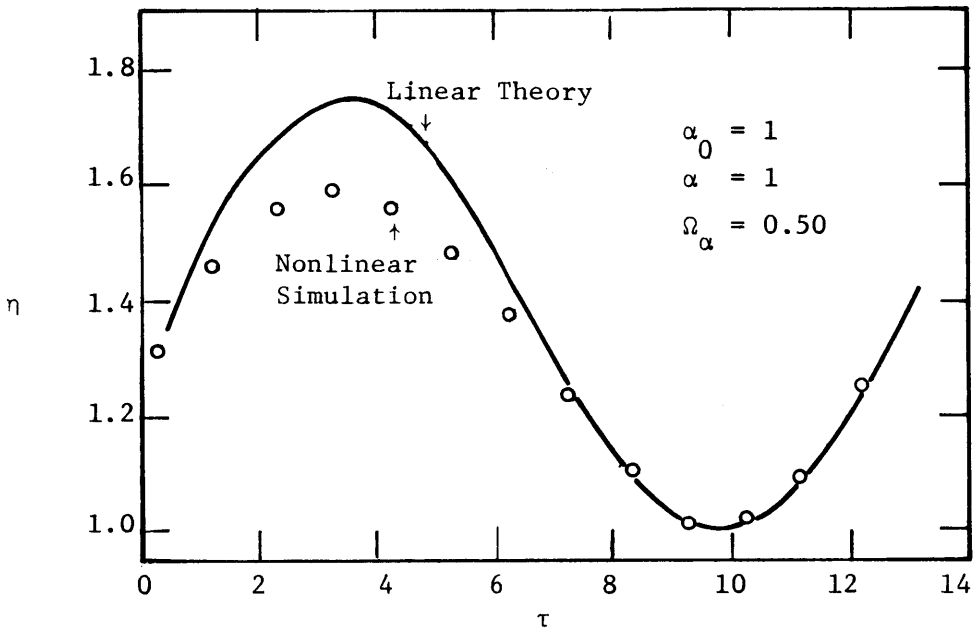

Figure 3.20 Nonlinear Simulation versus Linear Theory at x/L = 0.50 with Accretion Input, $\rho = \alpha_0 + \alpha \sin \Omega_\alpha \tau$

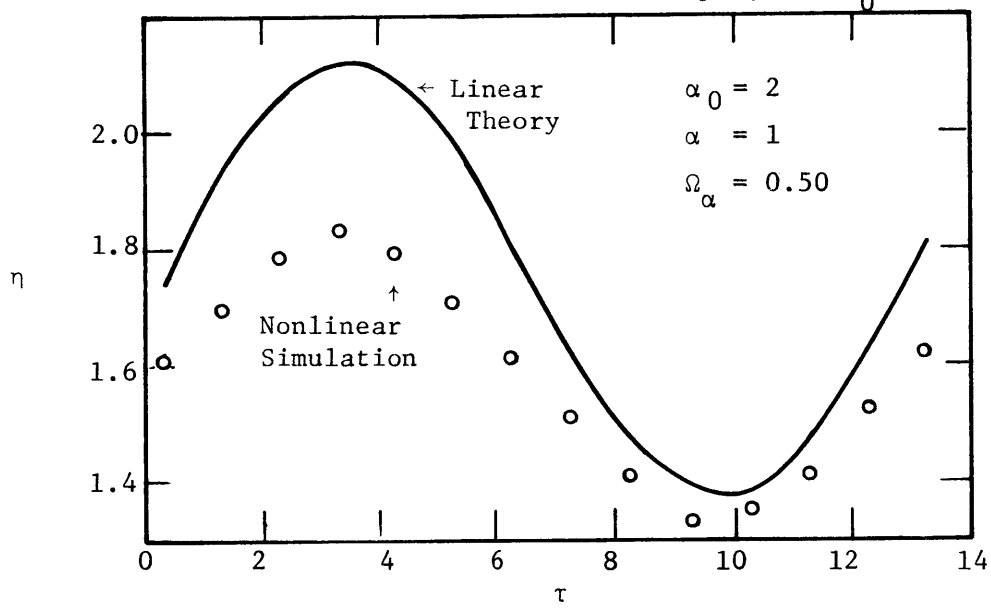

Figure 3.21 Nonlinear Simulation versus Linear Theory at x/L = 0.50 with Accretion Input, $\rho = \alpha_0 + \alpha \sin \Omega_\alpha \tau$

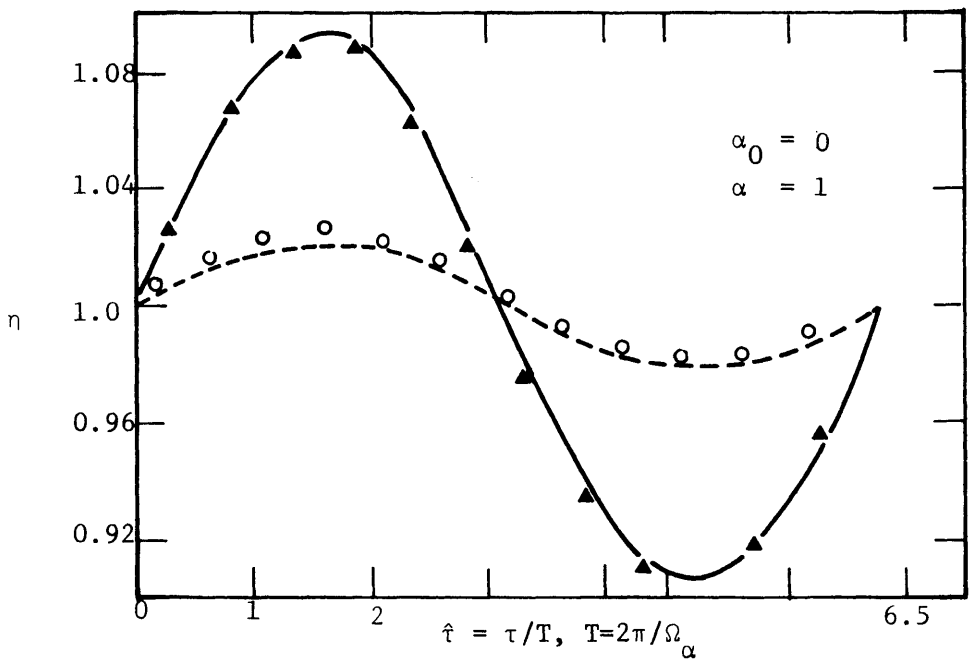

Figure 3.22 Nonlinear Simulation versus Linear Theory with Accretion Input, $\rho = \alpha_0 + \alpha \sin \Omega_\alpha \tau$

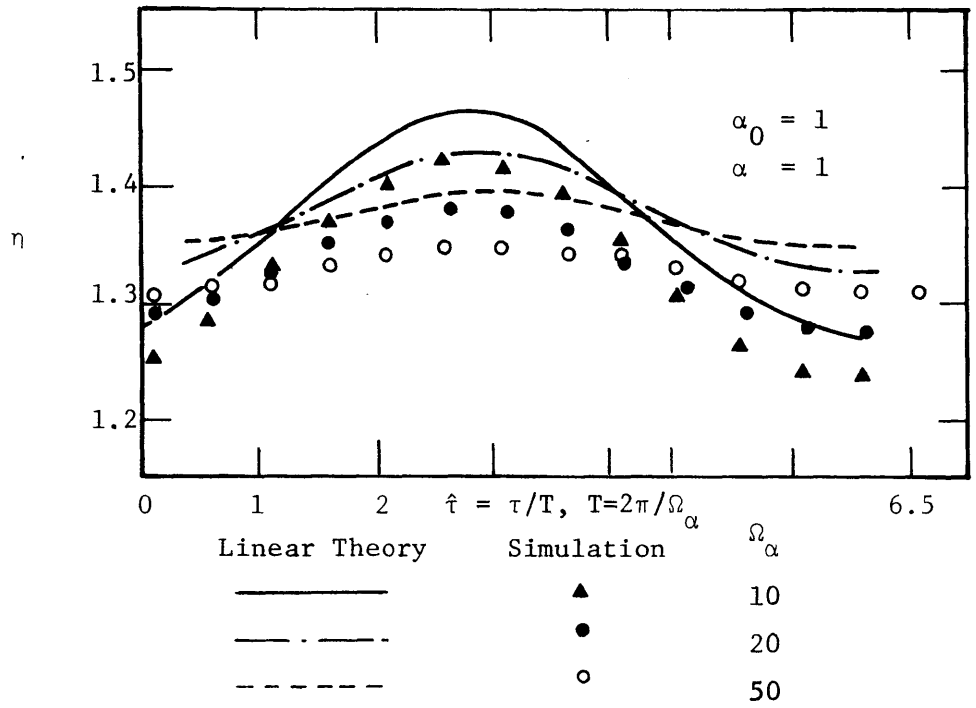

Figure 3.23 Nonlinear Simulation versus Linear Theory at x/L = 0.50 with Accretion Input, $\rho = \alpha_0 + \alpha \sin \Omega_\alpha \tau$

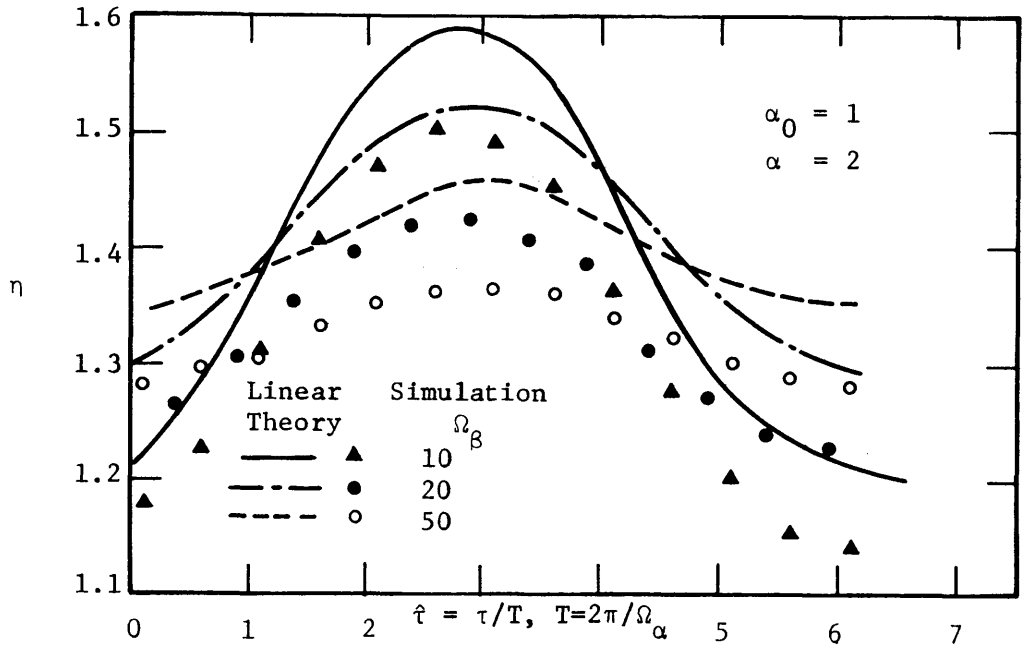

Figure 3.24 Nonlinear Simulation versus Linear Theory at x/L = 0.50 with Accretion Input, $\rho = \alpha_0 + \alpha \sin \Omega_\alpha \tau$

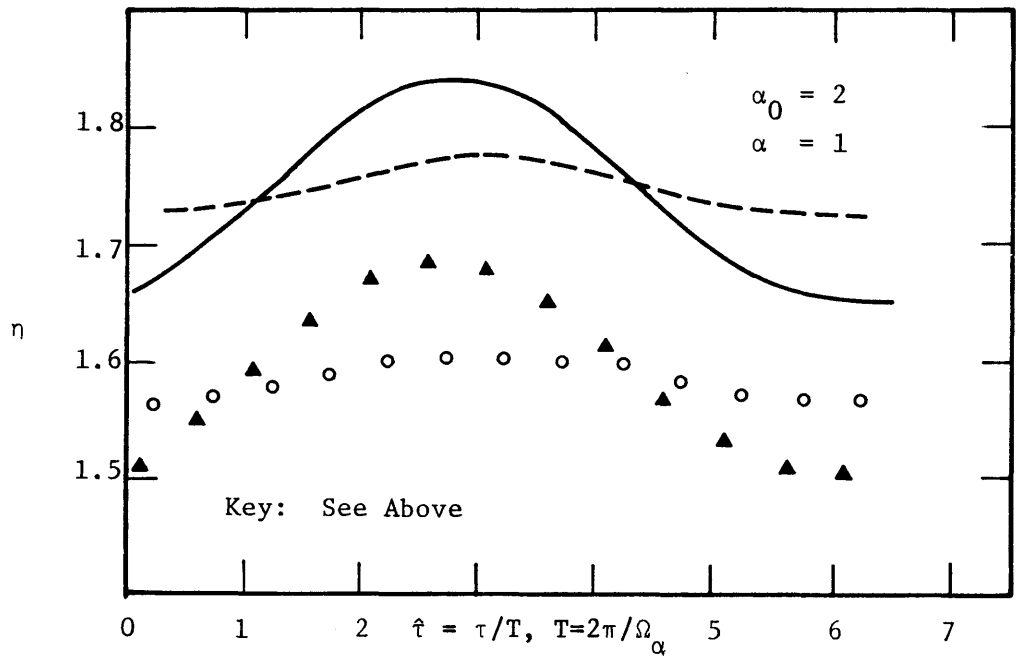

Figure 3.25 Nonlinear Simulation versus Linear Theory at x/L = 0.50 with Accretion Input, $\rho = \alpha_0 + \alpha \sin \Omega_\alpha \tau$

From these graphical results, it can be seen that the nonlinear solutions have sinusoidal shapes similar to those of the linear solutions. Hence, it may be concluded that the frequency of the response is quite close to that of the input. Furthermore, there is hardly any observable phase lag between the nonlinear and linear solutions. The only major difference is the upshift or downshift of the mean. These results show that the assumption in section 3.1 in the evaluation of nonlinear terms is reasonable. A number of points can be further confirmed by these results and are given as follows:

(a) Nonlinear deviations are significant in the range of low frequency in the case of accretion but are negligibly small in the case of stream interaction. See Figures 3.20, 3.21 and 3.17.

(b) Nonlinear deviations are approximately the same at higher frequency in both cases, accretion and stream interaction. In the former case, the nonlinear results are greater than those of the linear theory, while they are smaller in the latter case. See Figures 3.18 and 3.23.

(c) Nonlinear deviations are greater when the amplitude of fluctuation increases in the case of stream interaction. In Figures 3.18 and 3.19 one can see for $\beta=0.2$, the percentage of deviation is about 1%, whereas for $\beta=0.5$ the percentage of deviation is as much as 5%.

(d) Nonlinear deviations are greater when the amplitude of fluctuation increases in the case of accretion. In Figures 3.23 and 3.24 one can see when the amplitude $\alpha=1$, the percentage of deviation is less than 5%, but when $\alpha=2$ the percentage of deviation is as great as 10%.

(e) Nonlinear deviations are significant when the mean of accretion, α_0, increases. In Figures 3.23 and 3.25 one can see the deviation

increases from 5% at α_0=1 to 17% at α_0=2. In comparing Figures 3.23 to 3.25 one can see that nonlinear deviations are more significant when the mean is increased than when the amplitude is increased.

In conclusion, the study of the nonlinear simulation with sinusoidal inputs identifies a number of nonlinear parameters that are important in the later analysis of the stochastic simulation. These parameters include the mean and amplitude of accretion and the amplitude of stream stage fluctuation. Of these, it seems that the mean of accretion plays the most significant role.

3.3 Nonlinear Simulation of Spectral Response

Introduction

The major objective of this section is to investigate the spectral behavior of a nonlinear simulation of the stochastic phreatic aquifer system. The emphasis is on the transfer function rather than the phase spectrum of the system, since it was previously found that there is very small phase lag between the linear and nonlinear systems. (See sections 3.1 and 3.2) Using the transfer function determined from the simulation, we may make a more direct evaluation of the nonlinear Dupuit model subject to a given set of input statistical parameters. The simulation approach also has the advantage of permitting one to investigate models with further complexities, such as the spatial variability of the accretion rate or the hydraulic conductivity. In addition, the simulation requires the specification of certain characteristics of the numerical model. These are related to the physical parameters of the system, thus helping one to evaluate the effects of nonlinearity.

Characteristics of the Simulation of Spectral Response

A basic feature of the nonlinear simulation is the determination of the dimensionless time interval, $\Delta\tau$ in the numerical model. $\Delta\tau$ plays an important role in this study since it reflects both the physical and statistical aspects of the spectral analysis of the problem. The dimensionless parameters for both linear and nonlinear Dupuit equations are represented as:

dimensionless time $$\tau = \frac{T}{SL^2} t$$

dimensionless accretion $\rho = \frac{L^2}{Tm} \varepsilon(t)$

dimensionless stream stage $\eta_0 = \frac{H(t)}{m}$

where m is some characteristic aquifer thickness. In the linearized model, T is a constant; whereas in the nonlinear model T = Kh.

The simulation requires the determination of the time step interval, $\Delta\tau$. Once this is known, the physical parameters, S and T of the phreatic aquifer are implied and hence the output can be obtained. This time step interval is given by

$$\Delta\tau = \frac{T}{SL^2} \Delta t \qquad (3.3.1)$$

where Δt is the real time step interval in days, weeks, months or years.

At first, it seems that the determination of $\Delta\tau$ requires the explicit physical specification of the system, i.e. we need to know the physical parameters, S,T,m and L individually. However, $\Delta\tau$ could be estimated in a more implicit way using the sampling theorem in spectral analysis. This sampling theorem states that the shortest period that is theoretically possible to resolve with a given sampling interval, is one which is twice as large as the sampling interval. The maximum dimensionless frequency, Ω_c that can be specified by the sampling interval is given by (see Bendat & Piersol, 1971)

$$\Omega_c = \left(\frac{1}{2\Delta\tau}\right) 2\pi = \frac{\pi}{\Delta\tau} \qquad (3.3.2)$$

The determination of the dimensionless maximum frequency requires a physical understanding of the system. It has been shown previously (see section 3.2) that the dimensionless frequency, Ω, is related to

the aquifer physical properties by

$$\Omega = \left(\frac{SL^2}{T}\right) \omega$$

When Ω=100 it represents a typical aquifer system with a frequency of response of approximately 3 cycles/month, which is rather high for the natural frequency of hydrological processes. In this study the maximum dimensionless frequency, Ω_c chosen is 100 radians/dimensionless time = $100/2\pi$ cycles. Using equation 3.3.2

$$\Delta\tau = \frac{\pi}{100} \cong 0.031416$$

In the nonlinear system, the dimensionless time step, $\Delta\tau_N$ is chosen to be the same value. Hence we have

$$\Delta\tau_N = \Delta\tau$$

and the frequency is the same for both cases. In other words, the nonlinear and linear systems have the same dimensionless frequency scale. With such a choice of $\Delta\tau$, the dimensionless accretion in both systems is the same. Once the time step interval is determined the other parameters of the computer model can be established; e.g. the error criterion, E, which is given by $\Delta\tau/10$.

At each time step, input is generated into the model as was done in the deterministic simulation. The numerical error due to a stationary random time series input for the simulation could be regarded as a function of the mean and variance of the time series. From the nonlinear deterministic simulation it has been shown that this error increases slightly as the mean of dimensionless accretion, α_0 increases. This implies that the mean of the time series should have a similar

effect in the stochastic simulation. To show the importance of this numerical error in the spectral analysis consider the following rough estimate:

Let $\eta^s = (1+a)\eta$

where η^s = numerical output

η = theoretical output

a = numerical error

The spectral function for η^s is

$$S_{\eta^s\eta^s} = (1+a)^2 S_{\eta\eta}$$

Since the input accretion spectra is given by $S_{\rho\rho}$,

$$\frac{S_{\eta^s\eta^s}}{S_{\rho\rho}} = (1+a)^2 \frac{S_{\eta\eta}}{S_{\rho\rho}}$$

From the deterministic simulation, the numerical error for the steady accretion case is about 2% for α_0 as large as 3. Hence, the numerical and theoretical transfer functions are related by

$$\frac{S_{\eta^s\eta^s}}{S_{\rho\rho}} \cong 1.04 \frac{S_{\eta\eta}}{S_{\rho\rho}}$$

This 4% numerical error is sufficiently small for the purpose of this study.

The output from the simulation program and the input time series obtained from historical field data or generated synthetic data are analysed by the BMD02T program (Biomedical Computer Program—Autocovariance and Power Spectral Analysis) (see Dixon, 1973). The main error arising from this is the estimation of the spectrum. Appendix B con-

tains an evaluation of the confidence limits for the spectrum. The variance of the estimate is given by

$$\mathrm{Var}[\hat{S}_{XX}(\Omega)] \sim \frac{MS_{XX}^{2}(\ell)}{T} \tag{3.3.3}$$

where $S_{XX}(\Omega)$ = theoretical spectrum of X

$\hat{S}_{XX}(\Omega)$ = estimated spectrum of X

M = number of lags chosen for the spectral analysis

T = total record length.

Hence, a larger number of lags will, in general, produce a better resolution, but with a loss of confidence in the estimates. A reasonable choice of M is approximately 1/10 or less of the total record length, T. In this study, the total record length for the historical data with 30 days interval is 405 units and M is chosen to be 36. Since the dimensionless input and output spectra of the system are of the order of 0.1 (the dimensionless aquifer thichness η and the accretion, ρ or stream stage η_o are approximately of the order 0.1 to 1.0), hence one can see from equation 3.3.3 that the variance of the estimated spectrum is approximately 0.0001 and the standard deviation is about 1%. Thus, it can be concluded in this study that the error due to the numerical model and that due to the estimation of the spectrum are relatively small.

The basic feature of the numerical model as a transformation system (i.e. the determination of $\Delta\tau$) has been described, the characteristics of the inputs are now considered. These are the parameters controlling the nonlinearity of the system. The choice of these 'nonlinear' parameters forms the basis for the comparison of the transfer function of the simulation and that of the linear theory. In the simple evalua-

tion of the effects of nonlinearity via the deterministic simulation, it has been shown that α_0, α and β are the basic nonlinear parameters. The corresponding parameters in the analysis of a random stationary time series are the mean and standard deviation. To estimate the order of magnitude of these parameters, we require a certain degree of information about the physical system in terms of its properties and dimensions. Using the dimensionless accretion expression from the previous section, we could relate the nonlinear parameters, mean of accretion, α_0 and its amplitude α as given by

$$\alpha_0 = \bar{\rho} = \frac{L^2}{Km} \bar{\varepsilon} \tag{3.3.4}$$

$$\alpha^2 \sim \sigma^2_\rho = \frac{L^4}{K^2 m^2} \sigma^2_\varepsilon \tag{3.3.5}$$

where σ^2_ρ denotes the theoretical variance of ρ.

For a typical aquifer system with length of one mile, hydraulic conductivity of 10^4 gal/day/ft, aquifer thickness near stream of 30 ft. and average monthly precipitation of 3 in., the dimensionless mean of accretion, $\bar{\rho}$ is approximately 4. However, this must be corrected because not all precipitation is passed onto the water table; some being used by vegetation on the ground, some being retained in unsaturated zone above the water table, some being evaporated, etc. Jacob (1943) proposed that the accretion rate is directly proportional to the precipitation. This proportionality constant depends on the geological structure of the system and there is no simple way to determine it. In this study, this constant is assumed to be in the range from 10% to 50%. Hence, in the simulation study, the mean of dimensionless accretion is

chosen to be from 0.5 to 2 for a typical aquifer system.

From equation 4.2.1, the dimensionless accretion, $\bar{\rho}$, may be written as

$$\bar{\rho} = \frac{1}{Sm} \frac{\Delta t}{\Delta \tau} \bar{\varepsilon} \tag{3.3.6}$$

and using equation 4.2.2

$$\bar{\rho} = \frac{2\Omega_c}{Sm} \Delta t \ \bar{\varepsilon} \tag{3.3.7}$$

where $\bar{\varepsilon} = \gamma \bar{P}$

γ = percent of precipitation going to accretion

P = precipitation.

One can see that the $\bar{\rho}$ is proportional to the maximum frequency in the system. system. The choice of this frequency, as we have discussed, is based on the physical parameters and the characteristic frequency of response of the system. This characteristic frequency of response refers to the frequency due to the hydrological processes rather than to noise. The choice of the real time step, Δt depends on the amount of information we want to retrieve from the hydrological processes. In this study, the groundwater system has a relative slow response. In addition, we have a relatively long record of time span (about 36 years). Hence, a choice of 30 days or 1 month for each time interval was considered appropriate.

The dimensionless variance of the time series is related to the dimensionless mean as a ratio $\sigma_\rho / \bar{\rho}$. From equations 3.3.4 and 3.3.5 this ratio is equal to $\sigma_\varepsilon / \bar{\varepsilon}$, which is fixed in the historical data simulation, but which can be varied in the synthetic data. It is assumed that this ratio varies from 0.5 to 1.5 in realistic situations. In the stream interaction case, the dimensionless stream stage, η_0 is given by

$$\eta_0 = H/m$$

therefore $$\bar{\eta}_0 = \bar{H}/m$$

$$\sigma_{\eta_0} = \sigma_H/m$$

$$\sigma_{\eta_0}/\bar{\eta}_0 = \sigma_H/\bar{H}$$

The nonlinear parameter would seem to be given by the ratio $\sigma_{\eta_0}/\bar{\eta}_0$; however, the stream stage record is based on an arbitrary datum. Thus the ratio $\sigma_{\eta_0} = \sigma_H/m$ is more appropriate as a nonlinear parameter than the ratio $\sigma_H/\bar{H}$ which is varied by changing the arbitrary value $\bar{H}$.

In conclusion, one can see that the mean of the hydrological processes discussed above is related more to the physical dimensions and properties of the system, while the variance is related more to the statistical properties of the system and together they constitute the basic nonlinear parameters.

Nonlinear Simulation with Historical Data

The objectives of this section are to evaluate the numerical model with historical field data for the inputs and to compare the transfer function thus obtained to that from the linear spectral or sinusoidal theory.

The field data used throughout this section is a set of records of gauge height of a nearby stream and the precipitation at the city of Wichita, Kansas covering the period from January 1938 to September 1971. A listing of these input data is given at the end of the computer program in Appendix A. The geographical location and a more detailed description is given in Chapter 4. The real time interval, Δt chosen for

these 36 years of record is 30 days. The time series of the two inputs, stream stage and precipitation, is assumed to be stationary and the sample statistics for the first two moments are given in Table 4.1.

Parameters / Inputs	Sample Mean $\bar{X}$	Sample Variance s_X^2	Sample Standard Deviation s_X	$s_X/\bar{X}$
Precipitation	2.557 in.	5.411 in.^{2}	2.33 in.	0.9112
Stream Stage	2.739 ft.	5.426 ft.^{2}	2.34 ft.	0.8543

Table 3.2 Sample Statistics of Kansas Data

Single Input Case--

In this simulation study the aquifer thickness at the stream, m is needed to specify the complete description of the dimensionless stream stage. From communications with the U.S. Geological Survey Office in Kansas, this characteristic thickness at that particular location was estimated to be about 25 ft. This estimate is used to normalize the stream fluctuation and accretion.

Before going to the detailed study of the nonlinear simulation, it is worthwhile to look at a comparison to the linear simulation in one case. The rationale behind this is to show the accuracy of the spectral estimation and to identify the effects of nonlinearity, rather than the numerical error. This is shown in Figure 3.26, in which the linear theory, linear simulation and nonlinear simulation are compared in the stream interaction case. It is seen that the linear simulation results show close approximation to the linear theory, particularly in the range of higher frequency. For the nonlinear simulation, the amplitude is

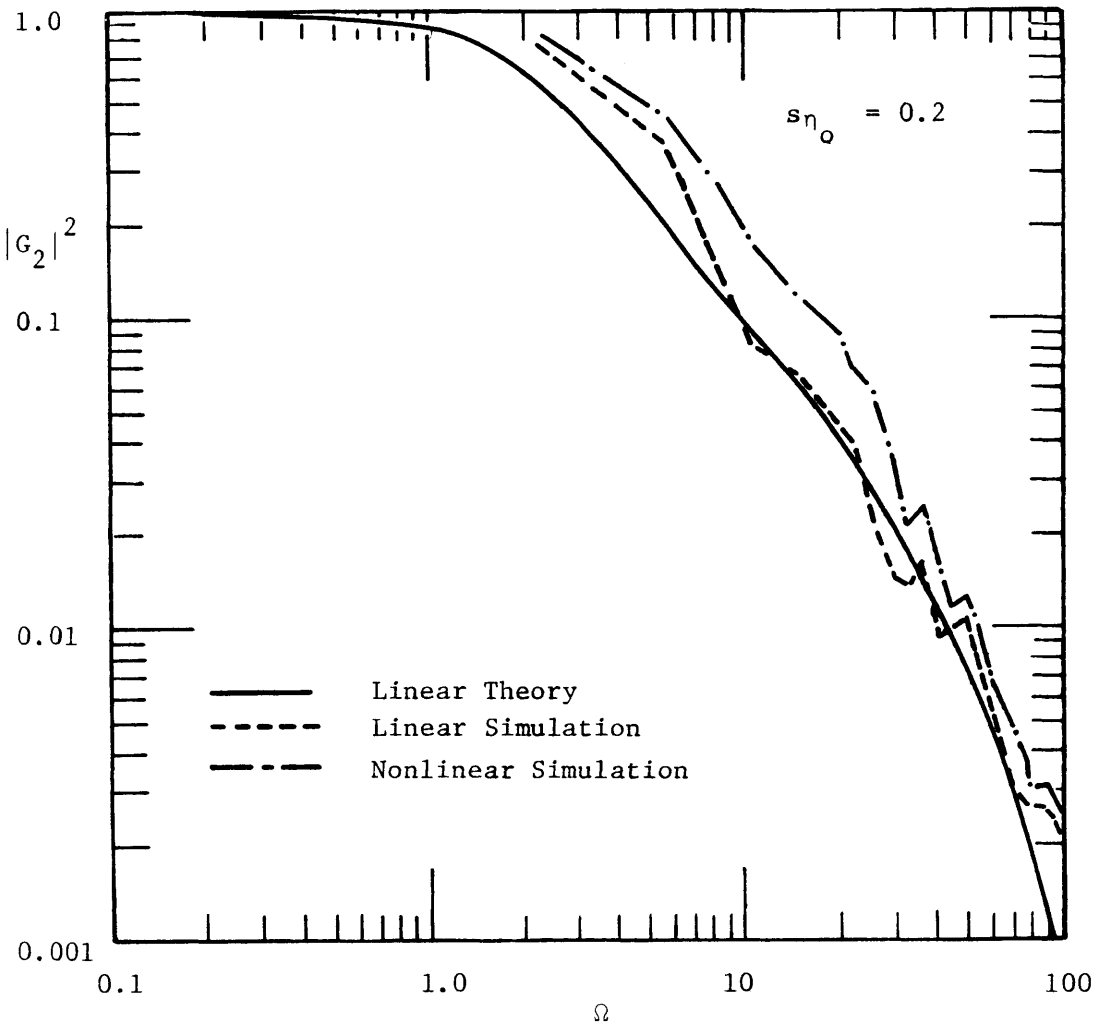

Figure 3.26 Comparison of the Linear Theory, Linear Simulation and Nonlinear Simulation for the Square of the Amplitude of the Transfer Function from Stream Stage to Response at x/L = 0.5

above both the linear theory and linear simulation. Since there is no significant difference between the linear simulation and theory, we can compare the linear theory to nonlinear simulation directly.

In the nonlinear simulation study, the major nonlinear parameter is $\bar{\rho}$, which is associated with the perturbation parameter, μ, characterizing nonlinearity found in Chapter 2. Their relationship is given by

$$\bar{\rho} = 2\mu$$

The dimensionless mean can be varied but the ratio $\frac{\sigma_\rho}{\bar{\rho}}$ remain constant for the historical data simulation, and be equal to the value given in Table 3.2. Table 3.3 lists some nonlinear simulation results over a range of different parameters.

In the accretion case (Figures 3.27 - 3.28) the simulation results show the amplitude of transfer function in the lower portion of the frequency range and is sensitive to changes of the mean of dimensionless accretion, $\bar{\rho}$ (or the perturbation parameter, μ).

As $\bar{\rho}$ or μ increases, the amplitude of the transfer function in the lower frequency drops. But, for $\bar{\rho}$ being less than 0.5, the nonlinear simulation results are close to the linear spectral theory. It may also be noticed that the effects of nonlinearity increase as the distance away from the stream increases. At relatively high frequency ($\Omega > 10$) the simulation results are quite close to the linear spectral theory regardless of the values of $\bar{\rho}$. Some of these results are in close agreement with the deterministic simulation (see Section 3.3), and the nonlinear perturbation analysis of Chapter 2.

Table 3.3 List of Nonlinear Simulation Parameters for the Single Input System

Figure Number	Dimensionless Accretion $\bar{\rho}$	Perturbation Parameter μ	Ratio of Sample s.d to mean $s_{\rho}/\bar{\rho}$	Sample s.d. s_{η_o}	Accretion or Stream Case
3.27	0.4589	0.22945	0.9112	-	Accretion
3.28	1.2785	0.63925	0.9112	-	Accretion
3.29	2	1.0	0.9112	-	Accretion
3.30	4	2.0	0.9112	-	Accretion
3.31	-	-	-	0.0468	Stream
3.32	-	-	-	0.0936	Stream
3.33	-	-	-	0.1872	Stream

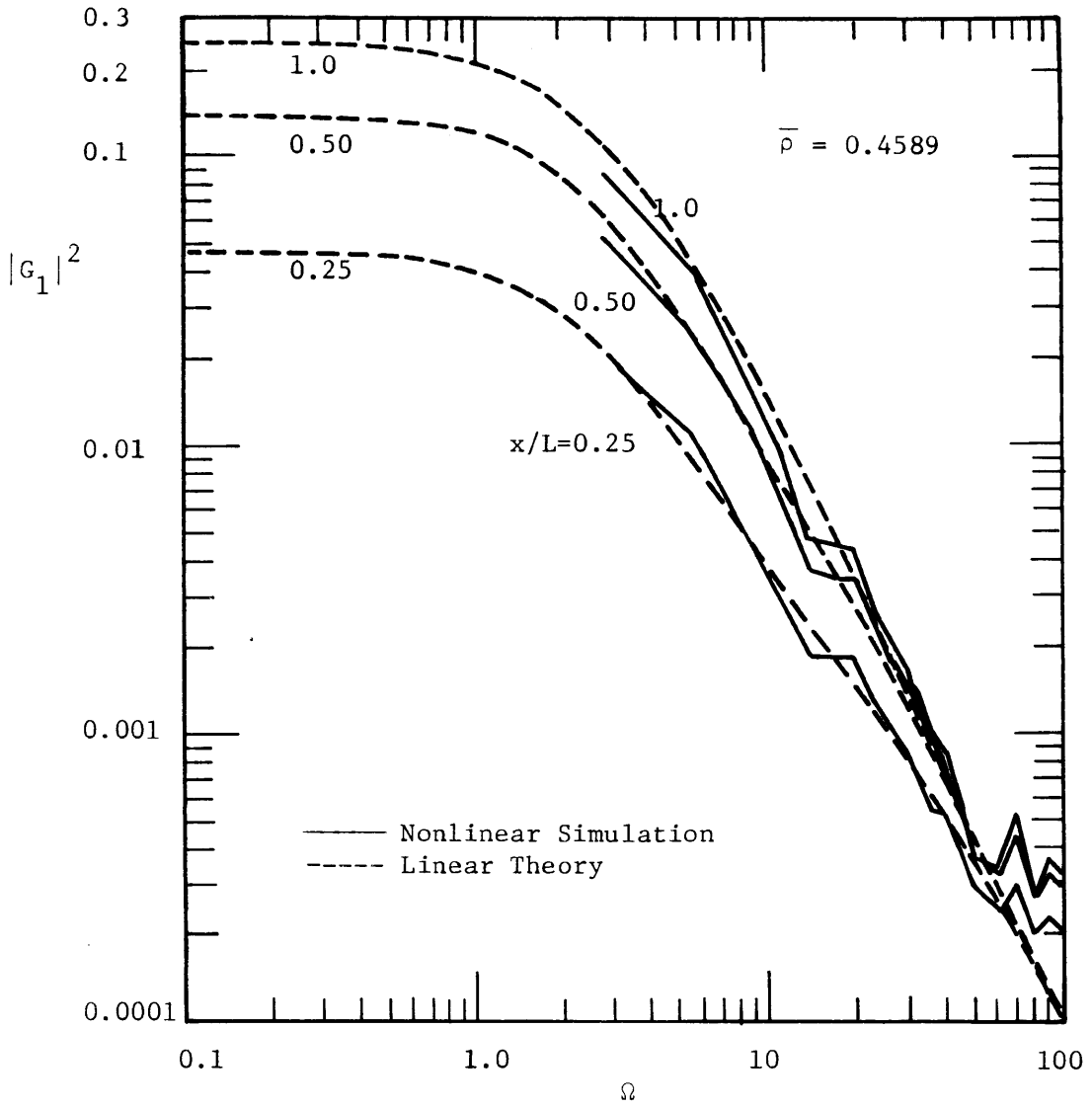

Figure 3.27 Square of the Amplitude of the Transfer Function of Nonlinear Simulation for the Aquifer System with Accretion Input,

$\bar{\rho}$ = 0.4589

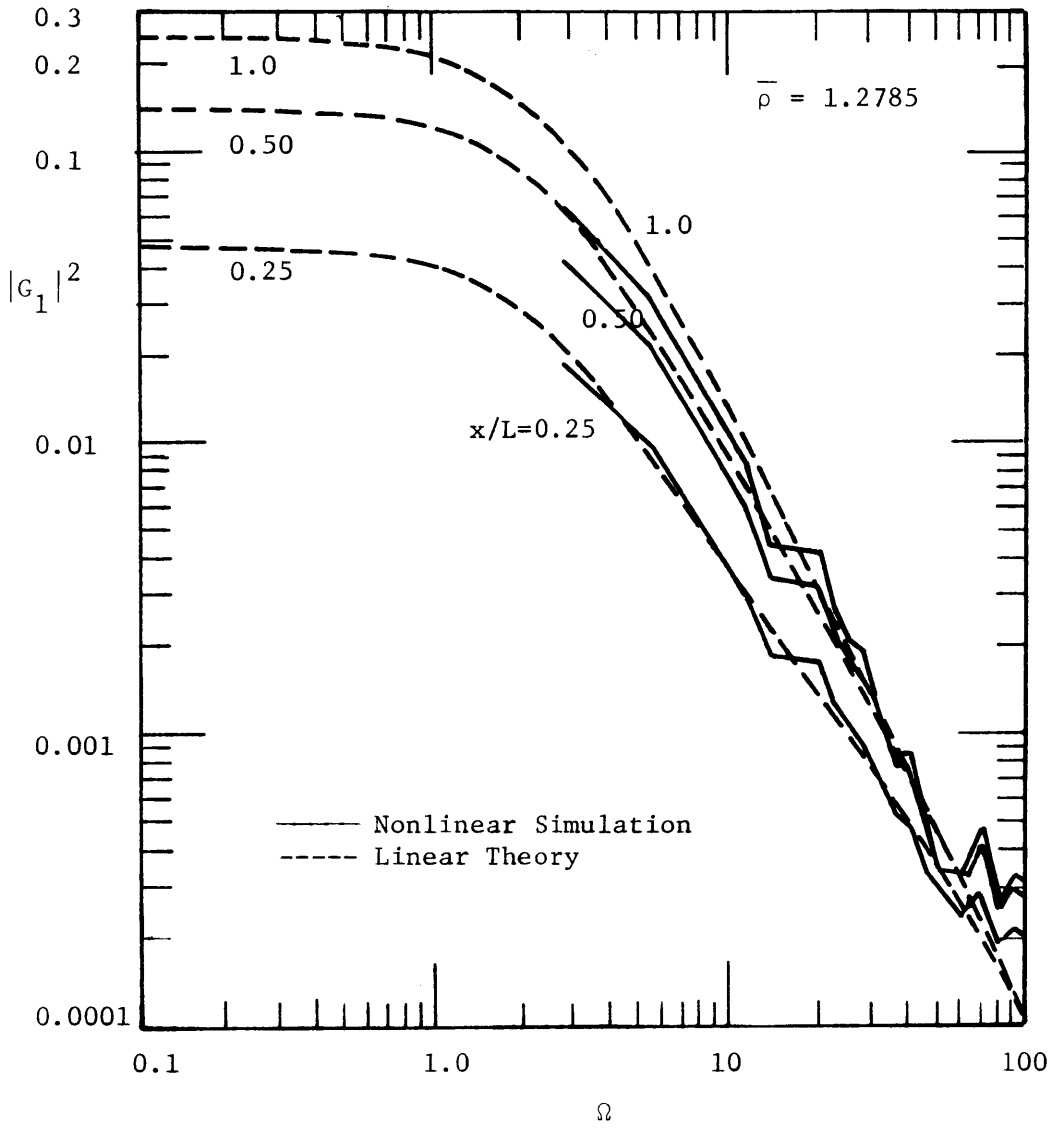

Figure 3.28 Square of the Amplitude of the Transfer Function of Nonlinear Simulation for the Aquifer System with Accretion Input,

$\bar{\rho}$ = 1.2785

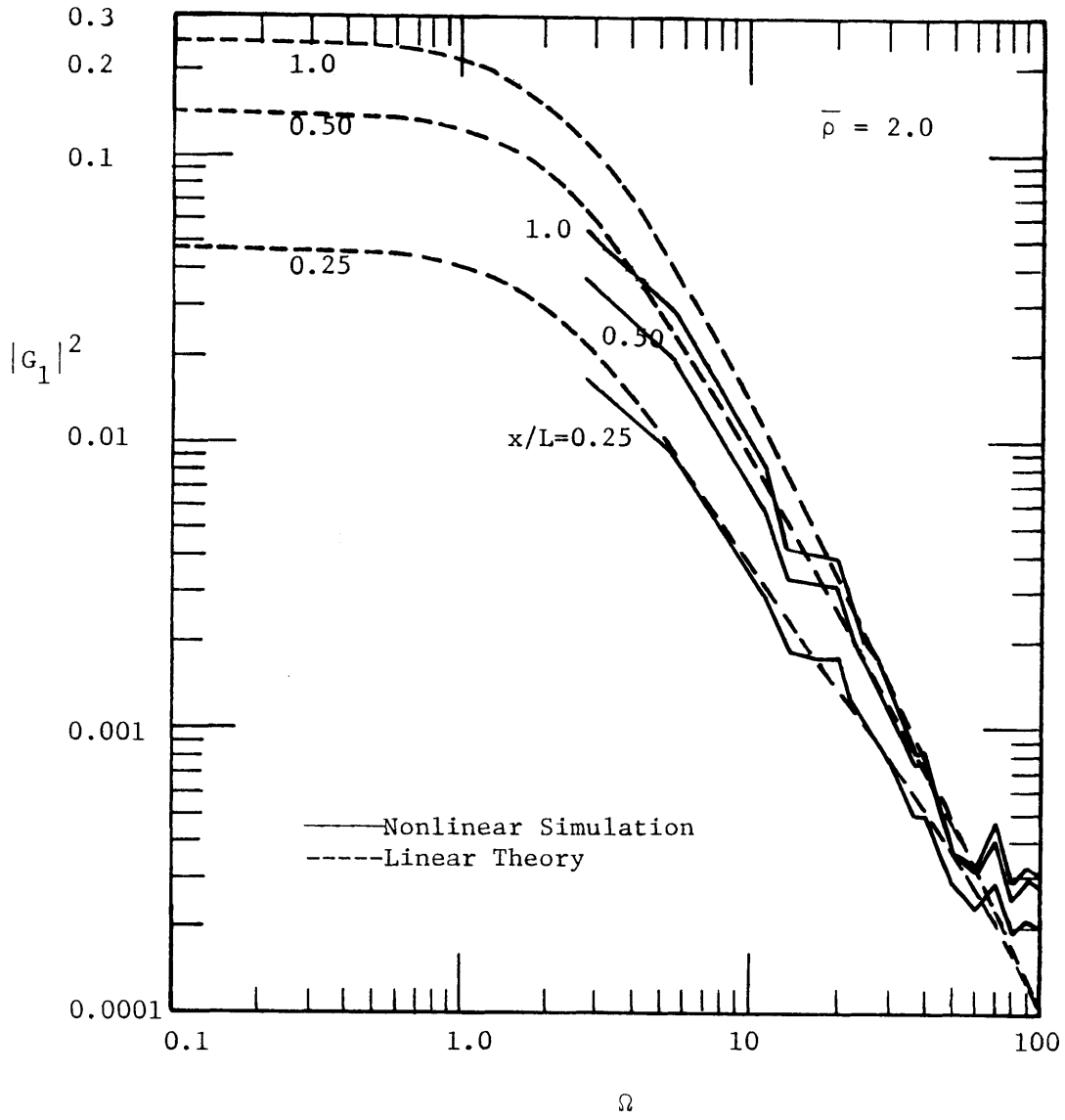

Figure 3.29 Square of the Amplitude of the Transfer Function of Nonlinear Simulation for the Aquifer System with Accretion Input,

$\bar{\rho}$ = 2.0

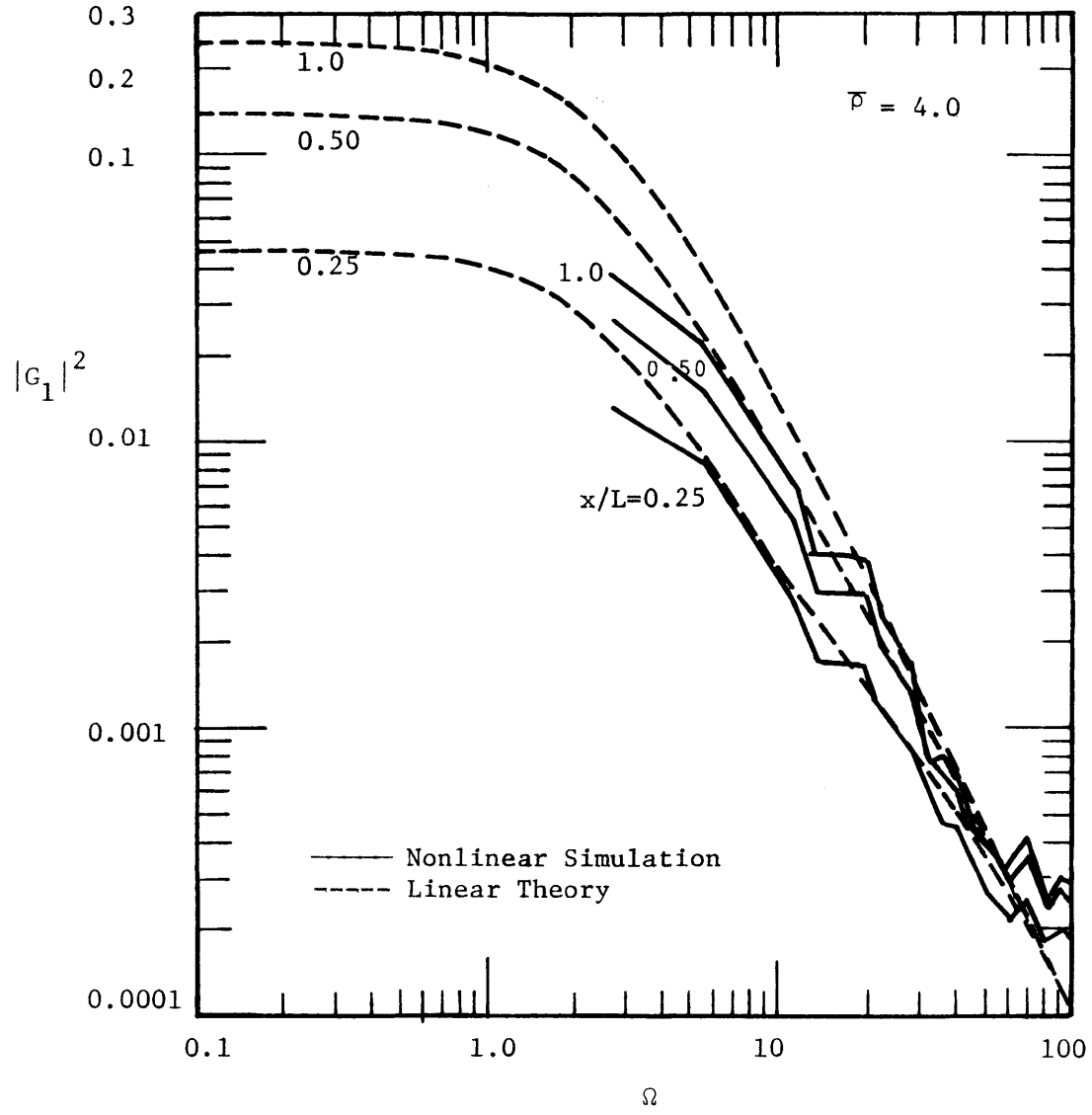

Figure 3.30 Square of the Amplitude of the Transfer Function of Nonlinear Simulation for the Aquifer System with Accretion Input,

$\overline{\rho}$ = 4.0

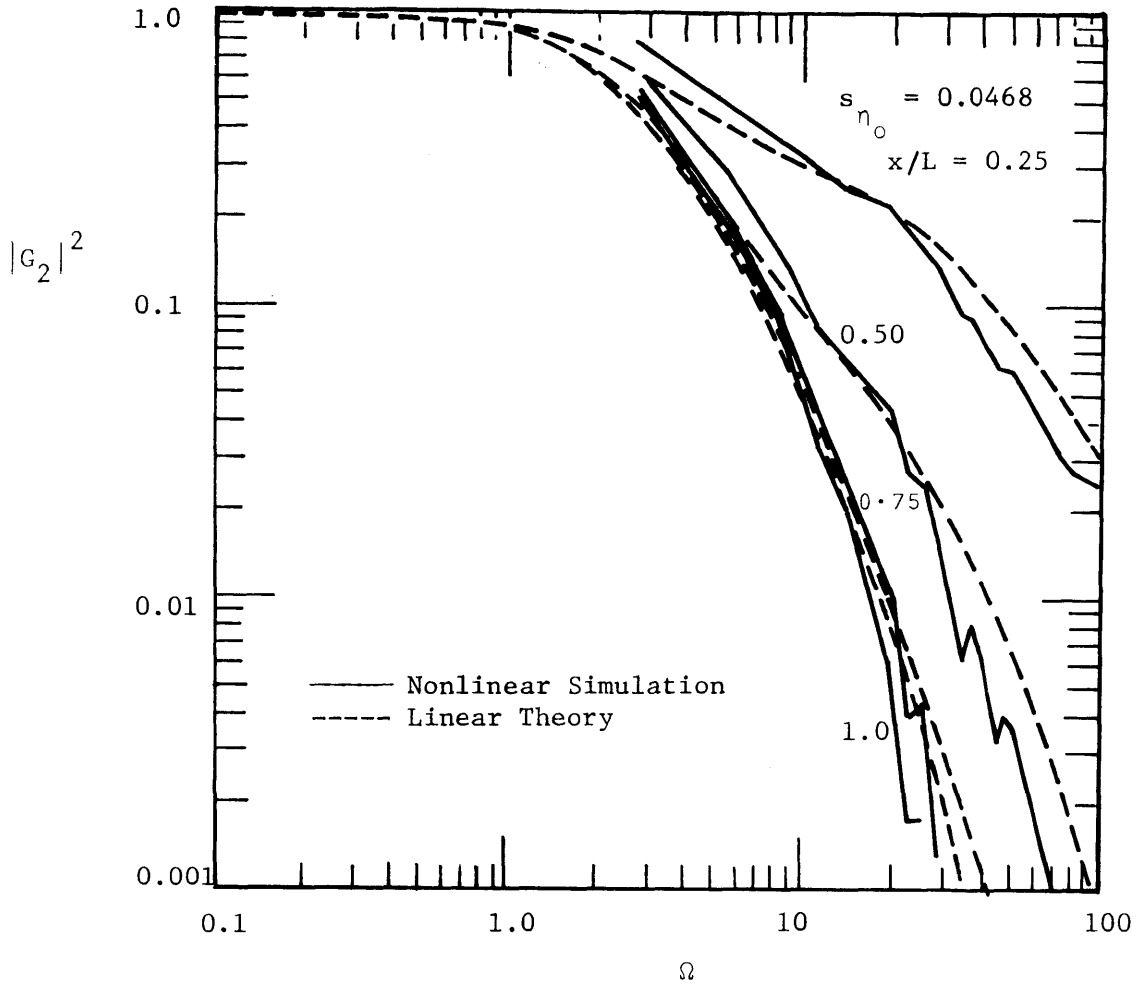

Figure 3.31 Square of the Amplitude of the Transfer Function of Nonlinear Simulation for the Aquifer System with Stream Stage Input,

$$s_{\eta_o} = 0.0468$$

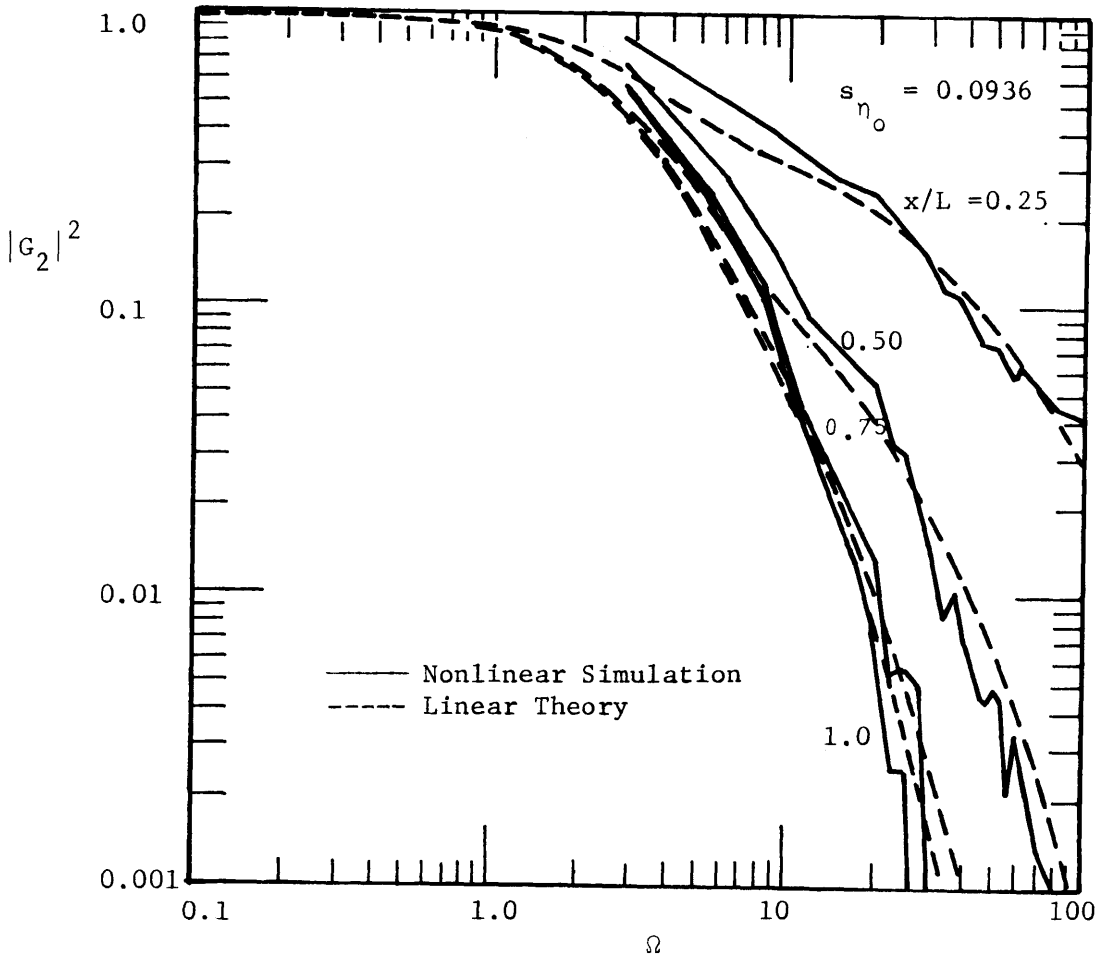

Figure 3.32 Square of the Amplitude of the Transfer Function of Nonlinear Simulation of the Aquifer System with Stream Stage Input,

$$s_{\eta_o} = 0.0936$$

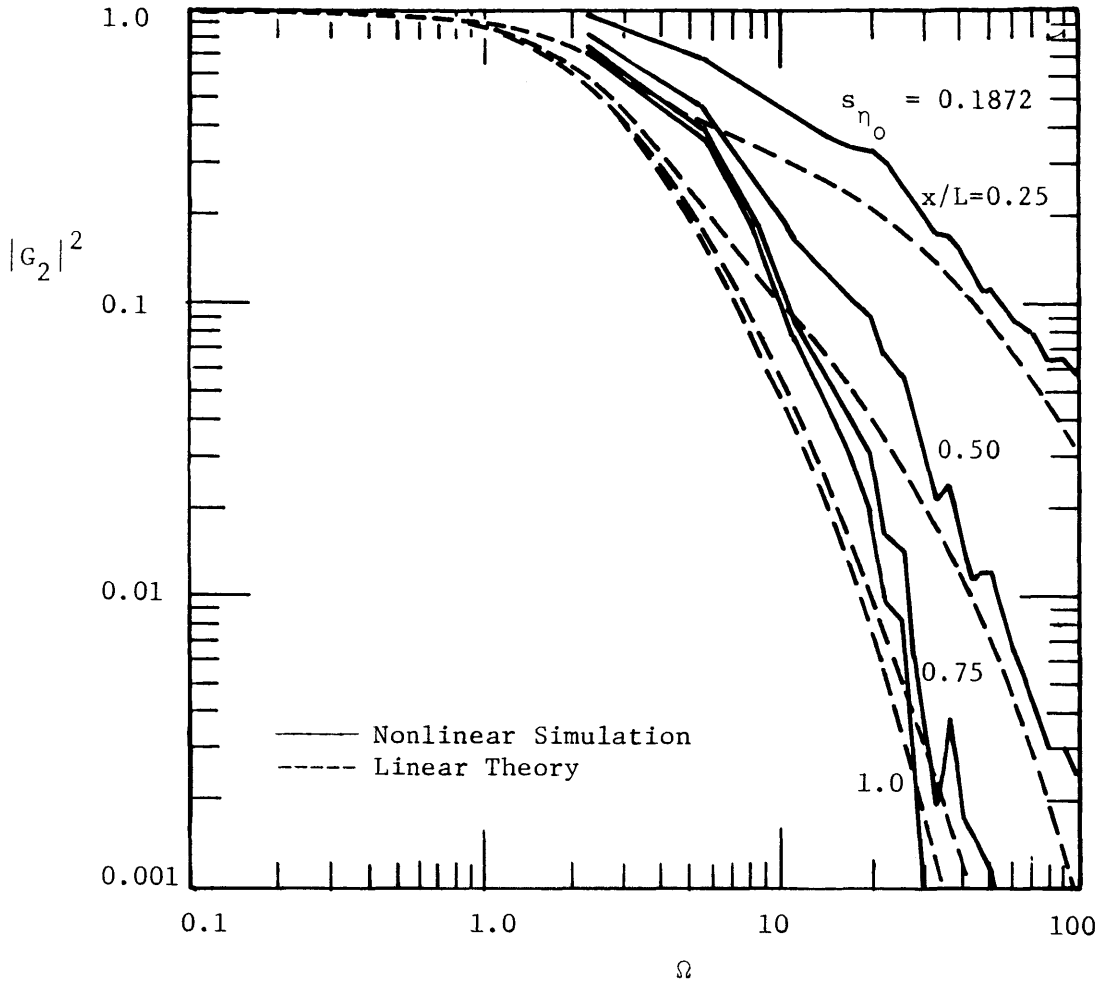

Figure 3.33 Square of the Amplitude of the Transfer Function of Nonlinear Simulation for the Aquifer System with Stream Stage Input,

$$s_{\eta_o} = 0.1872$$

It is noticed that at very high frequency ($\Omega > 60$) there is some deviation of the simulation from that of the linear theory. This is probably due to errors in the numerical simulation and the estimation of the spectrum.

In the stream interaction case, the nonlinear parameter s_{η_o} or $s_{H/m}$ is relatively insensitive to the effects of nonlinearity. Three cases have been tested with s_{η_o} approximately equal to 0.05, 0.1 and 0.2, respectively. The second case represents the dimensionless standard deviation for the Kansas case. The first and third cases represent the same data multiplied to produce standard deviations above and below this value. It is seen that the spectral amplitude increases at all frequencies as the amplitude of the input fluctuation increases. From these simulation results, it seems that nonlinear effects may be more significant when s_{η_o} or $s_{H/m}$ is greater than 0.2. In this case, it means either the aquifer thickness at the stream is relatively small or the variance of the stream fluctuation is very large. The combination of the statistical property, s_H and the physical characteristic, m of the system determines the magnitude of this nonlinear parameter. In realistic situations s_H has a relatively small range, say $s_H \sim 2$ to 5 ft., compared to the characteristic saturated thickness of the aquifer, m, which would be the more important determining importance of nonlinearity.

For the single input case involving stream stage fluctuation, the nonlinear effects can be evaluated by comparing the transmissivities of both nonlinear and linear systems. Since the porous medium of the

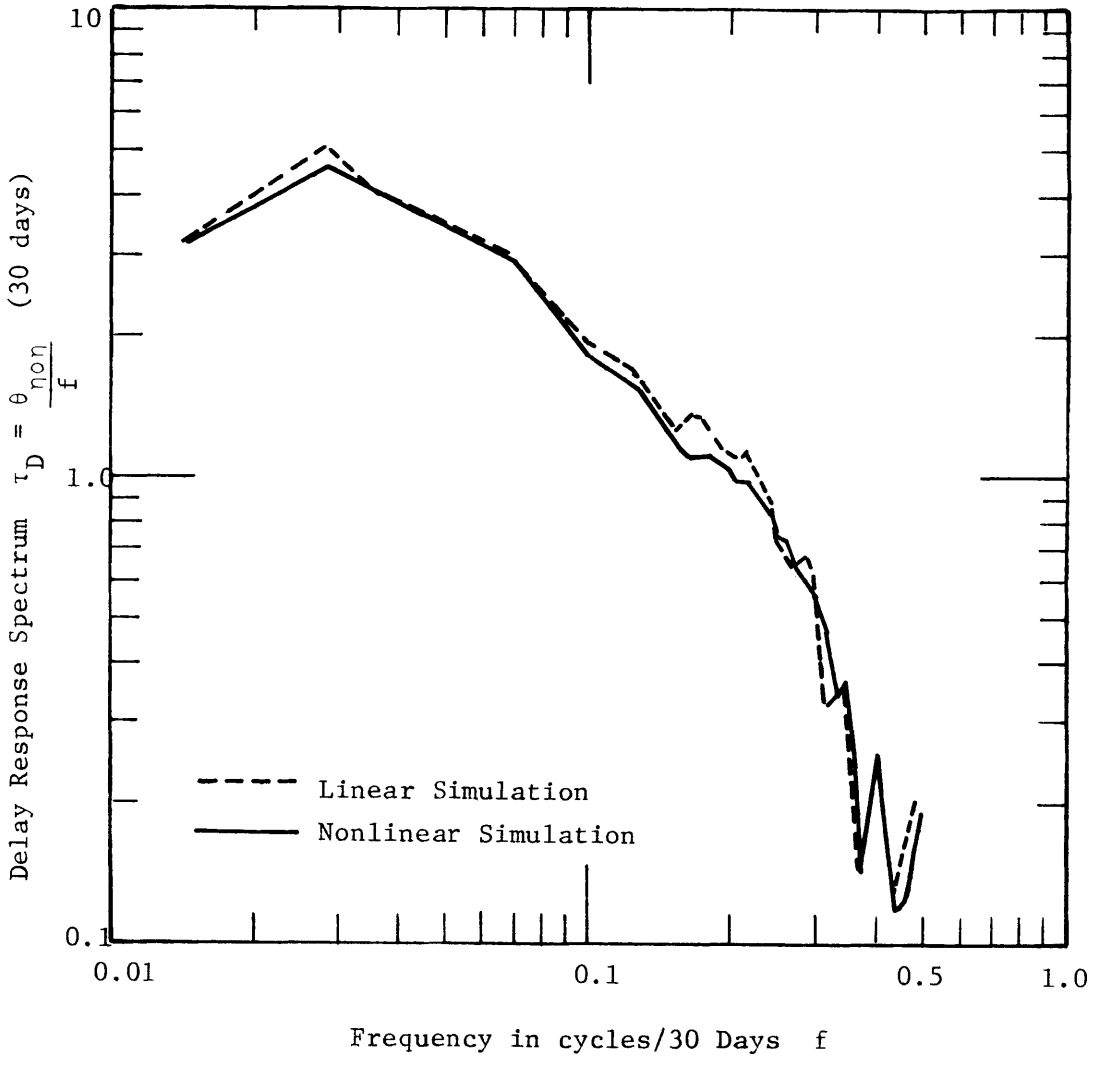

Figure 3.34 Delay Response Spectra for Linear and Nonlinear Stream Stage Input Systems

system is homogeneous it is reasonable to assume that the delay response time (See section 3.1) τ_D is inversely one location to the other. (See Chapter 14, Eagleson, 1970). Hence the ratio of transmissivities in nonlinear and linear cases are given by

$$\frac{T_N}{T_L} = \frac{\tau_D^L}{\tau_D^N}$$

where L indicates linear

N indicates nonlinear

The linear and nonlinear simulation of the delay response at x/L = 0.5 are plotted in Figure 3.34 for the case where the dimensionless stream stage sample standard deviation, s_{η_o}, is about 0.1 The results show the linear transmissivity is 5% to 10% lower than the nonlinear transmissivity. At other locations it has been found this ratio is approximately the same. It is expected that this deviation increases as s_{η_o} increases. This approach is applied only to the stream interaction case because it is assumed in this model that the flow in the aquifer is essentially horizontal. In the accretion case, the vertical recharge there are only small phase effects in the horizontal direction.

Dual Input Case -

In this system, both stream stage and accretion are used as inputs for the numerical model. For a linear system, the output of the dual system is simply the superposition of the two outputs due to each input system, i.e.,

$$Y = Y_1 + Y_2 \tag{3.3.8}$$

where Y = dual output

Y_1, Y_2 = outputs of single input system

In this study, Y_1 represents the output due to the accretion input and Y_2 represents the output due to the stream stage input. Their respective transfer functions were found (See section 3.1) to be

$$G_1 = \frac{i}{\Omega}(F-1) \tag{3.3.9}$$

$$G_2 = F \tag{3.3.10}$$

where $$F = \frac{\cosh \sqrt{i\Omega}(1-\xi)}{\cosh \sqrt{i\Omega}}$$

The dual spectral output can be easily obtained by assuming the dual system consists of two lumped parameter systems. The result obtained will be the same as that from the distributed parameter system.

From equation 4.3.1 we obtain the dual spectral output S_{YY} as

$$S_{YY} = S_{Y_1Y_1} + S_{Y_2Y_2} + S_{Y_1Y_2} + S_{Y_2Y_1} \tag{3.3.11}$$

Then, using the following relationships (See Chapter 10, Papoulis, 1965).

$$S_{Y_1Y_1} = |G_1|^2 S_{X_1X_1}$$

$$S_{Y_2Y_2} = |G_2|^2 S_{X_2X_2} \qquad (3.3.11)$$

$$S_{Y_1Y_2} = G_1^* G_2 S_{X_1X_2}$$

$$S_{Y_2Y_1} = G_1^* G_2 S_{X_2X_1}$$

in equation 4.3.4, we obtain

$$S_{YY} = |G_1|^2 S_{X_1X_1} + |G_1|^2 S_{X_2X_2} + G_1 G_2^* S_{X_1X_2}$$

$$+ G_1^* G_2 S_{X_2X_1} \qquad (3.3.12)$$

The quadspectrum, $Q_{X_1X_2}$ and cospectrum, $Co_{X_1X_2}$ for the two inputs X_1 and X_2 are related to the cross spectrum, $S_{X_1X_2}$ and $S_{X_2X_1}$ as

$$S_{X_1X_2} = Co_{X_2X_1} + iQ_{X_2X_1} \qquad (3.3.13)$$

$$S_{X_2X_1} = Co_{X_2X_1} - iQ_{X_2X_1}$$

Using equations 3.3.11 and 3.3.13 substituted into 3.3.12 we obtain the spectral dual output in dimensionless form with

$$\eta = Y, \quad \rho = X_1 \text{ and } \eta_o = X_2$$

as

$$S_{\eta\eta}(\Omega,\xi) = \frac{(F-1)\ (F^*-1)}{\Omega^2}\ S_{\rho\rho}(\Omega) + FF^*S_{\eta_o\eta_o}(\Omega)$$

$$- \frac{1}{\Omega}[2FF^* - (F+F^*)]\ Q_{\eta_o\rho}(\Omega) + \frac{i}{\Omega}(F-F^*)\ Co_{\eta_o\rho}(\Omega)$$

The transfer functions G_1 and G_2 for the dual input system can be found (See Chapter 4 or Bendat and Piersol, 1971, Chapter 5) as:

$$G_1 = \frac{S_{X_1Y}\ [1 - \frac{S_{X_1X_2}\ S_{X_2Y}}{S_{X_2X_2}\ S_{X_1Y}}]}{S_{X_1X_1}\ [1 - \gamma^2_{X_1X_2}]} \tag{3.3.15}$$

$$G_2 = \frac{S_{X_2Y}\ [1 - \frac{S_{X_2X_1}\ S_{X_1Y}}{S_{X_1X_1}\ S_{X_2Y}}]}{S_{X_2X_2}\ [1 - \gamma^2_{X_1X_2}]} \tag{3.3.16}$$

where $\gamma^2_{X_1X_2}$ = coherence square function between inputs X_1 and X_2.

However, for the nonlinear Dupuit equation, the superposition principle no longer holds. Hence, the theory developed so far is not completely applicable. In the Dupuit equation

$$\frac{\partial \eta}{\partial \tau} = \frac{\partial}{\partial \xi} \left(\eta \frac{\partial \eta}{\partial \xi}\right) + \rho$$

with the dual input system = $\eta_1 + \eta_2$ we obtain

$$\frac{\partial \eta_1}{\partial \tau} + \frac{\partial \eta_2}{\partial \tau} = \frac{\partial}{\partial \tau} \left(\eta_1 \frac{\partial \eta_1}{\partial \xi} + \eta_2 \frac{\partial \eta_2}{\partial \xi} + \eta_2 \frac{\partial \eta_1}{\partial \xi}\right) + \rho \qquad (3.3.17)$$

With the single input system we obtain

$$\frac{\partial \eta_1}{\partial \tau} = \frac{\partial}{\partial \xi} \left(\eta_1 \frac{\partial \eta_1}{\partial \xi}\right) + \rho$$

$$\frac{\partial \eta_2}{\partial \tau} = \frac{\partial}{\partial \tau} \left(\eta_2 \frac{\partial \eta_2}{\partial \xi}\right)$$

Adding these two equations we have

$$\frac{\partial \eta_1}{\partial \tau} + \frac{\partial \eta_2}{\partial \tau} = \frac{\partial}{\partial \xi} \left(\eta_1 \frac{\partial \eta_1}{\partial \xi} + \eta_2 \frac{\partial \eta_2}{\partial \xi}\right) + \rho \qquad (3.3.18)$$

Clearly $Y \neq Y_1 + Y_2$

In fact, it is seen that

$$Y = Y_1 + Y_2 + f(Y_1 Y_2) \tag{3.3.19}$$

In this nonlinear simulation of the dual input system, we use two methods to evaluate the effects of nonlinearity. The first method computes spectral dual output $S_{\eta\eta}$ in equation 4.3.6 or 4.3.8 based on G_1 and G_2 from linear theory and compares to $S_{\eta\eta}$ obtained directly from the nonlinear simulation. The second method compares transfer functions G_1 and G_2 obtained from linear theory (equations 3,3.9 and 3.3.10 to those computed from the nonlinear simulation results based on equations 3.3.15 and 3.3.16 which were derived via superposition principle. If the transfer functions for the dual system are close to the linear theory, the function $f(Y_1\ Y_2)$ would be negligibly small. On the other hand, if $f(Y_1\ Y_2)$ increases, the comparison between the linear theoretical transfer functions and the nonlinear transfer functions further identifies the nonlinear effects of the system. In general, it is seen from equation 3.3.19 that nonlinearity increases as the product of the amplitudes of the two single outputs increase. These products are proportional to those of the inputs. Hence, the basic nonlinear parameters of the dual input system are functions of the products of the amplitudes and means of the inputs.

Table 3.4 lists a number of typical cases of the nonlinear simulation for the dual system using both methods mentioned:

Table 3.4 List of Nonlinear Simulation Parameters for the Dual Input System

Figure Number	Basis for Comparison	Dimensionless Accretion Mean $\bar{\rho}$	Location x/L
3.35	$S_{\eta\eta}$ (Eq. 3.3.14)	1.0	0.25, 0.50, 1.0
3.36	$S_{\eta\eta}$ (Eq. 3.3.14)	1.0	0.50
3.37	$S_{\eta\eta}$ (Eq. 3.3.14)	2.0	0.50
3.38	$\|G_1\|^2$ (Eq. 3.3.15)	0.50	0.50
3.39	$\|G_1\|^2$ (Eq. 3.3.15)	2.0	0.50
3.40	$\|G_1\|^2$ (Eq. 3.3.15)	1.0	0.25, 0.50, 1.0
3.41	$\|G_2\|^2$ (Eq. 3.3.16)	0.50	0.50
3.42	$\|G_2\|^2$ (Eq. 3.3.16)	2.0	0.50
3.43	$\|G_2\|^2$ (Eq. 3.3.16)	1.0	0.25, 0.50, 1.0

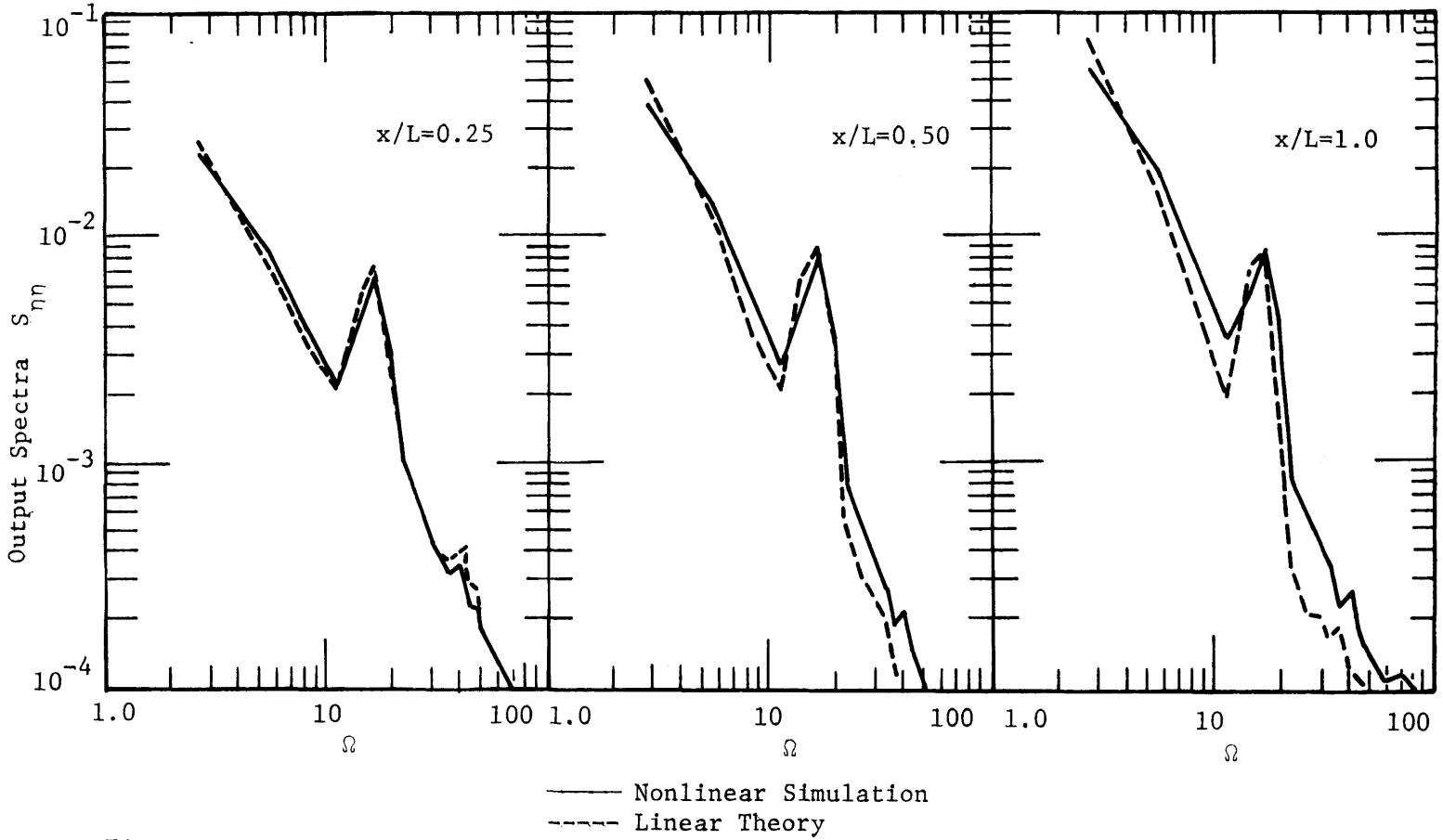

Figure 3.35 Output Spectra of Nonlinear Simulation for the Dual Input System with ρ = 1.0 at three locations

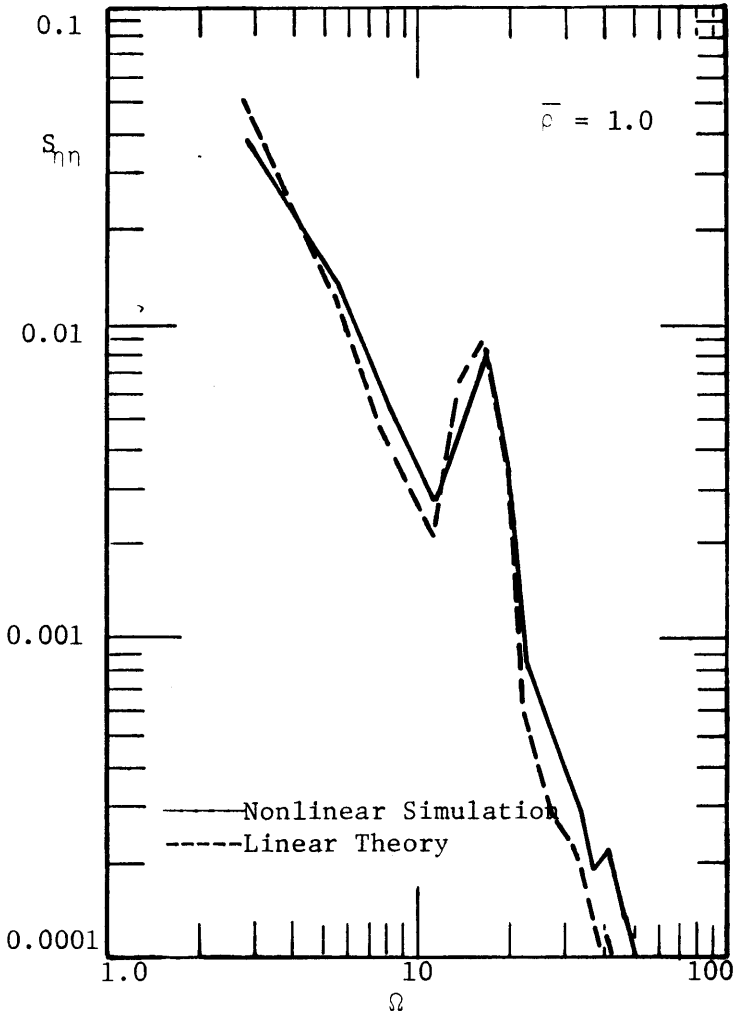

Figure 3.36

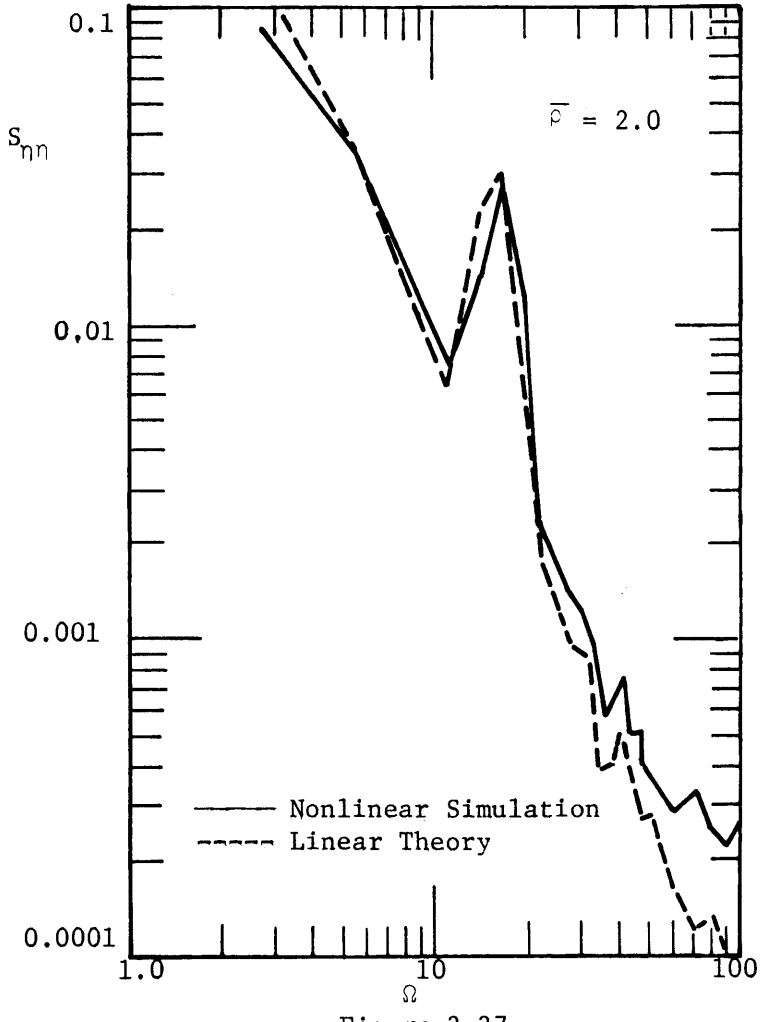

Figure 3.37

Figures 3.36-3.37 Output Spectra of Nonlinear Simulation for the Dual Input System with $\bar{\rho} = 1$ and $\bar{\rho} = 2$ at x/L = 0.5

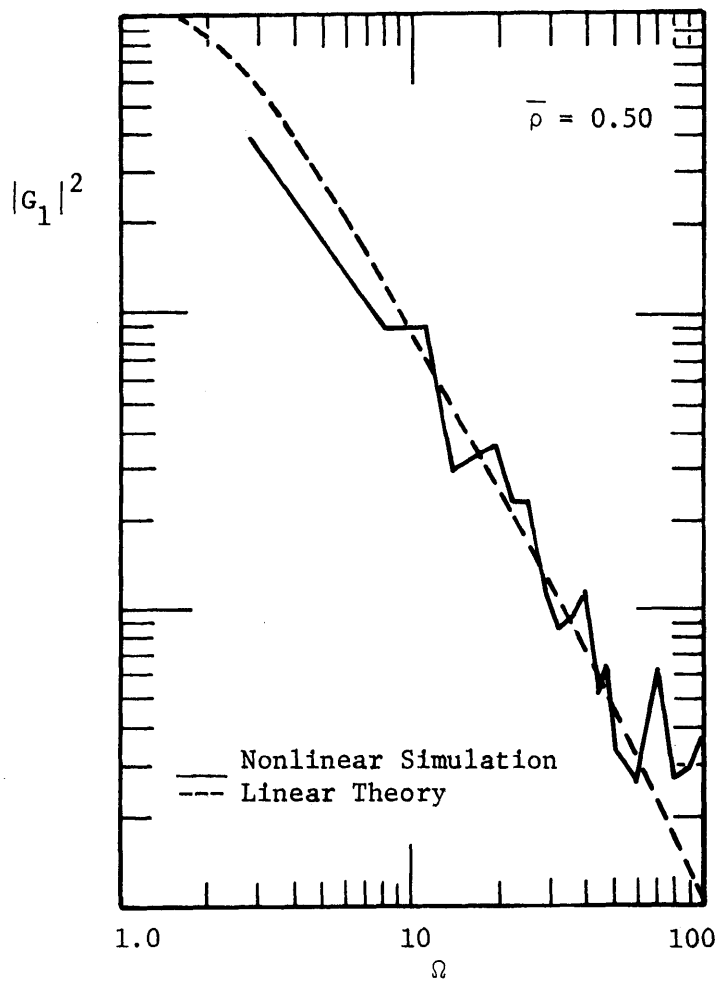

Figure 3.38

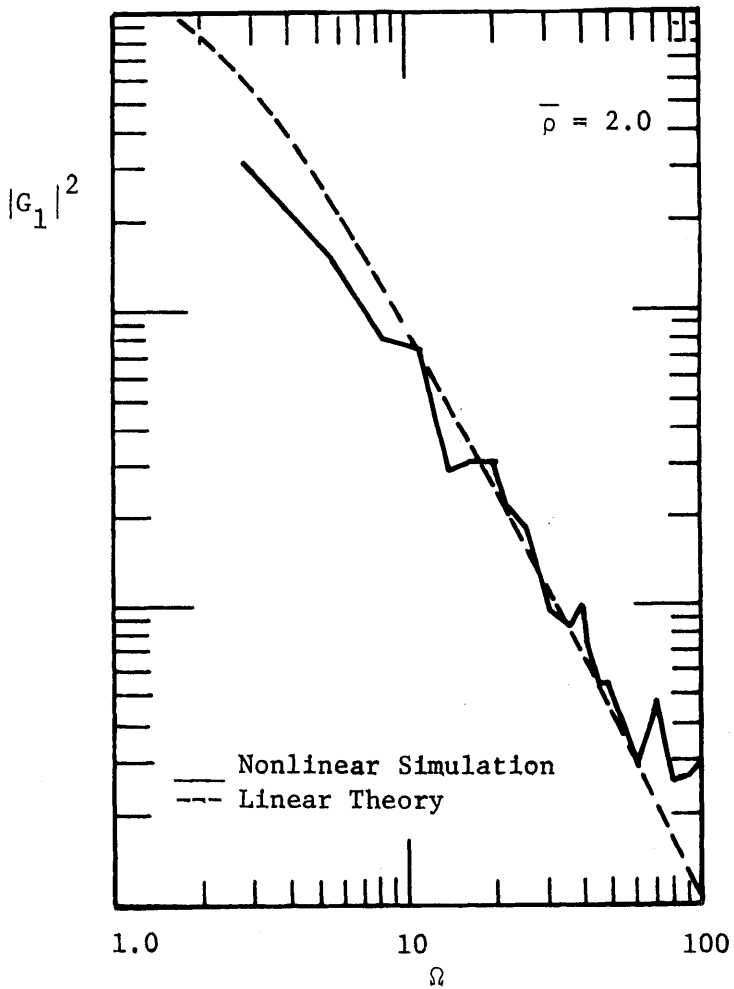

Figure 3.39

Figures 3.38-3.39 Square of the Amplitude of the Transfer Function of Nonlinear Simulation for the Dual Input System from Accretion Response at x/L=0.5, $\bar{\rho}$ = 0.5 and $\bar{\rho}$ = 2.0

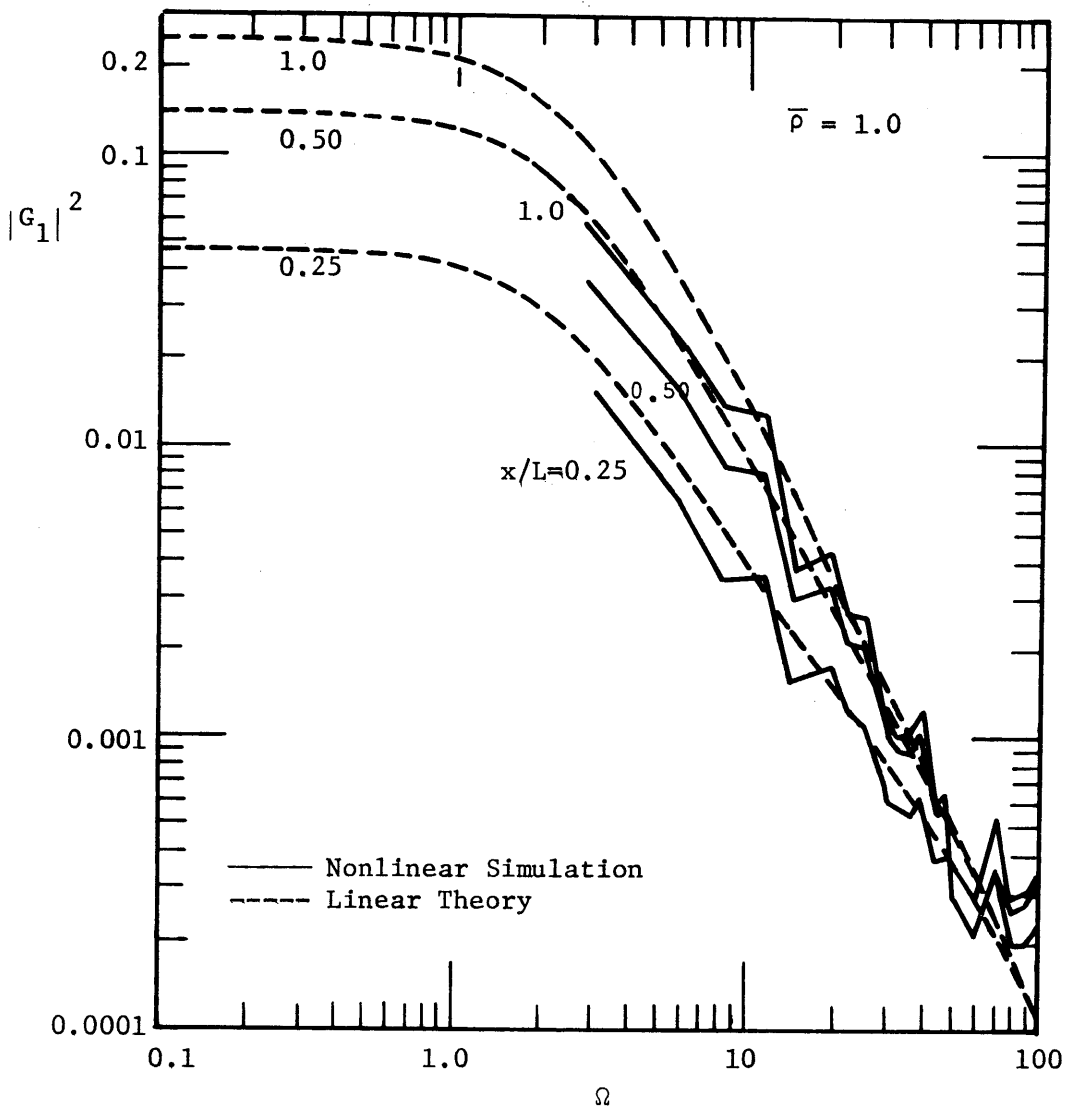

Figure 3.40 Square of the Amplitude of the Transfer Function of Nonlinear Simulation for the Dual Input System from Accretion Response at x/L = 0.25, 0.50, 1.0, $\overline{\rho}$ = 1.0

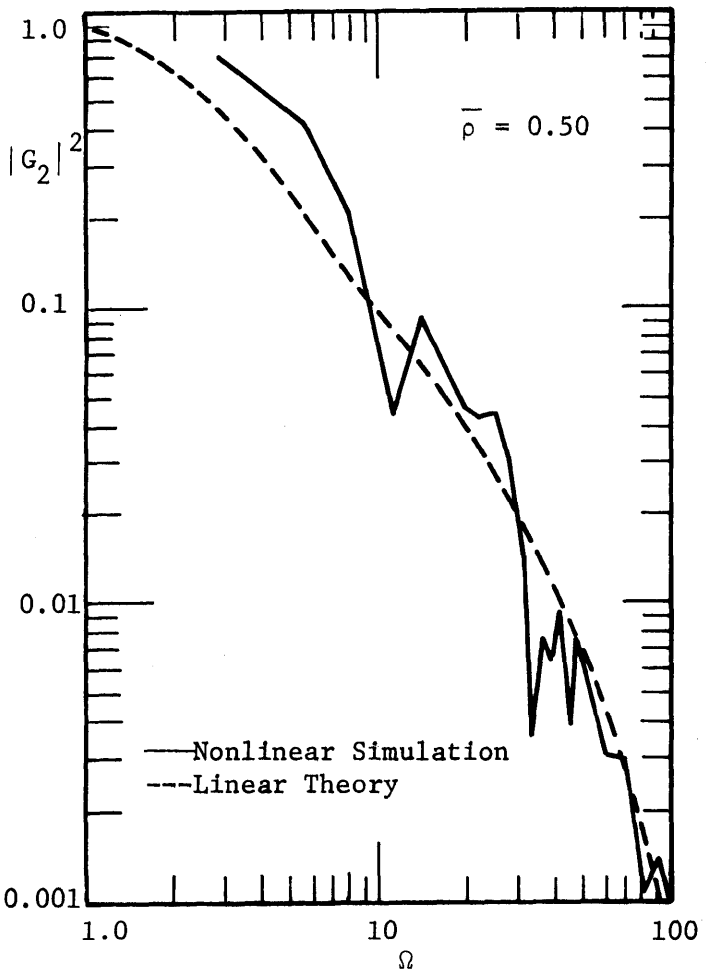

Figure 3.41

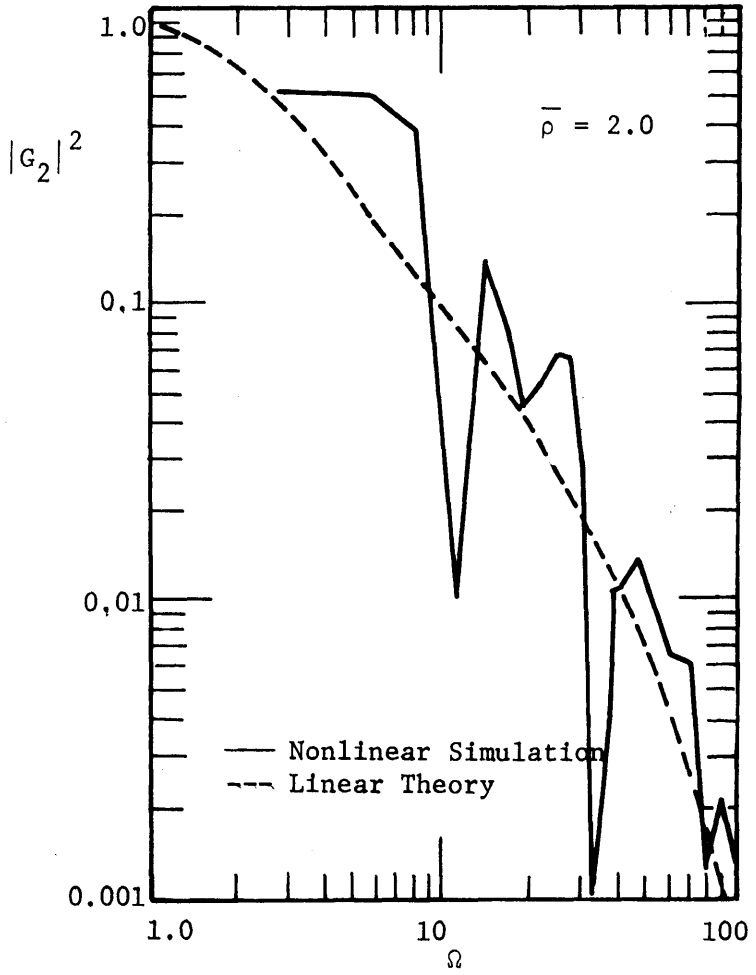

Figure 3.42

Figures 3.41-3.42 Square of the Amplitude of the Transfer Function of Nonlinear Simulation for the Dual Input System from Stream Stage Response at x/L = 0.50, $\bar{\rho}$ = 0.50 and $\bar{\rho}$ = 2.0

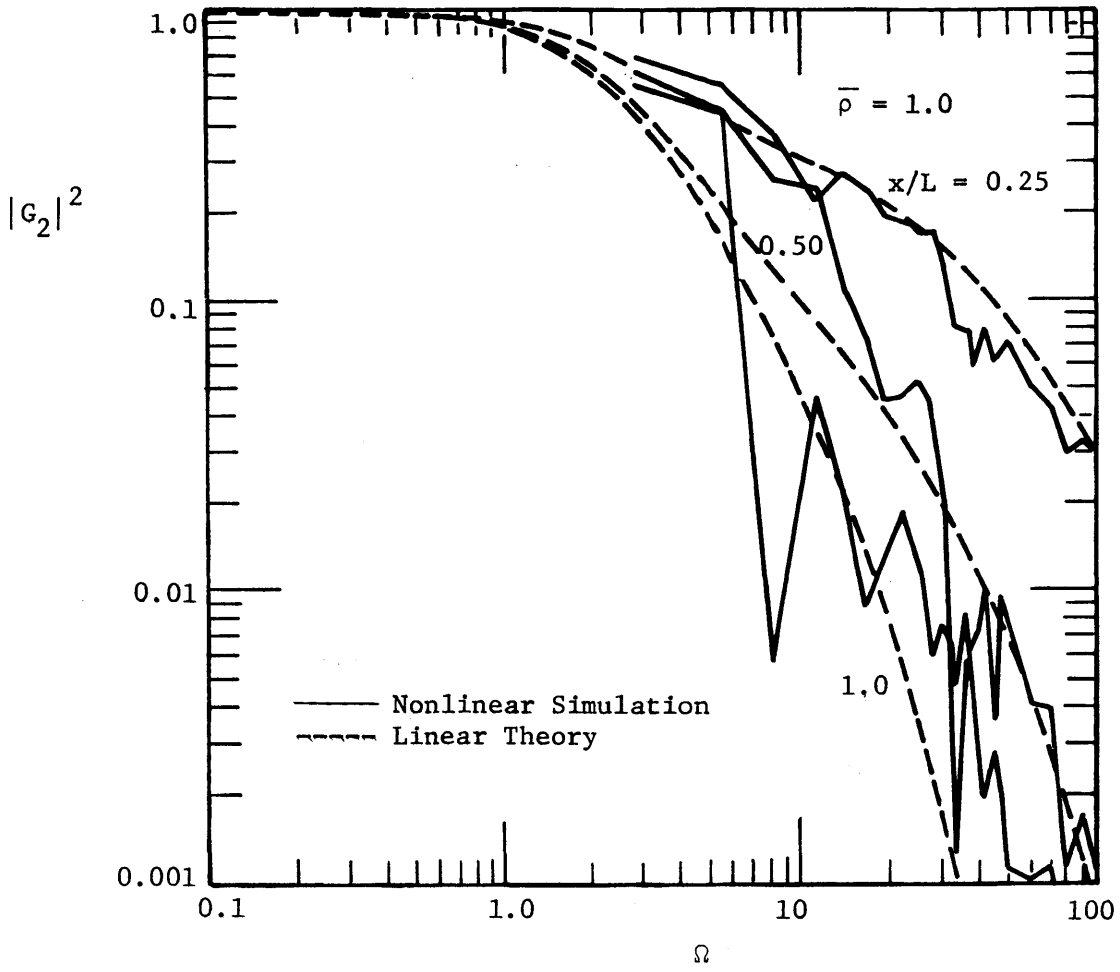

Figure 3.43 Amplitude of the Square of the Transfer Function of Nonlinear Simulation for the Dual Input System from Stream Stage Response at x/L = 0.25, 0.50 and 1.0, $\bar{\rho}$ = 1.0

The nonlinear parameter, s_{η_o} is fixed in all cases in the simulation of the dual input system. It is chosen to be about 0.1 in accordance with the information from the Kansas data. The rationale for this is based on the stream case, for which the effects of nonlinearity are relatively insensitive to changes of this parameter.

From Figure 3.35, it may be seen that nonlinear effects increase as the spatial coordinate x/L increases. This has a similar trend to that found for both the steady and transient deterministic cases (See section 3.2). Thus, the amount of nonlinearity is a function of the spatial parameter x/L. In addition, the mean of dimensionless accretion, $\bar{\rho}$ has significant nonlinear effects on the dual input system as in the single input system. The nonlinear deviation increases as this parameter increases. This is particularly significant in the low frequency range for which the nonlinear output spectrum, $S_{\eta\eta}$ falls below the linear one. (Compare Figures 3.27 and 3.37)

The graphical results of Figures 3.38 - 3.43 show the second method of analysis which computes the transfer function as in the case of a dual input lumped linear system. These simulation results show close agreement with the single input systems and they are quite close to the linear theory for small $\bar{\rho}$ and s_{η_o}. In the accretion case, the amplitude spectrum decreases slightly as $\bar{\rho}$ increases. (Compare Figures 3.38, 3.39 and 3.40). It is observed that the dual input system has slightly larger deviation in the lower frequency than the single input system (compare Figures 3.40 and 3.28). This is probably due to the interaction between the stream and accretion fluctuation in

the system. Mathematically this has been shown in equations 3.3.14 and 3.3.19 to be due to the product of the input amplitudes. In the stream interaction case, there is little significant difference as $\bar{\rho}$ increases. The only difference is that there is greater fluctuation of the amplitude of the function about a certain average value as $\bar{\rho}$ increases. This is probably due to errors of the estimation of the spectrum. Though this fluctuation is quite large, the transfer function from the linear theory fits rather smoothly about the mean of these fluctuations.

In conclusion, the linear theory is a good approximation to the nonlinear Dupuit equation in both single and dual input systems. Nonlinear effects play a more important role in the lower frequency as the mean of dimensionless accretion, $\bar{\rho}$ increases. In the stream case, the nonlinear effects are relatively small. From the study of the dual input system, it seems that the accretion plays a more important role than the stream stage.

In addition, the two methods show that the nonlinear effects are generally negligible. In particular, the second method based on the transfer function from the dual lumped system shows that the assumption that the superposition of the two single outputs from the dual output is quite reasonable. The validity of this assumption further confirms that in the analysis of field data, the transfer function for each single input system can be evaluated by this method.

Nonlinear Simulation with Synthetic Data

The previous section discusses the results of the nonlinear simulation using historical data from a particular location as input. This certainly has some limitations for a study with a more general framework. The objective of this section is to overcome these limitations by using generated synthetic input data. The following are some of the advantages:

(a) More information about the transfer function in the lower frequency range. For the historical data there is a fixed total record length of 405 units, with the number of lags used being set to 36. The resolution length is the dimensionless frequency interval, $\Delta\Omega = \frac{100}{36} \simeq 2.78$. Therefore the spectrum in the frequency range below $\Omega = 2.78$ cannot be evaluated. The number of lags is generally chosen as approximately 1/10 or less of the total record length. In order to improve the frequency resolution it is inadvisable to increase this number since the variance of the estimated spectrum would be increased. (See equation 3.3.3). But by using synthetic input data, we could increase the total record length, and hence, we could obtain information in a lower frequency range.

(b) Flexibility by varying the distribution and correlation properties of the input time series. In the historical data the major statistical property which may be varied is the mean of accretion, but not the variance which is fixed for a given set of data. Synthetic data can be generated with different typical variances

for investigating the more complete system. In addition, correlation properties may be introduced to the system in order to study possible effects on nonlinearity.

(c) Investigation of spatial variability of accretion.

Synthetic data enables us to explore a more complex model; i.e. accretion input with both temporal and spatial variability.

The generation of synthetic data for a hydrological process requires a physical understanding of the problem and the analysis of the available historical data. In this study the synthetic time series is considered to be stationary and random. This random time series, $X(\tau)$ may be considered to consist of two components, the deterministic $D(\tau)$ and the stochastic $S(\tau)$, i.e.

$$X(\tau) = D(\tau) + S(\tau) \tag{3.3.20}$$

The deterministic component accounts for the trend of the hydrological process, while the stochastic component accounts for the many unknown variables in the process. One particular characteristic of the trend of the process is the periodicity of the system. For a stationary process, the mean of both $D(\tau)$ and $S(\tau)$ is a constant. The deterministic component can be generated from a sinusoidal process, while the stochastic component is generated from some kind of random process for which we need to specify probability distribution properties. In other words, we must know the type of distribution and its mean, variance and autocorrelation.

The two inputs, accretion and stream stage, are first analyzed using the historical data. This is done in order to find out the dis-

tribution properties and sample statistics of these two time series. The input data were tested on log-normal probability paper (See Figures 3.44 and 3.45 and it was found the precipitation is approximately log-normally distributed. The mean and variance of precipitation and stream stage were already given in the previous section. Their autocorrelation functions are shown in Figures 3.46 and 3.47, respectively. It is observed that in both correlograms, particularly in the case of precipitation, the correlation function drops down significantly to approximately zero after one lag. This means there is very little correlation between the time records for intervals more than one lag unit (30 days). With such a property the process can be regarded as an independent one. Furthermore, the correlogram of precipitation shows that the process has an annual periodic component.

In this study synthetic accretion input is generated as it plays a more important role than stream stage in nonlinearity. The synthetic time series is of the form:

$$\rho(\tau) = A \cos\Omega\tau + e(\tau) \qquad (3.3.21)$$

where the sinusoidal term denotes the deterministic periodic component and the second term is a random process generated from an independent normally distributed process with sample mean $\bar{e}$ and sample variance s_e^2. The normal distribution is used instead of log-normal distribution simply for the sake of convenience. Furthermore, this serves as a test for an input with a different type of distribution.

From equation 3.3.21 the dimensionless accretion mean and its variance are given by

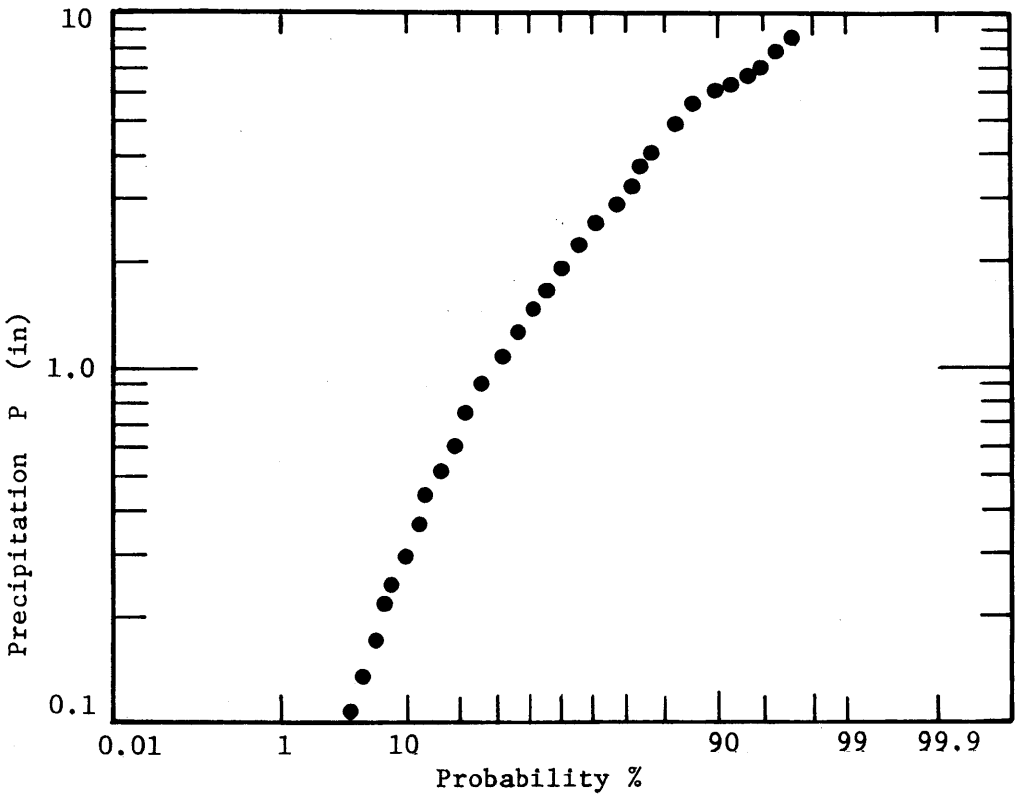

Figure 3.44 Precipitation of the Kansas Data Plotted on Log-Normal Probability Paper

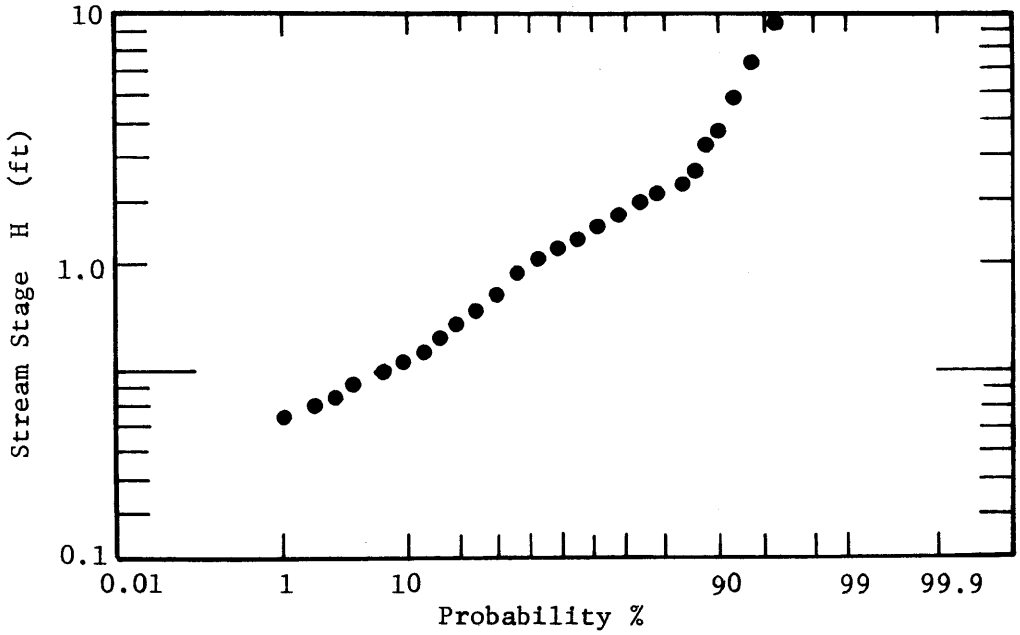

Figure 3.45 Stream Stage of the Kansas Data Plotted on Log-Normal Probability Paper

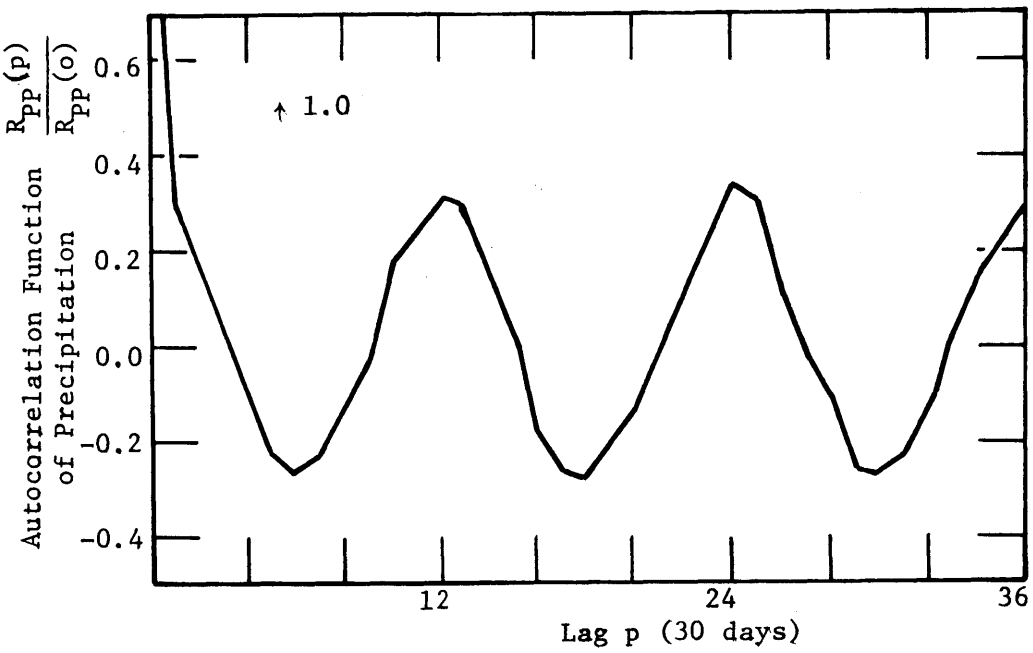

Figure 3.46 Correlogram of Precipitation of the Kansas Data

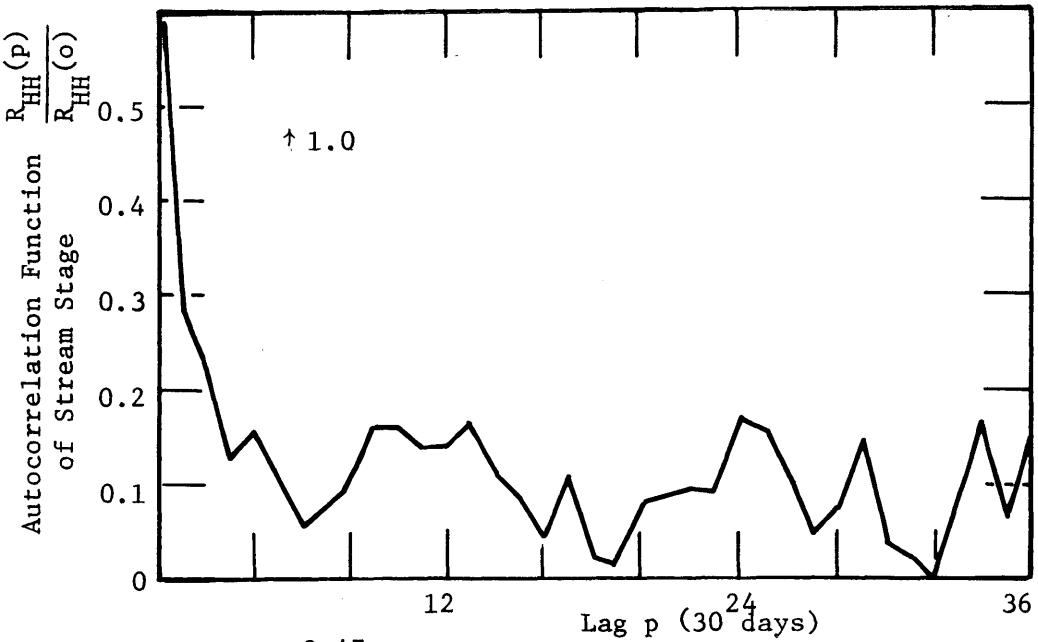

Figure 3.47 Correlogram of Stream Stage of the Kansas Data

$$\bar{\rho} = \bar{e}$$
$$\sigma_\rho^2 = \frac{A^2}{2} + \sigma_e^2 \qquad (3.3.22)$$

in which it is assumed that the deterministic and stochastic processes are independent. Table 3.5 lists the nonlinear simulation parameters for three cases with different variances.

Figure Number	Mean of Stochastic Component $\bar{e}$	s. d. of Stochastic Component s_e	Mean of Dimensionless $\bar{\rho}$	Amplitude of Deterministic Component A	Dim. frequency Ω
3.48	1	0.5	1	0.2	16
3.49	1	1.5	1	0.2	16
3.50	2	3.0	2	0.2	16

Table 3.5 List of Nonlinear Simulation Parameters for the Accretion Input System with Synthetic Data

The number of synthetic data generated in the first and third cases is 550 units and the number of lags is 50, while in the second case, the number of input time records is 1000 and the number of lags is 100. Clearly, there is no limit to the amount of data we can generate, but it becomes extremely costly. From Figures 3.48 - 3.50 it appears that the results are similar to those obtained from the historical data. In the historical data, we have a fixed dimensionless sample standard deviation, s_ρ of approximately 1. It is observed (compare Figures 3.48 and 3.49) that there is a relatively small increase of nonlinearity when the standard deviation of the input increases from

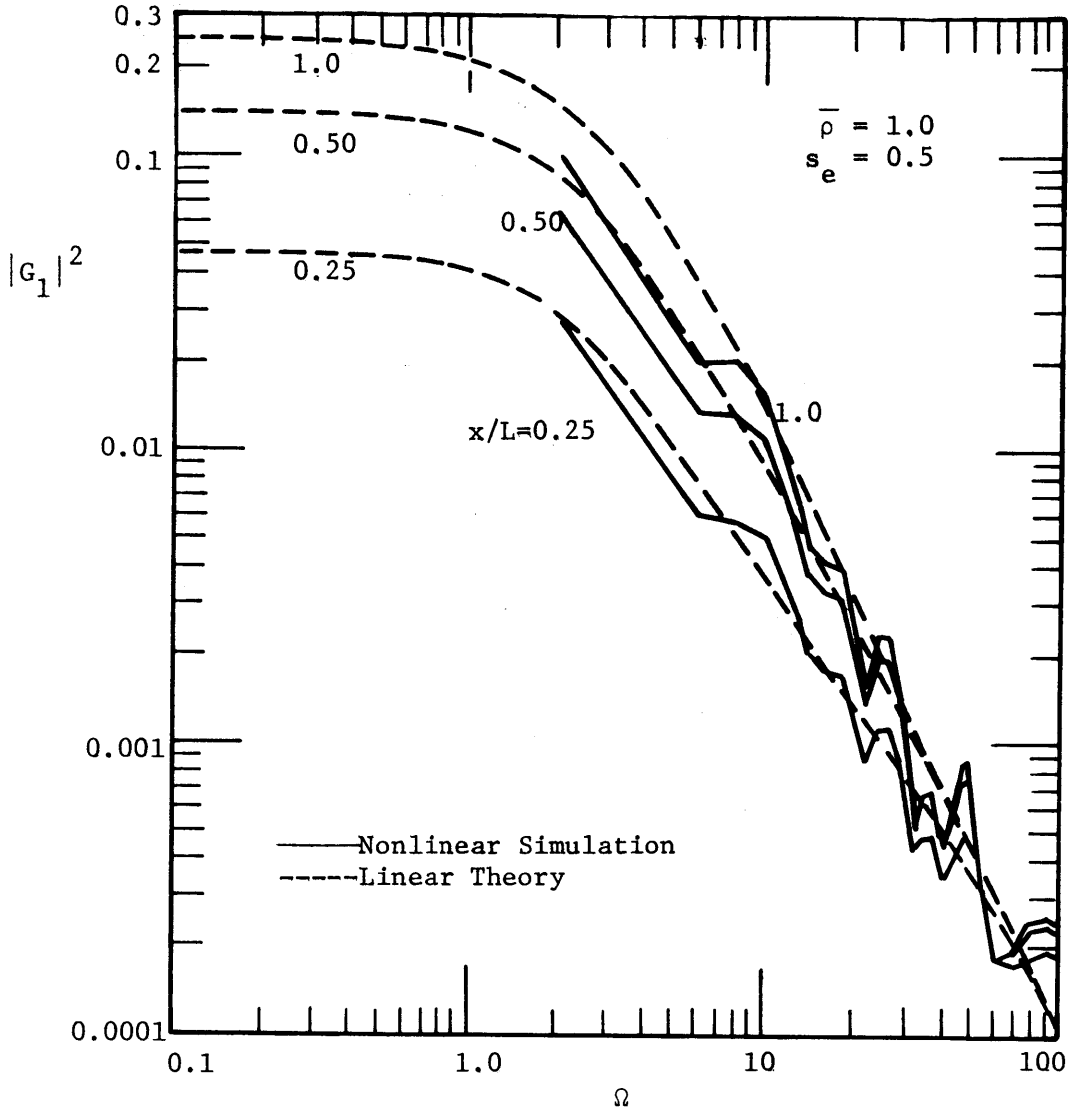

Figure 3.48 Square of the Amplitude of the Transfer Function of Nonlinear Simulation for the Aquifer System with Synthetic Accretion Input, $\bar{\rho}$ = 1.0 and s_e = 0.5

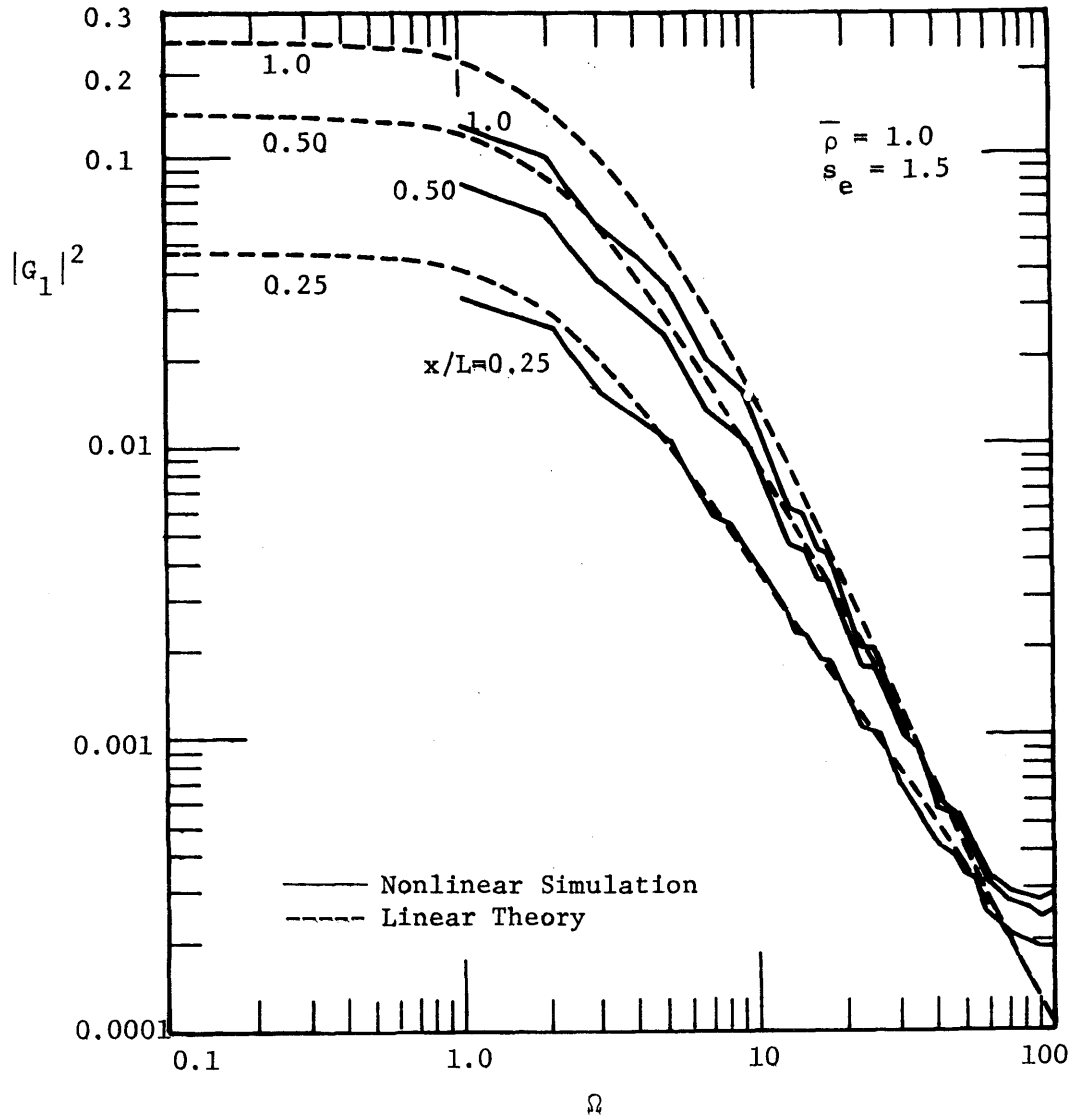

Figure 3.49 Square of the Amplitude of Transfer Function of Nonlinear Simulation for the Aquifer System with Synthetic Accretion Input, $\bar{\rho}$ = 1.0 and s_e = 1.5

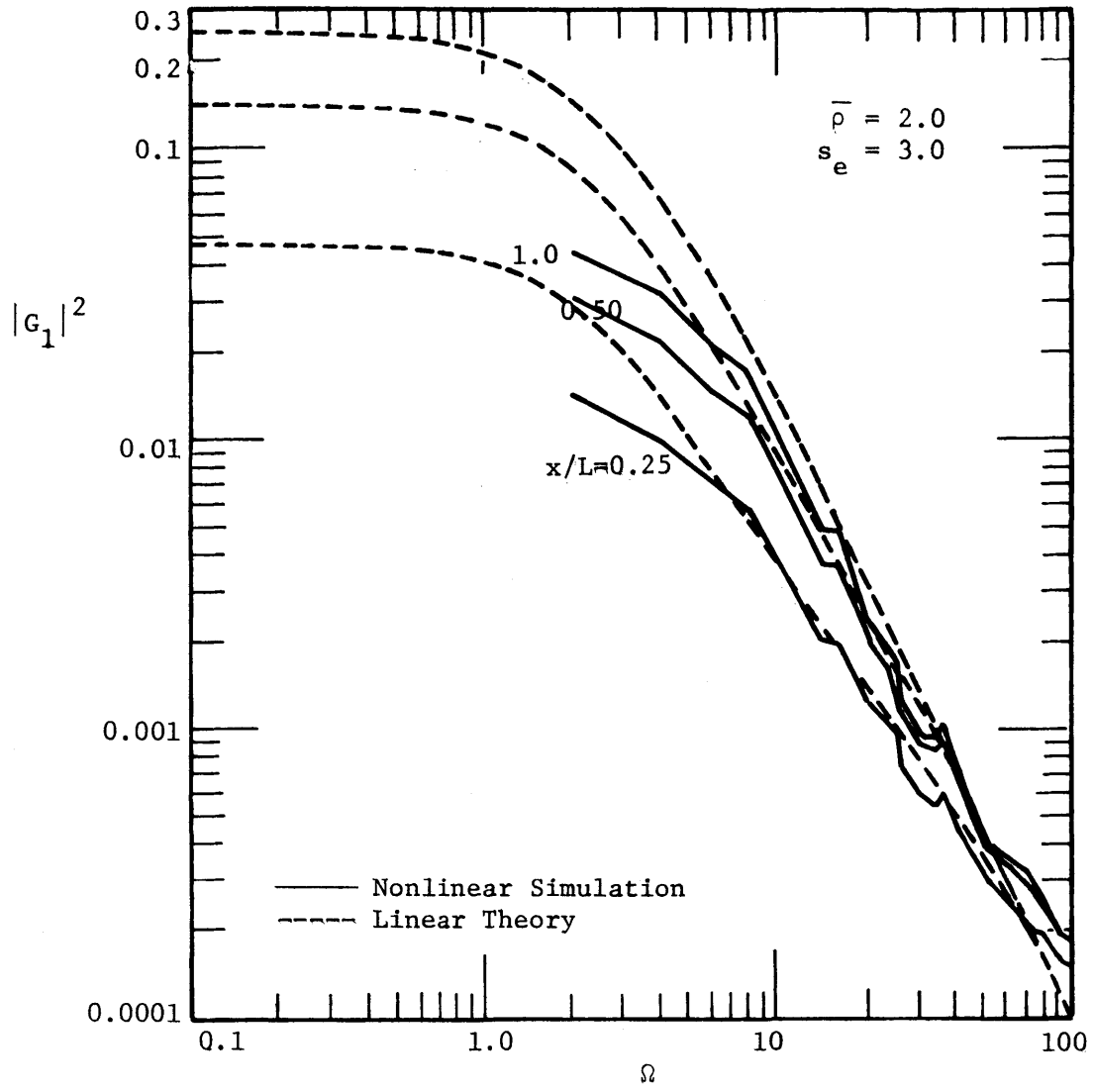

Figure 3.50 Square of the Amplitude of Transfer Function of Nonlinear Simulation for the Aquifer System with Synthetic Accretion Input, $\bar{\rho}$ = 2.0 and s_e = 3.0

0.5 to 1.5. The nonlinearity occurs in the range of lower frequency for which output amplitude decreases as s_ρ increases. There is some significant changes when the standard deviation increases to 3 (compare Figures 3.50 and 3.29). In realistic situations, a standard deviation of 3 for accretion, at a particular location over a significantly long record, is considered to be rare. Hence it can be concluded that the variance has a relatively small nonlinear effect on the groundwater system.

So far, precipitation records have been used to represent the accretion rate in order to facilitate the spectral analysis using field data input and output time records. In reality, precipitation and accretion differ not only in magnitude but also in spatial and temporal distributions due to the complicated processes occuring as water infiltrates into the ground and passes through the soil moisture zone. The two main topics to be considered in the simulation study will be the temporal and spatial distributions of the input accretion.

It has been shown in Figure 3.46 that the historical precipitation records have relatively uncorrelated temporal structure. We now incorporate into the synthetic accretion time series an arbitrary temporal correlation and study the behaviour of the transfer function of such a system. The time series is constructed in such a way that it depends on the accretion during the previous time steps. The intensity of dependence on the past is chosen by weights, w_i. The synthetic time series is represented in a discrete manner in the numerical model as

$$\rho(\tau_i) = A \cos \Omega\tau_i + \sum_{i=0}^{n} w_i e\ (\tau_i - i) \qquad (3.3.23)$$

where $\sum_{i=0}^{n} w_i = 1$

and $0 \leq w_i \leq 1$

e is generated from a normal distributed process as done previously. From equation 3.3.24 the mean and variance of the time series are found to be

$$\bar{\rho} = \bar{e}$$

$$\sigma_\rho^2 = \frac{A^2}{2} + \sum_{i=0}^{n} w_i^2 \sigma_e^2 + \Sigma_j \Sigma_i 2\, w_i w_j R_{ij} \qquad (3.3.24)$$

where $i \neq j$

R_{ij} = autocovariance of e between the i^{th} and j^{th} time step

σ_e^2 = theoretical variance of e

Since $\sum_{i=0}^{n} w_i = 1$

we have

$$\sigma_\rho^2 = \frac{A^2}{2} + \sigma_e^2 + \Sigma_j \Sigma_i 2\, w_i w_j (R_{ij} - \sigma_e^2)$$

One can see if there is strong correlation of the process between any two time steps, and if the weights, w_i are relatively high, the contribution to the dimensionless accretion variance, σ_ρ^2 would be high. Two cases are studied and are given in Table 3.6.

Figure Number	Dimensionless Accretion Mean $\bar{\rho}$	Sample Standard Deviation s_e	Amplitude of Deterministic Component A	Dimensionless Frequency Ω	Weights w_i
3.51	1	0.5	0	-	w_0=0.4 w_1=0.3 w_2=0.3
3.52	1	0.5	0.2	16	w_0=0.4 w_1=0.3 w_2=0.3

Table 3.6 List of Nonlinear Simulation Parameters for the Synthetic Accretion System with Temporal Correlation

It is seen that the correlational structure of the input time series has slightly greater nonlinear effects than the one without correlation (compare Figure 3.51 with 3.48). The nonlinear effects occur in the range of lower frequency such that the amplitude of transfer function is lower. One explanation of this is that for a correlated time series the total variance (sum of variance and auto-covariance as in equation 3.3.24 has larger value than that of the uncorrelated one. The interaction of covariance of the input series is further affected when the input is passed through the transformation system which also has a correlation structure. In other words the output time series has a correlation structure even if the input is white noise. The intensity of correlation will depend on the input series' structure. Another observation that may be made from Figures 3.51 and 3.52 is that there are some large fluctuations at

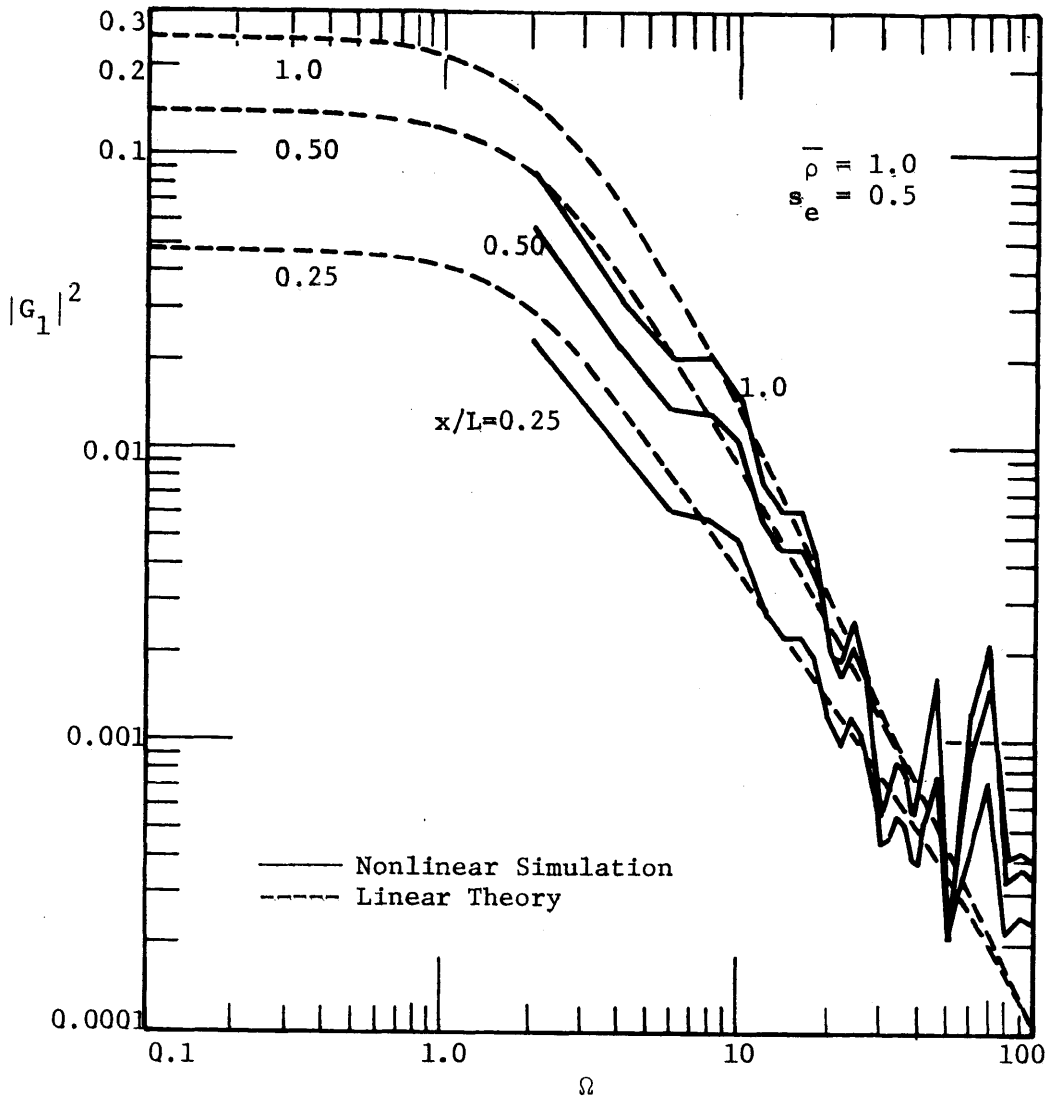

Figure 3.51 Square of the Amplitude of the Transfer Function of Nonlinear Simulation for the Aquifer System with a Temporally Correlated Synthetic Accretion Input, $\bar{\rho} = 1.0$ and $s_e = 0.5$

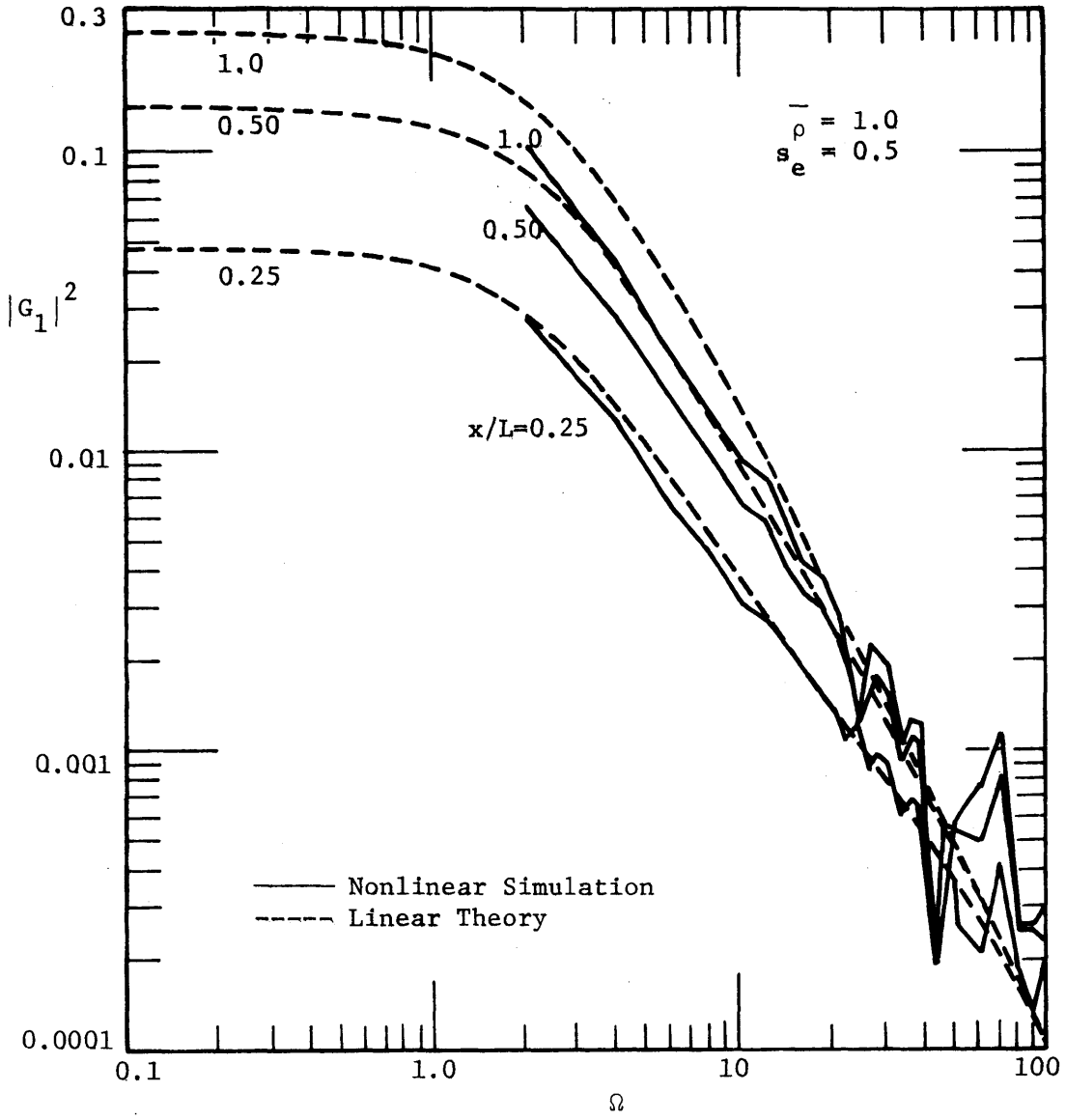

Figure 3.52 Square of the Amplitude of the Transfer Function of Nonlinear Simulation for the Aquifer System with a Temporally Correlated Synthetic Accretion Input, $\bar{\rho}$ = 1.0 and s_e = 0.5

high frequencies ($\Omega > 50$). At such high frequencies, the nonlinear simulation results show an amplitude of transfer function that is substantially higher than that of the linear theory. There are several possible sources of these effects including numerical error, aliasing error and the temporal correlation structure of the system. From the historical data analysis, and from the synthetic data analysis with no temporal correlation, we can see that these fluctuations do not exist at higher frequencies. Since the parameters used in these temporal correlation cases (compare Tables 3.5 and 3.6) are similar, it seems that numerical or aliasing error may not contribute to these fluctuations. Intuitively, this may be interpreted to mean that correlated accretion at high frequencies leads to a fluctuating system response, due to the interactions between the correlation of the input series and the transformation system.

Spatial as well as temporal distribution of accretion is of vital practical importance in this study. Four possible cases are considered. First, it is assumed that the spatial distribution is fixed for all time and is generated from a random normal process with a given mean and variance. Second, it is assumed that this spatial distribution varies randomly with time and has a mean equal to the uniform temporal fluctuation. Third and fourth, an arbitrary spatial correlation structure is incorporated in the above two cases. This structure is similar to that of the temporal structure, i.e. the spatial distribution depends on the weights w_i, given by the previous spatial coordinates starting from x/L =0 to 1. Hence the input accretion time series is

proportional to

$$\sum_{k=1}^{n} w_k e\ (i - k)$$

where n = number of horizontal spatial nodes in which there is dependence

i = number denotes the spatial horizontal coordinate

The following table lists the four cases.

Figure Number	Type of Spatial Distribution	Spatial Correlation Structure	Weights w_k	Dimensionless Accretion Mean $\bar{\rho}$
3.53	Fixed	Uncorrelated		2
3.54	Time variable	Uncorrelated		2
3.55	Fixed	Correlated	$w_1 = 0.4$, $w_2 = 0.3$ $w_3 = 0.2$, $w_4 = 0.1$	2
3.56	Time variable	Correlated	$w_1 = 0.4$, $w_2 = 0.3$ $w_3 = 0.2$, $w_4 = 0.1$	2

Table 3.7 List of Nonlinear Simulation Parameters for the Accretion Input System with Spatial Distribution

The temporal distribution of these four cases is the same as that of the historical data. The fixed spatial distribution is generated from a normal process with mean of 1 and standard deviation of 0.5 as shown in Figure 3.57. The linear theory for a spatially distributed accretion input developed in section 3.1 may be used for comparision to the nonlinear simulation results. There are two basic parameters to be chosen in order for comparision. These are the wave number, k

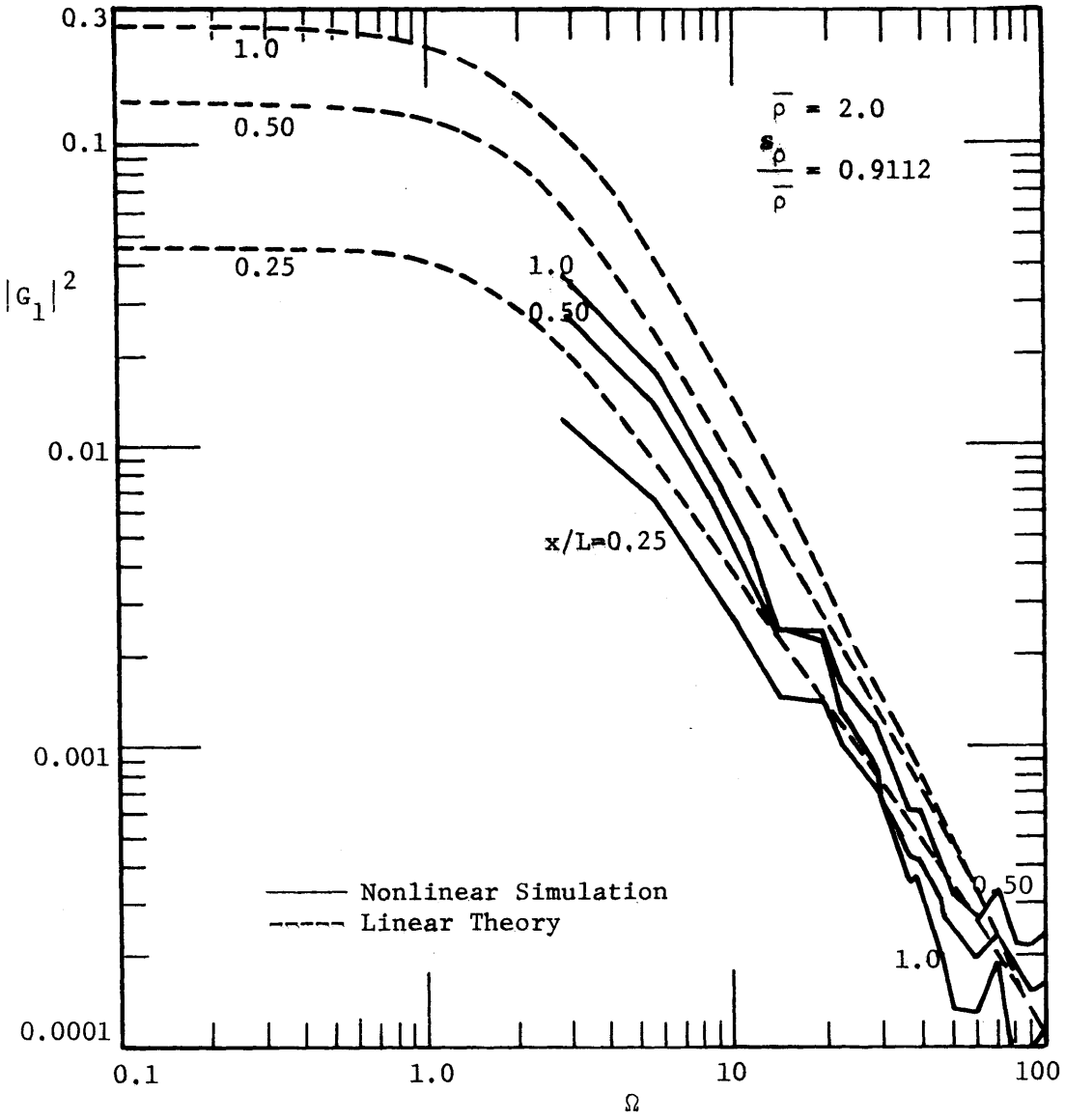

Figure 3.53 Square of the Amplitude of the Transfer Function of Nonlinear Simulation for the Accretion Input System with a Fixed and Uncorrelated Spatial Structure

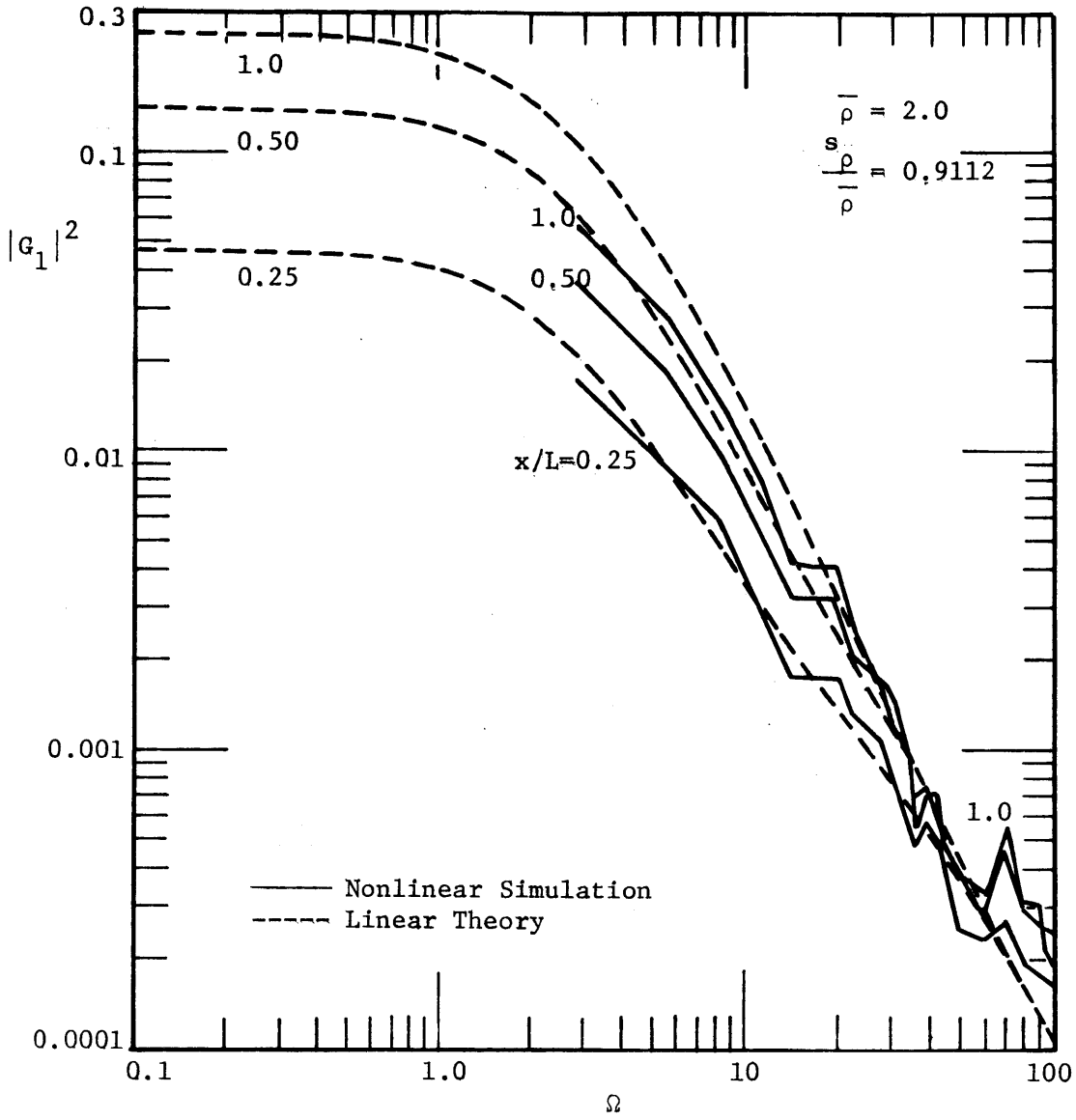

Figure 3.54 Square of the Amplitude of the Transfer Function of Nonlinear Simulation for the Accretion Input System with a Time Variable and Uncorrelated Spatial Structure

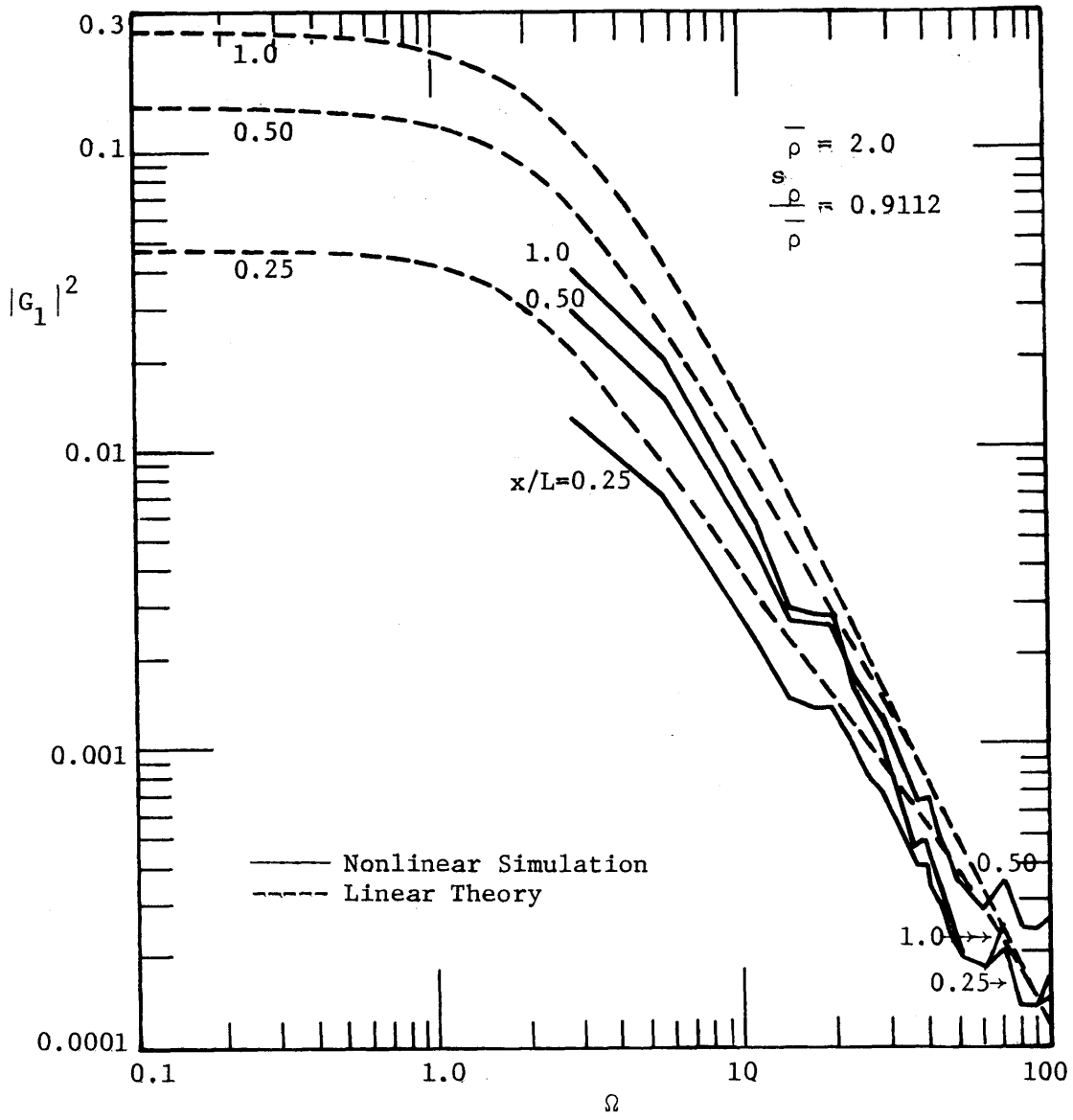

Figure 3.55 Square of the Amplitude of the Transfer Function of Nonlinear Simulation for the Accretion Input System with a Fixed and Correlated Spatial Structure

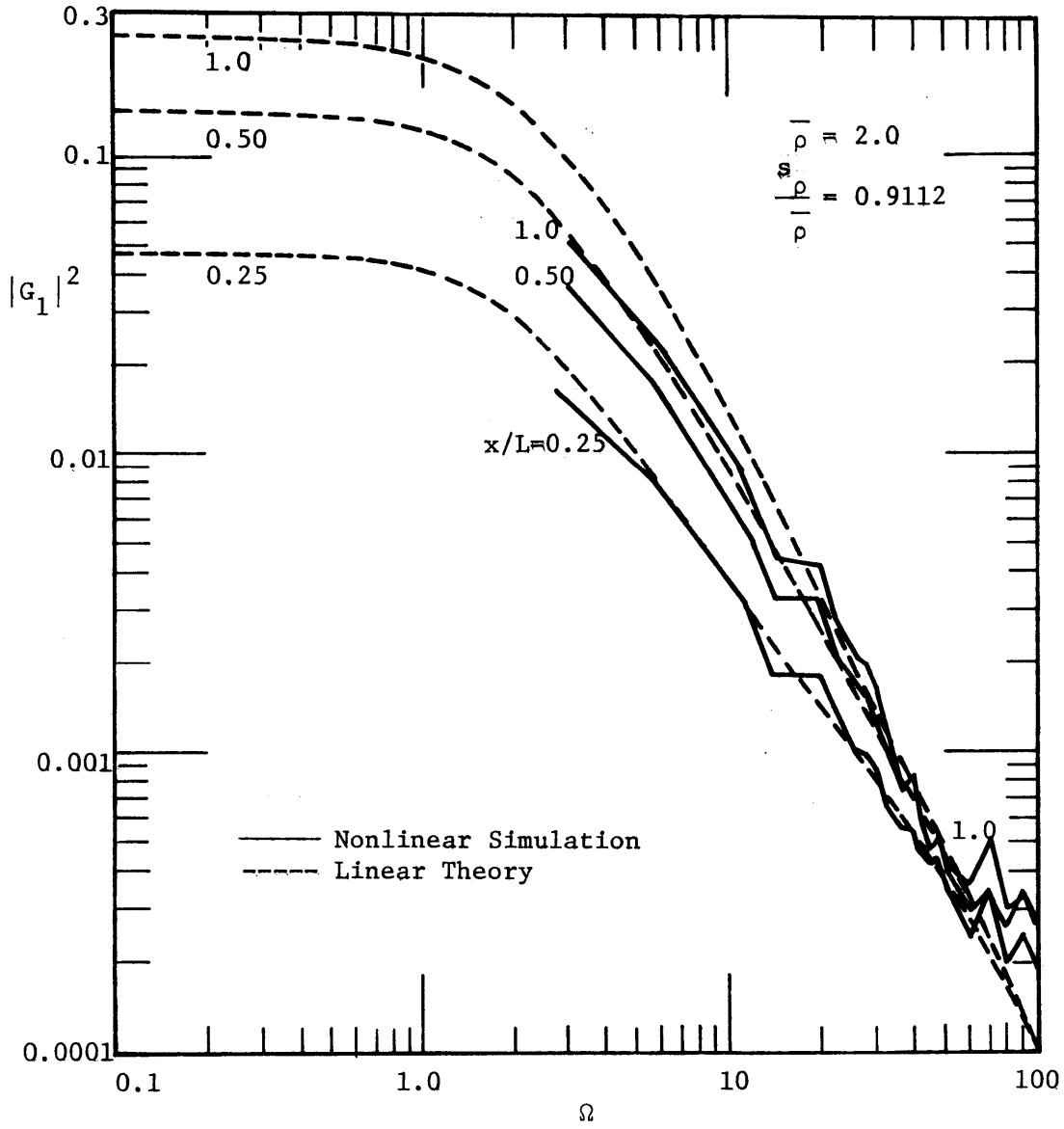

Figure 3.56 Square of the Amplitude of the Transfer Function of Nonlinear Simulation for the Accretion Input System with a Time Variable and Correlated Spatial Structure

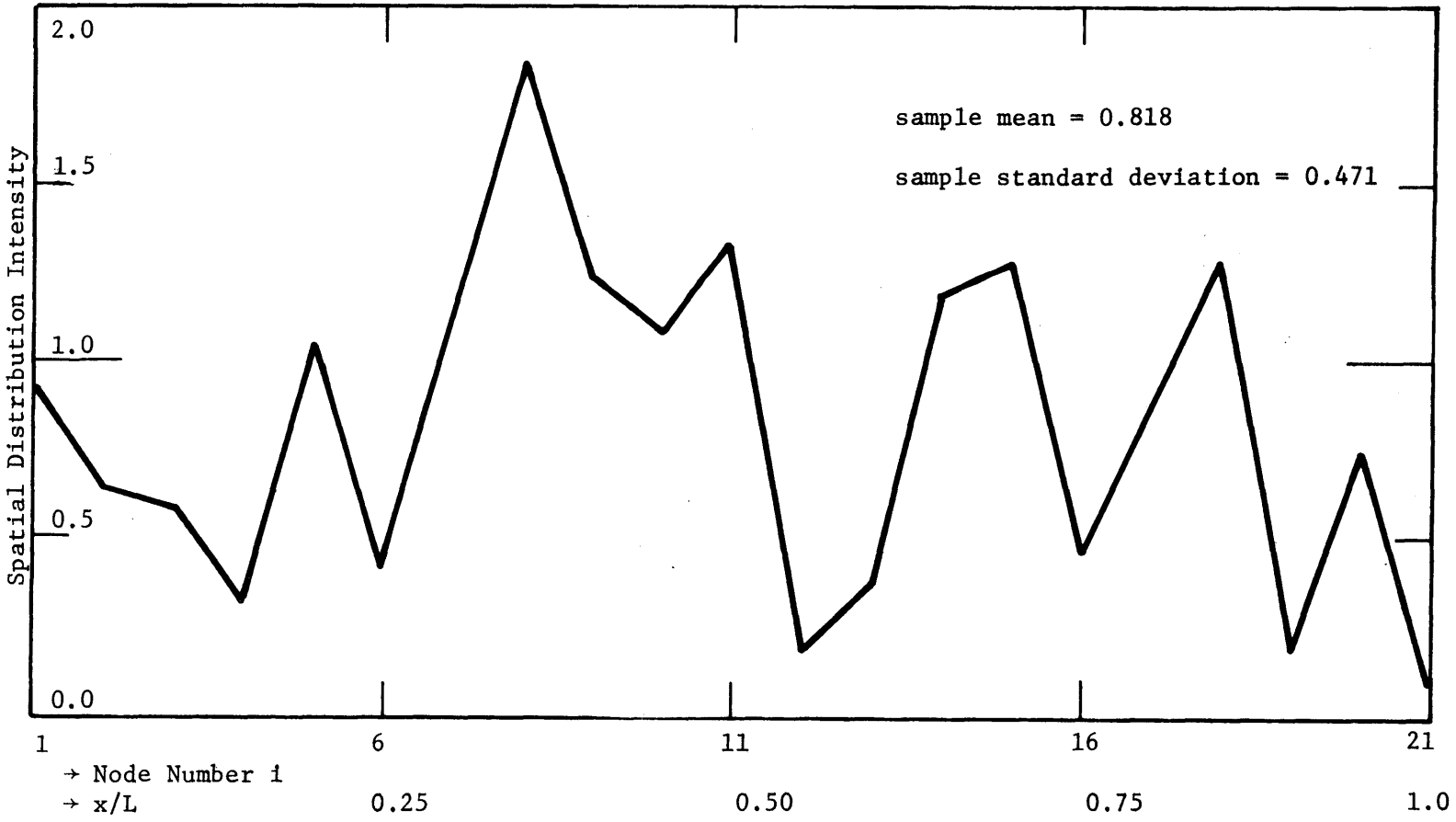

Figure 3.57 Fixed Spatial Distribution of Accretion for the Nonlinear Simulation of the Aquifer System

and the ratio of the amplitude of spatial fluctuation to that of the temporal fluctuation, α'/α. The choice of k depends on the intensity of the spatial fluctuation as shown in Figure 3.57. In this figure it can be estimated that the value of k is in the range from 8π to 10π. The comparison is based on the assumption that the spatial fluctuation is of the form of a sinusoidal wave $\alpha'/\alpha \cos k\xi$. The variance of this sinusoidal process, $0.5(\alpha'/\alpha)^2$, and the sample variance of the normal process from the simulation is equivalent as

$$s^2 = 0.5(\alpha'/\alpha)^2$$

$$\therefore \quad \alpha'/\alpha = \sqrt{2}\, s$$

Also in this case, s = 0.5, hence $\alpha'/\alpha = 0.707$. An example of the square of the amplitude of the transfer function with $k = 10\pi$ and $\alpha'/\alpha = 0.707$ has already been shown in Figure 3.10. There is virtually no difference from the case without spatial variability. The nonlinear simulation results for a fixed spatial distribution (see Figures 3.53 and 3.55 are somewhat different from those of the linear theory. Firstly, the amplitude of the transfer function is lower for all frequencies. This effect is observed in the linear theory for a spatially distributed accretion input (see Figure 3.9) but is not as significant as in the nonlinear system. Secondly, it is observed that the simulation results show a rather strong local spatial effect. In this example, it is seen that the amplitude drops down significantly at x/L = 1, below amplitudes for other locations at higher frequencies (Ω>30). This is due to the particular spatial structure of the system (see Figure 3.57 which shows that the sample mean is lower than 1 and the spatial

distribution intensity at x/L = 1 is substantially smaller than at other locations). This effect is not predicted in the linear theory. On the other hand, the cases with a time variable spatial distribution compare more closely with the linear theory. (See Figure 3.54 and 3.56). This seems reasonable as the random distribution has a mean which is equal to that of the uniform temporal distribution. The cases with spatial correlation for this system indicate little difference from the cases without correlation. The more significant difference is in the range of higher frequencies.

In the investigation of the two cases - fixed and time variable spatial structure - the former is probably more typical of field conditions because variations in accretion will be associated with soil conditions and vegetation. The time variable spatial structure relates to recharge variations associated with variable precipitation patterns and is useful in the initial investigation of this study.

In conclusion, the transfer function obtained from the spatially variable accretion input system is little different from the case where there is no spatial variability. This agrees closely with the linear theory for a spatially distributed input developed earlier. However, it seems that an extreme intensity of the spatial distribution at a particular location may have significant effects on the spectral response for higher frequencies at that location. The implications of these local effects require further investigation.

In this synthetic time series study, we see that the variance is relatively unimportant to the nonlinear effects. Also, the spatial

parameter, x/L may play an important role when the spatially distributed accretion input is subject to extreme local variations.

The simulation model can be further investigated with additional complexities. The most interesting items would be the incorporation of the spatial variability of hydraulic conductivity and the two dimensional spatial representation of the system. These can be easily implemented using the numerical model, but it would be expensive, especially the latter case. It is expected that in the case of spatial variability of hydraulic conductivity the behaviour of the transfer function may be more sensitive to changes of input parameters than in the case of spatial variability of accretion. In the two dimensional representation, some insight could be gained with regard to the two dimensional spatial distribution properties of the system.

3.4 Summary

In this study of the nonlinear simulation of the phreatic aquifer system, a finite difference model is regarded as a transformation system and the input time series are either obtained from historical field data or generated from synthetic data. Emphasis has been on the comparision of the transfer function of the nonlinear system, obtained from the spectral analysis of the simulation results, to the transfer function from the linear theory.

The linear theory for the Dupuit model is first developed and a simple evaluation of nonlinearity is discussed with emphasis on deterministic sinusoidal inputs. Then the numerical model is introduced and tested for a number of simple cases with sinusoidal inputs. It is found that the numerical error is sufficiently small and that the simple evaluation of nonlinearity is quite reasonable. This further confirms the identification of the parameters that control nonlinearity in the deterministic system. In the stochastic system, these parameters are correspondingly the mean, variance and autocovariance of the input stationary time series. This investigation leads to important physical and statistical interpretations of the phreatic aquifer system. The dimensionless mean is related to the physical dimensions and properties of the system, while the variance and autocovariance relate to the distribution properties of the input hydrological processes. The combination of these parameters leads to the evaluation of the nonlinear system.

The mean of dimensionless accretion is found to be the major cause of all nonlinear effects. This effect is significant in the range of lower frequency at which the amplitude of the transfer function for the nonlinear system is smaller, and this deviation increases as the dimensionless mean increases. In realistic situations, the dimensionless mean is found to be in the range from 0.1 to 2 and the nonlinear simulation results show relatively small deviation from the linear theory. Also, it is found that the deviation slightly increases as the spatial parameter - distance away from the stream - increases.

For a given system with fixed physical dimensions and properties, the probability distribution properties of the stream stage and accretion fluctuations are the more important determining factors of nonlinearity. It is found that the standard deviation of dimensionless accretion has similar effects on the amplitude of the transfer function as that of the dimensionless mean, but is less significant in the range from 0.5 to 1.5. Significant differences occur when the standard deviation is as high as 3, which is rare for a hydrological process with a long record. In the case of stream interaction, the standard deviation of dimensionless stream stage fluctuation is relatively unimportant in the range from 0.05 to 0.2, which can represent a good number of cases in realistic situations.

For the accretion input with both temporal and spatial distribution, it is found that there are negligible spatial effects. However, it seems that the extreme spatial distribution intensity at one location may have a significant effect on the spectral response for higher

frequencies at that particular location. Further investigation is required to identify the nonlinear effects of such a system.

The overall study of the stochastic groundwater systems is an exploratory investigation using spectral analysis to evaluate aquifer parameters with available data. The results of this portion of the study substantiate the reliability of the overall spectral simulation. This is because the transfer function obtained from inputs which have been passed through the numerical model and the spectral estimation process, shows excellent agreement with the linear theory. This simulation study further confirms that the linearized Dupuit model is a good approximation of the nonlinear model for typical aquifer physical dimensions and parameters, and input probability distribution properties. Future possible investigations, such as the spatial variability of hydraulic conductivity and the two dimensional spatial representation, can be easily implemented into the numerical model and should give additional insight into the system.

Chapter 4 DATA ANALYSIS AND PARAMETER EVALUATION

4.1 General Review of Spectral Analysis for Lumped Parameter Linear Systems

Single-input Linear Systems. A system is said to be a single-variable system if and only if it has only one input and one output, and if the input and output can be related by the convolution integral,

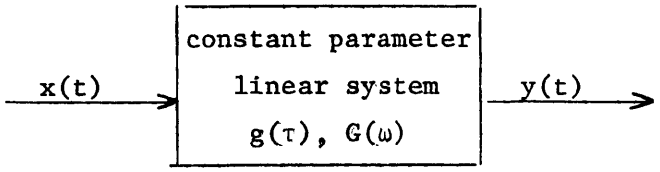

Figure 4.1 Single-input Linear System

namely,

$$y(t) = \int_{-\infty}^{\infty} g(\tau)x(t-\tau)\, d\tau \qquad (4.1.1)$$

For example, a first order linear system can be described by

$$C\,\frac{dy(t)}{dt} + y(t) = x(t) \qquad (4.1.2)$$

where C is called the time constant. It has to be assumed that the system is initially relaxed at $t \leq -\infty$. That is to say the output is excited solely and uniquely by the input applied thereafter.

The Convolution Theorem. The most useful relation between the Fourier transform and the convolution integral is the convolution

theorem. Taking the Fourier transform of the convolution integral as given by equation 4.1.1, we have

$$y(t) = \int_{-\infty}^{\infty} g(\tau)x(t-\tau)\, d\tau \qquad (4.1.3)$$

$$Y(\omega) = \int_{-\infty}^{\infty} y(t)\, e^{-i\omega t}\, dt$$

$$= \int_{-\infty}^{\infty}\int_{-\infty}^{\infty} g(\tau)x(t-\tau)\, e^{-i\omega t}\, d\tau\, dt$$

$$= \int_{-\infty}^{\infty}\int_{-\infty}^{\infty} g(\tau)\, e^{-i\omega\tau}x(t-\tau)\, e^{-i\omega(t-\tau)}\, d\tau\, dt$$

$$= \int_{-\infty}^{\infty} g(\tau)\, e^{-i\omega\tau} \int_{-\infty}^{\infty} x(t-\tau)\, e^{-i\omega(t-\tau)}\, dt\, d\tau$$

$$= \int_{-\infty}^{\infty} g(\tau)\, e^{-i\omega\tau}\, X(\omega)\, d\tau$$

$$Y(\omega) = G(\omega)\, X(\omega) \qquad (4.1.4)$$

where $Y(\omega)$, $G(\omega)$ and $X(\omega)$ are the Fourier transforms of $y(t)$, $g(t)$ and $x(t)$, respectively. Thus, the Fourier transform of the convolution of two functions is the product of their transforms.

Spectral Relationships for Single-input Linear Systems. Taking the product of $y(t)$ and $y(t+\tau)$ as given in equation 4.1.3, we have

$$y(t)y(t+\tau) = \int_{-\infty}^{\infty}\int g(\eta)x(t-\eta)g(\xi)x(t+\tau-\xi)d\eta\ d\xi \qquad (4.1.5)$$

The expectation of equation 4.1.5 gives the relation between the covariance functions of the input and output series in the time domain;

$$\mu_Y(\tau) = \int_{-\infty}^{\infty}\int g(\eta)g(\xi)\mu_X(\tau+\eta-\xi)\ d\eta\ d\xi \qquad (4.1.6)$$

Similarly, taking the expectation of the product of $x(t)$ and $y(t+\tau)$, we have, in time domain,

$$E[x(t)y(t+\tau)] = E[\int_{-\infty}^{\infty}\int g(\eta)x(t)x(t+\tau-\eta)d\eta]$$

$$\mu_{XY}(\tau) = \int_{-\infty}^{\infty} g(\eta)\mu_X(\tau-\eta)\ d\eta \qquad (4.1.7)$$

Using the convolution theorem, equations 2.1.8 and 2.1.23, equations 4.1.6 and 4.1.7 can be transformed into the frequency domain having the following relations:

$$S_{YY}(\omega) = |G(\omega)|^2\ S_{XX}(\omega) \qquad (4.1.8)$$

$$S_{XY}(\omega) = G(\omega)\ S_{XX}(\omega) \qquad (4.1.9)$$

Equation 4.1.8 shows the relation between the input and output spectra and is a real function, while equation 4.1.9 shows the relation between the input spectrum and the cross-spectrum of both input and output series. Note that $|G(\omega)|$ is the gain factor or the amplitude of the transfer function. If $S_{XX}(\omega)$, $S_{YY}(\omega)$ and $S_{XY}(\omega)$ are estimated by $\hat{S}_{XX}(\omega)$, $\hat{S}_{YY}(\omega)$ and $\hat{S}_{XY}(\omega)$ respectively, this gain factor, $|G(\omega)|$ is equivalent to equation 2.1.26, and equations 4.1.8 and 4.1.9 become

$$\hat{S}_Y(\omega) = |G(\omega)|^2 \hat{S}_X(\omega) \qquad (4.1.10)$$

$$\hat{S}_{XY}(\omega) = G(\omega) \hat{S}_X(\omega) \qquad (4.1.11)$$

Multiple-input Linear Systems and their Spectral Relationships. In direct generalization of equation 4.1.1, series $y(t)$, $g(\tau)$ and $x(t-\tau)$ can be thought of as vectors. Thus, we have

$$y_i(t) = \int_{-\infty}^{\infty} g_i(\tau) x_i(t-\tau)\, d\tau \quad i=1,\cdots,n \qquad (4.1.12)$$

If the inputs, $\{x_i(t), i = 1,\cdots,n\}$, are all mutually independent, equations 4.1.8, 4.1.9, 4.1.10 and 4.1.11 can simply be generalized

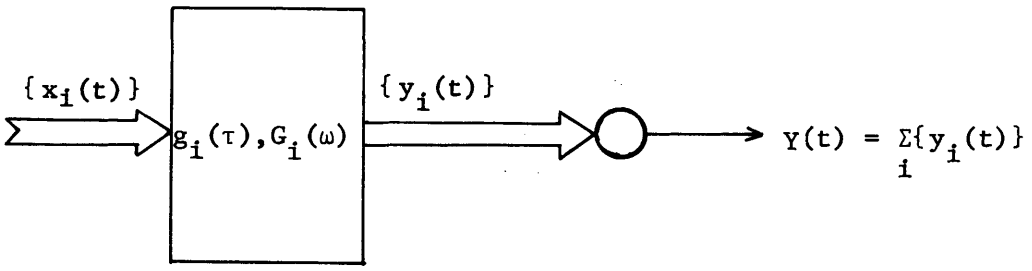

Figure 4.2 Multiple-Inputs Linear System.

respectively to:

$$S_{Y_i}(\omega) = |G_i(\omega)|^2 \, S_{X_i}(\omega) \tag{4.1.13}$$

$$S_{XY_i}(\omega) = G_i(\omega) \, S_{X_i}(\omega) \tag{4.1.14}$$

$$\hat{S}_{Y_i}(\omega) = |G_i(\omega)|^2 \, \hat{S}_{X_i}(\omega) \tag{4.1.15}$$

$$\hat{S}_{X_i Y_i}(\omega) = G_i(\omega) \, \hat{S}_{X_i}(\omega) \tag{4.1.16}$$

$$\text{for} \quad i = 1, \cdots, n$$

Owing to the linearity of the system, the spectrum of the final output, Y(t), can be found by simply summing over i, i.e.

$$S_Y(\omega) = \sum_{i=1}^{n} |G_i(\omega)|^2 S_{X_i}(\omega) \qquad (4.1.17)$$

For mutually correlated inputs, the auto-correlation function $\mu_Y(\tau)$ can be computed as follows:

$$\mu_Y(\tau) = E[y(t)y(t+\tau)] = E[\sum_{i=1}^{n} y_i(t) \sum_{j=1}^{n} y_j(t+\tau)]$$

$$= E[\sum_{i=1}^{n}\sum_{j=1}^{n} \int_{-\infty}^{\infty}\int_{-\infty}^{\infty} g_i(\eta)x_i(t-\eta)g_j(\xi)x_j(t+\tau-\xi)d\eta\, d\xi]$$

$$= \sum_{i=1}^{n}\sum_{j=1}^{n} \int_{-\infty}^{\infty}\int_{-\infty}^{\infty} g_i(\eta)g_j(\xi)\mu_{X_iX_j}(\tau+\eta-\xi)d\eta\, d\xi \qquad (4.1.18)$$

By multiplying equation 4.1.18 by $e^{-i\omega(\eta-\xi)}\, e^{i\omega(\eta-\xi)} = 1$ and taking the Fourier transform, the relationship between the input series and the output y(t) can then be found as,

$$S_Y(\omega) = \sum_{i=1}^{n}\sum_{j=1}^{n} \int_{-\infty}^{\infty}\int_{-\infty}^{\infty}\int_{-\infty}^{\infty} g_i(\eta)g_j(\xi)\mu_{X_iX_j}(\tau+\eta-\xi)$$
$$e^{-i\omega(\eta-\xi)}e^{i\omega(\eta-\xi)}e^{-i\omega\tau}d\eta d\xi d\tau$$

$$= \sum_{i=1}^{n}\sum_{j=1}^{n} \int_{-\infty}^{\infty}\int_{-\infty}^{\infty}\int_{-\infty}^{\infty} g_i(\eta)g_i(\xi)\mu_{X_iX_j}(\tau+\eta-\xi)$$
$$e^{-i\omega\eta}e^{i\omega\xi}e^{-i\omega(\tau+\eta-\xi)}d\eta d\xi d\tau$$

$$S_Y(\omega) = \sum_{i=1}^{n}\sum_{j=1}^{n} \int_{-\infty}^{\infty} g_i(\eta)e^{-i\omega\eta}d\eta \int_{-\infty}^{\infty} g_j(\xi)e^{i\omega\xi}d\xi \int_{-\infty}^{\infty} \mu_{X_iX_j}(\tau+\eta-\xi) e^{-i\omega(\tau+\eta-\xi)}d\tau$$

$$S_Y(\omega) = \sum_{i=1}^{n}\sum_{j=1}^{n} G_i(\omega)G_j^*(\omega)S_{X_iX_j}(\omega) \qquad (4.1.19)$$

In similar fashion, the cross-correlation function can be computed as:

$$\mu_{X_iY}(\tau) = E[x_i(t)y(t+\tau)] = E[x_i(t) \sum_{j=1}^{n} \int_{-\infty}^{\infty} g_j(\eta)x_j(t+\tau-\eta)d\eta]$$

$$= \sum_{j=1}^{n} \int_{-\infty}^{\infty} \mu_{X_iX_j}(\tau-\eta)\, g_j(\eta)\, d\eta \qquad (4.1.20)$$

By taking the Fourier transform of equation 4.1.20, the relations between the cross-spectra and the input spectra can be shown as

$$S_{X_iY}(\tau) = \sum_{j=1}^{n} \int_{-\infty}^{\infty} \int_{-\infty}^{\infty} g_j(\eta)\mu_{X_iX_j}(\tau-\eta)e^{-i\omega\tau}d\eta d\tau$$

$$= \sum_{j=1}^{n} \int_{-\infty}^{\infty} \int_{-\infty}^{\infty} g_j(\eta)e^{-i\omega\eta}\, \mu_{X_iX_j}(\tau-\eta)e^{-i\omega(\tau-\eta)}d\eta d\tau$$

$$S_{X_iY}(\omega) = \sum_{j=1}^{n} G_j(\omega)\, S_{X_iX_j}(\omega) \qquad (4.1.21)$$

Note that equations 4.1.19 and 4.1.21 are reducible to equations 4.1.13 and 4.1.14 if $S_{X_iX_j}(\omega) = 0$, for $i \neq j$, i.e., X_i and X_j are mutually independent. Note also that the property of cross-spectra,

$$S_{X_iX_j}(\omega) = S^*_{X_jX_i}(\omega) \tag{4.1.22}$$

Again, $S_Y(\omega)$, $S_{X_iY_j}(\omega)$, $S_{XY}(\omega)$ and $S_{X_iX_j}(\omega)$ in equations 4.1.19 and 4.1.20 are estimated, in practical computations, by $\hat{S}_Y(\omega)$, $\hat{S}_{X_iX_j}(\omega)$, $\hat{S}_{X_iY}(\omega)$ and $\hat{S}_{X_iX_j}(\omega)$, respectively. For a special case of two correlated inputs, $X_1(t)$ and $X_2(t)$, equation 4.1.19 gives,

$$S_Y(\omega) = |G_1(\omega)|^2 S_{X_1X_1}(\omega) + G_1(\omega)G_2^*(\omega)S_{X_1X_2}(\omega) +$$

$$G_1^*(\omega)G_2(\omega)S_{X_2X_1}(\omega) + |G_2(\omega)|^2 S_{X_2X_2}(\omega) \tag{4.1.23}$$

and equation 4.1.21 gives,

$$\begin{aligned} S_{X_1Y}(\omega) &= G_1(\omega)S_{X_1X_1}(\omega) + G_2(\omega)S_{X_1X_2}(\omega) \\ S_{X_2Y}(\omega) &= G_1(\omega)S_{X_2X_1}(\omega) + G_2(\omega)S_{X_2X_2}(\omega) \end{aligned} \tag{4.1.24}$$

$$G_1(\omega) = \frac{\begin{vmatrix} S_{X_1Y}(\omega) & S_{X_1X_2}(\omega) \\ S_{X_2Y}(\omega) & S_{X_2X_2}(\omega) \end{vmatrix}}{\begin{vmatrix} S_{X_1X_1}(\omega) & S_{X_1X_2}(\omega) \\ S_{X_2X_1}(\omega) & S_{X_2X_2}(\omega) \end{vmatrix}} \qquad (4.1.25)$$

and

$$G_2(\omega) = \frac{\begin{vmatrix} S_{X_1X_1}(\omega) & S_{X_1Y}(\omega) \\ S_{X_2X_1}(\omega) & S_{X_2Y}(\omega) \end{vmatrix}}{\begin{vmatrix} S_{X_1X_1}(\omega) & S_{X_1X_2}(\omega) \\ S_{X_2X_1}(\omega) & S_{X_2X_2}(\omega) \end{vmatrix}} \qquad (4.1.26)$$

After expanding equations 4.1.25 and 4.1.26,

$$G_1(\omega) = \frac{S_{X_1Y}(\omega)\left(1 - \frac{S_{X_1X_2}(\omega)\, S_{X_2Y}(\omega)}{S_{X_1Y}(\omega)\, S_{X_2X_2}(\omega)}\right)}{S_{X_1X_1}(\omega)\left(1 - \frac{S_{X_2X_1}(\omega) S_{X_1X_2}(\omega)}{S_{X_1X_1}(\omega) S_{X_2X_2}(\omega)}\right)} \qquad (4.1.27)$$

and

$$G_2(\omega) = \frac{S_{X_2Y}(\omega)\left(1 - \frac{S_{X_2X_1}(\omega)\, S_{X_1Y}(\omega)}{S_{X_1X_1}(\omega)\, S_{X_2Y}(\omega)}\right)}{S_{X_2X_2}(\omega)\left(1 - \frac{S_{X_2X_1}(\omega)\, S_{X_1X_2}(\omega)}{S_{X_1X_1}(\omega)\, S_{X_2X_2}(\omega)}\right)} \qquad (4.1.28)$$

Note that $S_{X_2X_1}(\omega) = S^*_{X_1X_2}(\omega)$, therefore by using equation 2.1.24, in the denominator of equations 4.1.27 and 4.1.28,

$$\frac{S_{X_2X_1}(\omega)\, S_{X_1X_2}(\omega)}{S_{X_1X_1}(\omega)\, S_{X_2X_2}(\omega)} = \gamma^2_{X_1X_2}(\omega) \qquad (4.1.29)$$

Note that equation 4.1.23 has a form identical to the linearized Dupuit aquifer model, equation 2.3.9, and this makes it possible to apply these results in the data analysis.

4.2 Numerical Procedure of Spectral Estimation

In order to use the relationships outlined in the previous section 4.1, we have to estimate the power spectra of the input and the output series as well as the cross-spectra between each of the input and the output series, i.e., $\hat{S}_{X_iY}$, and the cross-spectra between the input series, i.e., $\hat{S}_{X_iX_j}$, from equi-spaced time series data of limited length. First of all, these series of data are standardized by subtracting the mean and dividing by the standard deviation of the respective series. The autocovariances can then be computed as

$$\hat{R}_{XX}(p\Delta t) = \frac{1}{n-p} \sum_{k=1}^{n-p} x_k x_{k+p} \quad p = 0,1,2,3,\cdots k_m \tag{4.2.1}$$

where n = number of discrete data points taken at constant time interval of Δt and k_m = maximum number of lags. Then the raw estimate of the power spectrum can be obtained by discrete cosine transform.

$$\tilde{S}_{XX}(\omega_h) = \frac{2\Delta t}{\pi} \sum_{p=0}^{k_m} \alpha_p R_{XX}(p\Delta t) \cos \frac{hp\pi}{k_m} \tag{4.2.2}$$

$$h = 0,1,\cdots,k_m$$

where $$\alpha_p = \begin{cases} 1 & 0 < p < k_m \\ \frac{1}{2} & p = 0, k_m \end{cases}$$

and $$\omega_h = \frac{h\pi}{k_m \Delta t}$$

These raw estimates of the power spectrum are then smoothed by the following "hamming" window,

$$\hat{S}_{XX}(0) = .54 \tilde{S}_{XX}(0) + .46 \tilde{S}_{XX}(\omega_1)$$

$$\hat{S}_{XX}(\omega_h) = .23 \tilde{S}_{XX}(\omega_{h-1}) + .54 \tilde{S}_{XX}(\omega_h) + .23 \tilde{S}_{XX}(\omega_{h+1}) \tag{4.2.3}$$

$$\hat{S}_{XX}(\omega_{k_m}) = .54 \tilde{S}_{XX}(\omega_{k_m}) + .46 \tilde{S}_{XX}(\omega_{k_m-1})$$

The smoothed estimates of the power spectrum can be checked for accuracy with allowable truncation errors, by the following equality,

$$\hat{R}_{XX}(0) = \frac{\pi}{k_m \Delta t}\left[\frac{1}{2}(\hat{S}_{XX}(0)+\hat{S}_{XX}(\omega_{k_m})) + \sum_{h=1}^{k_m-1} S_{XX}(\omega_h)\right] \qquad (4.2.4)$$

Similar procedures can be used in computing the cross-spectra. The cross-covariance is computed by the formula

$$\hat{R}_{XY}(p\Delta t) = \frac{1}{n-p}\sum_{k=1}^{n-p} x_k y_{k+p} \qquad p=0,1,2,\cdots,k_m$$

$$\hat{R}_{XY}(-p\omega t) = \frac{1}{n-p}\sum_{k=1}^{n-p} x_{k+p} y_k \qquad p=0,1,2,\cdots,k_m \qquad (4.2.5)$$

Then taking the discrete cosine and sine transforms of equation 4.2.5, we have the raw estimates of the co-spectrum, Co_{XY}, and quadrature spectrum, Q_{XY}, respectively.

$$\tilde{Co}_{XY}(\omega_h) = \frac{\Delta t}{\pi}\sum_{p=0}^{k_m} \alpha_p[\hat{R}_{XY}(p\Delta t)+\hat{R}_{XY}(-p\Delta t)]\cos\left(\frac{hp\pi}{k_m}\right)$$

$$\tilde{Q}_{XY}(\omega_h) = \frac{\Delta t}{\pi}\sum_{p=0}^{k_m} \alpha_p[\hat{R}_{XY}(p\Delta t)+\hat{R}_{XY}(-p\Delta t)]\sin\left(\frac{hp\pi}{k_m}\right) \qquad (4.2.6)$$

$$h = 0,1,2,3,\cdots,k_m$$

where $$\alpha_p = \begin{cases} 1 & 0<p<k_m \\ \frac{1}{2} & p=0,k_m \end{cases}$$

and $$\omega_h = \frac{h\pi}{k_m \Delta t}$$

These raw estimates are again smoothed by the "hamming" window as given

in equation 4.2.3 to be $Co_{XY}(\omega_h)$ and $Q_{XY}(\omega_h)$. Now we have the cross-spectrum of X and Y, namely

$$S_{XY}(\omega_h) = Co_{XY}(\omega_h) + i\, Q_{XY}(\omega_h) \tag{4.2.7}$$

Then the gain factor or the amplitude of the transfer function can be computed as

$$|G(\omega_h)| = \frac{\sqrt{Co^2_{XY}(\omega_h)+Q^2_{XY}(\omega_h)}}{S_{XX}(\omega_h)} \tag{4.2.8}$$

and the phase shift of series Y with respect to series X is

$$\theta_{XY}(\omega_h) = \tan^{-1} \frac{Q(\omega_h)}{Co(\omega_h)} \tag{4.2.9}$$

Finally, the coherence square, between series X and Y, is given as

$$\gamma^2_{XY}(\omega_h) = \frac{Co^2_{XY}(\omega_h) + Q^2_{XY}(\omega_h)}{S_{XX}(\omega_h)\, S_{YY}(\omega_h)} \tag{4.2.10}$$

Due to availability and convenience, BMD T-series programs, from the Health Science Computing Facility, UCLA, have been used, in particular, the program BMD02T.

4.3 Estimation of Aquifer Parameters

Field Description. Through the U.S. Geological Survey, District Office at Lawrence, Kansas, we were able to obtain a relatively complete set of records of groundwater table fluctuations, gage height of the

nearby stream and the monthly precipitation at the city of Wichita, Kansas. The groundwater table fluctuations have been recorded since 1937 around the well field of the city of Wichita by means of observation wells. The well field is located mainly between the Arkansas River and the Little Arkansas River approximately 20 miles northwest of the city of Wichita. This well field is developed in alluvial material known as the Equus beds in south-central Kansas. The water-bearing materials consist of unconsolidated deposits of sand, gravel, silt and clay of Pleistocene age. The hydraulic gradient of the water table in the well field is toward the Little Arkansas River, and some water is being discharged into it, although most of the water moving across the well field is intercepted by pumping. The primary source of water for recharge to the well field is local precipitation. The geology and hydrology of this area had been studied extensively by Williams and Lohman (1949). For more detailed information of this area, readers are referred to the Bulletin No. 79, State Geological Survey of Kansas, 1949. Well no. 12 (no. 557 in Bulletin 79) and well no. 812 (no. 558 in Bulletin 79) have been chosen, in the following data analysis, on the grounds of the length of records, being from January 1938 to September 1971, and February 1937 to December 1962, respectively, and consistency of recording intervals. As reported by Williams and Lohman (1949), the average transmissivity of this area is of the order of 10^4 ft^2/day and, from a field test at well no. 12, the specific yield or storage coefficient is 0.33. (Table 7, Bulletin 79, USGS, 1949). There was no report at well no. 812. A map showing the relative location of well no. 12 and no. 812 is reproduced in Figure 4.3.

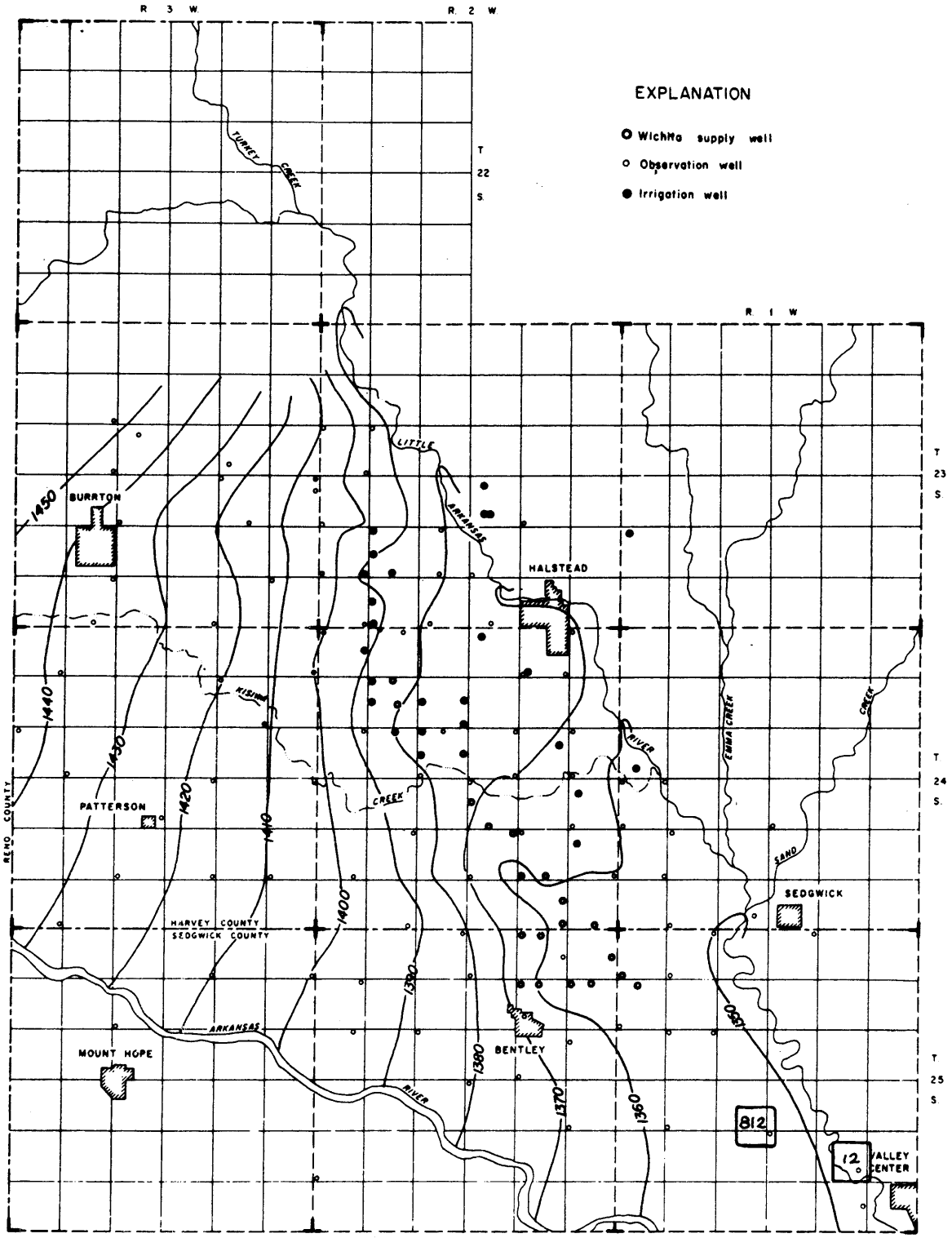

Figure 4.3 Map of Wichita Well Field (reproduced from Bulletin 119, State Geological Survey of Kansas, 1956)

Estimation of Aquifer Parameters. From the set of records obtained from the U.S. Geological Survey we can estimate the power spectra, cross-spectra and the gain factor or the amplitude of the transfer functions. The results are shown in Tables 4.1 and 4.2. Data is extracted at approximately 30 day intervals. Hence, we have 405 points for well no. 12 and 288 points for well no. 812. The time series are shown in Figures 4.4 and 4.5. The spectral calculations were made using 36 lags. The power spectra of the time series are shown in Figures 4.6 and 4.7 with the corresponding 95% confidence intervals. The transfer functions and spectra are related, for the case of independent inputs by equation 4.1.11, namely

$$\hat{S}_{XY} = G\,\hat{S}_X \tag{4.1.11}$$

where $|G|^2$ is the square of the amplitude of the transfer function; and for the case of correlated inputs, by equation 4.1.23, namely,

$$\hat{S}_Y = |G_1|^2\hat{S}_{X_1X_1} + G_1G_2^*\hat{S}_{X_1X_2} + G_1^*G_2\hat{S}_{X_2X_1} + |G_2|^2\hat{S}_{X_2X_2} \tag{4.1.23}$$

where G_1 and G_2 are given by equations 4.1.27 and 4.1.28. In both cases, Y is referred to as the output and X_i are the inputs. The values of $|G_P|^2$, $|G_H|^2$, $|G_1|^2$ and $|G_2|^2$ versus frequency are plotted in Figures 4.8-4.11, respectively, for well no. 12, and in Figures 4.12-4.15 respectively, for well no. 812.

Consider the horizontal bottom case of the linearized Dupuit Approximation. From equation 2.3.9, we have

FREQUENCY (CYCLES/ MONTH)	POWER SPECTRAL ESTIMATES OF SERIES 1	POWER SPECTRAL ESTIMATES OF SERIES 2	POWER SPECTRAL ESTIMATES OF SERIES 3
C.C	0.4616737	1.766C618	6.3718882
0.014	0.40CC797	1.0752516	4.C993395
C.028	0.2904645	C.477C665	1.4C86533
C.042	0.2214662	0.3459418	0.5118937
C.05E	C.1947339	0.2733959	0.2931146
C.C69	1.0026560	C.4343947	0.3065982
C.C83	2.0223532	0.5964674	0.3467798
0.097	0.9835154	0.4179365	C.2C75664
0.111	0.2144480	0.3081986	0.1272C72
C.125	0.2025C25	0.2775461	0.1014004
0.139	0.1556762	0.2285815	0.0675949
C.153	0.2378010	0.1841C76	0.C64C08C
C.167	0.2310787	0.2085326	0.0532606
C.181	0.1398047	C.2119500	0.0421772
C.194	0.1842604	0.2290967	0.0534783
0.208	0.2663465	0.2831765	0.0497491
C.222	0.2188570	0.2618365	0.0323070
0.236	0.2043062	0.3369848	0.0342543
0.250	0.2299384	0.2514215	0.0231870
C.264	0.1922260	0.1547332	0.0221578
0.278	0.2175524	0.2183325	0.0324012
C.292	0.2326224	0.2502175	0.0343981
0.30E	0.1975353	0.2251956	0.0235781
C.319	0.2578394	0.1837316	0.0261787
C.333	0.2502195	0.1927730	0.0353565
0.347	0.1914660	0.2193381	0.0281800
0.361	0.1985738	0.2041160	0.0136057
0.375	0.1933311	0.1819236	0.0113552
0.389	0.2222458	0.2101920	0.0131103
C.403	0.2479103	0.2472190	0.0129041
0.417	0.2183966	0.2956147	0.0122605
0.431	0.1810870	0.2315451	0.0155184
0.444	0.1769220	0.2715925	0.0110891
0.458	0.2118729	0.3244346	0.0127715
0.472	0.2450640	0.3240425	0.0237436
0.486	0.2150671	0.2789856	0.0238364
0.500	0.2178805	0.2635271	0.0167610

Table 4.1 Spectral Results for Well No. 12 (1=precipitation, 2=stream stage, and 3=well no. 12 elevation).

FREQUENCY (CYCLES/ MONTH)	CO-SPECTRUM OF SERIES 1 AND 2	QUADRATURE SPECTRUM OF SERIES 1 AND 2	CO-SPECTRUM OF SERIES 1 AND 3	QUADRATURE SPECTRUM OF SERIES 1 AND 3
0.0	0.5492625	0.0190047	-1.3272820	-0.3691775
0.014	0.4256815	0.0409466	-0.8723028	-0.5002798
0.028	0.2929254	0.0623291	-0.3176955	-0.4022828
0.042	0.2050447	0.0568162	-0.1274777	-0.2336676
0.056	0.1630077	0.0614800	-0.0614405	-0.1642944
0.069	0.4975184	0.0516860	-0.2204815	-0.2940277
0.083	0.8724203	-0.0576502	-0.4402660	-0.4511988
0.097	0.4153976	0.0143365	-0.2205715	-0.2465901
0.111	0.0912592	0.1368528	-0.0219914	-0.1096165
0.125	0.0492253	0.1719483	-0.0026751	-0.1040836
0.139	0.0277932	0.1387198	-0.0055513	-0.0575611
0.153	0.0117510	0.1152524	-0.0024248	-0.0359793
0.167	0.0453719	0.1413517	-0.0128043	-0.0481883
0.181	0.0410284	0.1068744	0.0024166	-0.0482872
0.194	0.0314140	0.1569433	0.0002797	-0.0719635
0.208	0.0165044	0.2065336	-0.0130033	-0.0698153
0.222	-0.0184029	0.1244329	-0.0222607	-0.0453012
0.236	-0.0553098	0.1468871	-0.0127094	-0.0314737
0.250	-0.0655937	0.1148209	-0.0072512	-0.0268367
0.264	-0.0151332	0.0498227	-0.0159597	-0.0284687
0.278	0.0110108	0.1243101	-0.0208474	-0.0476412
0.292	-0.0168739	0.1777741	-0.0124151	-0.0509917
0.306	-0.0497818	0.1211966	-0.0125382	-0.0155203
0.319	-0.0575510	0.0980981	-0.0287273	-0.0397460
0.333	-0.0601420	0.0893154	-0.0201196	-0.0504260
0.347	-0.0819513	0.0625255	0.0005166	-0.0190706
0.361	-0.0805233	0.0856179	-0.0104990	-0.0059157
0.375	-0.0741858	0.0874989	-0.0123814	-0.0072091
0.389	-0.1267378	0.0530410	0.0024627	-0.0108114
0.403	-0.0959663	0.0686592	-0.0033342	-0.0080163
0.417	-0.0748286	0.0624296	-0.0084673	-0.0072384
0.431	-0.0829571	0.0160047	-0.0000064	-0.0118076
0.444	-0.1208206	-0.0154884	0.0033890	-0.0036404
0.458	-0.1331828	0.0012722	-0.0078615	-0.0014138
0.472	-0.1406332	0.0790018	-0.0104317	-0.0104023
0.486	-0.0947788	0.0520430	-0.0103635	-0.0021318
0.500	-0.0630650	0.0120707	-0.0181379	0.0033710

Table 4.1 continued

FREQUENCY (CYCLES/ MONTH)	CO-SPECTRUM CF SERIES 2 AND 3	QUADRATURE SPECTRUM CF SERIES 2 AND 3	COHERENCE SQUARE CF SERIES 2 AND 3	(Independent Input) AMPLITUDE OF TRANSFER FUNCTION FROM 2 TO 3
0.0	-2.3253059	-0.3414624	0.4906533	1.3307819
0.014	-1.4926214	-0.4778031	0.5572397	1.4575481
0.028	-0.6113302	-0.4120255	0.8087377	1.5453119
0.042	-0.3007802	-0.2325832	0.8163494	1.0990725
0.056	-0.1719019	-0.1271662	0.5705467	0.7821108
0.069	-0.2081547	-0.1934170	0.6062143	0.6541175
0.083	-0.2597960	-0.2657448	0.7215000	0.6474648
0.097	-0.1691552	-0.1709676	0.6667858	0.5754615
0.111	-0.1437123	-0.0873871	0.7215837	0.5457374
0.125	-0.1104409	-0.0591664	0.5577835	0.4514245
0.139	-0.0583700	-0.0390752	0.3193281	0.3072946
0.153	-0.0590453	-0.0331152	0.3885020	0.3677066
0.167	-0.0753202	-0.0100368	0.5198600	0.3643841
0.181	-0.0624012	-0.0150806	0.4610268	0.3028902
0.194	-0.0902450	-0.0059112	0.6675885	0.3947607
0.208	-0.0947670	0.0006206	0.6375157	0.3346643
0.222	-0.0447346	0.0046611	0.2391362	0.1717726
0.236	-0.0360813	-0.0028283	0.1134749	0.1073995
0.250	-0.0252776	0.0062354	0.1162730	0.1035524
0.264	-0.0276535	0.0091424	0.2474220	0.1882309
0.278	-0.0468663	0.0097256	0.3238675	0.2192326
0.292	-0.0533637	0.0101923	0.3429253	0.2171241
0.306	-0.0255318	0.0126216	0.1527733	0.1264729
0.319	-0.0174880	0.0227974	0.1716382	0.1563827
0.333	-0.0322433	0.0220734	0.3034629	0.2359198
0.347	-0.0261183	0.0164261	0.1540189	0.1406695
0.361	-0.0088574	0.0060624	0.0516556	0.0586787
0.375	-0.0160190	0.0139999	0.2190973	0.1169421
0.389	-0.0226512	0.0085038	0.2124309	0.1151085
0.403	-0.0137318	0.0110983	0.0977185	0.0714185
0.417	-0.0170807	0.0138131	0.1331409	0.0743098
0.431	-0.0232923	0.0021455	0.1522694	0.1010211
0.444	-0.0153798	-0.0034149	0.0824112	0.0580074
0.458	-0.0130669	0.0096555	0.0637072	0.0500786
0.472	-0.0291670	0.0155243	0.1418933	0.1019654
0.486	-0.0133483	-0.0025389	0.0277600	0.0487028
0.500	0.0089366	-0.0078820	0.0355416	0.0475450

Table 4.1 continued

FREQUENCY (CYCLES/ MONTH)	COHERENCE SQUARE OF SERIES 1 AND 3	AMPLITUDE OF TRANSFER FUNCTION FROM 1 TO 3	(CORRELATED INPUT) AMPLITUDE OF THE TRANSFER FUNCTION FROM 1 TO 3	(CORRELATED INPUT) AMPLITUDE OF THE TRANSFER FUNCTION FROM 2 TO 3
0.0	0.6451867	2.9840708	2.2456646	.6586387
0.0139	0.6165560	2.5134487	1.7085054	.8321352
0.0278	0.6421922	1.7647696	.6785883	1.2940054
0.0417	0.6249697	1.2018919	.5308164	.9341296
0.0556	0.5390319	0.9007518	.5101726	.5245961
0.0694	0.4393591	0.3665377	.1125131	.5531303
0.0833	0.5666733	0.3117200	.0902898	.5221896
0.0972	0.5361804	0.3363903	.1609497	.4157547
0.1111	0.4582002	0.5213417	.2132902	.4644513
0.1250	0.5279362	0.5141564	.3666456	.3512720
0.1389	0.2528291	0.2955299	.2605913	.3061283
0.1528	0.0654329	0.1516432	.1190538	.4128620
0.1667	0.2019978	0.2157727	.0477656	.3900475
0.1806	0.3964162	0.3458227	.1965711	.2217188
0.1944	0.5255594	0.3905565	.1752162	.3301909
0.2083	0.6215476	0.3407254	.1907774	.2018524
0.2222	0.3603274	0.2306305	.2093571	.1264077
0.2361	0.1646279	0.1661377	.1954183	.1227025
0.2500	0.1449451	0.1208978	.1093718	.0845524
0.2639	0.2500818	0.1697847	.1397069	.1543639
0.2778	0.3836453	0.2390362	.1713266	.1266851
0.2917	0.3442098	0.2256073	.1443399	.1377625
0.3056	0.0654715	0.1010048	.0942609	.1388107
0.3194	0.3563027	0.1901991	.1709629	.0694463
0.3333	0.3331769	0.2169759	.1564174	.1567894
0.3472	0.0675613	0.0997180	.0481469	.1299758
0.3611	0.0537518	0.0606871	.0814133	.0789694
0.3750	0.0935044	0.0741075	.1129819	.1615283
0.3889	0.0421975	0.0498923	.0683258	.1508430
0.4028	0.0235626	0.0350209	.0291423	.0765520
0.4167	0.0463427	0.0510060	.0530125	.0793536
0.4306	0.0496121	0.0652038	.0831754	.1170568
0.4444	0.0126091	0.0281125	.0560938	.0705681
0.4583	0.0235785	0.0377000	.0855098	.0830916
0.4722	0.0372985	0.0601145	.1190172	.1486994
0.4861	0.0218368	0.0491978	.0886220	.0819165
0.5000	0.0931974	0.0846725	.0812124	.0387596

Table 4.1 continued

FREQUENCY (CYCLES/ MONTH	POWER SPECTRAL ESTIMATES OF SERIES 1	POWER SPECTRAL ESTIMATES OF SERIES 2	POWER SPECTRAL ESTIMATES OF SERIES 3
0.0	0.5374808	1.2685280	7.5446291
0.014	0.3837751	0.8597792	4.7825747
0.028	0.2173141	0.4381955	1.3861294
0.042	0.2153191	0.2512252	0.2511411
0.056	0.2332733	0.2239184	0.1932182
0.069	0.9996482	0.4708245	0.2120602
0.083	1.8161268	0.6250646	0.1392409
0.097	0.8645156	0.4285473	0.1139002
0.111	0.2524533	0.3583584	0.0873989
0.125	0.2644895	0.3161583	0.0598572
0.139	0.2270136	0.2389400	0.0474303
0.153	0.2797019	0.1821527	0.0314855
0.167	0.2960474	0.2133330	0.0311634
0.181	0.1716580	0.2338951	0.0242400
0.194	0.1944860	0.2702937	0.0244891
0.208	0.2838922	0.3319917	0.0234363
0.222	0.2465112	0.2963898	0.0192297
0.236	0.2317605	0.3909397	0.0146210
0.250	0.2459462	0.2833095	0.0118639
0.264	0.2086559	0.1864448	0.0106318
0.278	0.2216164	0.2646199	0.0079679
0.292	0.2031941	0.2625701	0.0084262
0.306	0.1393378	0.2096615	0.0095010
0.319	0.1768278	0.1573682	0.0103075
0.333	0.1921526	0.1958976	0.0117814
0.347	0.1662740	0.2520531	0.0109710
0.361	0.1730999	0.2030430	0.0108849
0.375	0.1717070	0.1653225	0.0099507
0.389	0.2172809	0.2151617	0.0081530
0.403	0.2540575	0.2459328	0.0058417
0.417	0.2455114	0.3216650	0.0083650
0.431	0.2244685	0.2708046	0.0097426
0.444	0.2079843	0.2879887	0.0130381
0.458	0.2432668	0.3442047	0.0153065
0.472	0.3040683	0.3669876	0.0149631
0.486	0.2521988	0.2921533	0.0175279
0.500	0.2480691	0.2584540	0.0166986

Table 4.2 Spectral Results for Well No. 812 (1=precipitation, 2=stream stage, and 3=well no. 812 elevation).

FREQUENCY (CYCLES/ MONTH)	CO-SPECTRUM OF SERIES 1 AND 2	QUADRATURE SPECTRUM OF SERIES 1 AND 2	CO-SPECTRUM OF SERIES 1 AND 3	QUADRATURE SPECTRUM OF SERIES 1 AND 3
0.0	0.5934544	0.0424455	-0.6505423	-0.5859277
0.014	0.4387881	0.0494298	-0.4209118	-0.6331782
0.028	0.2601902	0.0354270	-0.1225896	-0.2342375
0.042	0.1715844	0.0433205	-0.0064758	-0.0924887
0.056	0.1445757	0.0817950	0.0056685	-0.0959550
0.069	0.4958999	0.0509909	-0.0634411	-0.1000934
0.083	0.8613555	-0.0939653	-0.1846801	-0.0312619
0.097	0.4302959	0.0235687	-0.1069716	-0.0615308
0.111	0.1171054	0.1816434	0.0036852	-0.0480823
0.125	0.0554643	0.2089986	0.0148437	-0.0791034
0.139	0.0144547	0.1554420	0.0128739	-0.0429738
0.153	0.0064282	0.1237102	0.0161403	0.0004009
0.167	0.0589046	0.1547029	0.0003234	0.0012260
0.181	0.0438863	0.1351151	-0.0140864	-0.0218559
0.194	0.0351257	0.1939378	-0.0204440	0.0017919
0.208	0.0250411	0.2494217	-0.0203728	-0.0301657
0.222	-0.0208642	0.1474465	-0.0208998	-0.0345286
0.236	-0.0487455	0.1672570	-0.0245328	-0.0260277
0.250	-0.0657021	0.1113451	-0.0156738	-0.0233513
0.264	-0.0280692	0.0572293	-0.0066228	-0.0230150
0.278	0.0060719	0.1508234	-0.0121342	-0.0068546
0.292	-0.0091965	0.1765762	-0.0089311	-0.0138725
0.306	-0.0596035	0.0746194	-0.0108804	-0.0111758
0.319	-0.0558303	0.0447262	-0.0118123	-0.0172102
0.333	-0.0613305	0.0722870	-0.0131461	-0.0143624
0.347	-0.1011285	0.0930349	-0.0058837	-0.0070227
0.361	-0.0947801	0.0889423	-0.0038905	-0.0062667
0.375	-0.0919228	0.0643825	-0.0046817	-0.0047634
0.389	-0.1569659	0.0274889	-0.0076724	-0.0002818
0.403	-0.1139014	0.0479721	-0.0069335	-0.0114090
0.417	-0.0918743	0.0520705	-0.0009366	-0.0156151
0.431	-0.1046796	0.0092081	-0.0051403	-0.0126108
0.444	-0.1472512	-0.0286996	-0.0104580	-0.0215347
0.458	-0.1739575	0.0075133	-0.0182949	-0.0176749
0.472	-0.1837862	0.1228960	-0.0336563	-0.0184147
0.486	-0.1046023	0.0963448	-0.0363462	-0.0208492
0.500	-0.0651873	0.0384422	-0.0334923	-0.0146030

Table 4.2 continued

FREQUENCY (CYCLES/ MONTH)	CO-SPECTRUM OF SERIES 2 AND 3	QUADRATURE SPECTRUM OF SERIES 2 AND 3	COHERENCE SQUARE OF SERIES 2 AND 3	(Independent Input) AMPLITUDE OF TRANSFER FUNCTION FROM 2 TO 3
0.0	-2.2237883	-0.6888822	0.5662975	1.8352327
0.014	-1.3068628	-0.7961345	0.5694900	1.7798376
0.028	-0.3706064	-0.3770931	0.4602407	1.2065916
0.042	-0.0964719	-0.1002972	0.3069494	0.5539374
0.056	-0.0555385	-0.0430381	0.1141055	0.3137853
0.069	-0.0468276	-0.0855252	0.0952231	0.2070958
0.083	-0.0753059	-0.0563346	0.1016214	0.1504573
0.097	-0.0939134	-0.0574369	0.2482753	0.2568796
0.111	-0.0568609	-0.0282074	0.1286336	0.1771215
0.125	-0.0492156	-0.0541159	0.2827422	0.2313668
0.139	-0.0607753	-0.0365445	0.4437608	0.2967959
0.153	-0.0342762	-0.0341464	0.4081544	0.2656132
0.167	-0.0373897	-0.0011319	0.2104747	0.1753448
0.181	-0.0366297	0.0054816	0.2419537	0.1583513
0.194	-0.0099176	0.0317633	0.1672795	0.1231091
0.208	-0.0062384	0.0147100	0.0328123	0.0481282
0.222	-0.0002690	0.0378836	0.2518187	0.1278199
0.236	-0.0015383	0.0483079	0.4086855	0.1236312
0.250	-0.0072838	0.0359889	0.4011306	0.1296060
0.264	-0.0102035	0.0193590	0.2415853	0.1173717
0.278	-0.0158025	0.0225160	0.3588821	0.1039526
0.292	-0.0147248	0.0087558	0.1326499	0.0652449
0.306	-0.0056080	0.0112550	0.0793805	0.0599767
0.319	-0.0059049	0.0009023	0.0219977	0.0379582
0.333	-0.0137206	0.0157414	0.1889328	0.1065951
0.347	-0.0056710	0.0112043	0.0570268	0.0498215
0.361	0.0009507	0.0113620	0.0588206	0.0561543
0.375	0.0042891	-0.0078742	0.0488728	0.0542370
0.389	0.0096779	-0.0000056	0.0533927	0.0449798
0.403	0.0094477	0.0128159	0.1764547	0.0647408
0.417	0.0167387	0.0272489	0.3800777	0.0994187
0.431	0.0130876	0.0193366	0.2066409	0.0862218
0.444	0.0063050	0.0346488	0.3303198	0.1222889
0.458	0.0149681	0.0224903	0.1385306	0.0784878
0.472	0.0038127	0.0107906	0.0238513	0.0311847
0.486	0.0017760	0.0011684	0.0008825	0.0072763
0.500	0.0122587	-0.0036199	0.0378559	0.0494555

Table 4.2 continued

FREQUENCY (CYCLES/ MONTH)	COHERENCE SQUARE OF SERIES 1 AND 3	AMPLITUDE OF TRANSFER FUNCTION FROM 1 TO 3	(CORRELATED INPUT) AMPLITUDE OF THE TRANSFER FUNCTION FROM 1 TO 3	(CORRELATED INPUT) AMPLITUDE OF THE TRANSFER FUNCTION FROM 2 TO 3
0.0	0.1890256	1.6289120	2.2456646	.6586387
0.0139	0.3149563	1.9811506	1.7085054	.8321352
0.0278	0.2220367	1.2165680	.6785883	1.2940054
0.0417	0.1589648	0.4305941	.5308164	.9341296
0.0556	0.2063518	0.4134241	.5101726	.5245961
0.0694	0.0662472	0.1185467	.1125131	.5531303
0.0833	0.1387384	0.1031356	.0902898	.5221896
0.0972	0.1546583	0.1427454	.1609497	.4157547
0.1111	0.1053969	0.1910189	.2132902	.4644513
0.1250	0.4091610	0.3042993	.3666456	.3512720
0.1389	0.1869070	0.1976125	.2605913	.3061283
0.1528	0.0295997	0.0577233	.1190538	.4128620
0.1667	0.0001742	0.0042828	.0477656	.3900475
0.1806	0.1624870	0.1514758	.1965711	.2217188
0.1944	0.0884288	0.1055211	.1752162	.3301909
0.2083	0.1991499	0.1282206	.1907774	.2018524
0.2222	0.3436520	0.1637296	.2093571	.1264077
0.2361	0.3775325	0.1543285	.1954183	.1227025
0.2500	0.2710705	0.1143494	.1393718	.0845524
0.2639	0.2585449	0.1147773	.1397069	.1543639
0.2778	0.1099916	0.0628853	.1713266	.1266851
0.2917	0.1585867	0.0811970	.1443399	.1377625
0.3056	0.1837670	0.1119397	.0942609	.1388107
0.3194	0.2390589	0.1180465	.1709629	.0694463
0.3333	0.1674582	0.1013277	.1564174	.1567894
0.3472	0.0460128	0.0550999	.0481469	.1299758
0.3611	0.0288759	0.0426120	.0814133	.0789694
0.3750	0.0261074	0.0388970	.1129819	.1615283
0.3889	0.0332743	0.0353348	.0683258	.1508430
0.4028	0.1200966	0.0525496	.0291423	.0765520
0.4167	0.1191548	0.0637168	.0530125	.0793536
0.4306	0.0848027	0.0606687	.0831754	.1170568
0.4444	0.2113463	0.1151038	.0560938	.0785681
0.4583	0.1737868	0.1045695	.0855098	.0830916
0.4722	0.3234970	0.1261712	.1190172	.1486994
0.4861	0.3971792	0.1661446	.0888220	.0819165
0.5000	0.3222738	0.1472874	.0812124	.0387596

Table 4.2 continued

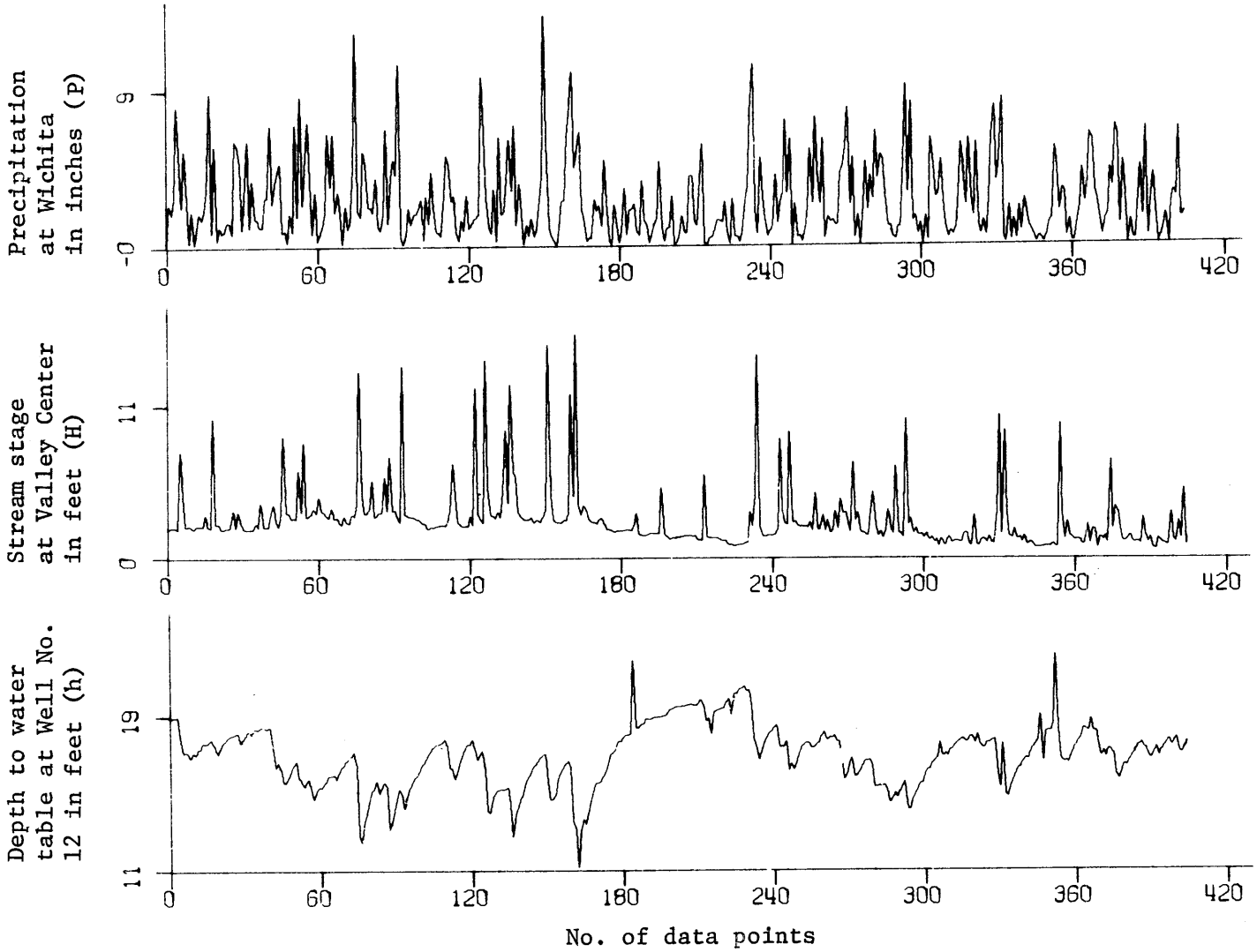

Figure 4.4 Input Data Taken Approximately Every Month from January 1938 to September 1971. (Well No. 12)

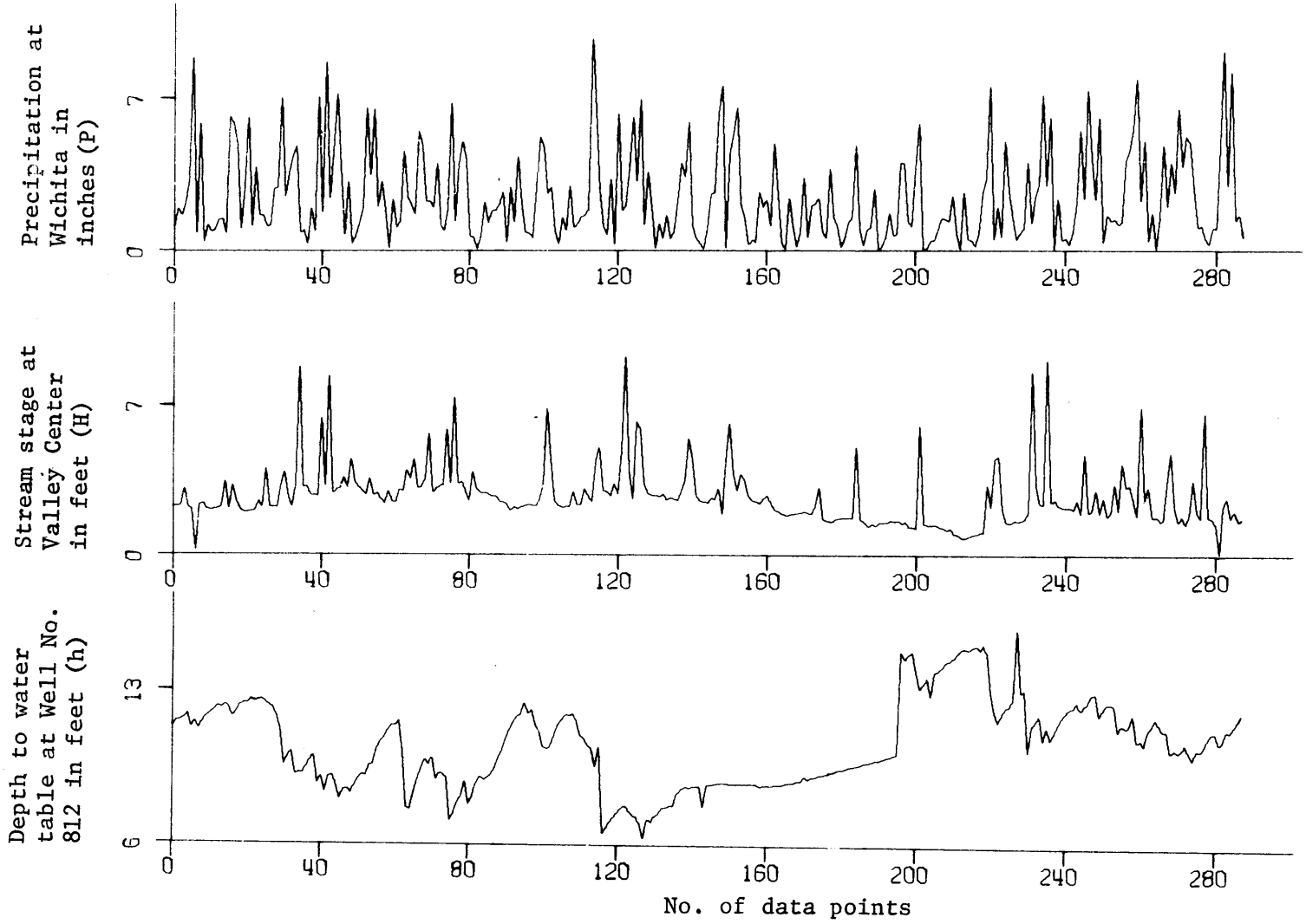

Figure 4.5 Input Data Taken Approximately Every Month from February 1937 to December 1962. (Well No. 812)

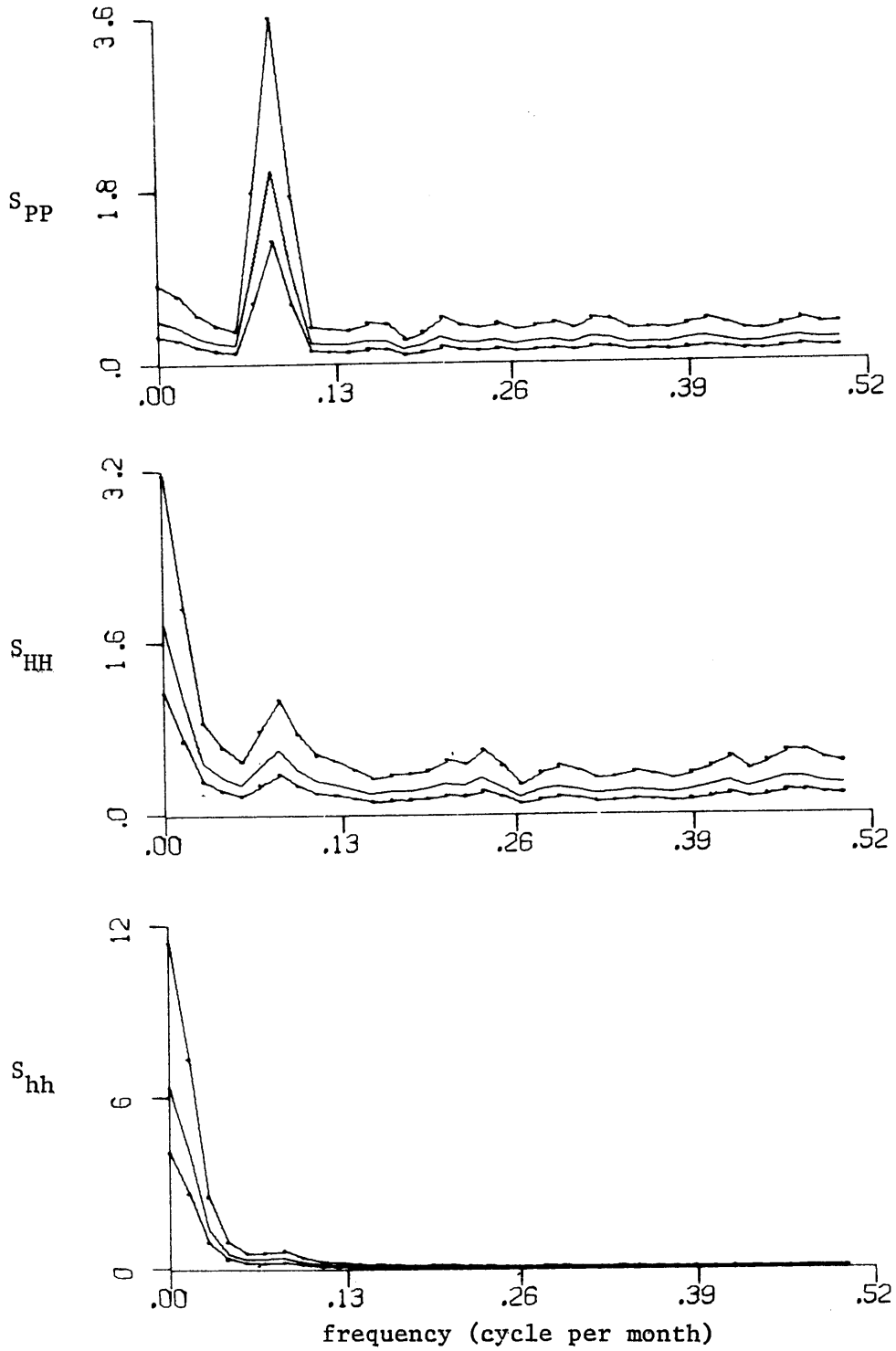

Figure 4.6 Power Spectra of Input Series with the Corresponding 95% Confidence Intervals for Well No. 12.

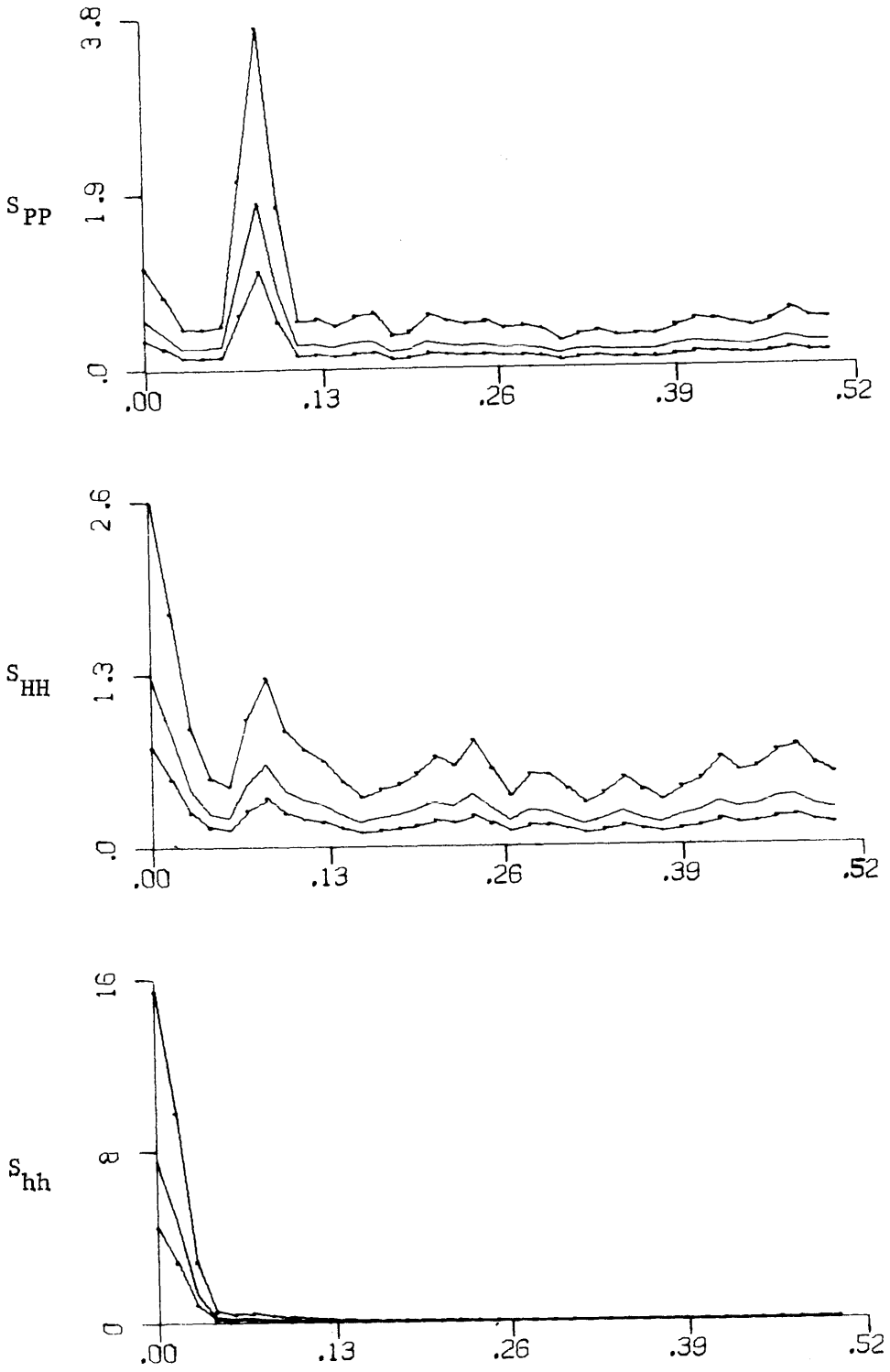

Figure 4.7 Power Spectra of Input Series with the Corresponding 95% Confidence Intervals for Well No. 812.

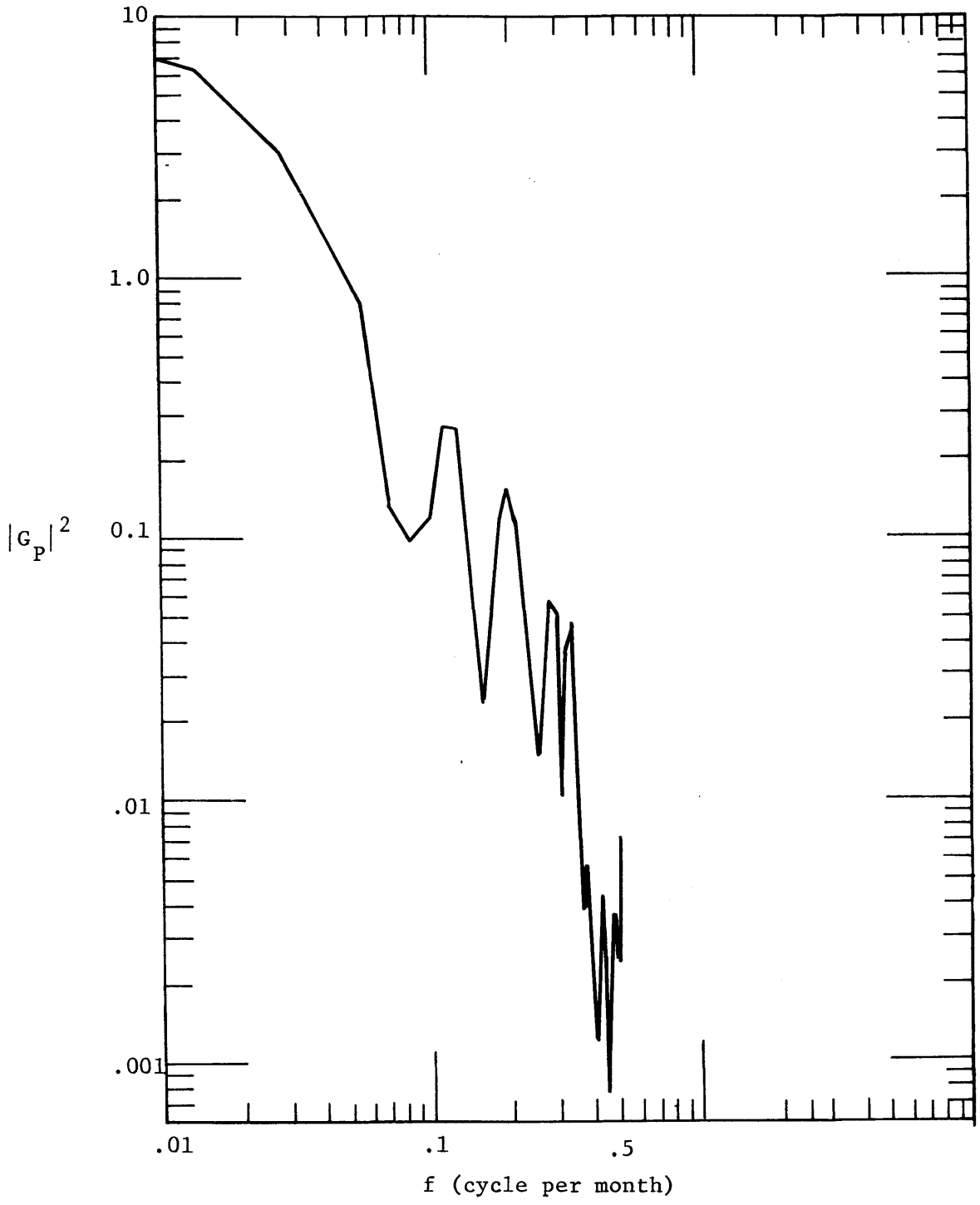

Figure 4.8 Square of the Amplitude of the Transfer Function from Series 1 (precipitation) to Series 3 (groundwater table fluctuations) for the Independent Input case for well No. 12.

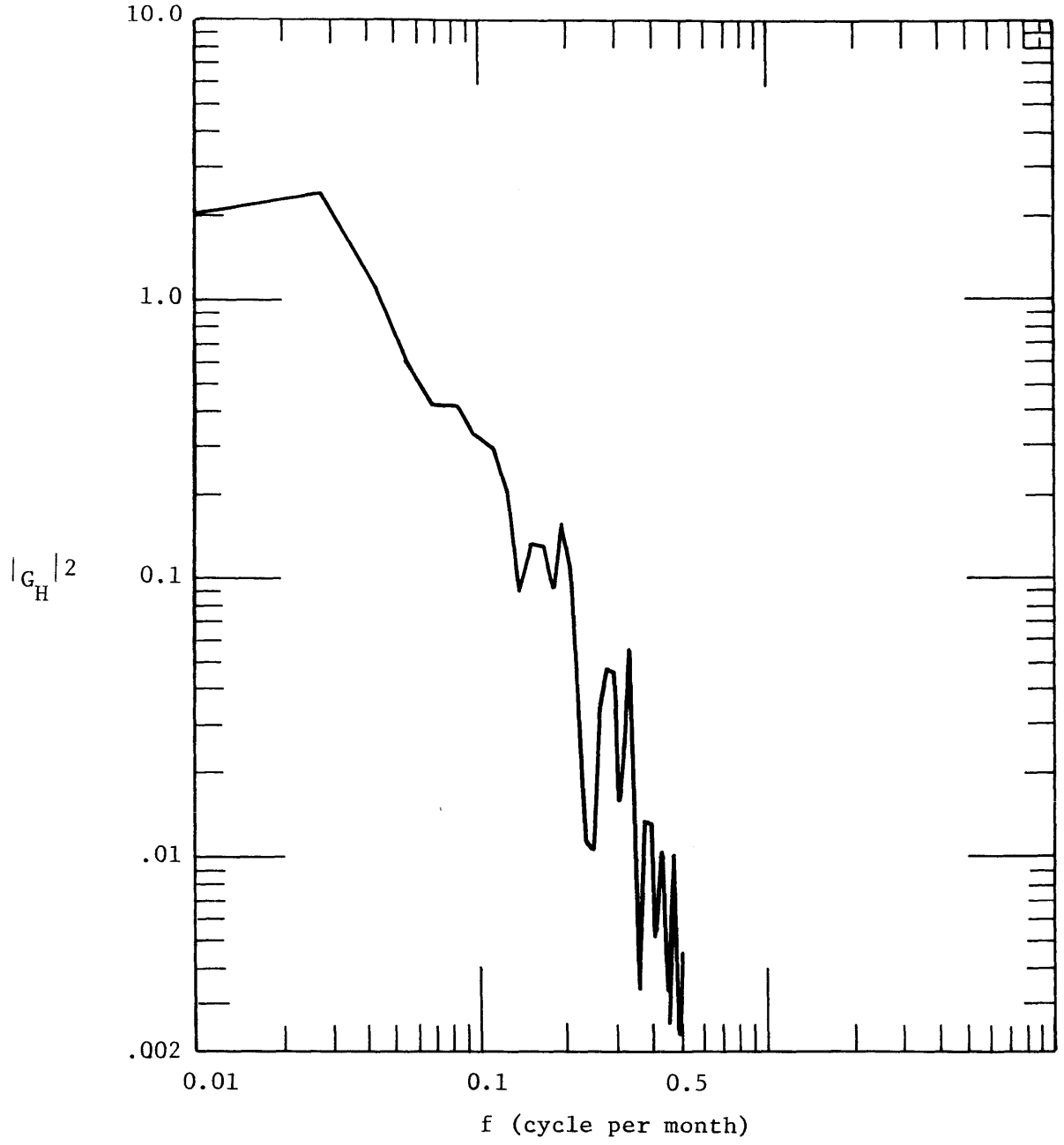

Figure 4.9 Square of the Amplitude of the Transfer Function from Series 2 (stream stage) to Series 3 (groundwater table fluctuation) for the Independent Input Case for well No. 12.

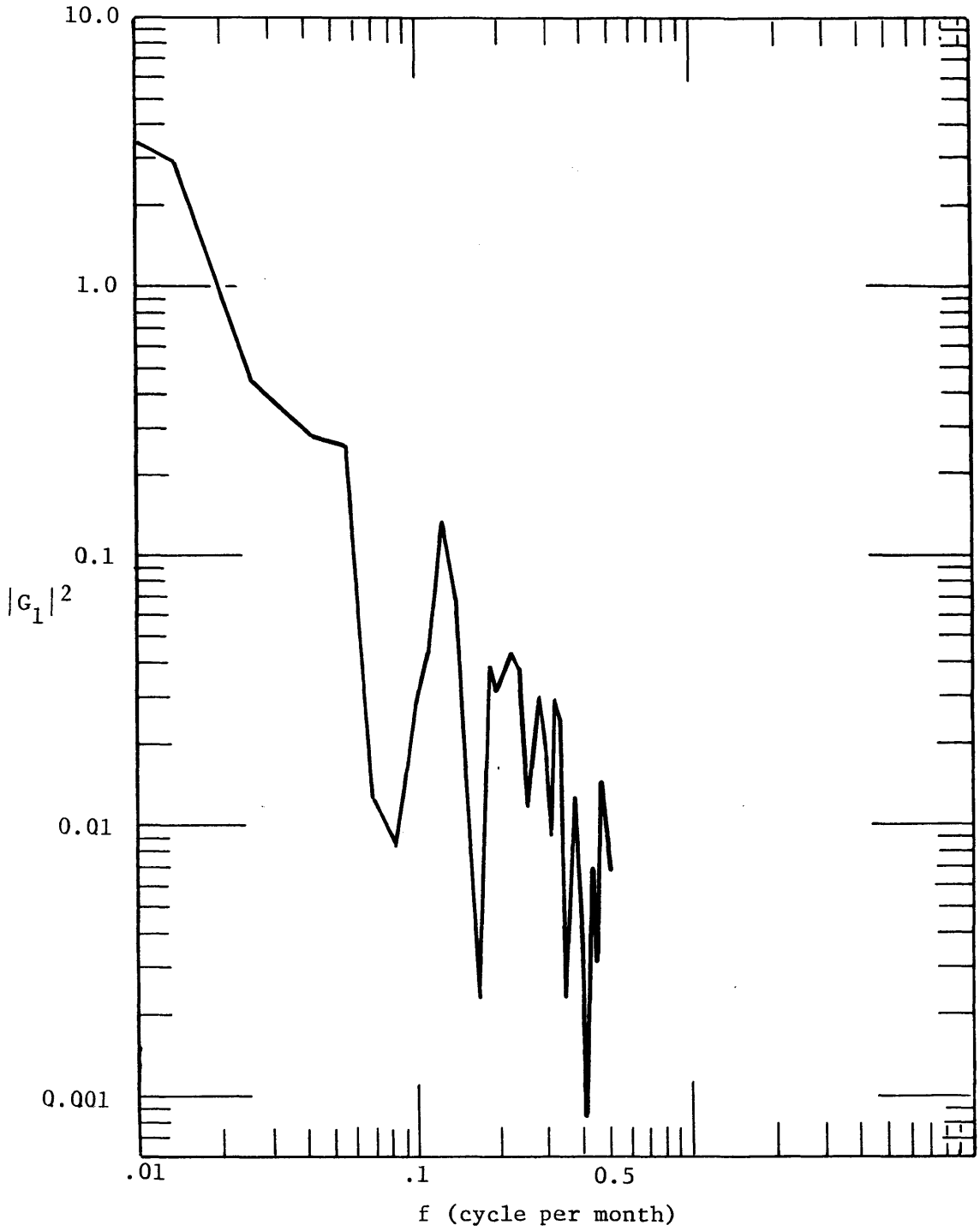

Figure 4.10 Square of the Amplitude of the Transfer Function from Series 1 (precipitation) to series 3 (groundwater table fluctuation) for Correlated-Input Case for Well No. 12.

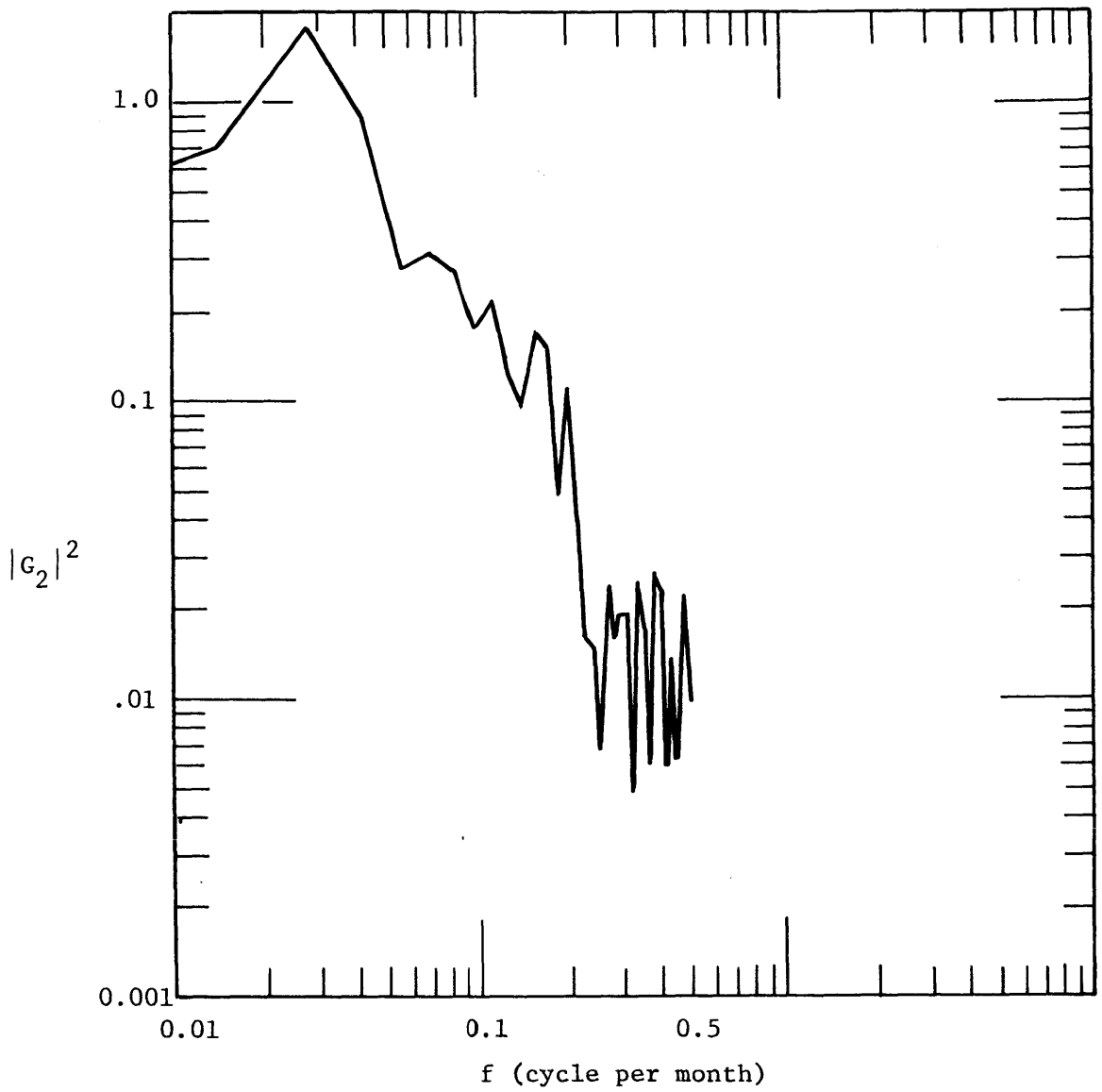

Figure 4.11 Square of the Amplitude of the Transfer Function from Series 2 (stream stage) to Series 3 (groundwater table fluctuation) for Correlated-Input Case for Well No. 12.

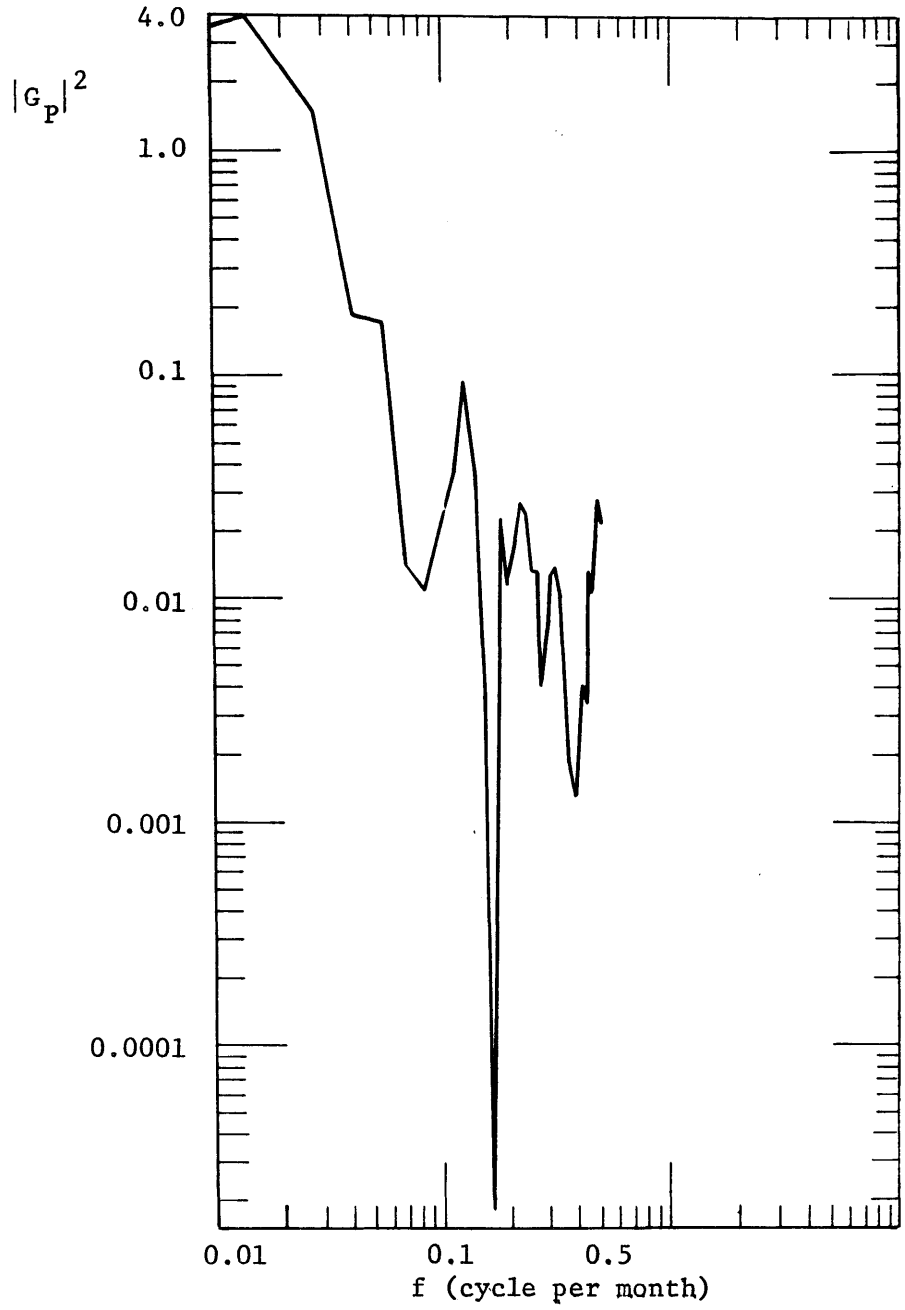

Figure 4.12 Square of the Amplitude of the Transfer Function from Series 1 (precipitation) to Series 3 (groundwater table fluctuation) for the independent input case for Well No. 812.

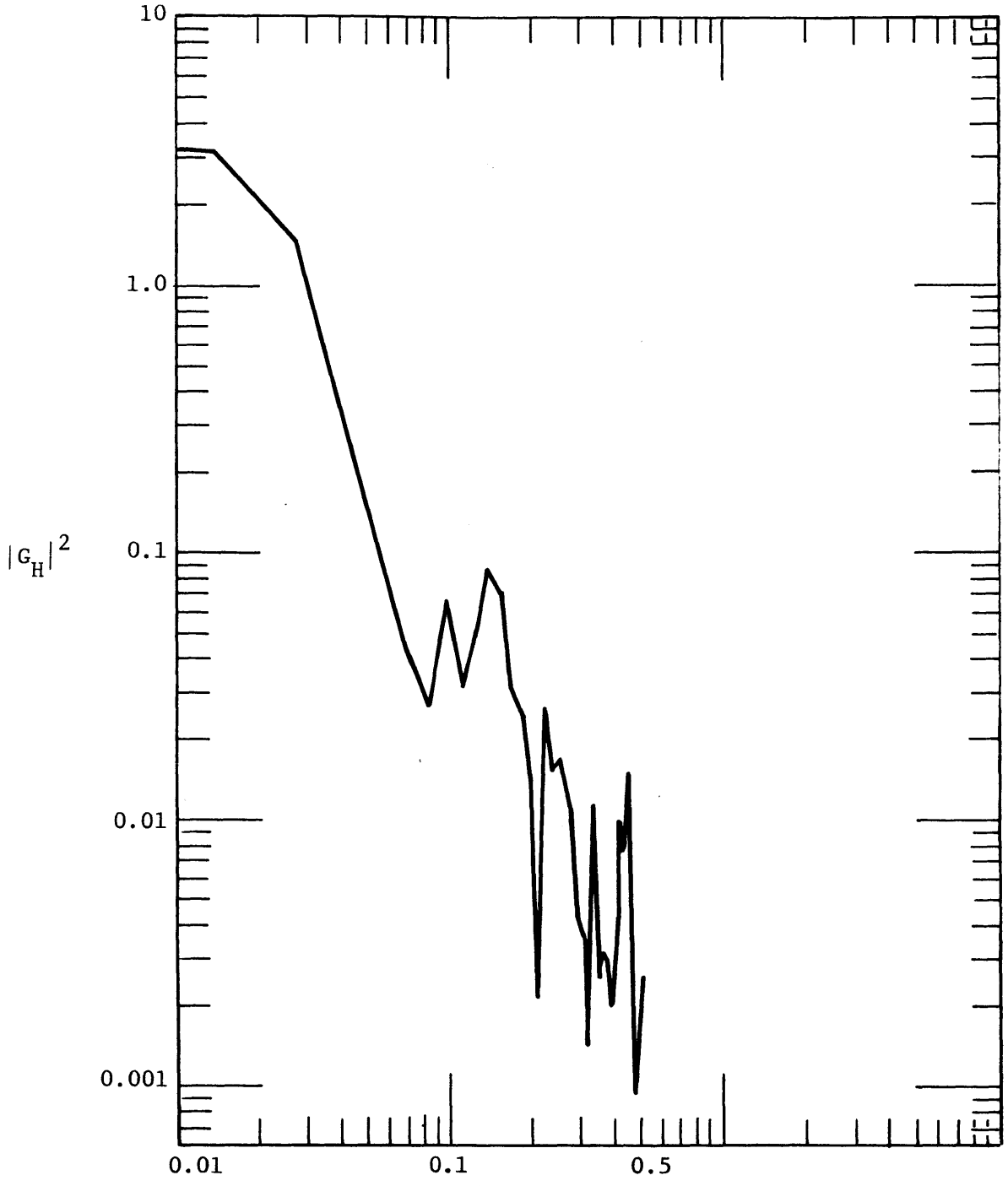

Figure 4.13 Square of the Amplitude of the Transfer Function from Series 2 (stream stage) to Series 3 (groundwater table fluctuation) for independent Input Case for Well No. 812.

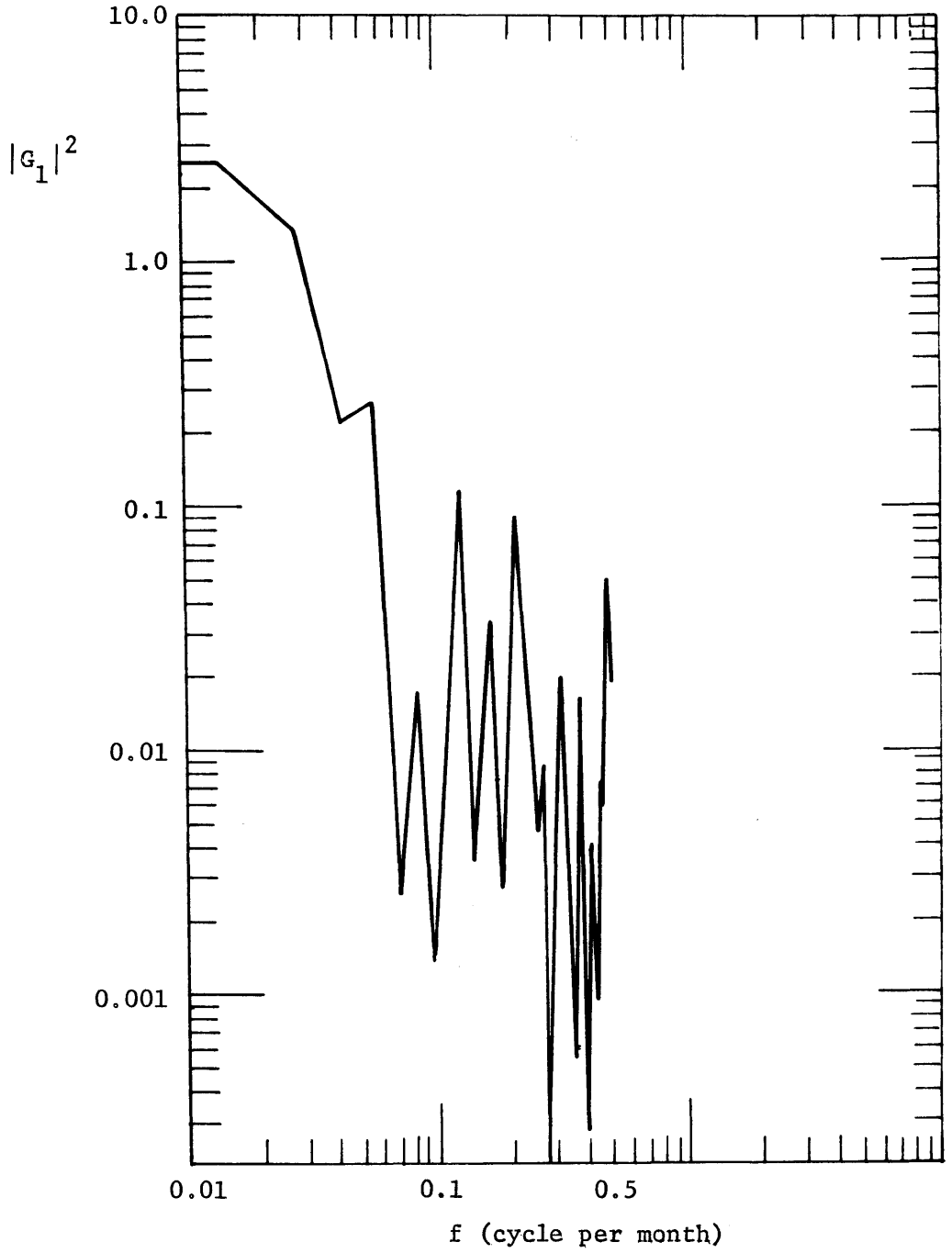

Figure 4.14 Square of the Amplitude of the Transfer Function from Series 1 (precipitation) to Series 3 (groundwater table fluctuation) for Correlated Input Case for Well No. 812.

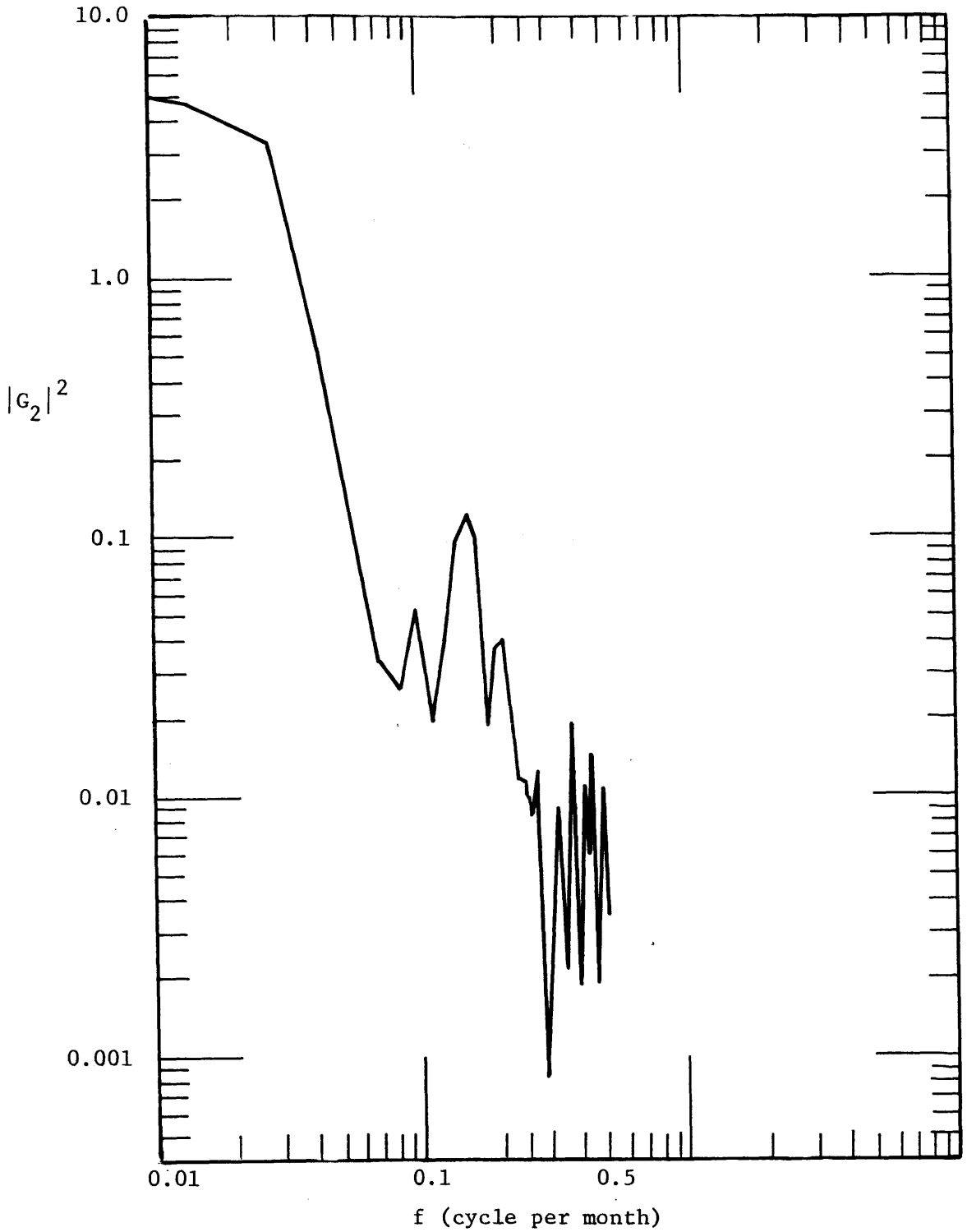

Figure 4.15 Square of the Amplitude of the Transfer Function from Series 2 (stream stage) to Series 3 (groundwater table fluctuation) for Correlated-Input Case for Well No. 812.

$$S_{hh} = \frac{(1-F)(1-F^*)}{\omega^2 S^2} S_{\varepsilon\varepsilon} - \frac{i}{\omega S}[(1-F)F^* S_{\varepsilon H} - (1-F^*)F\, S_{H\varepsilon}]$$

$$+ FF^*\, S_{HH} \qquad (4.3.1)$$

with $$F = \frac{\cosh[bL(\frac{x}{L} - 1)]}{\cosh(bL)}$$

$$bL = \frac{(1+i)}{\sqrt{2}}(\frac{\omega L^2}{\alpha})^{1/2}$$

and $$\alpha = \frac{T}{S}$$

The dimensionless parameter,

$$\frac{\omega L^2}{\alpha} \equiv \Omega \qquad (4.3.2)$$

is referred to as the dimensionless frequency. Note that equation 4.3.1 is exactly in the same form as equation 4.1.23 with the following equivalencies,

$$G_1 \equiv \frac{-i(1-F)}{\omega S} \qquad (4.3.3)$$

$$G_2 \equiv F$$

provided that X_1 is equivalent to ε and X_2 to H. In the independent input case, G can take on either form depending on which input series is being

used. Note that ε is referred to as the net accretion and that we have only precipitation records to work with. It is therefore necessary to assume a relationship between the total precipitation and the accretion. The simplest way is to assume that the accretion is a constant fraction of precipitation, i.e.,

$$\varepsilon = \gamma(\text{precipitation}) = \gamma P \tag{4.3.5}$$

where γ = constant < 1

By introducing this relation into the linearized Dupuit Approximation, it can be shown that equation 4.3.1 becomes

$$S_{hh} = \frac{(1-F)(1-F^*)}{\omega^2 S^2}\gamma^2 S_{PP} - \frac{i\gamma}{\omega S}[(1-F)F^* S_{\varepsilon H} - (1-F^*)F\, S_{H\varepsilon}] + FF^*\, S_{HH} \tag{4.3.6}$$

where F, Ω and α are as previously defined and S_{PP} is the power spectrum of the precipitation. With X_1 as the precipitation, equations 4.1.23 and 4.3.6 are compatible for comparisons. However, the function $\frac{(1-F)(1-F^*)\gamma^2}{\omega^2 S^2}$ can still not be computed. Instead $\frac{(1-F)(1-F^*)}{\Omega^2} = g(\Omega)$ together with $FF^* = f(\Omega)$ are computed and plotted in Figures 4.16 and 4.17 for a given value of x/L. We then have the following relationship

$$\frac{(1-F)(1-F^*)\gamma^2}{\omega^2 S^2} = g(\Omega)\,\frac{\gamma^2 L^4}{T^2} \tag{4.3.7}$$

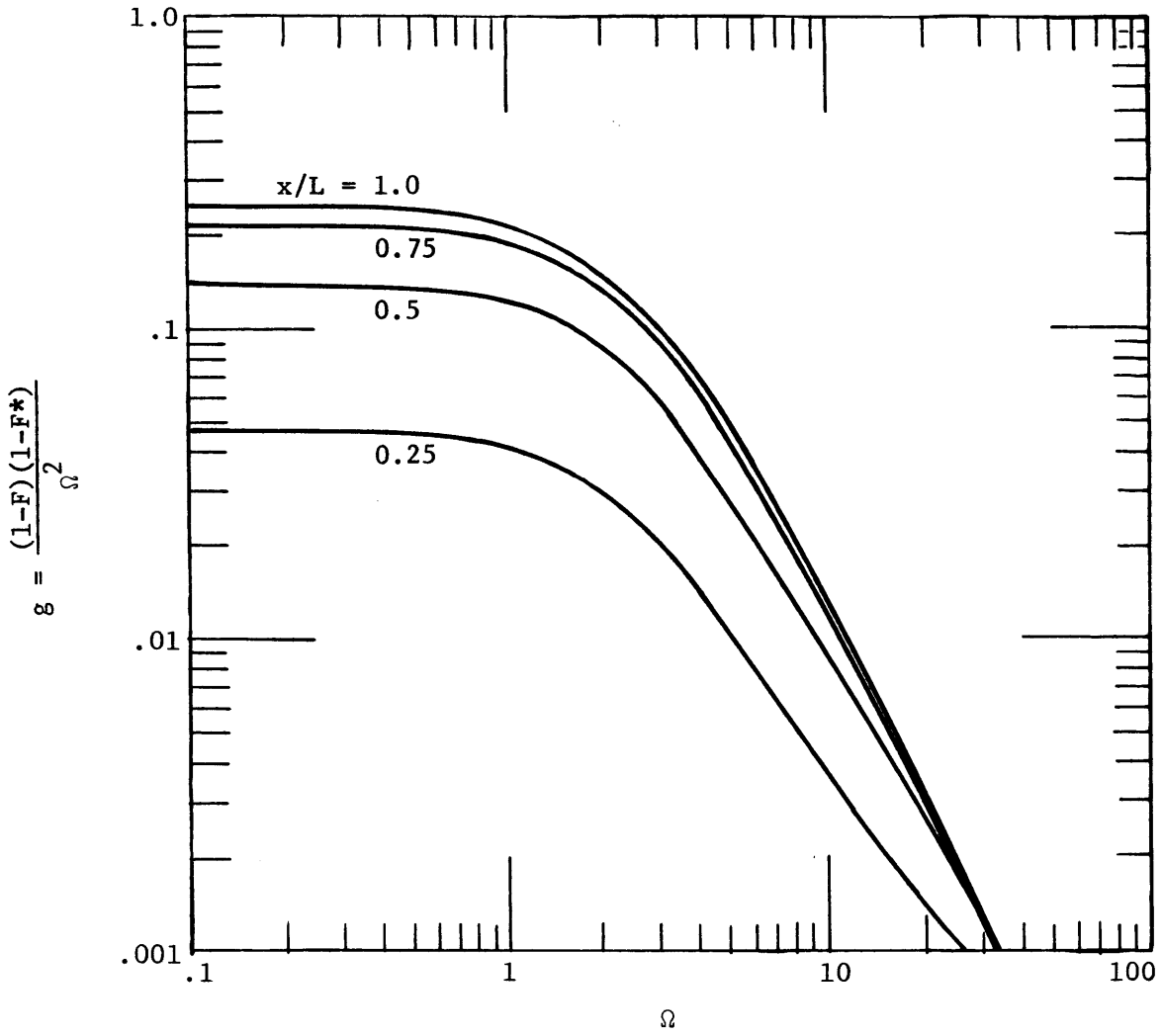

Figure 4.16 Aquifer Response to Accretion; Plot of g along the Aquifer with Horizontal Bottom ($\Gamma=0$).

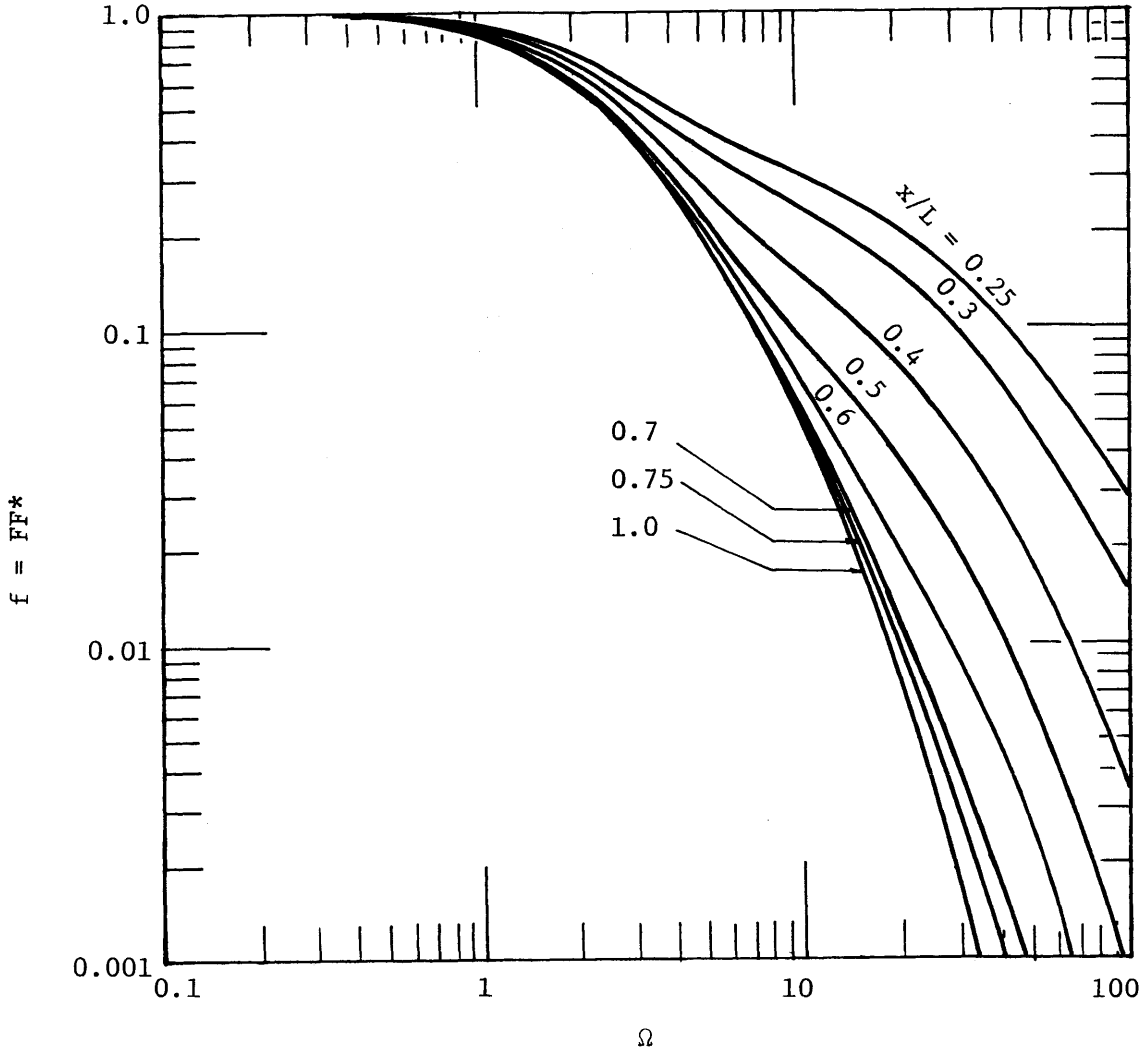

Figure 4.17 Aquifer Response to Stream Stage Fluctuations; Plot of f along the Aquifer with Horizontal Bottom (Γ=0).

The right hand side of equation 4.3.7 can be seen to be equivalent to $|G|^2$ in the single precipitation input case or $|G_1|^2$ of equation 4.1.23 for the correlated input case.

Matching Procedures for Independent Inputs. If it is assumed that the two inputs, precipitation and stream stage, are independent then the transfer function is calculated using the form of equation 4.1.11

$$\hat{S}_{Hh} = G_H \hat{S}_H \tag{4.3.8}$$

$$\hat{S}_{Ph} = G_P \hat{S}_P \tag{4.3.9}$$

which are simply special cases of equation 4.1.24 when $S_{X_1X_2}=S_{X_2X_1}=0$. It is obvious from Tables 4.1 and 4.2 that the inputs for these data are not independent; the co-spectrum and quadrature sepctrum of series 1 and 2 are non-zero. However, the following analysis will illustrate the procedure for the independent case and also demonstrate the effect of making that assumption. The theoretical transfer functions are

$$|G_H|^2 = f(\Omega) = FF^* \tag{4.3.10}$$

$$|G_P|^2 = g(\Omega) \quad \gamma^2 L^4/T^2 \tag{4.3.11}$$

Thus, for well no. 12, by matching Figures 4.9 and 4.17 and shifting along the abscissa, a best fit curve corresponding to a value of x/L can be chosen. The value of Ω corresponding to a particular value of f can be found. Then by matching Figures 4.8 and 4.16, holding the same relative position along the abscissa with the same value of x/L, a value of $g(\Omega)$ corresponding to a particular value of $|G_P|^2$ can be determined by just shifting along the ordinate. A similar procedure holds for well no. 812. A set of sample matched positions can be found in Figures 4.18

and 4.19 for well no. 12 and in Figures 4.20 and 4.21 for well no. 812. From the matching procedure of well no. 12, we have

$$\log\left(\frac{\omega L^2}{\alpha}\right) = \log(f) + \log\left(\frac{2\pi L^2}{\alpha}\right)$$

$$\frac{T}{S} = \frac{2\pi L^2}{34} \qquad (4.3.12)$$

$$\log[g(\Omega)] + \log\left[\frac{\gamma^2 L^4}{T^2}\right] + \log|G_p|^2$$

$$\frac{\gamma L^2}{T} = 2 \qquad (4.3.13)$$

The distance of the well no. 12 from the stream can be estimated from the topographic map to be 1200 feet (Figure 4.22). Then L can be computed as

$$L = \frac{x}{.75} \cong 1600 \text{ feet}$$

Using $\gamma = 0.05$, S and T can be determined from equations 4.3.12 and 4.3.13 to be 0.135 and 0.212×10^4 ft^2/day, respectively. Similarly, for well no. 812, we have

$$\frac{T}{S} = \frac{2\pi L^2}{70}$$

and

$$\frac{\gamma L^2}{T} = 1.949$$

with

$$L = 6000 \text{ ft.}$$

Using $\gamma = 0.05$, S and T can be determined to be 0.285 and 3.078×10^4 ft^2/day, respectively.

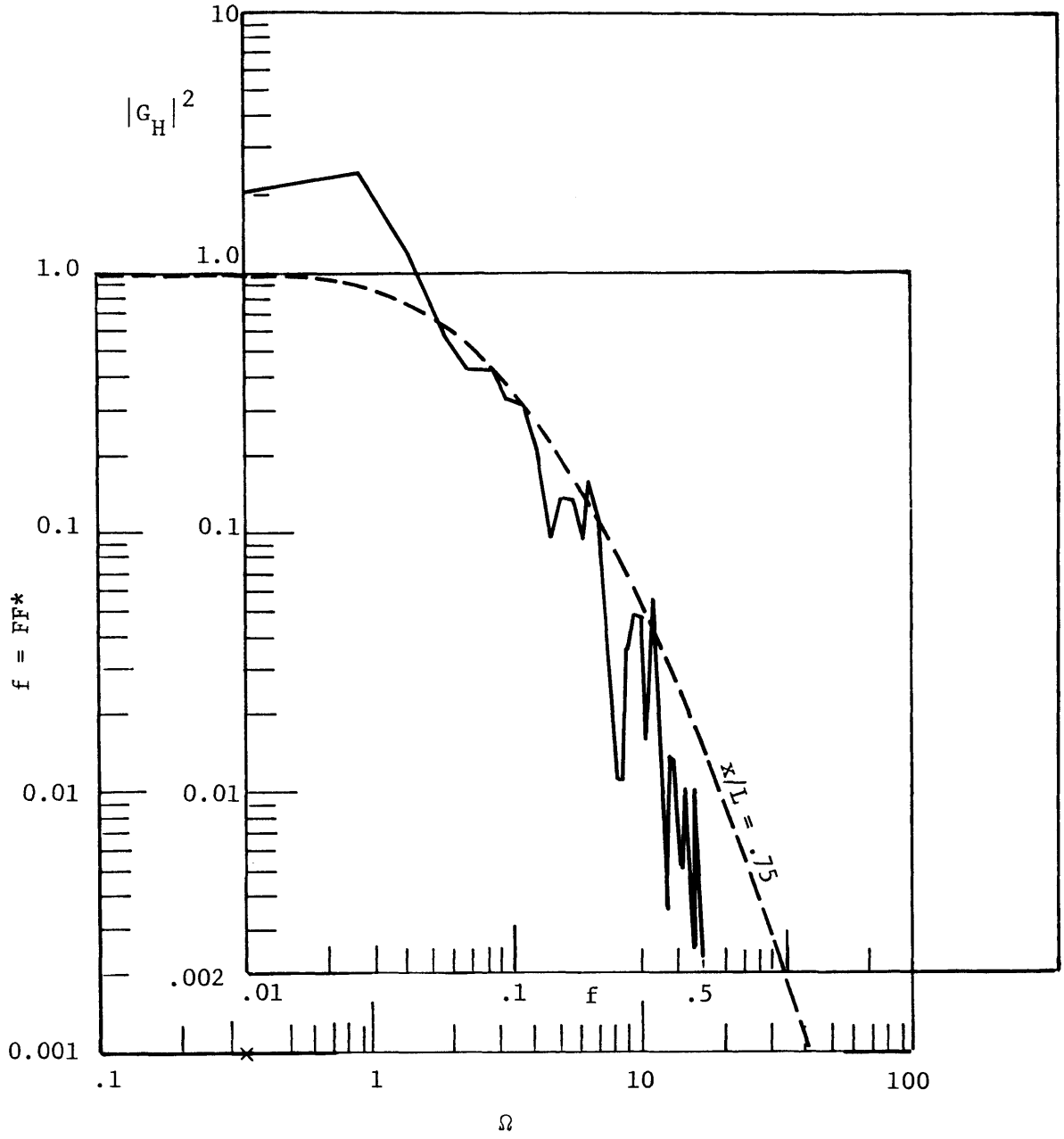

Figure 4.18 Sample Matching of Figure 4.9 and Figure 4.17 for the Independent-Input Case. (x) is the point used in the estimation of parameters at well no. 12.

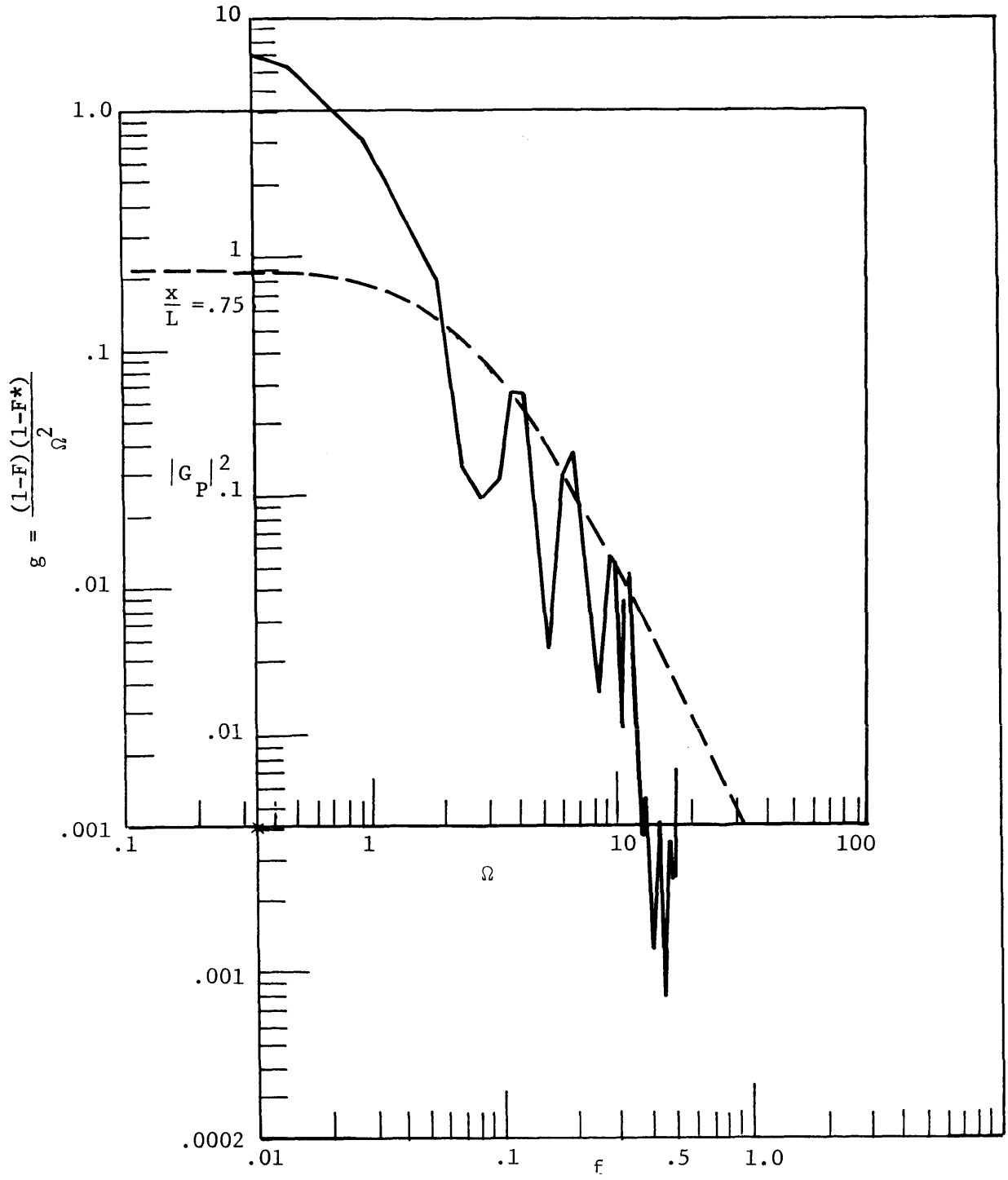

Figure 4.19 Sample Matching of Figure 4.8 and 4.16 for theIndependent Input Case. (×) is the point used in the estimation of parameters at well no. 12.

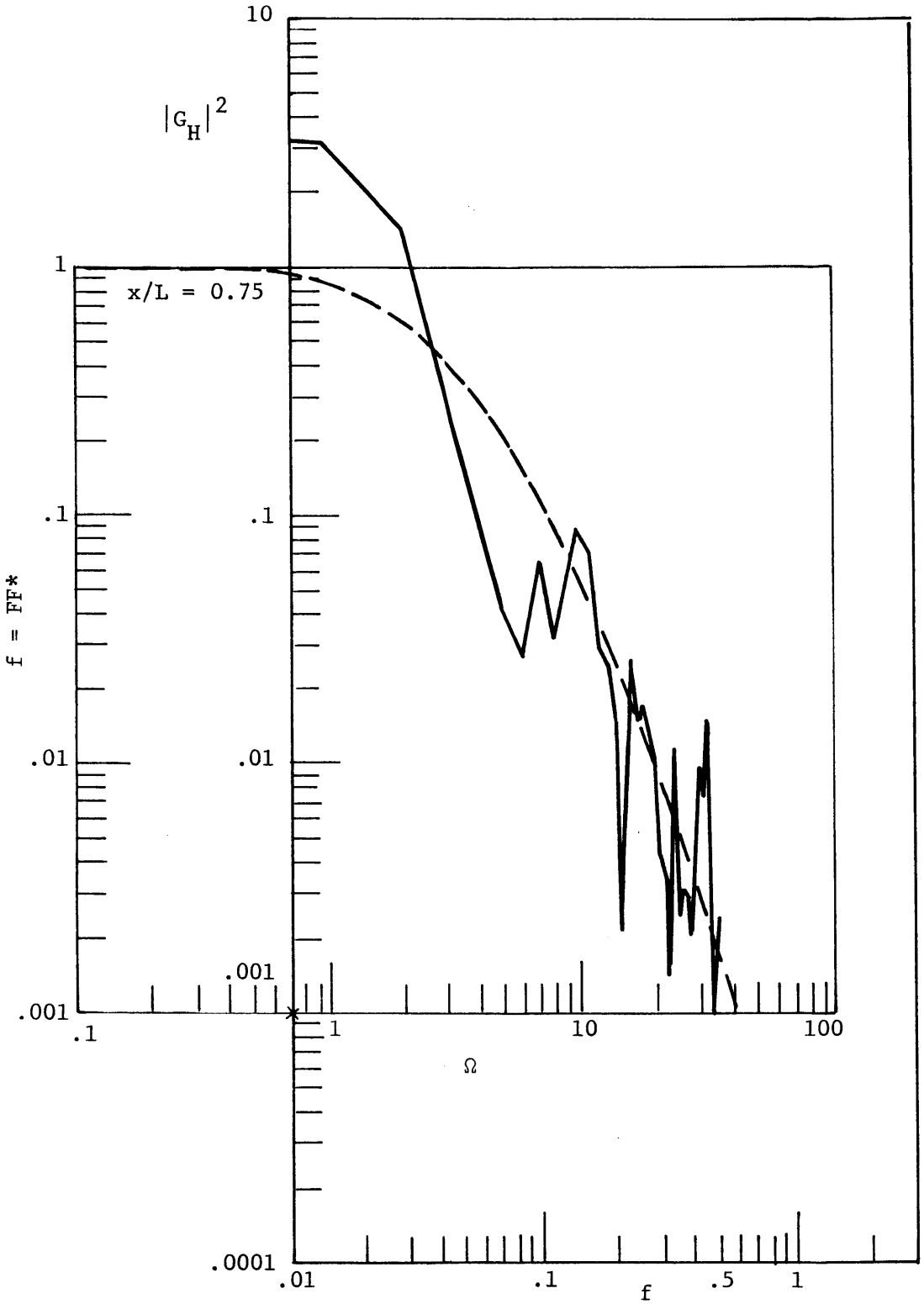

Figure 4.20 Sample Matching of Figures 4.13 and 4.17 for the Independent Input Case. (×) is the point used in the estimation of parameters at well no. 812.

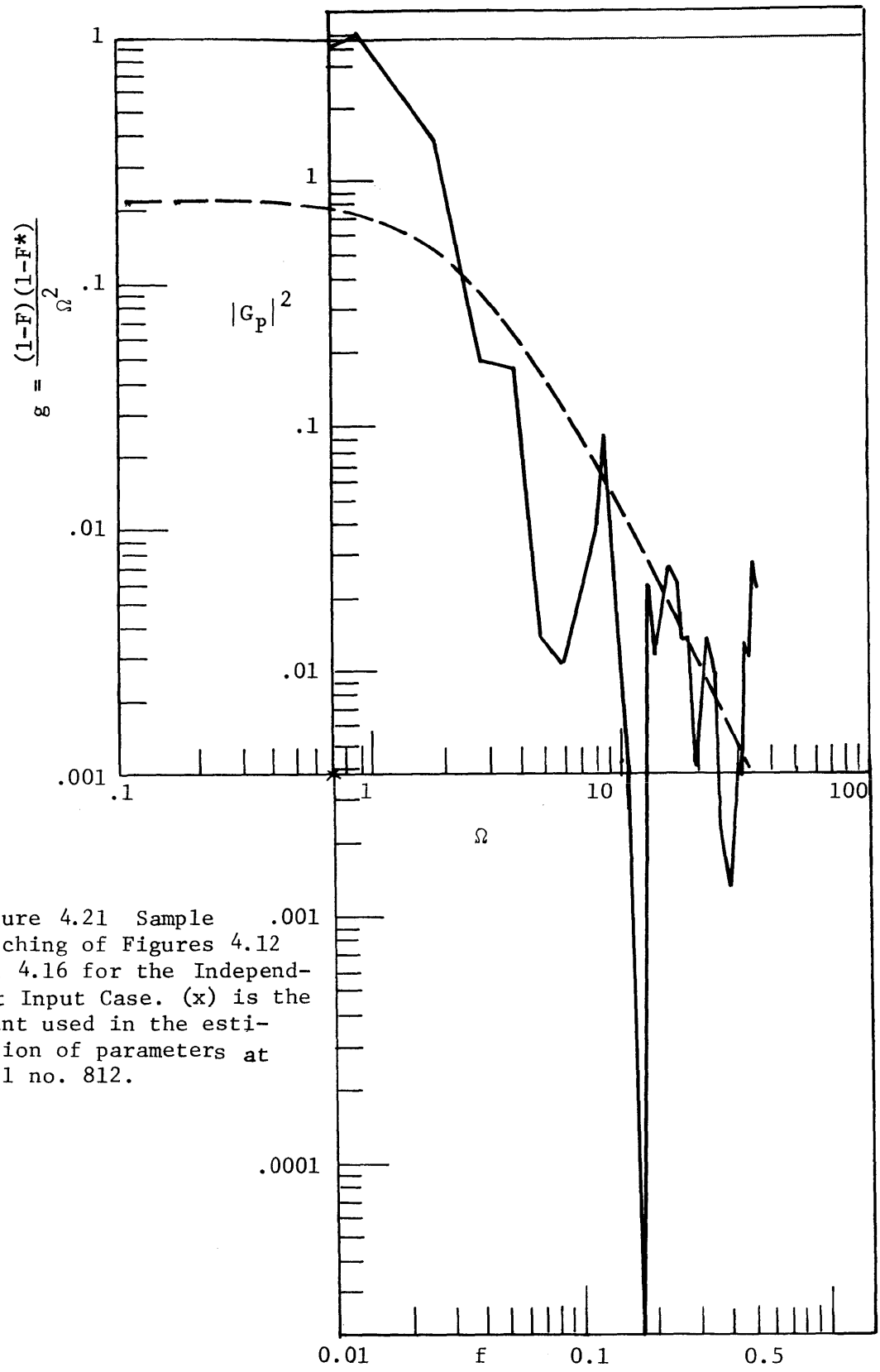

Figure 4.21 Sample Matching of Figures 4.12 and 4.16 for the Independent Input Case. (x) is the point used in the estimation of parameters at well no. 812.

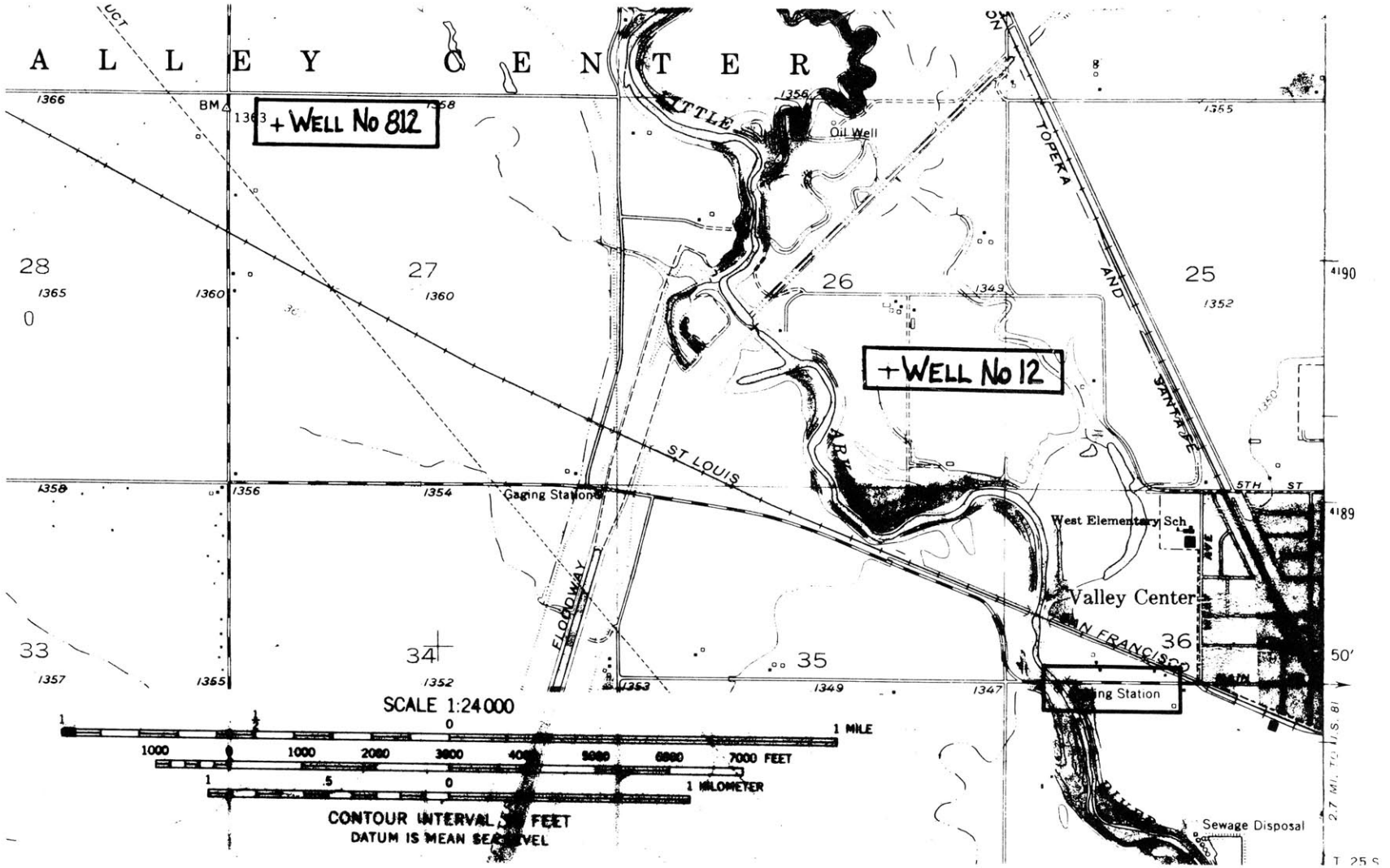

Figure 4.22 Map Showing the Location of Well No. 12, Well No. 812 and the Gaging Station.

Matching Procedure for Correlated Inputs. From equation 4.1.23, we have

$$S_{hh} = |G_1|^2 S_{PP} + G_1 G_2^* S_{PH} + G_1^* G_2 S_{HP} + |G_2|^2 S_{HH} \qquad (4.3.14)$$

Compared to equation 4.3.6, we can see the following equivalencies

$$\frac{(1-F)(1-F^*)\gamma^2}{\omega^2 S^2} \equiv |G_1|^2 \qquad (4.3.15)$$

$$FF^* \equiv |G_2|^2 \qquad (4.3.16)$$

Similar procedures, as in the independent inputs, can be employed for Figures 4.10, 4.11, 4.16 and 4.17. A set of sample matched positions can be found in Figures 4.23 and 4.24 for well no. 12 and in Figures 4.25 and 4.26 for well no. 812. Hence, we have, for well no. 12

$$\log[g(\Omega)] + \log \frac{\gamma^2 L^4}{T^2} = \log|G_1|^2$$

$$\frac{\gamma^2 L^4}{T^2} = 1.8$$

$$\frac{\gamma L^2}{T} = 1.341 \qquad (4.3.17)$$

and

$$\log(\frac{\omega L^2}{\alpha}) = \log(f) + \log(\frac{2\pi L^2}{\alpha})$$

$$\frac{T}{S} = \frac{2\pi L^2}{46} \qquad (4.3.18)$$

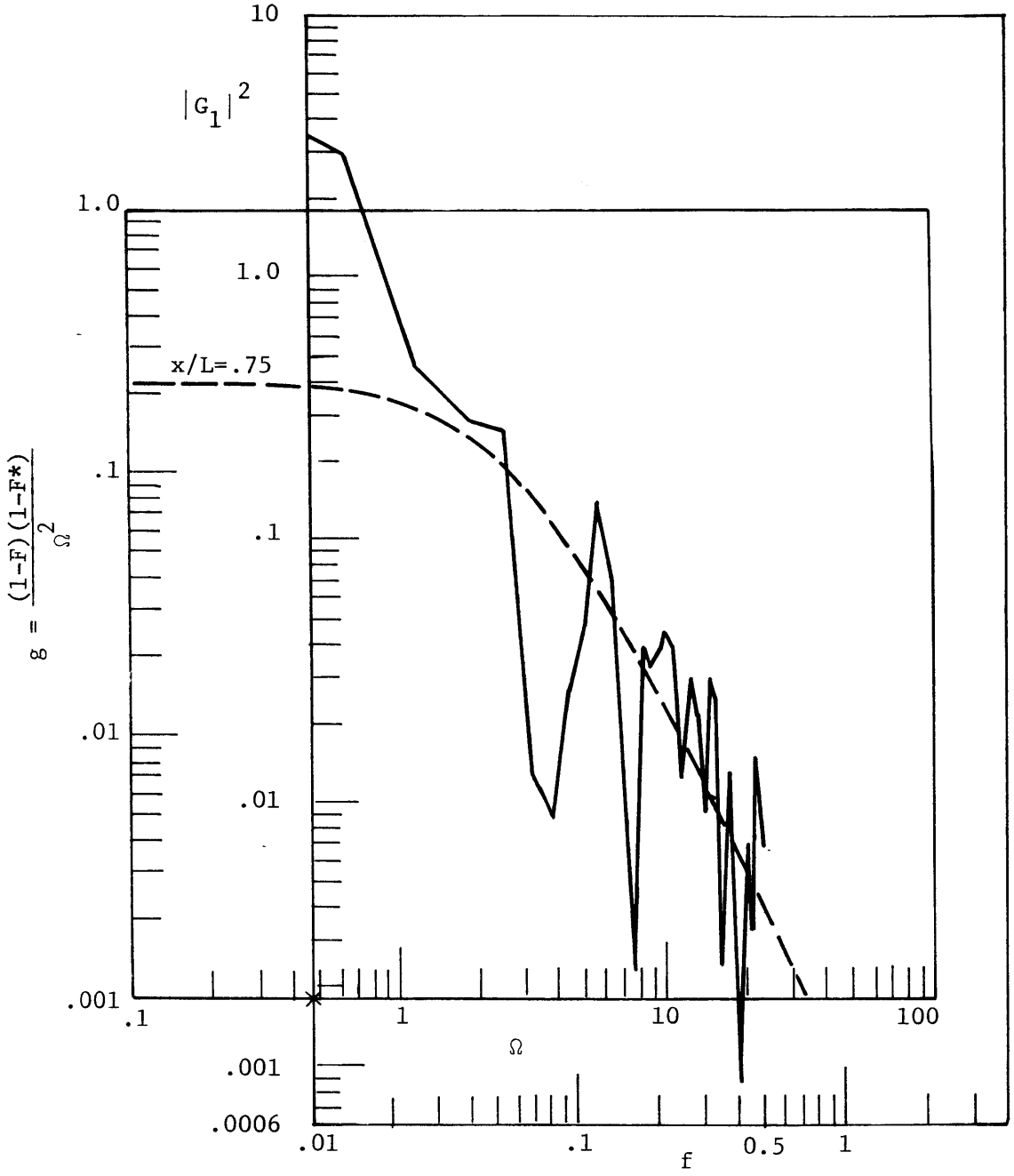

Figure 4.23 Sample Matching of Figures 4.10 and 4.16 for the Correlated-Input Case. (x) is the point used in the estimation of parameters at well no. 12.

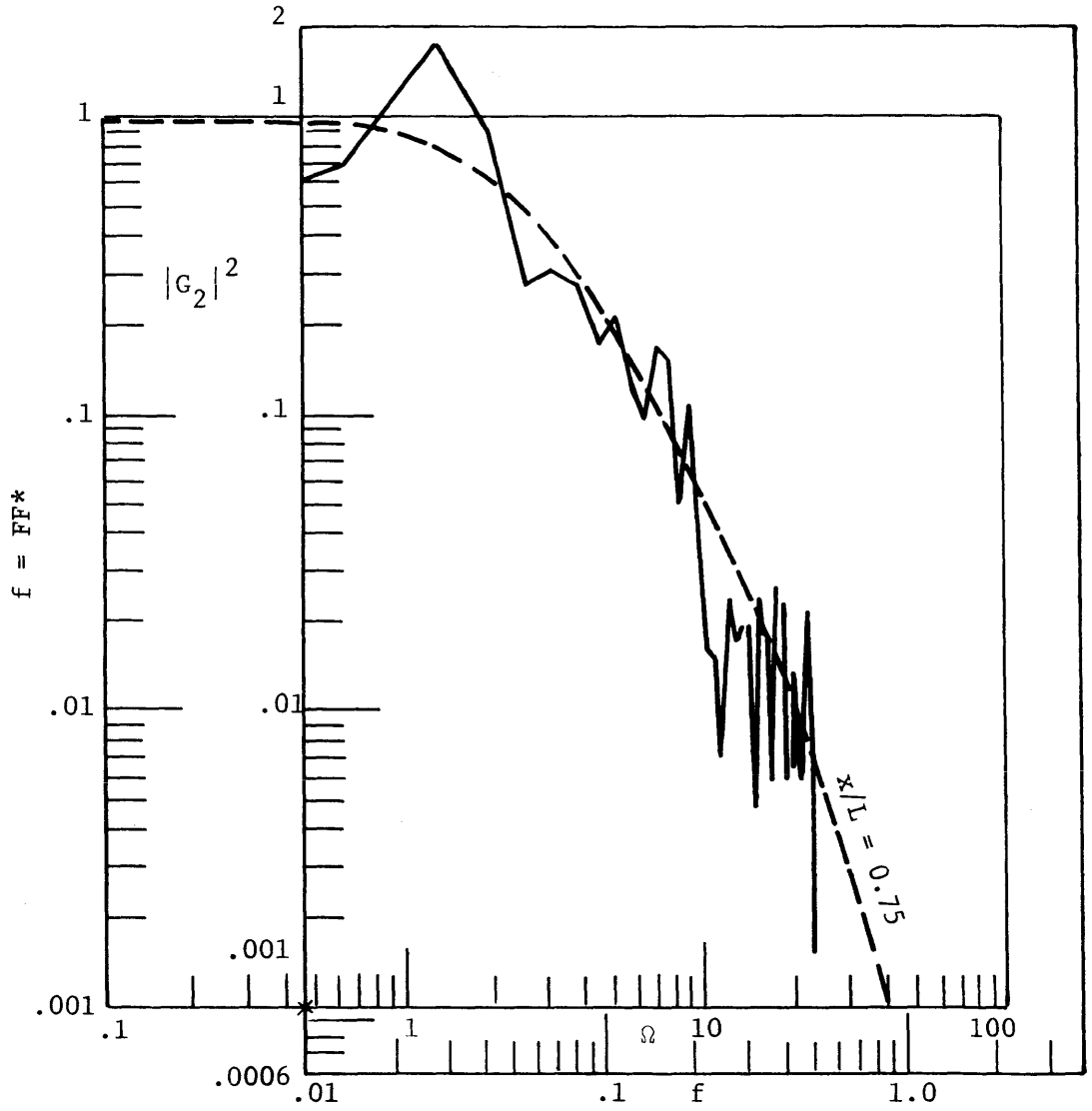

Figure 4.24 Sample Matching of Figures 4.11 and 4.17 for the Correlated-Input Case. (x) is the point used in the estimation of parameters at well no. 12.

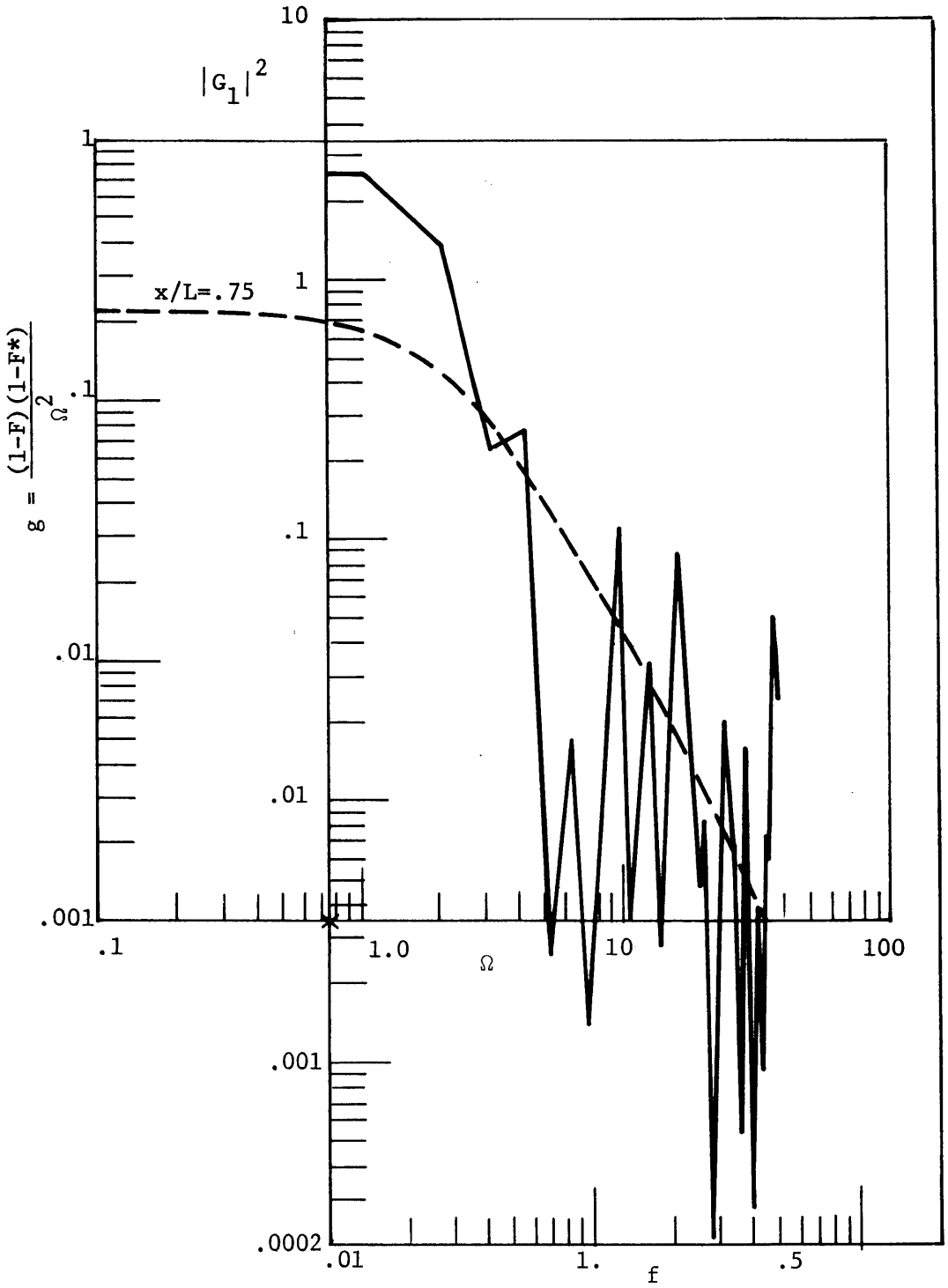

Figure 4.25 Sample Matching of Figures 4.14 and 4.16 for the Correlated-Input Case. (x) is the point used in the estimation of parameters at well no. 812.

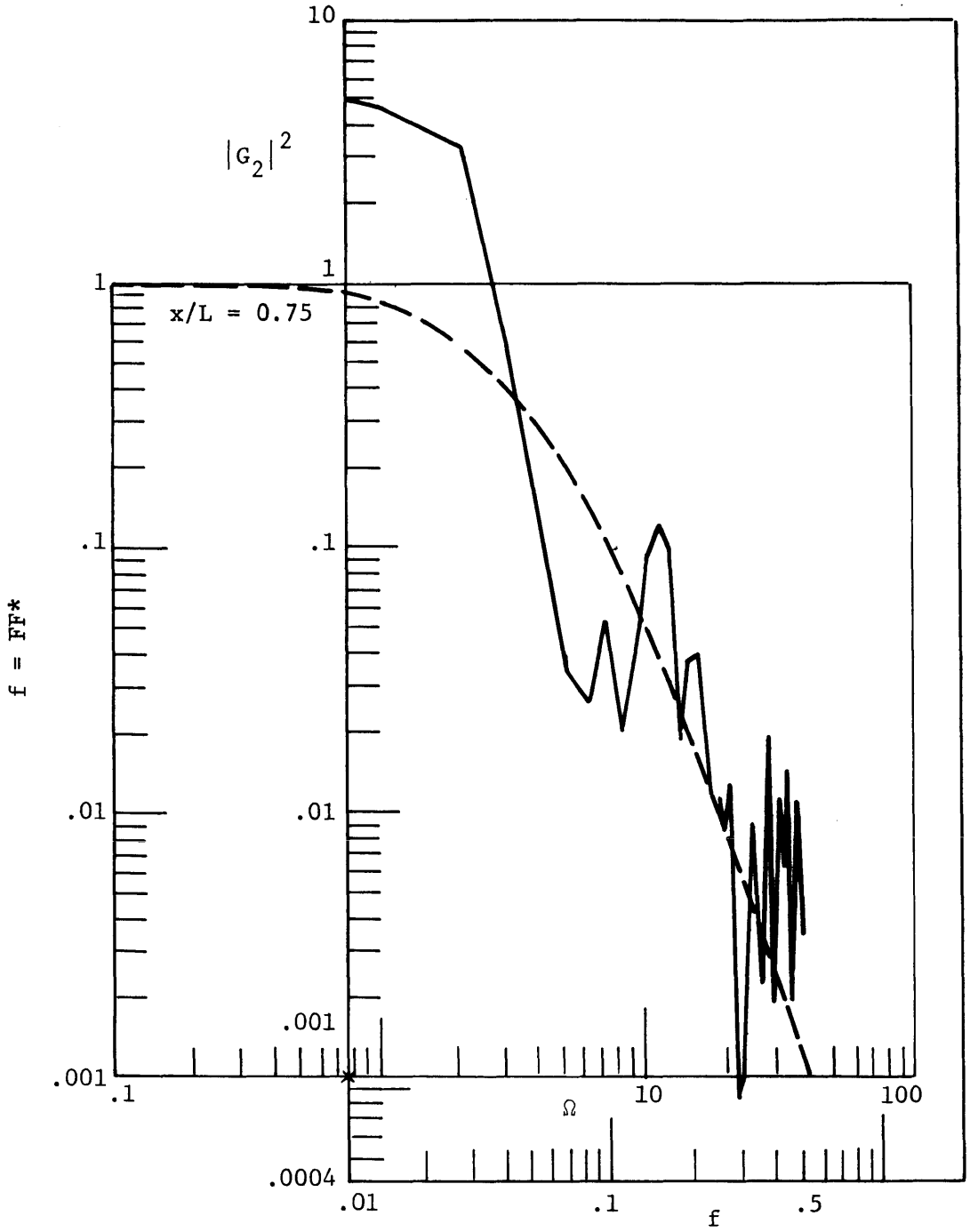

Figure 4.26 Sample Matching of Figures 4.15 and 4.17 for the Correlated-Input Case. (x) is the point used in the estimation of parameters at well no. 812.

Taking x = 1200 feet, L = 1600 feet and γ = 0.05, S and T can be determined to be 0.27 and 0.32×10^4 ft^2/day, respectively. Similarly, for well no. 812, we have

$$\frac{\gamma L^2}{T} = 1.844$$

and

$$\frac{T}{S} = \frac{2\pi L^2}{75}$$

with

$$L = 6000 \text{ feet}$$

Using γ = 0.05, S and T can be determined to be 0.32 and 3.25×10^4 ft^2/day, respectively. Note that S is directly proportional to γ in these computations so that a reduction in the estimated value of γ will produce a corresponding decrease in S. However, S is independent of the estimation of L. A summary of the values S and T as estimated by the two approaches and the values given by Williams and Lohman (1949) are given in Table 4.3.

4.4 Discussion

The above results demonstrate that the spectral analysis technique can yield reasonable estimates of aquifer parameters in a complex natural setting. It should be emphasized that the site and data selection for this analysis was based largely on the availability of a relatively long term record of the type that would be available at many sites. That is, to demonstrate the method in a realistic setting, we purposely selected a site which involved a complex unknown aquifer configuration rather than a restricted known configuration which would reproduce the idealized geometry of the theoretical model. The objective was to demonstrate the technique for realistic field conditions. It was not felt that the model required

verification in the idealized geometry because the basic aquifer equation (2.3.1) is well established and the validity of linearization in the stochastic case has been demonstrated by the simulations in Chapter 3.

The input time series for the numerical spectral estimates were, in the case of the stream stage and aquifer water level, values extracted at monthly intervals, this being the smallest time period for which data were consistently available. However, in the case of the precipitation data, total monthly values (actually the average rate over the month) were used. The use of monthly average precipitation may appear to be inconsistent, but actually on both physical and theoretical grounds it is more appropriate than using discrete values. Theoretically, the effect of using the average of a time series can be evaluated by analyzing the averaging process as a filter using linear system theory (see e.g., Chapter 2 of Jenkins and Watts, 1968). This analysis shows that spectral amplitude is attenuated near the Nyquist frequency (0.5 cycle/mo) but that the spectrum is undistorted at the lower frequencies. The effect is very much like that shown in Figure 2.33 which demonstrates the effect of storage in the unsaturated zone. Physically it is recognized that, because of the storage effects in the unsaturated zone, the recharge input will not be proportional to the instantaneous precipitation rate. The use of the average precipitation rate implicitly accounts for storage in the unsaturated zone in a way which is theoretically sound and hence appropriate.

Our experience, based on some preliminary numerical spectral analysis of daily precipitation and groundwater levels for a well in Wilmington, Massachusetts, is that monthly data will addquately characterize the spectral response of most phreatic aquifer systems. The energy content of the higher frequencies (>0.5 cycle/mo) is very small and has no effect on

the estimated transfer function. The Wilmington aquifer had a response time (S/a in equation 2.2.4) of around 3 months; the Kansas site shows a response time of the same magnitude (response time = $SL^2/3T$ from equation 4.3.18). Only for very small response times (say less than 1 month), i.e., small highly permeable aquifers, will a smaller sampling interval be required.

Because of the fluctuations in the calculated transfer functions (see e.g., Figures 4.23 and 4.24), the matching procedure may appear to be somewhat subjective. Our experience was that completely independent matching analyses produced essentially the same results; however, a more objective procedure such as a least squares fitting could be used. The fluctuations in the estimated transfer functions could be eliminated by introducing more smoothing (e.g., fewer lags) in the spectral calculation; however, this would be at the risk of introducing bias in the spectral estimates. This is the well known tradeoff between stability and fidelity in spectral estimation (Jenkins and Watts, Chapter 7). We have opted for a scheme which retains spectral detail although there is the possibility that some of the fluctuation is spurious. The theoretical comparisons could be made to appear more favorable by introducing more smoothing. The results summarized in Table 4.3 show that the effects of correlated inputs are significant and should be included.

In this data analysis a simple linear relationship between recharge and precipitation was assumed, recognizing this as a crude approximation of the actual recharge process. It was beyond the scope of this work to even attempt to solve the difficult problem of recharge prediction. Most hydrologists recognize this as a basically unresolved problem, but if and when improved predictive methods become available, they can easily be in-

Source	Well No.	Transmissivity T (ft^2/day)	Storage Coef. S	γ	Length of Aquifer L (ft.)
independent input case	12	$.212\times10^4$	.135	.05	1600
	812	3.08×10^4	.285	.05	6000
correlated input case	12	0.32×10^4	.27	.05	1600
	812	3.25×10^4	.32	.05	6000
Bulletin 79 (William & Lohman 1949)		$.615\times10^4$ to 4.41×10^4	.33 (at well #12)		

Table 4.3 Summary of Aquifer Parameters

corporated in the spectral model. Given a functional relationship for recharge in terms of precipitation, temperature, and other climatological data, a multiple-input analysis is carried out with these additional input series. The procedure is outlined in Section 2.6 for the case of evapotranspiration losses linearly related to temperature. The seasonal effects of evapotranspiration losses are likely to be significant in some cases and should be explored in future research. The use of spectral analysis as a method of estimating groundwater recharge from water level fluctuations should also be explored.

Although there are natural complexities as indicated above, the generally favorable results of the spectral method applied to the Kansas site suggest that there could be significant potential for such methods in the interpretation of natural groundwater level fluctuations. The large amount of existing data on groundwater levels could provide more quantitative information through spectral analysis and the analyses would be performed routinely as the data becomes computer accessible. As experience is developed, it may also be possible to recognize certain descriptive features of groundwater systems by inspection of spectra. Other methods of data interpretation may be useful; for example, the simpler linear reservoir model (Section 2.2) may be desirable for some problems (Gelhar and Wilson, 1974). The parameters for this lumped parameter model (S and a in equation 2.2.4) can be found by spectral transfer function analysis but the theoretical transfer functions are simpler (see equation 2.2.9). Methods based on cross spectral analysis of water levels from several wells in an aquifer are also attractive.

Chapter 5 CONCLUSIONS

Several major results of significance in relation to temporal variability of groundwater systems have been established. These fall into the following categories:

1. Linear aquifer models provide theoretical predictions of the spectral response characteristics of several phreatic aquifer configurations. The effects of aquifer slope, flow zone thickening, vertical flow, etc. are analyzed and the conditions under which these factors can be neglected are determined. The horizontal Dupuit aquifer model is reasonable for application under many field conditions, but the other effects can be included if the aquifer configuration is known.

2. Nonlinear aquifer simulations predict the overall effects of nonlinearity on the spectral response of phreatic aquifers. The nonlinear effects are typically quite small for field conditions, and the linear analytical models therefore provide a reasonable basis for the interpretation of field observations. The effects of spatially variable accretion rate on the frequency spectrum are also quite small.

3. Aquifer parameters can be determined by comparing the observed spectral response of an aquifer with the linear theory. From precipitation, stream stage and aquifer water level data, the storage coefficient and transmissivity of a stream-connected aquifer can be estimated using a spectral matching procedure.

In addition, it was established that the spectral distortion associated with flow phenomena in the unsaturated zone above the water table will be quite small for a sampling interval of one month or greater. In the design of simple flow measuring networks it was shown that spatial variability of hydraulic conductivity, as characterized by a spatial correlation function, is an important factor which should be included.

The results of this study should be widely applicable for the estimation of aquifer parameters from natural fluctuations of groundwater level. Thus it should be possible to make much better use of extensive existing data of this type for the evaluation of groundwater resources. Important items which should be explored in future studies are techniques for dealing with nonstationary aquifer response and methods of incorporating spatial variability of hydrologic parameters into the design of complex multiple-well observation networks. More realistic recharge models including the effect of temperature on evapotranspiration losses should also be investigated.

REFERENCES

Bear, J., Dynamics of Fluids in Porous Media, American-Elsevier Publishing Co., Inc., 1972.

Bendat, J. S. and Piersol, A. G., Random Data: Analysis and Measurement Procedures, Wiley-Interscience, John Wiley & Sons, Inc., 1971.

Brooks, R. H.,"Unsteady Flow of Groundwater into Drain Tile", J. Irr. and Drain. Div., ASCE, Vol. 87, IR2, pp. 27-37, 1961.

Buyevick, Y. A., Leonov, A. I. and Safrai, V. M., "Variations in Filtration Velocity Due to Random Large-Scale Fluctuations of Porosity", J. Fluid Mech., Vol. 37, pp. 371-381, 1969.

Cooper, H. H., Jr., and Rorabaugh, M. I., "Changes in Ground-Water Movement and Bank Storage Caused by Flood Waves in Surface Streams", U.S.G.S. Prof. Paper 475-B, B192-195, 1963.

Dagan, G., "Linearized Solution of Unsteady Deep Flow toward an Array of Horizontal Drains", J. Geophys. Res., Vol. 69, No. 16, pp. 3361-3369, 1964.

Dixon, W. J. (editor), BMD Biomedical Computer Programs, University of California Press, 1973.

Dooge, J. C. I., "The Routing of Groundwater Recharge through Typical Elements of Linear Storage", International Association of Scientific Hydrology, Publication No. 52, General Assembly of Helsinki, pp. 286-300, 1960.

Eagleson, P. S., Dynamic Hydrology. McGraw-Hill, New York, 1970.

Eriksson, E., "Groundwater Time-Series: An Exercise in Stochastic Hydrology", J. Nordic Hydrol., Vol. 3, pp. 181-205, 1970a.

Eriksson, E., "Cross-Spectrum Analysis of Groundwater Levels in an Esker", J. Nordic Hydrol., Vol. 4, pp. 245-259, 1970b.

Freeze, R. A. and Banner, J., "The Mechanism of Natural-Ground-Water Recharge and Discharge 2. Laboratory Column Experiments and Field Measurements", Water Resour. Res., Vol. 6, pp. 138-155, 1970.

Gardner, W. R., "Gravity Drainage of Soils", Soil Sci. Soc. Am. Proc., Vol. 26, pp. 129-132, 1962.

Gelhar, L. W., "Stochastic Analysis of Phreatic Aquifers", Water Resour. Res., Vol. 10, pp. 539-545, 1974.

Gelhar, L. W. and Wilson, J. L., "Ground-Water Quality Modeling", Ground Water, Vol. 12, pp. 399-408, 1974.

Glover, R. E. and Bittinger, N. W., "Drawdown Due to Pumping from an Unconfined Aquifer", Transactions, ASCE, Vol. 26, pp. 176-183, 1961

Glover, R. E., "Seasonal Fluctuations of Return Flows", Proc. National Symposium on Ground-Water Hydrology, American Water Resources Association, Proc. Series No. 4, pp. 272-278, 1967.

Granger, C. W. J. and Hatanaka, M., Spectral Analysis of Economic Time Series, Princeton University Press, Princeton, New Jersey, 1964.

Hall, F. R. and Moench, A. F., "Application of the Convolution Equation to Stream-Aquifer Relationships", Water Resour. Res., Vol. 8, pp. 487-493, 1972.

Hannan, E. J., Time Series Analysis, Science Paperbacks, Metheun & Co., Ltd., London, 1960.

Haushild, W. and Kruse, G., "Unsteady Flow of Groundwater into a Surface Reservoir", J. Hydrau. Div., ASCE, Vol. 86, HY7, pp. 13-20, 1960.

Hornberger, G., Ebert, J. and Remson, I., "Numerical Solution of the Boussinesq Equation for Aquifer-Stream Interaction", Water Resour. Res., Vol. 6, pp. 601-608, 1970.

Hunt, B. W., "Vertical Recharge of Unconfined Aquifer", J. Hydrau. Div., ASCE, Vol. 97, HY7, pp. 1017-1030, 1971.

Jackson, R. E., Gilliland, J. A. and Adamowski, K., "Time Series Analysis of the Hydrologic Regimen of a Groundwater Discharge Area", Water Resour. Res., Vol. 9, pp. 1411-1419, 1973.

Jacob, C. E., "Correlation of Ground-Water Levels and Precipitation on Long Island, New York", Transactions, A.G.U., Vol. 24, pp. 564-572, 1943.

Jenkins, G. M. and Watts, D. G., Spectral Analysis and Its Applications, Holden-Day, Inc., 1968.

Karadi, G., Krizek, R. and Elnagger, H., "Unsteady Seepage Flow Between Fully Penetrating Trenches", J. Hydrol., Vol. 6, pp. 417-430, 1968.

Kraijenhoff van de Leur, D. A., "A Study of Non-Steady Groundwater Flow with Special Reference to a Reservoir-Coefficient", De Ingenieur, No. 19, pp. 87-94, 1958.

Kriz, G. J., "Determination of Unconfined Aquifer Characteristics", J. Irr. and Drain. Div., ASCE, Vol. 93, IR2, pp. 37-47, 1967.

Kriz, G. J., Scott, V. H. and Burgy, R. H., "Analysis of Parameters of an Unconfined Aquifer", J. Hydrau. Div., ASCE, Vol. 92, HY5, pp. 49-56, 1966.

Murray, W. A. and Monkmeyer, P. L., "Validity of Dupuit-Forchheimer Equation", J. Hydrau. Div., ASCE, HY9, pp. 1573-1577, 1973.

Papoulis, A., Probability, Random Variables and Stochastic Processes, McGraw-Hill, New York, 1965.

Peaceman, D. W. and Rachford, H. H., Jr., "The Numerical Solution of Parabolic and Elliptic Differential Equations", J. Soc. Ind. and Appl. Math., Vol. 3, pp. 28-41, 1955.

Pinder, G. F., Bredehoeft, J. D. and Cooper, H. H., Jr., "Determination of Aquifer Diffusivity from Aquifer Response to Fluctuations in River Stage", Water Resour. Res., Vol. 5, pp. 850-855, 1969.

Polubarinova-Kochina, P. Y., Theory of Ground Water Movement, Translated by R. J. M. DeWiest, Princeton University Press, Princeton, New Jersey, 1962.

Prickett, T. A. and Lonnquist, C. G., Selected Digital Computer Techniques for Groundwater Resource Evaluation, Illinois State Water Survey, Urbana, 1971.

Remson, I., Hornberger, G. M. and Moltz, F. J., Numerical Methods in Subsurface Hydrology, Wiley-Interscience, John Wiley & Sons, Inc., 1971

Singh, K. P., "Theoretical Baseflow Curves", J. of Hydrau. Div., ASCE, Vol. 95, HY6, pp. 2029-2048, 1969.

Stramel, G. J., "Progress Report on the Ground-Water Hydrology of the Equus Beds Area, Kansas", State Geological Survey of Kansas, Bulletin 119, Part 1, 1956.

Stramel, G. J., "Progress Report on the Ground-Water Hydrology of the Equus Beds Area, Kansas - 1966", State Geological Survey of Kansas, Bulletin 187, Part 2, 1967.

Swartzendruber, D., "The Flow of Water in Unsaturated Soils", in Flow in Porous Media, R. J. M. DeWiest, Ed., Academic Press, New York, 1969.

Thornthwaite, C. W., "An Approach Toward a Rational Classification of Climate", American Geographical Review, Vol. 38, pp. 55-94, 1948.

Tison, G., Jr., "Fluctuations of Ground-Water Levels", in Advances in Geophysics, Vol. 2, pp. 303-325, 1965.

van Schilfgaarde, J., "Transient Design of Drainage Systems", ASCE Water Resources Engineering Conference Preprint 172, Mobile, Alabama, March 8-12, 1965.

Venetis, C., "Estimating Infiltration and/or the Parameters of Unconfined Aquifers from Groundwater Level Observations", J. Hydrol., Vol. 12, pp. 161-169, 1971.

Williams, C. C. and Lohman, S. W., "Geology and Ground-Water Resources of a Part of South-Central Kansas with Special Reference to the Wichita Municipal Water Supply", State Geological Survey of Kansas, Bulletin 79, 1949.

Yeh, W., "Nonsteady Flow to Surface Reservoir", J. Hydrau. Div., ASCE, Vol. 96, HY6, pp. 609-618, 1970.

Youngs, E. G., "The Drainage of Liquids from Porous Materials", J. Geophys. Res., Vol. 65, pp. 4025-4030, 1960.

LIST OF SYMBOLS

The following list covers the symbols which are widely used in the report. The dimensions of dimensional quantities are given in brackets. Also shown is the section in which the term is first used.

Symbol	Definition	Section
a	linear reservoir coefficient [1/T]	2.2
Co_{XY}	cospectrum of X and Y	2.1
e	random noise generated from a normal process	3.3
f	square of the amplitude of the normalized transfer function for a stream stage input	2.3
g	square of the amplitude of the normalized transfer function for an accretion input	2.3
G	transfer function	2.1
G_1	transfer function from accretion to aquifer response	3.1
G_2	transfer function from stream stage to aquifer response	3.1
h	thickness of the saturated zone [L]	2.1
h_o	elevation of water outfall of the linear reservoir in the coupled system [L]	2.3
H	stream or reservoir stage [L]	2.1
i	$\sqrt{-1}$	
i	discrete x-coordinate of the finite difference model	3.2
j	discrete y-coordinate of the finite difference model	3.2
k_m	maximum number of lags	4.2
K	hydraulic conductivity [L/T]	2.1

Symbol	Definition	Section
L	horizontal aquifer length [L]	2.1
m	a characteristic aquifer [L] thickness generally taken at stream	3.1
m_x	mean value of x	2.1
p(x)	probability density function	2.1
n	effective porosity	
P	precipitation rate [L/T]	3.2
q	outflow per unit area, linear reservoir [L/T]	2.2
Q	discharge [L^3/T]	2.5
Q_{XY}	quadrature spectrum of X and Y	2.1
R_{XX}	autocorrelation function X	2.1
$\hat{R}_{XX}$	estimated autocorrelation function of X	2.1
R_{XY}	cross correlation function of X and Y	2.1
$\hat{R}_{XY}$	estimated cross correlation function of X and Y	2.1
s_X^2	sample variance of X	3.3
S	storage coefficient in Dupuit aquifer	2.1
S_{XX}	power spectrum of X(t)	2.1
$\hat{S}_{XX}$	smoothed estimate of power spectrum of X(t)	2.1
S_{XY}	cross spectrum of X(t) and Y(t)	2.1
$\hat{S}_{XY}$	smoothed estimate of cross spectrum of X(t) and Y(t)	2.1
t	time [T]	2.1
T	aquifer transmissibility [L^2/T]	2.1
x	horizontal spatial coordinate [L]	2.1
X	an arbitrary input random time series	

Symbol	Definition	Section
y	elevation of water table above datum ($= h + \zeta$) [L]	2.5
z	vertical spatial coordinate [L]	2.3
α	$= T/S$ $[L^2/T]$	2.3
β	slope of aquifer bottom	2.3
γ	fraction of precipitation producing recharge	3.3
γ^2_{XY}	coherence squared function between X and Y	2.1
ϵ	accretion [L/T]	
ζ	elevation of aquifer bottom above datum [L]	2.1
η	dimensionless thickness of saturated zone ($= h/m$)	3.1
η_o	dimensionless stream stage elevation ($= H/m$)	3.1
θ_{XY}	phase spectrum from X to Y	2.1
μ	a perturbation parameter ($= \epsilon L^2/2K\bar{H}$)	2.3
μ_X	autocovariance function of X	2.1
ξ	dimensionless horizontal coordinate ($= x/L$)	3.1
ρ	dimensionless accretion ($= L^2\epsilon/Tm = 2\mu$)	3.1
τ	dimensionless time ($= Tt/SL$)	3.1
ϕ	piezometric head [L]	2.4
ω	dimensional circular frequency [1/T]	2.1
Ω	dimensionless frequency ($= S\omega L^2/T$)	2.3

APPENDIX A

Listing of the Computer Program

This program is based on the aquifer simulation program with water table conditions written by Prickett and Lonnquist in 1971. There are minor modifications which include the incorporation of the proper boundary conditions and the one dimensional representation. This listing is for the particular case of a dual input system with stream stage and accretion inputs. The data were obtained from the U.S. Geological Survey of Kansas at Wichita and are given at the end of the program. Also listed is the procedure for the BMD 02T (Biomedical Computer Program, Autocovariance and Power Spectral Analysis) which is used for the data analysis of the input and output time series, the latter of which is obtained directly from the numerical simulation program.

```
C     BASIC AQUIFER SIMULATION PROGRAM                                    BASP0001
C     WITH WATER-TABLE CONDITIONS                                         BASP0002
C     DEFINITION OF VARIABLES                                             BASP0003
C     HO(I,J)-----HEADS AT START OF TIME                                  BASP0004
C                 INCREMENT (I,J)                                         BASP0005
C     H(I,J)------HEADS AT END OF TIME                                    BASP0006
C     SF2(I,J)----STORAGE FACTOR FOR WATER-                               BASP0007
C                 TABLE CONDITIONS                                        BASP0008
C                 INCREMENT                                               BASP0009
C     Q(I,J)------CONSTANT WITHDRAWAL                                     BASP0010
C                 RATES                                                   BASP0011
C     T(I,J,1)----AQUIFER TRANSMISSIVITY                                  BASP0012
C                 BETWEEN I,J AND I,J+1                                   BASP0013
C     T(I,J,2)----AQUIFER TRANSMISSIVITY                                  BASP0014
C                 BETWEEN I,J AND I+1,J                                   BASP0015
C     AA,BB,CC,DD-COEFFICIENTS IN WATER                                   BASP0016
C                 BALANCE EQUATIONS                                       BASP0017
C     NR----------NO. OF ROWS IN MODEL                                    BASP0018
C     NC----------NO. OF COLUMNS IN MODEL                                 BASP0019
C     NSTEPS------NO. OF TIME INCREMENTS                                  BASP0020
C     DELTA-------TIME INCREMENTS                                         BASP0021
C     HH,S2,QQ,TT-DEFAULT VALUES                                          BASP0022
C     PERM(I,J,1)-AQUIFER PERMEABILITY                                    BASP0023
C                 BETWEEN I, J AND I, J+1                                 BASP0024
C     PERM(I,J,2)-AQUIFER PERMEABILITY                                    BASP0025
C                 BETWEEN I, J AND I+1, J                                 BASP0026
C     BOT(I,J)----ELEVATION OF BOTTOM OF                                  BASP0027
C                 AQUIFER                                                 BASP0028
C     RR(ISTEP)---ACRETION RATE AT TIME STEP ISTEP                        BASP0029
C     HX(ISTEP)---PRECIPITATION DATA AT EACH TIME STEP                    BASP0030
C     HX1(ISTEP)--STREAM GAUGE DATA AT EACH TIME STEP                     BASP0031
C     HY(ISTEP)---DIMENSIONLESS ACCRETION RATE                            BASP0032
C     RO----------PARAMETER OF DIMENSIONLESS ACCRETION MEAN               BASP0033
C     UM----------COEFFICIENT OF WITHDRAWAL RATES                         BASP0034
      DIMENSION H(50,50),HO(50,50),                                       BASP0035
     1SF2(50,50),Q(50,50),T(50,50,2),                                     BASP0036
```

```
     2E(50),G(50),DL(50,50),HY(1000),,HX1(1000)                        BASP0037
     3,PERM(50,50,2),BOT(50,50),HX(1000),RR(1000)                      BASP0038
C     TURN OFF UNDERFLOW TRAP                                          BASP0039
C     DEFINE INPUT AND OUTPUT DEVICE NUMBERS                           BASP0040
      INTEGER OUT                                                      BASP0041
      IN=5                                                             BASP0042
      OUT=6                                                            BASP0043
C     READ PARAMETER CARD AND                                          BASP0044
C     DEFAULT VALUE CARD                                               BASP0045
      READ(IN,10)NSTEPS,DELTA,ERROR,                                   BASP0046
     1NC,NR,TT,HH,QQ,S2,PP,BOTT                                        BASP0047
10    FORMAT(I6,2F8.0/2I6,1F6.0,6X,2F6.0                               BASP0048
     1,18X,1F6.0,6X,2F6.0)                                            BASP0049
C     FILL ARRAYS WITH DEFAULT VALUES                                  BASP0050
      DO 20 I=1,NC                                                     BASP0051
      DO 20 J=1,NR                                                     BASP0052
      SF2(I,J)=S2                                                      BASP0053
      PERM(I,J,1)=PP                                                   BASP0054
      PERM(I,J,2)=PP                                                   BASP0055
      BOT(I,J)=BOTT                                                    BASP0056
      T(I,J,1)=TT                                                      BASP0057
      T(I,J,2)=TT                                                      BASP0058
      H(I,J)=HH                                                        BASP0059
      HO(I,J)=HH                                                       BASP0060
20    Q(I,J)=QQ                                                        BASP0061
C     READ NODE CARDS                                                  BASP0062
      DO 30 I=1,NC                                                     BASP0063
      DO 30 J=1,NR                                                     BASP0064
30    READ(5,40) I,J,T(I,J,1),                                         BASP0065
     1T(I,J,2),H(I,J),Q(I,J),                                          BASP0066
     2SF2(I,J),PERM(I,J,1),PERM(I,J,2),BOT(I,J)                        BASP0067
40    FORMAT(2I3,2F6.0,2F4.0,F10.0,3F6.0)                              BASP0068
C     READ PRECIPITATION DATA                                          BASP0069
      READ(5,45)(HX(K),K=1,405)                                        BASP0070
C     READ STREAM GAUGE DATA                                           BASP0071
      READ(5,45)(HX1(K),K=1,405)                                       BASP0072
```

```
45    FORMAT(8X,12F6.2)                                                    BASP0073
C     START OF SIMULATION                                                  BASP0074
50    TIME=0                                                               BASP0075
C     DIMENSIONLESS ACCRETION INPUT                                        BASP0076
      HY(ISTEP)=HX(ISTEP)/2.557                                            BASP0077
      RC=1.                                                                BASP0078
      RR(ISTEP)=.0025*RO*HY(ISTEP)                                         BASP0079
C     DIMENSIONLESS STREAM INPUT                                           BASP0080
      H(1,1)=1.+HX1(ISTEP)/25.                                             BASP0081
      H(1,2)=H(1,1)                                                        BASP0082
C     NO FLOW BOUNDARY CONDITIONS                                          BASP0083
      H(22,1)=H(20,1)                                                      BASP0084
      H(22,2)=H(20,2)                                                      BASP0085
C     PREDICT HEADS FOR NEXT                                               BASP0086
C     TIME INCREMENT                                                       BASP0087
      DO 70 I=1,NC                                                         BASP0088
      DO 70 J=1,NR                                                         BASP0089
      D=H(I,J)-HO(I,J)                                                     BASP0090
      HC(I,J)=H(I,J)                                                       BASP0091
      F=1.0                                                                BASP0092
      IF(DL(I,J).EQ.0.0)GO TO 60                                           BASP0093
      IF(ISTEP.GT.2)F=D/DL(I,J)                                            BASP0094
      IF(F.GT.5)F=5.0                                                      BASP0095
      IF(F.LT.0.0)F=0.0                                                    BASP0096
60    DL(I,J)=D                                                            BASP0097
      H(I,J)=H(I,J)+D*F                                                    BASP0098
70    IF(H(I,J).LE.BOT(I,J))H(I,J)=BOT(I,J)+0.01                           BASP0099
C     REFINE ESTIMATES OF HEADS BY IADI METHOD                             BASP0100
      ITER=0                                                               BASP0101
80    E=0.0                                                                BASP0102
      ITER=ITER+1                                                          BASP0103
C     TRANSMISSIVITY CONTROL                                               BASP0104
      DO 83 I=1,NC                                                         BASP0105
      DO 83 J=1,NR                                                         BASP0106
        IF(I.LT.NC)T(I,J,2)=PERM(I,J,2)*(H(I,J)+H(I+1,J))/2                BASP0107
83    IF(J.LT.NR)T(I,J,1)=PERM(I,J,1)*(H(I,J)+H(I,J+1))/2                  BASP0108
```

```
C       COLUMN CALCULATIONS                                                 BASP0109
        DO 190 II=1,NC                                                      BASP0110
        I=II                                                                BASP0111
        IF(MOD(ISTEP+ITER,2).EQ.1) I=NC-I+1                                 BASP0112
        DO 170 J=1,NR                                                       BASP0113
C       CALCULATE B AND G ARRAYS                                            BASP0114
        BB=SF2(I,J)/DELTA                                                   BASP0115
        UM=0.                                                               BASP0116
        DD=HO(I,J)*SF2(I,J)/DELTA+RR(ISTEP)-UM*Q(I,J)                       BASP0117
        AA=0.0                                                              BASP0118
        CC=0.0                                                              BASP0119
        IF(J-1)90,100,90                                                    BASP0120
90      AA=-T(I,J-1,1)                                                      BASP0121
        BB=BB+T(I,J-1,1)                                                    BASP0122
100     IF(J-NR)110,120,110                                                 BASP0123
110     CC=-T(I,J,1)                                                        BASP0124
        BB=BB+T(I,J,1)                                                      BASP0125
120     IF(I-1)130,140,130                                                  BASP0126
130     BB=BB+T(I-1,J,2)                                                    BASP0127
        DD=DD+H(I-1,J)*T(I-1,J,2)                                           BASP0128
140     IF(I-NC)150,160,150                                                 BASP0129
150     BB=BB+T(I,J,2)                                                      BASP0130
        DD=DD+H(I+1,J)*T(I,J,2)                                             BASP0131
160     W=BB-AA*B(J-1)                                                      BASP0132
        B(J)=CC/W                                                           BASP0133
170     G(J)=(DD-AA*G(J-1))/W                                               BASP0134
C       RE-ESTIMATE HEADS                                                   BASP0135
        E=E+ABS(H(I,NR)-G(NR))                                              BASP0136
        H(I,NR)=G(NR)                                                       BASP0137
        N=NR-1                                                              BASP0138
180     HA=G(N)-B(N)*H(I,N+1)                                               BASP0139
        E=E+ABS(HA-H(I,N))                                                  BASP0140
        H(I,N)=HA                                                           BASP0141
        N=N-1                                                               BASP0142
        IF(N.GT.0)GO TO 180                                                 BASP0143
        DO 190 N=1,NR                                                       BASP0144
```

```
      IF(H(I,N).GT.BOT(I,N))GO TO 190                                    BASP0145
      E=E+BOT(I,N)+0.01-H(I,N)                                           BASP0146
      H(I,N)=BOT(I,N)+0.01                                               BASP0147
190   CONTINUE                                                           BASP0148
C     TRANSMISSIVITY CONTROL                                             BASP0149
      DO 193 J=1,NR                                                      BASP0150
      DO 193 I=1,NC                                                      BASP0151
      IF(I.LT.NC)T(I,J,2)=PERM(I,J,2)*(H(I,J)+H(I+1,J))/2                BASP0152
193   IF(J.LT.NR)T(I,J,1)=PERM(I,J,1)*(H(I,J)+H(I,J+1))/2                BASP0153
C     ROW CALCULATIONS                                                   BASP0154
      DO 300 JJ=1,NR                                                     BASP0155
      J=JJ                                                               BASP0156
      IF(MOD(ISTEP+ITER,2).EQ.1) J=NR-J+1                                BASP0157
      DO 280 I=1,NC                                                      BASP0158
      BB=SF2(I,J)/DELTA                                                  BASP0159
      DD=HO(I,J)*SF2(I,J)/DELTA+RR(ISTEP)-UM*Q(I,J)                      BASP0160
      AA=0.0                                                             BASP0161
      CC=0.0                                                             BASP0162
      IF(J-1)200,210,200                                                 BASP0163
200   BB=BB+T(I,J-1,1)                                                   BASP0164
      DD=DD+H(I,J-1)*T(I,J-1,1)                                          BASP0165
210   IF(J-NR)220,230,220                                                BASP0166
220   DD=DD+H(I,J+1)*T(I,J,1)                                            BASP0167
      BB=BB+T(I,J,1)                                                     BASP0168
230   IF(I-1)240,250,240                                                 BASP0169
240   BB=BB+T(I-1,J,2)                                                   BASP0170
      AA=-T(I-1,J,2)                                                     BASP0171
250   IF(I-NC)260,270,260                                                BASP0172
260   BB=BB+T(I,J,2)                                                     BASP0173
      CC=-T(I,J,2)                                                       BASP0174
      W=BB-AA*B(I-1)                                                     BASP0175
      GO TO 275                                                          BASP0176
270   W=BB-(AA+CC)*B(I-1)                                                BASP0177
275   B(I)=CC/W                                                          BASP0178
280   G(I)=(DD-AA*G(I-1))/W                                              BASP0179
C     RE-ESTIMATE HEADS                                                  BASP0180
```

```
      E=E+ABS(H(NC,J)-G(NC))                                                    BASP0181
      H(NC,J)=G(NC)                                                             BASP0182
      N=NC-1                                                                    BASP0183
290   HA=G(N)-B(N)*H(N+1,J)                                                     BASP0184
      E=E+ABS(H(N,J)-HA)                                                        BASP0185
      H(N,J)=HA                                                                 BASP0186
      N=N-1                                                                     BASP0187
      IF(N.GT.0)GO TO 290                                                       BASP0188
      DO 300 N=1,NC                                                             BASP0189
      IF(H(N,J).GT.BOT(N,J))GO TO 300                                           BASP0190
      E=E+BOT(N,J)+0.01-H(N,J)                                                  BASP0191
      H(N,J)=BOT(N,J)+0.01                                                      BASP0192
300   CONTINUE                                                                  BASP0193
C     PRINT RESULTS                                                             BASP0194
      IF(E.GT.ERROR) GO TO 80                                                   BASP0195
315   DO 320 J=1,1                                                              BASP0196
      WRITE(6,330)ISTEP,HY(ISTEP),(H(I,J),I=1,NC,5)                             BASP0197
C     STORE DATA IN TAPE                                                        BASP0198
320   WRITE(12,330)ISTEP,HY(ISTEP),(H(I,J),I=1,NC,5)                            BASP0199
330   FORMAT(I6,6F12.5)                                                         BASP0200
340   CONTINUE                                                                  BASP0201
      STOP                                                                      BASP0202
      END                                                                       BASP0203
C     CONTROL CARDS(OMITTED) FOR GENERATED DATA IN TAPE                         BASP0204
C     TO BE USED IN THE BMD 02T PROGRAM                                         BASP0205
C     LISTING OF DATA                                                           BASP0206
  405 0.0314 0.003                                                            BASP0207
   21     2 1.0         1.0   0.0                          0.0025     1.0   0.0  BASP0208
C     NODE CARDS                                                                BASP0209
  1  1 1.0   1.0  1.0 0.0 900C0000.0 1.0  1.0    0.0                           BASP0210
  1  2 1.0   1.0  1.0 0.0 900C0000.0 1.0  1.0    0.0                           BASP0211
  2  1 1.0   1.0  1.0 0.0  0.0025    1.0  1.0    0.0                           BASP0212
  2  2 1.0   1.0  1.0 0.0  0.0025    1.0  1.0    0.0                           BASP0213
  3  1 1.0   1.0  1.0 0.0  0.0025    1.0  1.0    0.0                           BASP0214
  3  2 1.0   1.0  1.0 0.0  0.0025    1.0  1.0    0.0                           BASP0215
  4  1 1.0   1.0  1.0 0.0  0.0025    1.0  1.0    0.0                           BASP0216
```

```
 4  2 1.0    1.0   1.0  0.0   0.0025    1.0   1.0     0.0                BASP0217
 5  1 1.0    1.0   1.0  0.0   0.0025    1.0   1.0     0.0                BASP0218
 5  2 1.0    1.0   1.0  0.0   0.0025    1.0   1.0     0.0                BASP0219
 6  1 1.0    1.0   1.0  0.0   0.0025    1.0   1.0     0.0                BASP0220
 6  2 1.0    1.0   1.0  0.0   0.0025    1.0   1.0     0.0                BASP0221
 7  1 1.0    1.0   1.0  0.0   0.0025    1.0   1.0     0.0                BASP0222
 7  2 1.0    1.0   1.0  0.0   0.0025    1.0   1.0     0.0                BASP0223
 8  1 1.0    1.0   1.0  0.0   0.0025    1.0   1.0     0.0                BASP0224
 8  2 1.0    1.0   1.0  0.0   0.0025    1.0   1.0     0.0                BASP0225
 9  1 1.0    1.0   1.0  0.0   0.0025    1.0   1.0     0.0                BASP0226
 9  2 1.0    1.0   1.0  0.0   0.0025    1.0   1.0     0.0                BASP0227
10  1 1.0    1.0   1.0  0.0   0.0025    1.0   1.0     0.0                BASP0228
10  2 1.0    1.0   1.0  0.0   0.0025    1.0   1.0     0.0                BASP0229
11  1 1.0    1.0   1.0  0.0   0.0025    1.0   1.0     0.0                BASP0230
11  2 1.0    1.0   1.0  0.0   0.0025    1.0   1.0     0.0                BASP0231
12  1 1.0    1.0   1.0  0.0   0.0025    1.0   1.0     0.0                BASP0232
12  2 1.0    1.0   1.0  0.0   0.0025    1.0   1.0     0.0                BASP0233
13  1 1.0    1.0   1.0  0.0   0.0025    1.0   1.0     0.0                BASP0234
13  2 1.0    1.0   1.0  0.0   0.0025    1.0   1.0     0.0                BASP0235
14  1 1.0    1.0   1.0  0.0   0.0025    1.0   1.0     0.0                BASP0236
14  2 1.0    1.0   1.0  0.0   0.0025    1.0   1.0     0.0                BASP0237
15  1 1.0    1.0   1.0  0.0   0.0025    1.0   1.0     0.0                BASP0238
15  2 1.0    1.0   1.0  0.0   0.0025    1.0   1.0     0.0                BASP0239
16  1 1.0    1.0   1.0  0.0   0.0025    1.0   1.0     0.0                BASP0240
16  2 1.0    1.0   1.0  0.0   0.0025    1.0   1.0     0.0                BASP0241
17  1 1.0    1.0   1.0  0.0   0.0025    1.0   1.0     0.0                BASP0242
17  2 1.0    1.0   1.0  0.0   0.0025    1.0   1.0     0.0                BASP0243
18  1 1.0    1.0   1.0  0.0   0.0025    1.0   1.0     0.0                BASP0244
18  2 1.0    1.0   1.0  0.0   0.0025    1.0   1.0     0.0                BASP0245
19  1 1.0    1.0   1.0  0.0   0.0025    1.0   1.0     0.0                BASP0246
19  2 1.0    1.0   1.0  0.0   0.0025    1.0   1.0     0.0                BASP0247
20  1 1.0    1.0   1.0  0.0   0.0025    1.0   1.0     0.0                BASP0248
20  2 1.0    1.0   1.0  0.0   0.0025    1.0   1.0     0.0                BASP0249
21  1 1.0    1.0   1.0  0.0   0.0025    1.0   1.0     0.0                BASP0250
21  2 1.0    1.0   1.0  0.0   0.0025    1.0   1.0     0.0                BASP0251
C      30 DAYS-INTERVAL DATA OF PRECIPITATION FROM 1938 TO 1971           BASP0252
```

1938	0.12	2.48	1.91	2.83	8.14	4.49	2.24	5.60	2.62	0.16	2.05	0.15	BASP0253
1939	1.09	1.93	1.57	2.14	3.25	8.90	0.72	5.84	0.30	1.14	0.81	0.95	BASP0254
1940	1.40	1.43	0.74	6.15	5.82	4.83	0.94	2.87	6.14	1.05	3.82	1.56	BASP0255
1941	1.53	1.09	1.11	2.83	2.89	7.03	2.41	3.54	4.29	4.81	0.78	0.92	BASP0256
1942	0.23	1.93	0.83	7.08	1.67	8.69	2.34	4.51	7.21	3.77	0.68	3.14	BASP0257
1943	0.27	0.67	1.21	1.94	6.59	3.43	6.51	1.95	3.14	1.83	0.07	2.33	BASP0258
1944	1.01	1.34	4.55	12.42	2.04	1.60	5.49	4.77	2.20	2.20	1.93	3.98	BASP0259
1945	1.07	0.84	1.85	6.79	1.28	4.00	5.01	4.11	10.58	0.51	0.05	0.62	BASP0260
1946	2.21	1.23	1.81	1.87	2.11	2.71	0.32	2.90	1.27	4.32	2.14	0.78	BASP0261
1947	0.71	0.52	2.91	5.20	4.69	2.57	2.89	0.82	0.25	1.50	0.89	2.98	BASP0262
1948	1.00	1.19	1.51	1.65	1.86	9.76	6.39	2.72	1.05	0.67	3.30	0.23	BASP0263
1949	6.29	1.80	2.01	3.83	6.15	3.16	6.97	1.13	3.62	1.91	0.06	1.22	BASP0264
1950	0.52	1.61	0.50	0.88	2.24	4.02	13.37	5.93	1.04	0.48	0.26	0.02	BASP0265
1951	1.03	2.58	2.69	6.33	7.60	10.07	4.45	5.38	6.59	2.05	1.47	0.24	BASP0266
1952	0.41	0.35	2.68	1.97	2.31	1.08	4.94	2.52	0.28	0.00	2.40	1.09	BASP0267
1953	0.15	0.82	3.35	0.57	2.02	2.17	2. 9	0.82	0.53	3.77	1.46	1.06	BASP0268
1954	0.09	0.57	1.30	1.54	4.84	0.94	0.19	0.96	1.09	2.83	0.00	0.18	BASP0269
1955	0.61	1.71	0.68	0.72	4.02	3.98	1.30	1.06	3.79	5.84	0.03	0.03	BASP0270
1956	0.43	0.45	0.91	1.46	1.40	1.28	2.51	0.70	0.03	2.69	0.48	0.39	BASP0271
1957	0.19	0.77	2.60	3.31	7.57	10.46	1.99	0.59	5.05	2.72	1.45	0.45	BASP0272
1958	0.81	1.03	4.07	1.23	2.44	3.00	7.19	2.93	6.11	0.00	2.39	0.46	BASP0273
1959	0.53	0.23	0.85	2.17	5.53	2.35	7.38	4.20	2.31	6.13	0.30	1.60	BASP0274
1960	1.37	1.41	1.18	1.28	4.10	4.59	5.57	7.91	2.25	5.03	0.37	1.73	BASP0275
1961	0.02	1.51	4.83	2.00	4.02	2.61	6.56	3.80	5.24	4.87	2.80	1.01	BASP0276
1962	1.07	0.47	0.26	1.02	0.99	4.80	9.22	2.95	8.23	1.32	1.62	0.60	BASP0277
1963	1.22	0.02	1.67	0.22	6.15	4.51	2.70	2.86	4.90	2.47	1.04	0.34	BASP0278
1964	0.71	0.53	0.89	2.97	5.84	3.73	2.23	6.10	2.66	1.64	5.88	1.03	BASP0279
1965	0.56	1.39	0.48	2.63	6.26	8.00	3.62	4.91	8.44	0.32	0.11	2.25	BASP0280
1966	0.23	1.44	0.26	2.21	0.76	2.67	1.78	1.09	0.72	0.47	0.09	0.43	BASP0281
1967	0.28	0.09	0.57	1.30	1.42	5.62	4.28	1.91	3.19	2.98	0.39	1.41	BASP0282
1968	0.14	0.20	1.36	2.16	4.37	2.38	3.65	6.41	5.91	3.06	2.47	1.31	BASP0283
1969	0.45	1.35	1.73	4.30	3.28	6.82	6.23	1.07	4.77	2.80	0.01	1.36	BASP0284
1970	0.28	0.21	2.70	4.49	1.58	6.72	0.47	2.37	4.04	1.88	0.05	0.49	BASP0285
1971	0.98	1.70	0.01	2.35	3.02	2.70	6.65	1.49	1.73	5.54	2.49	0.95	BASP0286
C	30 DAYS-INTERVAL DATA OF STREAM GAUGE FROM 1938 TO 1971												BASP0287
1938	2.09	2.19	2.22	2.08	2.05	7.77	4.46	2.20	2.31	2.14	2.10	2.27	BASP0288

```
1939      2.23   2.26   2.30   3.07   2.20   2.08  10.18   2.34   2.42   2.10   2.06   2.15 BASP0289
1940      2.16   2.29   3.43   2.14   3.26   2.48   2.11   1.96   1.98   2.04   2.06   2.48 BASP0290
1941      2.21   4.02   2.20   2.22   2.18   3.21   3.88   2.65   2.20   3.27   8.83   3.15 BASP0291
1942      3.14   2.78   2.75   2.69   6.40   3.18   8.40   2.85   3.01   3.08   3.60   3.13 BASP0292
1943      4.48   3.36   3.12   2.94   2.78   3.56   2.76   2.86   2.54   2.39   2.98   2.50 BASP0293
1944      2.43   3.03   2.94   3.96  13.52   4.47   3.08   3.18   3.53   5.66   2.84   3.07 BASP0294
1945      3.21   3.26   5.86   3.29   7.37   3.28   3.39   2.93   2.50  13.90   3.05   2.87 BASP0295
1946      2.87   2.80   2.69   2.70   2.52   2.41   2.35   2.07   2.21   2.12   2.25   2.31 BASP0296
1947      2.34   2.29   2.26   2.60   3.33   6.87   4.46   2.47   2.24   2.18   2.25   2.25 BASP0297
1948      2.93   2.31  12.36   3.07   2.68   2.44  14.34   5.05   2.97   2.90   2.74   3.31 BASP0298
1949      2.84   4.86   9.31   3.90  12.58   6.22   5.88   3.32   2.85   2.72   2.72   2.71 BASP0299
1950      2.84   2.59   2.66   2.60   2.53   2.97   3.48  15.43   4.47   2.72   2.48   2.46 BASP0300
1951      2.42   2.62   2.59   3.11  11.88   4.42  16.16   3.77   2.96   3.78   3.50   2.72 BASP0301
1952      2.52   2.45   2.39   2.62   2.80   2.46   2.09   1.98   1.89   1.81   1.90   1.94 BASP0302
1953      1.95   1.98   2.02   1.94   1.92   2.33   3.20   1.65   1.56   1.55   1.66   1.74 BASP0303
1954      1.74   1.72   1.74   1.72   5.09   1.64   1.51   1.34   1.44   1.35   1.49   1.49 BASP0304
1955      1.53   1.62   1.57   1.62   1.46   1.58   1.34   1.28   1.21   6.04   1.45   1.36 BASP0305
1956      1.39   1.41   1.31   1.25   1.17   1.25   1.01   0.96   0.80   0.81   0.92   0.99 BASP0306
1957      1.01   1.08   1.10   3.29   2.25   4.53  14.66   2.14   1.51   1.47   1.61   1.58 BASP0307
1958      1.60   1.73   2.01   8.62   3.24   2.37   2.33   9.12   2.45   2.60   2.32   2.20 BASP0308
1959      2.19   2.22   2.11   2.54   1.92   4.72   1.96   2.11   3.04   1.92   2.65   1.77 BASP0309
1960      2.00   3.33   2.05   4.30   3.17   3.25   2.53   1.82   6.93   2.56   3.20   1.75 BASP0310
1961      1.78   1.61   1.66   3.32   4.79   2.25   1.55   1.79   1.44   1.92   3.48   1.98 BASP0311
1962      1.70   6.66   1.76   1.64   1.45  10.04   2.29   2.71   1.73   2.08   1.60   1.68 BASP0312
1963      1.45   1.64   1.40   1.42   1.21   1.25   0.95   1.19   0.98   1.07   1.49   1.16 BASP0313
1964      1.13   1.20   1.12   1.08   1.71   1.83   1.06   0.83   3.00   0.92   0.85   1.35 BASP0314
1965      1.25   1.11   1.44   1.03   0.99   3.28  10.34   1.63   9.24   3.12   1.46   1.34 BASP0315
1966      2.02   1.38   1.41   1.14   1.47   0.96   1.10   1.01   0.76   0.70   0.71   0.75 BASP0316
1967      0.80   0.83   0.78   1.00   0.84   0.82   9.75   3.07   1.29   2.58   1.56   1.30 BASP0317
1968      1.23   1.25   1.15   0.95   1.12   2.39   0.97   2.01   1.87   0.66   1.48   1.28 BASP0318
1969      1.47   1.13   7.11   2.01   3.66   3.23   2.00   1.15   1.23   1.39   1.60   1.05 BASP0319
1970      1.09   1.08   0.95   2.88   1.58   1.05   1.40   0.73   0.54   1.40   1.13   0.97 BASP0320
1971      0.90   0.96   3.32   1.29   1.08   2.61   1.35   4.99   0.94      .      .      . BASP0321
C     CONTROL CARDS(OMITTED) FOR THE BMD 02T PROGRAM                                        BASP0322
C     NUMBER OF INPUT DATA FOR EACH SERIES IS 405                                           BASP0323
C     NUMBER OF LAGS IS 36                                                                  BASP0324
```

```
C     BASE SERIES IS ACCRETION                                                  BASP0325
PROBLMKANSA2                    6 495 36 100 1.00MONTHYES          112 1      BASP0326
(6X,6F12.5)                                                                   BASP0327
SELECT YES YES YES 01   05 02     03     04     05     06                      BASP0328
C     BASE SERIES IS STREAM                                                   BASP0329
PROBLMKANSA2                    5 405 36 100 1.00MONTH             112 1      BASP0330
(18X,5F12.5)                                                                  BASP0331
FINISH                                                                        BASP0332
```

APPENDIX B

Confidence Limits for the Spectrum

The sampling distribution of a smoothed estimate of a spectrum is approximately chi-square with ν degrees of freedom. Hence, for a spectral density $S_{XX}(\Omega)$ based upon an estimate $\hat{S}_{XX}(\Omega)$ measured with the number of lags, M and a total record length T, a $1-\alpha$ confidence interval is given by

$$\frac{\nu \hat{S}_{XX}(\Omega)}{\chi^2_{\nu;\, \alpha/2}} \leq S_{XX}(\Omega) \leq \frac{\nu \hat{S}_{XX}(\Omega)}{\chi^2_{\nu;\, 1-\alpha/2}} \qquad \text{(B 1)}$$

where $\nu = 2.667\ T/M$ for the Turkey window used in this program (See p. 252, Jenkins and Watts, 1968.)

APPENDIX C

List of Figures

APPENDIX D

List of Tables